



TECHNISCHE UNIVERSITÄT MÜNCHEN

Ingenieurfacultät Bau Geo Umwelt

Lehrstuhl für Statik

Numerical Methods for the Design and Analysis of Tensile Structures

Falko Hartmut Dieringer

Vollständiger Abdruck der von der Ingenieurfacultät Bau Geo Umwelt der
Technischen Universität München zur Erlangung des akademischen Grades eines

Doktor-Ingenieurs

genehmigten Dissertation.

Vorsitzender:

Univ.-Prof. Dr.-Ing. habil. Fabian Duddeck

Prüfer der Dissertation:

1. Univ.-Prof. Dr.-Ing. Kai-Uwe Bletzinger
2. Univ.-Prof. Dr.-Ing. Rainer Barthel
3. Prof. Eugenio Oñate Ph.D., Universitat Politècnica de Catalunya

Die Dissertation wurde am 05.03.2014 bei der Technischen Universität München
eingereicht und durch die Ingenieurfacultät Bau Geo Umwelt am 05.06.2014
angenommen.

Abstract

In the present thesis the design and analysis process for tensile structures is discussed from a numerical point of view. The special characteristics of the load bearing behavior of tensile structures introduce the necessity of adapted numerical methods for the individual design and analysis steps. The required governing equations are formulated based on continuum mechanics. Therefore, standard numerical strategies, e.g. the Finite Element Method, can be applied for the solution of the governing equations. In addition, there are strong interactions between the individual design steps. These interactions are discussed in detail and the effects on the numerical results are presented.

Because of the slenderness of tensile structures external loads are only restrained by in-plane stresses. Therefore, a feasible design has to be found which satisfies the requirements from an engineering and architectural point of view. Based on a predefined stress distribution and various boundary conditions, the shape of equilibrium is evaluated in the design step of *form finding*. For the solution of this numerically inverse problem, the Updated Reference Strategy is applied. After a detailed discussion of this method, an extension can be presented which is introduced as the eXtended Updated Reference Strategy. The integration of elastic elements in a tensile structure can be introduced as a hybrid structure. Based on this definition, the effects on the numerical form finding process are discussed in detail for this type of structures.

The shape of equilibrium is the basis for the subsequent design steps. In the *structural analysis* the behavior of the tensile structure based on external loads will be evaluated. In this thesis the general numerical process for the transient and steady state case is discussed. For the numerical modeling, different finite elements have to be applied. Therefore, a set of typical elements are discussed in detail and a general discussion on other types of elements is given. In addition, the special characteristics of external loads w.r.t. large deformations of tensile structures are shown.

In general, tensile structures are double curved surfaces which introduce the necessity of a *cutting pattern generation* for the manufacturing. Based on the general discussion of the underlying mechanical problem the principle of the Variation of Reference Strategy is introduced. Here, the resulting stresses from the assembly process and the intended stress distribution are minimized in order to evaluate the cutting patterns. Besides the discussion of the solution process of the governing equations, the introduction of requirements from the manufacturing process is shown. In addition, a discussion on the sensitivities of the cutting pattern generation process is given.

The individual design steps can be combined to two principal design approaches. The standard and the extended design approach are discussed in detail and the respective effects on the numerical results are presented. The integration of elastic elements in the presented design approaches is shown and a detailed discussion of the effects on the numerical modeling for hybrid structures is given. Hence, an integrated numerical design and analysis process is introduced for the simulation of arbitrary tensile structures.

Zusammenfassung

In der vorliegenden Arbeit wird der Entwurfs- und Berechnungsprozess von Membrantragwerken aus numerischer Sicht betrachtet. Das besondere Lastabtragverhalten von Membrantragwerken erfordert angepasste numerische Methoden für die einzelnen Entwurfs- und Berechnungsschritte. Die beschreibenden Gleichungen werden hierbei aus einer kontinuumsmechanischen Sichtweise abgeleitet. Dies ermöglicht den Einsatz von numerischen Standardverfahren, wie der Methode der Endlichen Elemente, zur Lösung der beschreibenden Gleichungen. Zusätzlich können Interaktionen zwischen den einzelnen Entwurfs- und Berechnungsschritten identifiziert werden. Diese Interaktionen werden im Detail diskutiert und die sich hieraus ergebenden Effekte auf die numerischen Ergebnisse vorgestellt.

Auf Grund der extremen Schlankheit von Membrantragwerken erzeugen äußere Lasten ausschließlich Spannungen in der Tangentialebene. Daher muss ein Entwurf gefunden werden, der sowohl den Anforderungen aus ingenieurtechnischer wie auch aus architektonischer Sicht genügt. Basierend auf einem vordefinierten Spannungszustand und verschiedenen Randbedingungen wird im Entwurfsschritt der *Formfindung* die Gleichgewichtsfläche gefunden. Das hierbei vorhandene numerisch inverse Problem wird mittels der Updated Reference Strategy gelöst. Aufbauend auf der detaillierten Diskussion dieser Methode wird die eXtended Updated Reference Strategy als Erweiterung vorgestellt. Die Integration von elastischen Strukturelementen in Membrantragwerke wird als hybride Tragwerke eingeführt. Mit dieser Begriffsdefinition werden für diese Tragwerke die Einflüsse auf den numerischen Formfindungsprozess im Detail diskutiert.

Die Gleichgewichtsfläche stellt die Basis für die weiteren Entwurfsschritte dar. In der *Strukturanalyse* wird das Verhalten der Membrantragwerke bzgl. äußerer Lasten berechnet. In der vorliegenden Arbeit wird der allgemeine numerische Prozess hinsichtlich transienter und stationärer Fälle diskutiert. Für die numerische Simulation werden hierfür verschiedene Finite Elemente angewendet. Daher werden typische Finite Elemente im Detail beschrieben und weiter in einer allgemeinen Diskussion behandelt. Zusätzlich wird der Einfluss der großen Verformungen eines Membrantragwerks auf die äußeren Lasten detailliert diskutiert.

Im Allgemeinen weisen Membrantragwerke eine doppelte Krümmung auf, welche die Notwendigkeit einer *Zuschnittsermittlung* für den Herstellprozess begründet. Aufbauend auf der grundlegenden Diskussion der mechanischen Fragestellung wird das Verfahren der Variation of Reference Strategy vorgestellt. Hierbei wird der Unterschied zwischen den sich ergebenden Spannungen aus dem Herstellprozess und den vordefinierten Spannungen minimiert, um die Zuschnitte zu ermitteln. Neben der Diskussion des eigentlichen Lösungsprozesses der beschreibenden Gleichungen, werden Nebenbedingungen, die sich aus dem Herstellprozess ergeben, miteinbezogen. Ergänzend werden die Sensitivitäten des Prozesses der Zuschnittsermittlung vorgestellt und diskutiert.

Die einzelnen Entwurfsschritte können prinzipiell zu zwei verschiedenen Entwurfsansätzen kombiniert werden. Der gewöhnliche und der erweiterte Entwurfsansatz

werden detailliert diskutiert und die Effekte auf die numerischen Ergebnisse werden dargelegt. Die Integration von elastischen Elementen in den Entwurfsansatz wird aufgezeigt und die grundsätzlichen Effekte auf den numerischen Simulationsprozess werden angegeben. Somit wird ein integraler numerischer Entwurfs- und Berechnungsprozess für die Simulation von beliebigen Membrantragwerken vorgestellt.

Acknowledgments

This dissertation was written from 2009 to 2014 during my time as research assistant at the Chair of Structural Analysis (Lehrstuhl für Statik) at the Technische Universität München, Munich, Germany.

I would like to thank sincerely Prof. Dr.-Ing. Kai-Uwe Bletzinger for giving me the possibility to work in his research group. I want to thank him not only for his helpful and inspiring guidance as doctoral supervisor, but also for providing me the academic freedom to develop and realize new ideas and methods. I also want to thank Dr.-Ing. Roland Wüchner for many fruitful discussions.

Furthermore, I would like to address my thanks to the members of my examining jury, Univ.-Prof. Dr.-Ing. Rainer Barthel and Univ.-Prof. Dr.-Ing. Eugenio Oñate. Their interest in my work is gratefully appreciated. Also, I want to thank Univ.-Prof. Dr.-Ing. habil. Fabian Duddeck for chairing the jury.

I also want to thank all coworkers at the Chair of Structural Analysis for the friendly cooperation and the pleasant time that I had working with them. I want to especially mention Armin Widhammer and Benedikt Philipp who inspired my work with numerous discussions.

Finally, I want to thank my family for their support during my study of civil engineering and my dear girlfriend Miriam for her patience, understanding and advice at all times.

Munich, June 2014
Falko Hartmut Dieringer

Contents

1	Introduction	1
1.1	Motivation	1
1.2	Objective and Outline	4
2	Fundamentals	9
2.1	Numerical Modeling	9
2.2	Tensors	10
2.2.1	Tensor Calculus	13
2.3	Differential Geometry of Surfaces in Space	15
2.4	Continuum Mechanics	23
2.4.1	Configurations	24
2.4.2	Deformation Gradient	25
2.4.3	Strains	27
2.4.4	Stresses	29
2.4.5	Material Modeling	31
2.4.6	Equilibrium	40
2.5	Discretization in Time and Space	42
2.5.1	Space discretization	43
2.5.2	Time discretization	44
2.5.3	Linearization of the Equilibrium Equation	45
3	Form Finding	47
3.1	What is form finding?	48
3.2	Numerical form finding of tensile structures	51
3.3	Stabilization of the inverse problem	53
3.3.1	Updated Reference Strategy	55
3.3.1.1	Membrane element	57
3.3.1.2	Cable element	60
3.3.1.3	Existence of a solution for the form finding problem	62

3.3.1.4	Isotropic prestress	66
3.3.1.5	Anisotropic prestress	68
3.4	eXtended Updated Reference Strategy (X-URS)	72
3.5	Form finding of hybrid structures	82
4	Structural Analysis	89
4.1	Transient Analysis	89
4.1.1	Internal Forces in the Transient Analysis	90
4.1.2	Mass Inertia in the Transient Analysis	91
4.1.3	Damping in the Transient Analysis	92
4.1.4	Solution process for the Transient Analysis	92
4.2	Steady State Analysis	95
4.3	Finite Element Formulations	99
4.3.1	Truss or Cable Element	99
4.3.2	Membrane Element	100
4.3.3	Spring-Damper Element	101
4.3.4	Further Finite Elements	103
4.4	External Loads	104
5	Cutting Pattern Generation	109
5.1	Cutting Pattern Generation for Tensile Structures	110
5.2	Solution approach for the Cutting Pattern Generation	115
5.2.1	Minimization of the Work of Stress Differences	118
5.2.2	Minimization of Potential Energy	119
5.2.3	Least Square Approach	121
5.2.4	Summary of the Cutting Pattern Methods	122
5.2.5	General Statements	122
5.2.6	Ensure equal seam length of multi-strip cutting patterns	131
5.2.7	Influence of the Seams	137
6	Design Loops and Interfaces	143
6.1	Standard Design Approach	144
6.2	Extended Design Approach	145
6.3	Elastic Members in the Design Process	153
6.4	Requirements for the Interfaces	159
7	Projects	163
7.1	Student Project	163
7.2	Wide-span Umbrella Structure	169
7.3	Cushions	174
8	Concluding Remarks	183
	List of Figures	186
	Bibliography	191

Introduction

"Leichtbau ist eine Forderung unserer Zeit... Leichtbau muß in immer stärkerem Maße für alle Bauteile gefordert werden, die aus knappen Baustoffen gefertigt werden..." (engl. *"Lightweight construction is a requirement of our time... Lightweight construction has to be required increasingly for all structural components which are made of limited building materials..."*) [Leo40]. This quote from *Fritz Leonhardt*, one of the most important pioneers in modern civil engineering, was written in 1940 in a totally different social period. However, in the context of modern discussions and needs for the construction of sustainable and efficient buildings the formulated requirements are still valid. The principles published by *Fritz Leonhardt* can be mentioned as milestones in modern lightweight design for all types of construction methods in civil engineering [Web11]. Based on the requirements of *Fritz Leonhardt* different effects on the individual construction methods have to be discussed. In general the main motivation is the minimization of material which is used to build a certain structure. The most appropriate method to meet the requirement of minimization of used material is that of tensile structures. Tensile structures are lightweight structures, which combine optimal stress state of the material with an impressive design vocabulary. In the following a brief introduction to this fascinating type of structures will be given to motivate a detailed discussion related to the open questions in the numerical design and analysis of tensile structures.

1.1 Motivation

One of the most important innovations for the development of tensile structures was around 60'000 B.C. [Hop07]. With the innovation of the needle, humans were able to manufacture textiles and mesh works, which are used to cover the sleeping-place or fire pit. In principle these were the first tensile structures. Of course, there was still a long path ahead in developing a tensile structure of the sort that will be discussed in the following chapters. More professional, and based on early "engineering" experience built tensile structures are nomad living tents or roman tents for military camps. Also small scale tents like canopies or awnings were important sources of experience in the development of engineering methods for tensile struc-

1.1 Motivation

tures. Another not less important area of application for the progression of tensile structures are sails for ships. All of these types of structures were the beginning of experience and innovations for the modern state of the art methods for designing tensile structures (cf. figure 1.1) The main advantage of tensile structures in antiq-

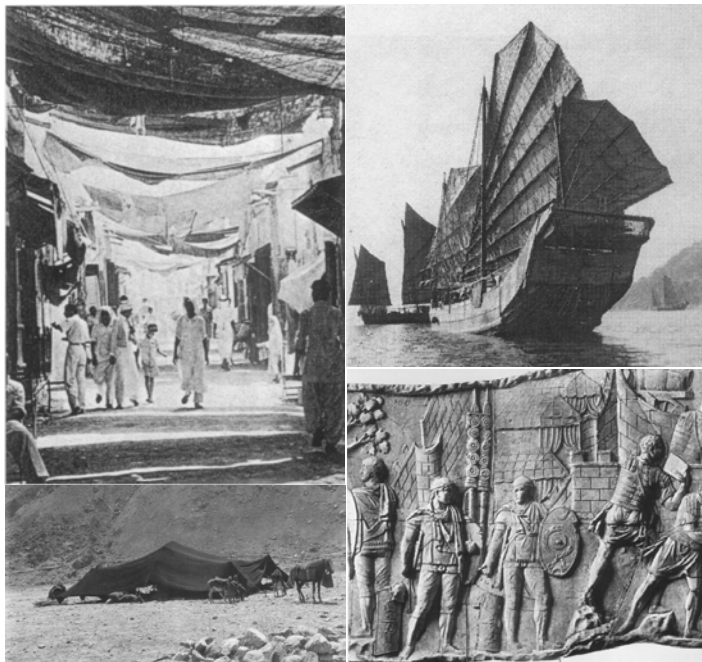


Figure 1.1: Early tensile structures (top left: Canopy on a bazaar in Bahrain [Koc04]; top right: Sail ship [Ber05]; bottom left: Nomad tent [Rob96]; bottom right: Figure of roman military tents [Koc04])

uity was the minimal weight effort for a certain application, due to their needs of mobility, simple assembly and flexibility. Of course, these arguments are still valid for modern tensile structures.

Through the centuries the applications of tensile structures didn't change much. They were mostly used for temporary tents and roofs. The limitation of permanent applications, was due to the lack of appropriate materials, which have an acceptable long term behavior. With the innovation of new materials for industrial products, the possibilities for architectural tensile structures changed fundamentally. Materials which were made of fabric and a protective coating, made tensile structures also interesting for long term architectural buildings. Of course their advantage, in terms of minimization of material needed, is still an interesting point in the current discussion on limited resources. New materials like PTFE (polytetrafluoroethylene),

coated woven glass fibers or foils made of ETFE (ethylene tetrafluoroethylene) are the most common materials in modern tensile structures. A detailed discussion on current materials used in tensile architecture can be found in [Mor00], [Koc04], [Sei08], [Kni+11].

Based on these new possibilities created by newly available materials, architects and engineers have been started to think in new ways and applications. There are many architects and engineers to be named who were responsible or had an important impact on this development. However, the most outstanding contribution to this type of structure was made by *Frei Otto* at the University of Stuttgart. *Frei Otto* was consistently introducing the basic ideas of *Fritz Leonhardt* into tensile architecture. Most probably, without knowing his paper mentioned above. The work of *Frei Otto* is discussed in detail in [OR95], [Sch90]. Some of the most important and groundbreaking structures were designed by *Frei Otto*. The roof of the Olympic stadium in Munich or the Tanzbrunnen at the Bundesgartenschau in Cologne are just two examples of the impressive number of tensile structures which *Frei Otto* was involved (cf. figure 1.2). Of course, there are many more pioneers who can be named such as Richard Buckminster Fuller, Edmund Happold, Ludwig Stromeyer or Jörg Schlaich. The groundbreaking work of these pioneers inspired modern ar-

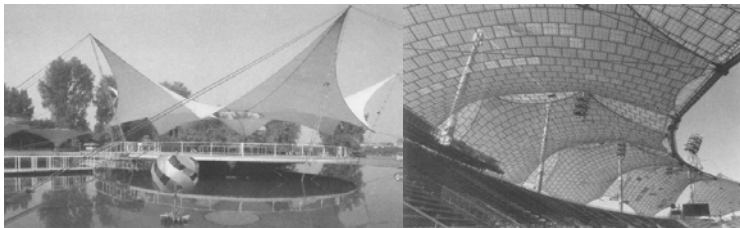


Figure 1.2: Tensile structures designed by *Frei Otto* (left: Tanzbrunnen in Cologne 1957 [Sch90]; right: Roof of the Olympic stadium in Munich 1972 (Architect: Behnisch & Partners) [Sch90])

chitects and engineers to design more challenging structures which are built all over the world. The Expo-Axis in Shanghai or the Bangkok international airport are examples of the current state-of-the-art tensile structures (cf. figure 1.3). Detailed reviews of modern tensile architecture can be found in [Sei08], [Ber05], [Koc04], [Kni+11], [Hop07], [Rob96], [Sch97].

Despite the innovations in modern materials, the design process for tensile structures were still mainly based on experiments and experience. The main merit of *Frei Otto's* work is the ability to transfer the experimental based models of a tensile structure to the final real scale. The development of numerical methods which were appropriate for the design and analysis of these structures began with the design of the Olympic stadium in Munich in 1972. The well known *Force Density Method*, which was introduced by Klaus Linkwitz at the University of Stuttgart in 1971, was the first numerical method fitted for the special requirements in the design process of tensile structures [LS71]. As the *Force Density Method* is limited to cable nets,

1.2 Objective and Outline

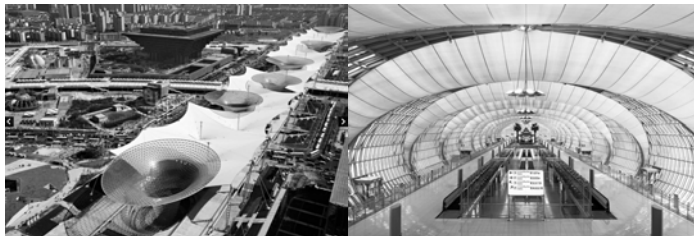


Figure 1.3: Modern tensile structures (left: Expo axis in Shanghai (*copyright: Knippers Helbig - Advanced Engineering*); right: Bangkok international airport (*copyright: Werner Sobek Group GmbH*))

in [HP72] and [Hau72] the principles for the analysis including cables and membranes are presented. Most of the numerical methods, which were developed in the following, are based on the ideas which were introduced in the Force Density Method. The development of numerical methods for tensile structures based on the Finite Element Method (FEM), introduced in the 1960s, were not continued in the same intensity. The introduction of methods based on the FEM were done with the application of the *Dynamic Relaxation Method* for tensile structures [Bar74], [Bar88]. However, the development of appropriate numerical methods were not as proceeding as experimental methods. Despite modern computational methods there are still open questions in the numerical modeling of tensile structures. Form finding, cutting pattern generation, transient load conditions (e.g. wind loads) and appropriate material modeling introduce questions which have to be discussed. Additionally, current tensile structures are more and more combined structures, where the supporting frame and the tensile itself influence each other. Therefore, all of the structural members have to be considered in one computational model. This introduces additional efforts in the numerical modeling of the tensile structure. In the following chapters a contribution to the available methods for the numerical design and analysis of tensile structures will be done.

1.2 Objective and Outline

The objective of the present thesis is to contribute to the numerical modeling of the design and analysis process of tensile structures. In contrast to "conventional" structures (e.g. steel frames, concrete slabs) the overall shape and the structural capacity are strongly coupled in the case of tensile structures. In addition, the structural behavior of tensile structures differs fundamentally from "conventional" structures as they have a negligible bending stiffness. Due to that, appropriate and specific computational methods have to be applied. As a consequence, the individual design steps interact with each other and have to be understood as an integrated design and analysis loop.

In general the design and analysis steps of a tensile structure can be divided into form finding, structural analysis and cutting pattern generation [GB09]. In this the-

sis the individual design and analysis steps are going to be discussed in a separated from. For each step, adapted computational methods will be presented. The derived governing equations for the individual task will be solved by the Finite Element Method. Based on the discussion of existing approaches, improvements for all design steps are going to be depicted. The extensions for the available methods will be purely derived from continuum mechanics and numerical optimization. Therefore, it is ensured that the derived extensions are general and flexible for the application of tensile structures. Because of the fact that modern tensile structures have to be more and more computed together with the supporting frames, due to the structural interaction, the impact of these "conventional" structural elements in the design and analysis process is going to be discussed.

Based on the individual design and analysis steps, possible design loops will be presented. In common practice the design of a tensile structure starts with identifying a satisfying form from an architectural point of view. The solution of the form finding problem is the underlying mechanical question. This step has to be repeated until all architectural and engineering requirements are satisfied. Subsequent to the form finding, the engineer is performing a structural analysis w.r.t. certain load conditions (e.g. wind and snow load) which is followed by the decision about the layout and the computation of the cutting patterns. The individual steps are repeated as long as all of the architectural and structural requirements are fulfilled. From an engineering point of view the natural requirements are the limit stress in the structural members, the supporting forces and the overall deflection of the structure.

In this design loop it is common practice to exclude the supporting frame during the computation of the tensile structure and apply the resulting boundary forces to the elastic supporting members. It is obvious, that this standard approach neglects some important effects on the final structural behavior of the tensile structure, such as the influence of the flexibility of the supporting frames or the change of stress distribution due to the non-developability of the doubly curved shape. The integration of these influences leads to the extended design approach shown in figure 1.4. Here, an integrated numerical design and analysis approach for tensile structures is proposed. Because of this approach, a more accurate structural assessment can be achieved. Of course, this extended design approach includes some difficulties for the design process. For instance, to include the influence of the non-developability into the structural analysis, the layout of the cutting patterns have to be set in an early phase of the design process. In the present thesis the result of the two available design loops w.r.t. the final structural behavior of the tensile is going to be discussed.

In addition to the discussion of the individual design loops and the included design steps, the definition of the demands at the transitions between the individual design steps is a crucial discussion. At a first glance it seems that the requirements at the interfaces between the individual design steps are clear and well defined, but it will be shown that there are different possibilities of handling the requirements at the interfaces from a mechanical point of view, which results in a different structural response of the tensile structures.

1.2 Objective and Outline

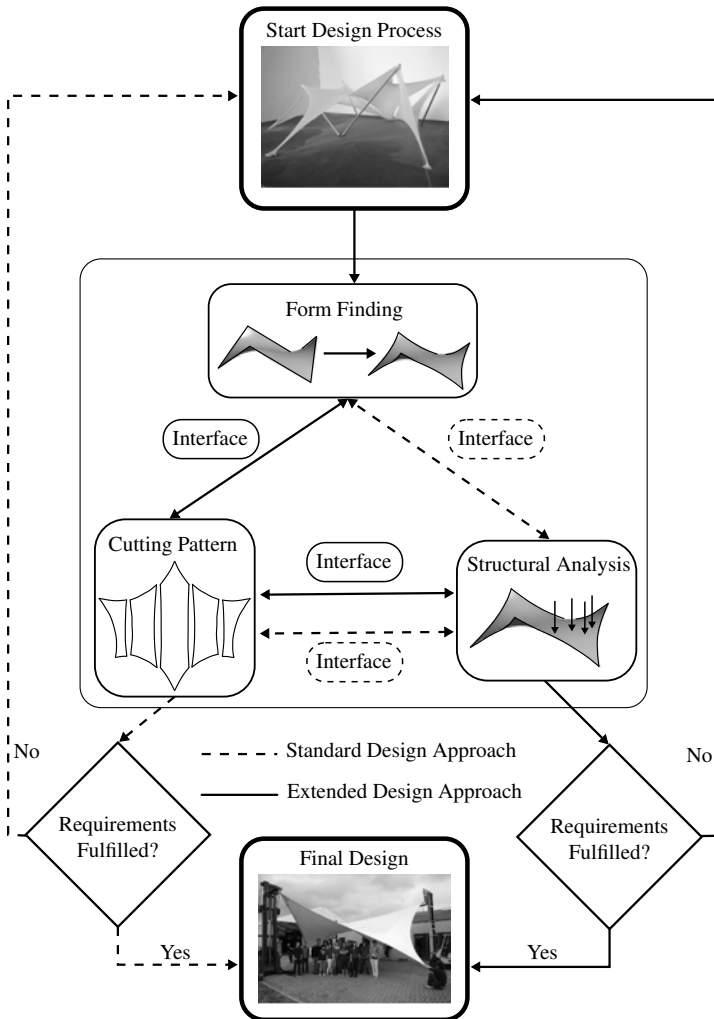


Figure 1.4: Design process for tensile structures

The present thesis will include a detailed discussion on the individual disciplines which are needed to develop an integrated state-of-the-art numerical design and analysis process for tensile structures. Starting with the discussion of the fundamentals from differential geometry and continuum mechanics, the individual design steps are going to be presented and will result in a discussion of the overall design loops and their consequences. The structure of the presented thesis is outlined as follows:

Chapter 2 includes the fundamentals which are needed for the numerical description of tensile structures. In the beginning the basics from differential geometry will be depicted in order to have the possibility of the mathematical description of surfaces in a 3 dimensional space. With the basics from the geometrical description of tensile structures, the governing equations from continuum mechanics are derived. In this chapter the main focus is on the governing equations for strains and stresses for a geometrical nonlinear behavior of the structure. In addition, a discussion of the currently used material models is given. Subsequently the governing equations for the equilibrium in steady state and transient conditions will be derived and the solution techniques in combination with time and space discretization will be depicted.

Chapter 3 describes the beginning steps of designing a tensile structure. Form finding is the first step to a feasible design. As form finding is exclusively a design step for tensile structures, an answer to the question *What is form finding?* will be given. Based on the description of the underlying mechanical problem, a solution technique, called the *Updated Reference Strategy*, introduced in [BR99], will be presented. With the discussion and presentation of additional enhancements to this method, e.g. handling of anisotropic prestress distributions, an extension towards the mathematically consistent solution of the form finding problem will be introduced. At the end, a discussion of the influence of the integrated form finding of tensile and supporting structure completes this chapter.

Chapter 4 contains the description of the process of structural analysis. Beginning with the governing equations for the structural analysis in transient and steady state conditions, different finite elements will be formulated. The main focus in this chapter is on the presentation of all required element types, which have to be available for state of the art tensile structures. Based on benchmark examples, the individual requirements for the structural analysis will be presented. Subsequently, special effects from follower forces (e.g. wind loads) resulting in the formulation of the equilibrium conclude this chapter.

Chapter 5 addresses the topic of cutting pattern generation. Here, the principal problem of computing plane patterns for a doubly curved surface is addressed. The main objective is to develop a doubly curved surface into a plane with the fewest compromises possible w.r.t. the resulting stress distribution after the assembly of the tensile structure. In this chapter a method based on ideas from structural optimization [LWB08] is going to be presented. Starting with a discussion of the principles of the method, extensions to apply the method on state of the art tensile structures will be presented. Additionally, a discussion of the sensitivity of the resulting cut-

1.2 Objective and Outline

ting patterns w.r.t. different input parameters is included.

Chapter 6 contains the description of the different possible design loops. Besides the basics of the individual design loops, a discussion of the results in the structural response of the tensile structure is also included. A standard and extended design loop are discussed from a mechanical point of view. Especially the different possibilities in describing the equilibrium through all the design stages. The influence of including the supporting structures in the design loops will be discussed as well. The special requirements on the numerical methods will be shown and the principal results and differences from a mechanical point of view will be presented. A discussion of the requirements of the individual interfaces concludes this chapter.

Chapter 7 a collection of different projects, in which the presented methodologies are applied will be shown. The principle applicability for the design and analysis of tensile structures of the derived and introduced methods is presented.

Chapter 8 concludes the present thesis with a discussion of the introduced methods for the design and analysis of tensile structures. Finally, pending research topics will be reviewed to ensure that this thesis will be an inspiration for further research on the topic of the numerical design and analysis of tensile structures.

Remark: All numerical results in the present thesis were obtained by the research code Carat++.

Fundamentals

In this chapter, the fundamentals for the geometrical and mechanical description of tensile structures will be given. In the beginning there is a brief discussion of the aspects of numerical modeling. The geometrical description of surfaces in 3D-space is an elementary topic to comprehend the mechanical behavior of tensile structures. For this purpose a discussion of the most important definitions and equations from differential geometry is included in this chapter. On this basis it is possible to depict the mechanics of tensile structures. In general, they have small thickness and undergo large deflections, which introduce the requirement to the underlying mechanical descriptions to be able to cover the full appearing kinematic. Hence, a brief discussion of the most important content from tensor calculus for the description of the mechanics of large deformations is included. Combining differential geometry and tensor calculus, it is possible to introduce strains and stresses into continuum mechanics to describe the behavior of tensile structures in an appropriate form. In order to complete the discussion on the mechanical characteristics, some comments on the material modeling are included as well. With the principles from differential geometry and continuum mechanics, the governing equations for the equilibrium will be derived. Based on a description for the discretization in time and space, a solution technique for the obtained equilibrium equation is included in this chapter, as well.

2.1 Numerical Modeling

The geometry of a tensile structure is embedded in the 3 dimensional space. There are two main lengths L_X and L_Y which define the overall shape. The third length defines the thickness L_Z of the shape (cf. figure 2.1). In general, the thickness of a tensile structure is much smaller in comparison to the other two main lengths and is in general assumed to be constant all over the surface. The applied materials for tensile structures are highly advanced and most adapted for the special application of architectural applications. Fabric materials like PTFE or foils like ETFE have an complex micro structure, containing fibers and coating in case of PTFE. From a numerical point of view it would be possible to model the material in its details,

2.2 Tensors

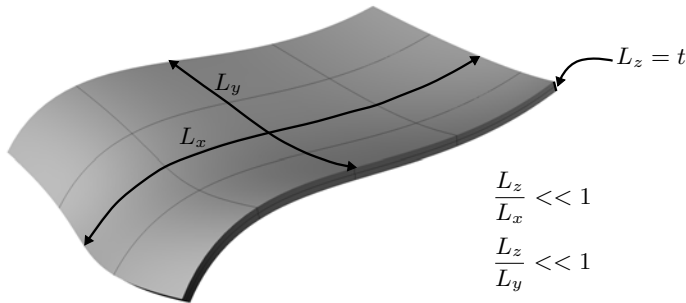


Figure 2.1: Length-to-Thickness ratio for a tensile structure

starting from its micro structure and including this into the full scale computation of the tensile structure [STT95], [KJS05], [XN11], [ZP06]. It is obvious that the effort for the solution process of the resulting numerical model is highly time consuming. The advantage from this approach is that the results are more detailed and precise. The application of this approach is most appropriate if a detailed analysis of a small scale structure has to be done. The simulation of car body parts made out of carbon fiber reinforced plastics is just one example for the application of this approach. In the case of architectural tensile structures this approach can't be applied because of the time effort required for the numerical solution process and the variation in the material properties. It is more suitable to introduce models which are able to describe the material behavior in a homogenized way. For this, the assumption is introduced that for a certain piece of material the properties are constant all over the volume.

With the assumption of a small thickness and a homogenized material it is possible to reduce the numerical model from a full continuum to a description of the mid surface of the tensile structure [Bis+04]. In figure 2.2 the steps for the numerical modeling of homogenization and dimension reduction are illustrated. For the step of dimension reduction the following assumption is introduced additionally: If measuring the stresses at a certain point through the thickness, the change will be negligible. Hence, it is assumed that the stress doesn't change through the thickness. In general, this stress situation is called *membrane stress state*. Therefore, tensile structures are often also described as *membrane structures*. In this thesis both names are valid and understood as equivalent. It is also assumed that the tensile structure has no bending stresses, as they would result in a change of the normal stresses through the thickness.

2.2 Tensors

In this section an introduction to tensor calculus will be given. For the geometrical and mechanical description of tensile structures, tensors are the most appropriate

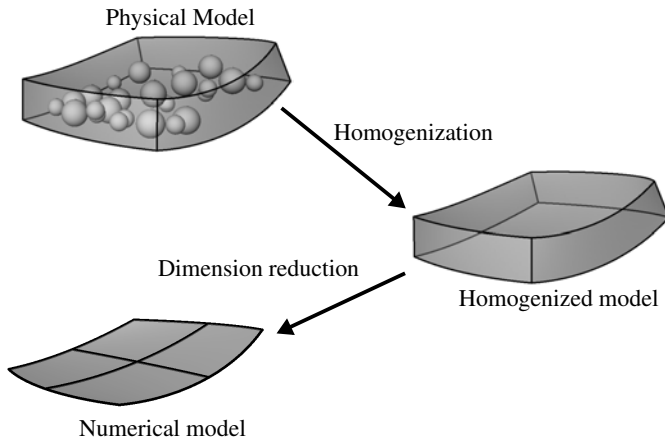


Figure 2.2: Numerical modeling steps for a tensile structure

quantities. With the introduction of tensors in the governing equations it is possible to reduce the complexity and state them in a compact form. The following content from tensor calculus is not a complete discussion of the topic, just the most relevant calculation rules will be depicted.

Of course, in the beginning the question arises "What is a Tensor?". The answer to that question can be found in [Käs64]: *Sämtliche Größen der Physik sind Tensoren* (engl.: All physical quantities are tensors). Tensors in general are quantities which can be represented by their individual values (here: coefficients) and their directions (here: base vectors). For a detailed introduction to the topic of tensor calculus, many sources are available (e.g. [Bet87]). In general, there is a distinction between different types of tensors:

Zero-Order Tensor: Objects which consist of a scalar value without a certain direction (e.g. density of a material, temperature, etc.)

First-Order Tensor: Objects which consist out of coefficients where each is related to a certain direction. For instance, a vector \mathbf{v} is a first order tensor. It can be given in terms of its coefficients v^i and the related directions \mathbf{e}_i . The directions of the tensor are referenced as the base vector of the tensor. These can be understood as the coordinate system in which the tensor is defined. It is important to state that the tensor itself is invariant to the change of the coordinate system. In principle the coordinate system can be chosen arbitrarily, but of course the coefficients of the tensor are changing through the change of the coordinate system. Examples for first-order tensors are geometrical vectors, force vectors, etc..

Second-Order Tensor: Objects which can be represented by coefficients and two

2.2 Tensors

base vectors. A second-order tensor \mathbf{T} can be obtained by the dyadic product, or tensor product, of the two vectors \mathbf{a} and \mathbf{b} :

$$\mathbf{T} = \mathbf{a} \otimes \mathbf{b} = (a^i \mathbf{e}_i) \otimes (b^j \mathbf{e}_j) = a^i b^j \mathbf{e}_i \otimes \mathbf{e}_j = T^{ij} \mathbf{e}_i \otimes \mathbf{e}_j \quad (2.1)$$

Here, the tensor product is introduced by \otimes . In equation (2.1) the vectors \mathbf{e}_i and \mathbf{e}_j represents the Cartesian base vectors. For the example of the second-order tensor \mathbf{T} it would be stated that the tensor is defined in the dimension of the vectors \mathbf{a} and \mathbf{b} [Hol00]. It is also possible to define the tensor \mathbf{T} in terms of its coefficients and base vectors. In the following example the mathematical operation related to the tensor product is shown.

Example: The dyadic product of the tensors \mathbf{a} and \mathbf{b} can be computed as:

$$\mathbf{a} \otimes \mathbf{b} = \begin{bmatrix} a_1 \\ a_2 \\ a_3 \end{bmatrix} \begin{bmatrix} b_1 & b_2 & b_3 \end{bmatrix} = \begin{bmatrix} a_1 b_1 & a_1 b_2 & a_1 b_3 \\ a_2 b_1 & a_2 b_2 & a_2 b_3 \\ a_3 b_1 & a_3 b_2 & a_3 b_3 \end{bmatrix}$$

Additionally, in equation (2.1) the *Einstein summation convention* is introduced [BZ13], [Haz88]. According to the Einstein summation convention a summation is carried out over an identical super- and subscript index appearing in the same equation. In order to describe this operation the following example shall explain the application of the Einstein summation convention.

Example: The Einstein summation convention is evaluated for the example:

$$\sum_{i=1}^3 a_i b^i = a_i b^i = a_1 b^1 + a_2 b^2 + a_3 b^3$$

In the following chapters the assumption is made, that in case of Latin letters it will be summarized from 1 to 3 ($i \in 1, 2, 3$) and in case of Greek letters from 1 to 2 ($\alpha \in 1, 2$).

Higher-Order Tensor: Objects which can be represented by coefficients and n base vectors. The resulting tensors are stated as n^{th} -order tensors (e.g. Elasticity Tensor).

In order to distinguish between the different types of tensors, zero-order tensors will be written in plain letters and all higher order tensors (e.g. first, second, etc.) in bold letters. A further distinction is made between first order tensors, which will be written in small letters, and higher order tensors, which will be written in capital letters.

2.2.1 Tensor Calculus

Based on the given definitions, tensors will be introduced in the geometrical and mechanical description of tensile structures. For this purpose, detailed knowledge of tensor calculus is required. Therefore, a basic introduction to the topic will be given. Of course, this introduction just addresses the most important definitions which are used in the following chapters. There exists a wide range of literature for a detailed study of the topic. The later stated definitions and equations can be found in [Alt12], [Hol00], [Par03], [Cha14], [Kli93], [Baş00], [Bet01] .

Summation and multiplication of tensors: The properties for the summation of tensors are mainly coincident to the properties which are known from ordinary arithmetic.

The commutative rule:

$$\mathbf{A} + \mathbf{B} = \mathbf{B} + \mathbf{A} \quad (2.2)$$

In general, the dot product of tensors isn't commutative:

$$\mathbf{AB} \neq \mathbf{BA} \quad (2.3)$$

The associative rule:

$$(\mathbf{A} + \mathbf{B}) + \mathbf{C} = \mathbf{A} + (\mathbf{B} + \mathbf{C}) \quad (2.4)$$

$$(\mathbf{AB})\mathbf{C} = \mathbf{A}(\mathbf{BC}) \quad (2.5)$$

Multiplication by scalars:

$$\alpha\mathbf{A} = (\alpha\mathbf{A}) = \alpha(\mathbf{A}) \quad (2.6)$$

Single and Double Contraction of Tensors: The single and double contraction are scalar products for tensors. It will be obtained by the scalar product of the base vectors of the tensor.

Single contraction:

$$\mathbf{A} \cdot \mathbf{u} = (A^{ij}\mathbf{e}_i \otimes \mathbf{e}_j) \cdot (u^k\mathbf{e}_k) = A^{ij}u^k g_{jk}\mathbf{e}_i = A^{ij}u_j\mathbf{e}_i \quad (2.7)$$

As a result of the single contraction, the order of the tensor will be reduced by one. In the example given in equation (2.7) it can be seen that the second order tensor \mathbf{A} will be transformed into a first order tensor by the single contraction.

Double contraction:

$$\begin{aligned} \mathbf{A} : \mathbf{B} &= (A^{ij}\mathbf{e}_i \otimes \mathbf{e}_j) : (B^{mn}\mathbf{e}_m \otimes \mathbf{e}_n) \\ &= A^{ij}B^{mn}(\mathbf{e}_i\mathbf{e}_m)(\mathbf{e}_j\mathbf{e}_n) \\ &= A^{ij}B^{mn}g_{im}g_{jn} = A_{mn}B^{mn} = A^{ij}B_{ij} \end{aligned} \quad (2.8)$$

2.2 Tensors

The order of the resulting tensor of a double contraction will be decreased by two. For the given example in equation (2.8) the reduction of the second-order tensor \mathbf{A} by the double contraction with the second-order tensor \mathbf{A} can be seen. The resulting tensor is reduced to a zero order.

Calculation rules for dyads and contractions: For the derivation of the governing equations in the later chapters, particular calculation rules for dyadic products as well as for single and double contractions are applied. The following list of equations specify the most important rules which are used in the following chapters.

Calculation rules for dyadic products:

$$\mathbf{A} \otimes \mathbf{B} \neq \mathbf{B} \otimes \mathbf{A} \quad (2.9)$$

$$\mathbf{u}(\mathbf{v} \otimes \mathbf{w}) = (\mathbf{u}\mathbf{v})\mathbf{w} \quad (2.10)$$

$$(\mathbf{u} \otimes \mathbf{v})(\mathbf{w} \otimes \mathbf{x}) = (\mathbf{v}\mathbf{w})\mathbf{u} \otimes \mathbf{x} \quad (2.11)$$

Calculation rule for single contraction:

$$(\mathbf{A}\mathbf{B})^T = \mathbf{B}^T \mathbf{A}^T \quad (2.12)$$

Calculation rules for double contraction:

$$\mathbf{A} : (\mathbf{B}\mathbf{C}) = (\mathbf{B}^T \mathbf{A}) : \mathbf{C} = (\mathbf{A}\mathbf{C}^T) : \mathbf{B} \quad (2.13)$$

$$\mathbf{A} : (\mathbf{B} + \mathbf{C}) = \mathbf{A} : \mathbf{B} + \mathbf{A} : \mathbf{C} \quad (2.14)$$

For the special case that tensor \mathbf{A} is symmetric:

$$\mathbf{A} : \mathbf{B} = \mathbf{A} : \mathbf{B}^T \quad (2.15)$$

Transformation of coefficients of tensors: In the later chapters all tensors are represented in terms of coefficients and base vectors. For the derivation of the governing equations it is essential to be able to represent a tensor in different coordinate systems w.r.t. different base vectors respectively. In order to be able to transform tensors into different base systems, below a general approach for this purpose will be illustrated. The basic idea behind the derived transformation rule is based on the previous definition of a tensor (cf. section 2.2), which states that a tensor is invariant w.r.t. the chosen coordinate system. The same tensor can be represented by different coefficients and respective base vectors. In order to obtain the transformation rule, a second order tensor \mathbf{A} should be represented by two tensors with different coefficients and base vectors.

The second order tensor \mathbf{A} will be represented w.r.t. two different covariant base vector systems $\mathbf{u}_i \otimes \mathbf{u}_j$ and $\mathbf{v}_i \otimes \mathbf{v}_j$. Due to the equivalence of the tensor representation the tensor \mathbf{A} can be obtained by the multiplication of the different coefficients and the respective base vectors:

$$\mathbf{A} = u^{ij} \mathbf{u}_i \otimes \mathbf{u}_j = v^{ij} \mathbf{v}_i \otimes \mathbf{v}_j \quad (2.16)$$

If assuming that one representation of the tensor is already given (e.g. $v^{ij}\mathbf{v}_i \otimes \mathbf{v}_j$ is given) the coefficients of the second representation can be evaluated. The idea underlying the derivation of the transformation rule is to cancel out the base vectors of the unknown coefficients. This can be achieved by multiplying the equation (2.16) with the counterpart of the base vectors from both sides (here the contravariant base vectors \mathbf{u}^i and \mathbf{u}^j). For the computation of the unknown coefficients, additionally equation (2.22) and equation (2.10) have to be applied. Finally, the transformation rule for the coefficients v^{ij} into u^{ij} can be formulated as follows:

$$\begin{aligned} u^{ij}\mathbf{u}^m(\mathbf{u}_i \otimes \mathbf{u}_j)\mathbf{u}^n &= v^{ij}\mathbf{u}^m(\mathbf{v}_i \otimes \mathbf{v}_j)\mathbf{u}^n \\ u^{ij}(\mathbf{u}^m\mathbf{u}_i)(\mathbf{u}_j\mathbf{u}^n) &= v^{ij}(\mathbf{u}^m\mathbf{v}_i)(\mathbf{v}_j\mathbf{u}^n) \\ u^{ij}\delta_i^m\delta_n^j &= v^{ij}(\mathbf{u}^m\mathbf{v}_i)(\mathbf{v}_j\mathbf{u}^n) \\ u^{mn} &= v^{ij}(\mathbf{u}^m\mathbf{v}_i)(\mathbf{v}_j\mathbf{u}^n) \end{aligned} \quad (2.17)$$

In the derivation of equation (2.17) the contravariant base vector as well as the Kronecker Delta δ_i^j are introduced. A detailed explanation of these quantities will be given in the next section. It is obvious that this kind of methodology can be applied to each kind of tensor transformation, whether it is a second-order tensor or another kind of order. Hence, the derivation of more transformation rules won't be given here, as the same principle steps have to be carried out.

2.3 Differential Geometry of Surfaces in Space

The topic of differential geometry offers the possibility to describe surfaces in a 3 dimensional space in a mathematical closed form. Based on this representation, different quantities of surfaces can be derived. They can be used in order to assess the geometrical and mechanical behavior of the surface. The metric of the surface is used in order to compute mechanical properties like strains. Additionally, the curvature or the area content of the surface are important quantities for geometrical and mechanical interpretation of the surface. In this section the principal fundamentals of differential geometry are formulated. Of course, the later definitions and equations are just an extract of the wide content of differential geometry. In the following descriptions the main focus is on the representation and investigation of arbitrary surfaces in a 3 dimensional space. Beginning with the representation of points, the mathematical description of surfaces will be obtained. Subsequently, the investigation of the surface properties is included as well in this chapter.

A certain point in space \mathbf{P} can be uniquely indicated by its position vector \mathbf{r} . The position vector of the point \mathbf{P} can be formulated in terms of the individual coefficients x^i and the respective base vectors \mathbf{e}_i as it is a tensor of first order (cf. figure 2.3). In general, for the description of point \mathbf{P} an arbitrary coordinate system could be chosen. Here, the stationary global Cartesian coordinate system is used, which indicates the *Euclidean Space* by the base vectors \mathbf{e}_i with $i \in 1, 2, 3$. The position vector \mathbf{r} can be mathematically obtained by:

$$\mathbf{r} = x^1\mathbf{e}_1 + x^2\mathbf{e}_2 + x^3\mathbf{e}_3 = \sum_{i=1}^3 x^i\mathbf{e}_i = x^i\mathbf{e}_i \quad (2.18)$$

2.3 Differential Geometry of Surfaces in Space

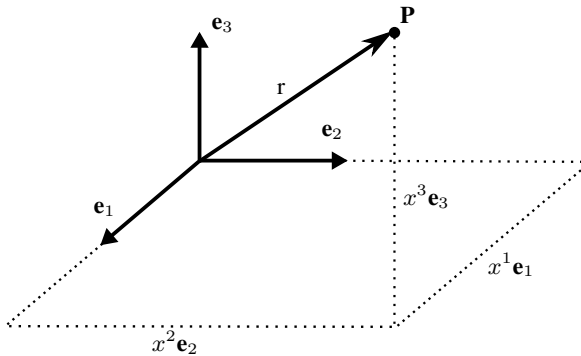


Figure 2.3: Position vector \mathbf{r} of point \mathbf{P} in a cartesian coordinate system

In equation (2.18) again the Einstein summation convention is introduced in order to simplify the mathematical expression for the representation of point \mathbf{P} .

In principle it is possible to describe a surface in space by the definition of each point on the surface explicitly. It is obvious that this approach of point-wise representation of a surface has limitations, due to the fact that all points have to be tackled by a single set of functions in the euclidean space. In order to describe arbitrarily shaped surfaces in space it is advantageous to apply a parametric description of the surface. The parametric representation of a surface can be understood as a net which is superimposed over the given surface. In the parametric space a local coordinate system is introduced. The local directions θ^1 and θ^2 form an orthogonal coordinate system in the parametric space. The net of parametric lines superimposed over the surface are aligned w.r.t. to this local coordinate system. The parametric lines won't remain orthogonal after assembling it to the surface. Due to that property the parametric description of a surface is also stated as a curvilinear representation of the surface. In figure 2.4 the mapping of the parametric space into the euclidean is illustrated. Of course, it is possible to define the point \mathbf{P} in terms of the curvilinear coordinate system θ^1 and θ^2 . In order to obtain the coordinates of a point \mathbf{P} on the surface in a 3 dimensional space the X,Y and Z coordinates have to be expressed in terms of the surface parameters. To find the parametric representation of a surface can be challenging as well. There is a wide range of literature that discusses this topic [Bär10], [Car76], [Kre91], [Küh06].

For the description of point \mathbf{P} the tensor representation can again be applied. Based on this, the point \mathbf{P} consists of coefficients and respective base vectors. In this case the base vectors are the stationary global Cartesian base vectors \mathbf{e}_i . Due to the fact, that the base vectors are constant, the parametric description just has to be included in the respective coefficients. Based on this the parametric description of point \mathbf{P}

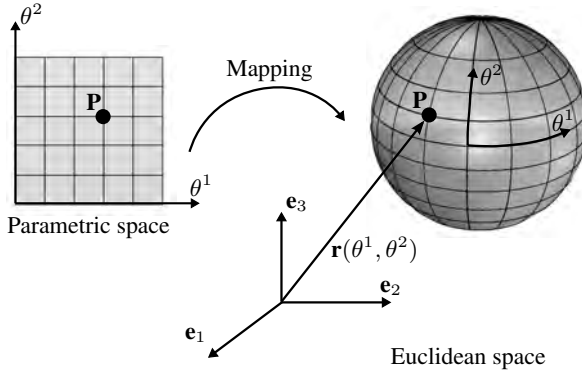


Figure 2.4: Parametric description of a surface

can be formulated as follows:

$$\mathbf{r}(\theta^1, \theta^2) = x^i(\theta^1, \theta^2)\mathbf{e}_i = \begin{bmatrix} x(\theta^1, \theta^2) \\ y(\theta^1, \theta^2) \\ z(\theta^1, \theta^2) \end{bmatrix} \quad (2.19)$$

With the parametric representation of the surface it is possible to introduce a local coordinate system in each point of the surface. By taking the partial derivative of the position vector $\mathbf{r}(\theta^1, \theta^2)$ w.r.t. the surface parameters θ^1 and θ^2 the covariant base vectors can be introduced:

$$\begin{aligned} \mathbf{g}_1 &= \frac{\partial \mathbf{r}(\theta^1, \theta^2)}{\partial \theta^1} \\ \mathbf{g}_2 &= \frac{\partial \mathbf{r}(\theta^1, \theta^2)}{\partial \theta^2} \end{aligned} \quad (2.20)$$

The base vectors \mathbf{g}_1 and \mathbf{g}_2 are tangential to the surface at each point. Due to the change of the parameter lines the base vectors are changing depending on the position in which they were computed. As the parameter lines aren't orthogonal, neither are the base vectors. In general, there have to be 3 base vectors in order to describe a full coordinate system in the Euclidean space (like in case of the global Cartesian coordinate system \mathbf{e}_1 to \mathbf{e}_3). In principle the third base vector can be chosen arbitrarily in the case of surfaces. In fact there are some advantages to align the third base vector w.r.t. the surface normal \mathbf{n} . Additionally, the assumption is made, that the third base vector has the length of 1. Therefore, the third base vector can be obtained by the normalized cross product of the in-plane base vectors \mathbf{g}_1 and \mathbf{g}_2 :

$$\mathbf{g}_3 = \frac{\mathbf{g}_1 \times \mathbf{g}_2}{\|\mathbf{g}_1 \times \mathbf{g}_2\|} = \mathbf{n} \quad (2.21)$$

2.3 Differential Geometry of Surfaces in Space

At point \mathbf{P} a further type of base vectors is defined. The contravariant base vectors are reciprocal to the covariant base vectors [Hol00]. They are indicated with super-script indices \mathbf{g}^i and they are a part of the tangential plane defined by the covariant base vectors. Therefore, the third contravariant is aligned with the third covariant base vector $\mathbf{g}^3 = \mathbf{g}_3$. The scalar product of the different in-plane base vectors fulfills the following condition:

$$\mathbf{g}^\alpha \cdot \mathbf{g}_\beta = \delta_\beta^\alpha = \begin{cases} 1 & \text{for } \alpha = \beta \\ 0 & \text{for } \alpha \neq \beta \end{cases} \quad (2.22)$$

In equation (2.22) the *Kronecker Delta* δ_β^α is introduced. It describes the relation between the co- and contravariant base vectors. The previously defined properties of the base vectors are illustrated in figure 2.5. By using the defined base vectors,

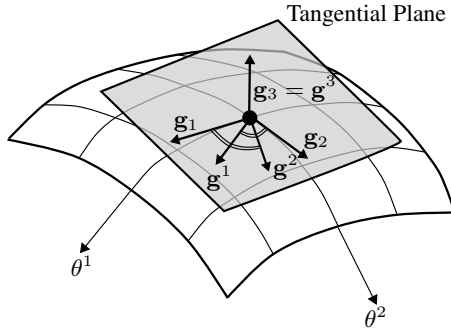


Figure 2.5: Co- and contravariant base vectors

an important quantity for the description of a surface in space can be defined. The *Metric Tensor* contains all important surface properties like the area content, the angles between the individual base vectors and the lengths of the base vectors. The metric tensor, also called the first fundamental form, can be obtained by the scalar product of the surface base vectors and the dyadic product of the same ones:

$$\begin{aligned} \mathbf{I} &= (\mathbf{g}^\alpha \cdot \mathbf{g}^\beta) \mathbf{g}_\alpha \otimes \mathbf{g}_\beta = g^{\alpha\beta} \mathbf{g}_\alpha \otimes \mathbf{g}_\beta \\ \mathbf{I} &= (\mathbf{g}_\alpha \cdot \mathbf{g}_\beta) \mathbf{g}^\alpha \otimes \mathbf{g}^\beta = g_{\alpha\beta} \mathbf{g}^\alpha \otimes \mathbf{g}^\beta \end{aligned} \quad (2.23)$$

The summation in equation (2.23) just has to be carried out by considering the in-plane base vectors as the third base vector hasn't any influence and does not introduce additional information to the metric tensor. In general, the metric tensor can be represented by a 3×3 matrix. As the third base vector is assumed to have the length of 1 and is identical in the co- and contravariant representation, the metric tensor can be reduced to a 2×2 matrix. In equation (2.23) the covariant metric

coefficients $g_{\alpha\beta}$ are introduced. They can be computed by the scalar product of the covariant base vectors. The metric tensor can also be represented by the contravariant metric coefficients $g^{\alpha\beta}$. They can be computed by the inverse of the covariant metric coefficients:

$$[g^{\alpha\beta}] = \begin{bmatrix} g^{11} & g^{12} \\ g^{21} & g^{22} \end{bmatrix} = [g_{\alpha\beta}]^{-1} = \begin{bmatrix} g_{11} & g_{12} \\ g_{21} & g_{22} \end{bmatrix}^{-1} \quad (2.24)$$

Applying the co- and contravariant metric coefficients, the co- and contravariant base vectors can be transformed into each other:

$$\begin{aligned} \mathbf{g}_\alpha &= g_{\alpha\beta} \mathbf{g}^\beta \\ \mathbf{g}^\alpha &= g^{\alpha\beta} \mathbf{g}_\beta \end{aligned} \quad (2.25)$$

One of the most important purposes of the metric coefficients is the evaluation of the surface area content. In order to compute the surface area content the infinitesimal area element has to be obtained. This can be done by the infinitesimal lengths dr_1 and dr_2 along the parameter lines θ^1 and θ^2 respectively:

$$\begin{aligned} dr_1 &= \frac{\partial \mathbf{r}(\theta^1, \theta^2)}{\partial \theta^1} d\theta^1 = \mathbf{g}_1 d\theta^1 \\ dr_2 &= \frac{\partial \mathbf{r}(\theta^1, \theta^2)}{\partial \theta^2} d\theta^2 = \mathbf{g}_2 d\theta^2 \end{aligned} \quad (2.26)$$

Based on equation (2.26) the infinitesimal area content da can be derived by the parallelogram spanned by dr_1 and dr_2 :

$$da = \|\mathbf{g}_1 \times \mathbf{g}_2\| d\theta^1 d\theta^2 = \sqrt{(\mathbf{g}_1 \times \mathbf{g}_2) \cdot (\mathbf{g}_1 \times \mathbf{g}_2)} d\theta^1 d\theta^2 \quad (2.27)$$

The achieved equation is defined as the *Lagrange Identity*. In [Kli93] an alternative representation for the computation of the area content based on equation (2.27) is given as follows:

$$da = \sqrt{g_{11}g_{22} - (g_{12})^2} d\theta^1 d\theta^2 \quad (2.28)$$

By integration over the surface parameters θ^1 and θ^2 the overall area content a can be obtained:

$$a = \int_a da = \int_{\theta^2} \int_{\theta^1} \sqrt{g_{11}g_{22} - (g_{12})^2} d\theta^1 d\theta^2 \quad (2.29)$$

In order to illustrate the application of equation (2.29), a simple example will be presented in the following.

Example: With the derived equation (2.28) the area content of a plane rectangle with side length a and b should be computed. It is obvious, that the result of the calculation should lead to the well known solution $A_{\text{Rectangle}} = a \cdot b$. In figure 2.6 the example is illustrated. The position vector for this example can be given as

2.3 Differential Geometry of Surfaces in Space

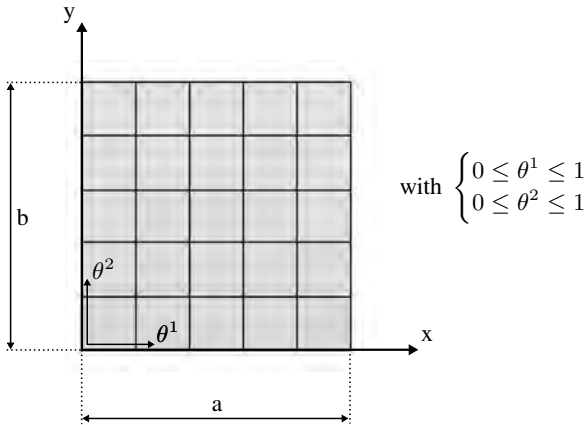


Figure 2.6: Example for the calculation of the area content of a rectangle surface

follows:

$$\mathbf{r}(\theta^1, \theta^2) = \begin{cases} \theta^1 a \\ \theta^2 b \\ z = \text{const} \end{cases} \quad \text{for } \begin{cases} 0 \leq \theta^1 \leq 1 \\ 0 \leq \theta^2 \leq 1 \end{cases}$$

With equation (2.20) the base vectors can be computed to:

$$\mathbf{g}_1 = \frac{\partial \mathbf{r}(\theta^1, \theta^2)}{\partial \theta^1} = \begin{pmatrix} a \\ 0 \\ 0 \end{pmatrix}$$

$$\mathbf{g}_2 = \frac{\partial \mathbf{r}(\theta^1, \theta^2)}{\partial \theta^2} = \begin{pmatrix} 0 \\ b \\ 0 \end{pmatrix}$$

Applying equation (2.29) the area content can be evaluated to:

$$A = \int_0^1 \int_0^1 \sqrt{a^2 b^2 - 0^2} d\theta^1 d\theta^2 = a \cdot b$$

It can be seen that the expected result for the area content is achieved.

The curvature has a major importance in the evaluation of surfaces. In principle, the curvature can be understood as the deviation of a surface from a plane. In order

to obtain the curvature the second fundamental form or *Curvature Tensor* has to be evaluated:

$$\mathbf{k} = b_{\alpha\beta} \mathbf{g}^\alpha \otimes \mathbf{g}^\beta \quad (2.30)$$

The coefficients of the curvature tensor $b_{\alpha\beta}$ in equation (2.30) can be obtained in different ways [Bär10], [Kli93], [BK85]:

$$\begin{aligned} b_{\alpha\beta} &= -\mathbf{g}_\alpha \frac{\partial \mathbf{n}}{\partial \theta^\beta} \\ b_{\alpha\beta} &= \frac{\partial \mathbf{g}_\alpha}{\partial \theta^\beta} \cdot \mathbf{n} \end{aligned} \quad (2.31)$$

For the characterization of spatial surfaces the knowledge of the *Gaussian Curvature* K is of importance. Based on the Gaussian curvature a classification of the individual surfaces can be made [Hsi97]. A surface can be classified as

- elliptic or synclastic, for ($K > 0$) or
- hyperbolic or anticlastic, for ($K < 0$) or
- parabolic or developable, for ($K = 0$).

The Gaussian Curvature can be expressed by the ratio between the determinants of the first and second fundamental forms [LB73], [Bär10]:

$$K = \frac{\det[b_{\alpha\beta}]}{\det[g_{\alpha\beta}]} = \frac{b_{11}b_{22} - (b_{12})^2}{g_{11}g_{22} - (g_{12})^2} \quad (2.32)$$

An important characteristic of spatial surfaces is their developability. A surface can be understood as developable if it can be developed into a flat situation without compromises like strains or stresses. In other words each surface which can be assembled from a flat configuration is developable. From a mathematical point of view, if the Gaussian curvature vanishes (i.e. $K = 0$) the surface is developable. In the following example a spherical surface will be investigated for its curvature properties. It is obvious that the sphere contains to the non-developable surfaces, so the Gaussian curvature should be unequal to zero.

Example: For the following spherical surface (cf. figure 2.7) the Gaussian curvature will be evaluated. As surface parameters to describe each point on the surface, the angles $\theta^1 = \vartheta$ and $\theta^2 = \varphi$ will be chosen. The position vector \mathbf{R} can be evaluated by the two surface parameters and the radius r of the sphere.

$$\mathbf{R} = \begin{bmatrix} r \sin(\theta^1) \cos(\theta^2) \\ r \sin(\theta^1) \sin(\theta^2) \\ r \cos(\theta^1) \end{bmatrix}$$

2.3 Differential Geometry of Surfaces in Space

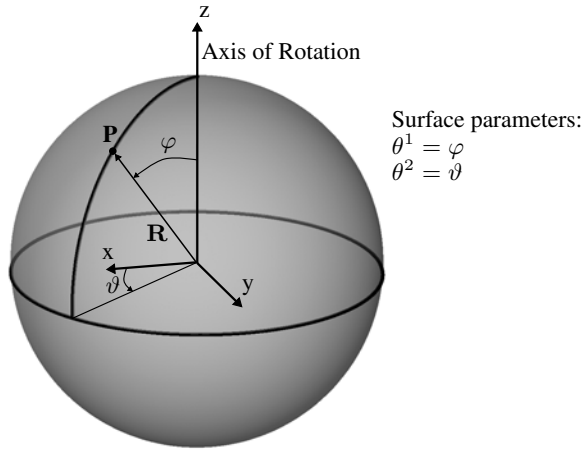


Figure 2.7: Example for the calculation of the curvature of a sphere

With the position vector \mathbf{R} the covariant base vectors of the surface can be calculated with equation (2.20) and the surface normal with equation (2.21) respectively. The covariant base vectors \mathbf{g}_1 and \mathbf{g}_2 of the tangential surface are given by:

$$\mathbf{g}_1 = \frac{\partial \mathbf{R}}{\partial \theta^1} = r \begin{bmatrix} \cos(\theta^1) \cos(\theta^2) \\ \cos(\theta^1) \sin(\theta^2) \\ -\sin(\theta^1) \end{bmatrix}$$

$$\mathbf{g}_2 = \frac{\partial \mathbf{R}}{\partial \theta^2} = r \begin{bmatrix} -\sin(\theta^1) \sin(\theta^2) \\ \sin(\theta^1) \cos(\theta^2) \\ 0 \end{bmatrix}$$

The surface normal is computed as follows:

$$\mathbf{n} = \begin{bmatrix} \sin(\theta^1) \cos(\theta^2) \\ \sin(\theta^1) \sin(\theta^2) \\ \cos(\theta^1) \end{bmatrix}$$

Due to the normalization it turns out that the surface normal is independent of the radius of the sphere. With the covariant base vectors the covariant metric coefficient can be evaluated with equation (2.24). The metric coefficients are obtained by:

$$g_{\alpha\beta} = \begin{bmatrix} r^2 & 0 \\ 0 & r^2 \sin^2(\theta^1) \end{bmatrix}$$

In order to compute the Gaussian curvature the coefficients of the curvature tensor have to be evaluated by applying equation (2.30) based on the covariant base vectors. Using the second relation of equation (2.31) the coefficients of the curvature

tensor are computed by the scalar product of the first order derivative of the base vectors w.r.t. the surface parameters $\frac{\partial \mathbf{g}_\alpha}{\partial \theta^\beta}$ and the surface normal vector \mathbf{n} . The first order derivative of the covariant base vector w.r.t. the surface parameters is given by:

$$\begin{aligned}\frac{\partial \mathbf{g}_1}{\partial \theta^1} &= r \begin{bmatrix} -\sin(\theta^1) \cos(\theta^2) \\ -\sin(\theta^1) \sin(\theta^2) \\ -\cos(\theta^1) \end{bmatrix} \\ \frac{\partial \mathbf{g}_1}{\partial \theta^2} &= \frac{\partial \mathbf{g}_2}{\partial \theta^1} = r \begin{bmatrix} -\cos(\theta^1) \sin(\theta^2) \\ \cos(\theta^1) \cos(\theta^2) \\ 0 \end{bmatrix} \\ \frac{\partial \mathbf{g}_2}{\partial \theta^2} &= r \begin{bmatrix} -\sin(\theta^1) \cos(\theta^2) \\ -\sin(\theta^1) \sin(\theta^2) \\ 0 \end{bmatrix}\end{aligned}$$

Using the evaluated first order derivatives of the covariant base vectors the coefficients of the curvature tensor can be obtained by:

$$b_{\alpha\beta} = \begin{bmatrix} -r & 0 \\ 0 & -r \sin^2(\theta^1) \end{bmatrix}$$

With the covariant metric and the curvature coefficients the Gaussian curvature can be evaluated by applying equation (2.32):

$$K = \frac{1}{r^2} > 0$$

It can be seen that the Gaussian curvature of the sphere is constant and unequal to zero. From this mathematical approach the obvious result turns out, that a sphere is non-developable.

2.4 Continuum Mechanics

The subject of continuum mechanics is applied for the description of the mechanical behavior of structures in time and space. In general, the main task which will be addressed by the continuum mechanics is the description of the occurring strains and stresses of an elastic body. Continuum mechanics can be applied to various applications in engineering. In this section, an introduction with the focus on tensile surface structures will be given. A detailed introduction into the general application of continuum mechanics in a wide range of engineering tasks can be found in [Meh97], [Bet01], [Alt12], [Hol00], [Baş00], [Par03], [Cha14], [Man13], [Mar94]. In the beginning of this section an introduction to the idea of different configurations will be given. Based on this, the definitions for strains and stresses are obtained. For the connection between strains and stresses, appropriate material models are introduced. Integrating these definitions into the characteristic equations for the motion

of an elastic body, it is possible to derive the equilibrium in time and space in the strong and weak form. At the end of this section a discretization in time and space will be introduced.

2.4.1 Configurations

The basis of the mechanical description of a tensile structure is the possibility to introduce their large deformations into the governing equations. To be able to describe the full deformation of an elastic body, it has to be ensured that the position of a defined material point can be identically given at a specific time t during the deformation process. To provide this description of the deformation process two individual configurations are introduced. The reference or material configuration is defined as the starting point of the motion at $t = 0$. The current or spatial configuration is supposed to be the current position of the material point at $t = t_{current}$. The difference between these two configurations are indicated as the deformation of the material point expressed by the displacement vector \mathbf{u} ($t = t_{current}$). In figure 2.8 the individual configurations are illustrated for a certain point on a surface. At the investigated point it is possible to evaluate the base vectors as shown in section 2.3. Of course, the base vectors can be evaluated in both configurations. In the following, the quantities which are defined w.r.t. the reference configuration are indicated with capital letters and in the case of the current configuration with small letters.

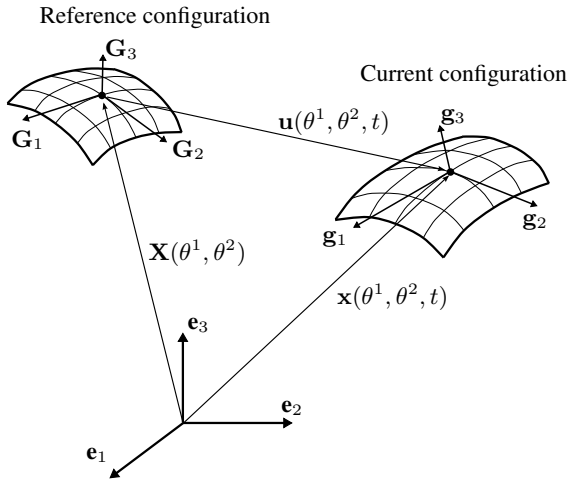


Figure 2.8: Reference and current configuration in continuum mechanics

In general, there are two ways of investigating the deformation process. The first possibility is to investigate a certain surface point and observe what happens to it during the deformation. This way of investigating the motion of a body is referred

as the material or the *Lagrangian description* of motion. The second possibility is to investigate a certain point in space and observe what happens at this specific point as time changes. This method is referred as the spatial or *Eulerian description* of motion. In the context of structural mechanics the Lagrangian description is most appropriate for the formulation of the governing equations and will be used in the following chapters as well. The Eulerian description is mostly applied in cases of fluid dynamic problems. Based on the definition of the reference and current configuration and the Lagrangian description of motion, the deformation of a specific material point on the surface can be obtained by:

$$\mathbf{u}(\theta^1, \theta^2, t) = \mathbf{x}(\theta^1, \theta^2, t) - \mathbf{X}(\theta^1, \theta^2) \quad (2.33)$$

With the possibility to describe the deformation of an elastic body at each time for arbitrary large deformations the related quantities like strains and stresses can be evaluated. Based on the description of the deformation process in the following the governing equations and quantities will be derived.

2.4.2 Deformation Gradient

The deformation gradient transfers quantities from the reference to the current configuration and vice versa. It can be derived by the mapping of a infinitesimal line element in the reference configuration $d\mathbf{X}$ into the current configuration $d\mathbf{x}$. A detailed derivation of the deformation gradient can be found in [Alt12], [Hol00]. The mapping between the configurations with the deformation gradient can be given by:

$$d\mathbf{x} = \mathbf{F} \cdot d\mathbf{X} \quad (2.34)$$

The equation (2.34) can also be formulated by:

$$\mathbf{F} = \frac{d\mathbf{x}}{d\mathbf{X}} \quad (2.35)$$

Based on the chain rule and equation (2.35) a mapping between the base vectors of the individual configuration can be derived:

$$\mathbf{g}_i = \frac{\partial \mathbf{x}}{\partial \theta^i} = \frac{\partial \mathbf{x}}{\partial \mathbf{X}} \frac{\partial \mathbf{X}}{\partial \theta^i} = \mathbf{F} \cdot \mathbf{G}_i \quad (2.36)$$

Of course, with the deformation gradient a transformation for all types of base vectors can be indicated [Hol00]:

$$\begin{aligned} \mathbf{g}_i &= \mathbf{F} \cdot \mathbf{G}_i; & \mathbf{g}^i &= \mathbf{F}^{-T} \cdot \mathbf{G}^i \\ \mathbf{G}_i &= \mathbf{F}^{-1} \cdot \mathbf{g}_i; & \mathbf{G}^i &= \mathbf{F}^T \cdot \mathbf{g}^i \end{aligned} \quad (2.37)$$

For the application of the defined transformation rules the knowledge of the deformation gradient is essential. With equation (2.36) the evaluation of the deformation gradient can be derived by:

$$\mathbf{g}_i = (\mathbf{g}_j \otimes \mathbf{G}^j) \cdot \mathbf{G}_i = \mathbf{g}_j \delta_i^j = \mathbf{F} \cdot \mathbf{G}_i \quad (2.38)$$

Based on the relation of equation (2.38) the following definitions for the deformation gradient can be given [Cha14]:

$$\begin{aligned} \mathbf{F} &= \mathbf{g}_i \otimes \mathbf{G}^i; & \mathbf{F}^{-T} &= \mathbf{g}^i \otimes \mathbf{G}_i \\ \mathbf{F}^{-1} &= \mathbf{G}_i \otimes \mathbf{g}^i; & \mathbf{F}^T &= \mathbf{G}^i \otimes \mathbf{g}_i \end{aligned} \quad (2.39)$$

The deformation gradient will be introduced for the general transformation of mechanical quantities in various cases. One important application is derived from Nanson's formula [Hol00]. Here, a relation between the infinitesimal surface element in the reference configuration dA and in the current configuration da can be obtained:

$$\mathbf{n}da = \det \mathbf{F} \mathbf{F}^{-T} \mathbf{N}dA \quad (2.40)$$

In equation (2.40) the normal vector in the reference configuration is indicated by \mathbf{N} and in the current configuration by \mathbf{n} . The determinant of the deformation gradient in equation (2.40) can be evaluated from the relation between the infinitesimal volume elements [Par03]. With the assumption w.r.t. to the calculation of \mathbf{g}_3 from equation (2.21) the determinant of the deformation gradient can be given by:

$$\det \mathbf{F} = \frac{dv}{dV} = \frac{(\mathbf{g}_1 \times \mathbf{g}_2) \mathbf{g}_3}{(\mathbf{G}_1 \times \mathbf{G}_2) \mathbf{G}_3} = \frac{da}{dA} \quad (2.41)$$

From equation (2.40) and equation (2.41) it can be seen that there exists a transformation between the infinitesimal surface element in the reference and the current configuration:

$$da = \det \mathbf{F} dA \quad (2.42)$$

The deformation gradient itself describes the full deformation of a continuum body. The process can be divided into two principle motions. First, each position vector of a material point can be moved from the reference to the current configuration and then be rotated into the final position. This decomposition is known as the *Polar Decomposition* [Hol00]. It decomposes the deformation gradient in the *Rotation Tensor* \mathbf{R} and the *Right Stretch Tensor* \mathbf{U} or *Left Stretch Tensor* \mathbf{v} :

$$\mathbf{F} = \mathbf{R}\mathbf{U} = \mathbf{v}\mathbf{R} \quad (2.43)$$

As for every physical quantity, there exist principal directions for the deformation gradient. They can be understood as a set of directions which remain orthogonal during the deformation process. They can be obtained by an eigenvalue analysis of the deformation gradient. The related eigenvalues are known as the *Principal Stretches* which measure the elongation of the principal directions w.r.t. the deformations. The deformation gradient can be given in terms of the principal stretches and principal directions as follows:

$$\mathbf{F} = \sum_{k=1}^3 \lambda_k \mathbf{n}_k \otimes \mathbf{N}_k \quad (2.44)$$

In equation (2.44) \mathbf{n}_k are the principal directions w.r.t the current configuration and \mathbf{N}_k w.r.t. the reference configuration. The principle stretches are given as λ_k .

The eigenvalue analysis causes some mathematical problems as the deformation gradient is defined in the reference and the current configuration. To avoid this kind of issue, another quantity can be introduced which is exclusively defined in the reference configuration with the same eigenvalues and directions. The *Right Cauchy Green Tensor* \mathbf{C} provides the same eigenvalues and directions as the deformation gradient, but with a complete definition in the reference configuration the solution of the eigenvalue problem cause no mathematical issues. To evaluate the Right Cauchy Green Tensor various possibilities are existing. In the following, the evaluation of the Right Cauchy Green Tensor based on the definition from [Baş00], [Hol00], [Par03] is stated:

$$\mathbf{C} = C_{ij} \mathbf{G}^i \otimes \mathbf{G}^j = \mathbf{F}^T \mathbf{F} = \sum_{k=1}^3 \lambda_k^2 \mathbf{N}_k \otimes \mathbf{N}_k = \mathbf{g} = g_{ij} \mathbf{G}^i \otimes \mathbf{G}^j \quad (2.45)$$

The knowledge of the principal directions and principal stretches is crucial for the formulation of nonlinear material models. The derivation of the governing equations for this kind of materials is often done in terms of the principal directions as it is more convenient from a mathematical point of view. In section 2.4.5 the formulation of a nonlinear material model in principal directions will be introduced.

2.4.3 Strains

In the previous section the deformation gradient was introduced. It is a quantity to analyze the overall deformation process of a continuum body. Due to that the deformation gradient also includes rigid body motions. For the structural behavior of a continuum body the local deformations are decisive. Hence, the deformation gradient can't be used to measure this local deformation. For this purpose, strains will be introduced as mechanical quantities. In general, strains are not unique from a physical point of view, as they are defined as normalized local deformations w.r.t. a certain reference length. Due to this there exist various different strain measurements. In general, the difference between the strains are based on their individual capabilities for the description of large or small deformations. Typically, strain measures for small deformations are misinterpret the rigid body motions to achieve a simple representation in the respective equations. Another classification can be made due to the magnitude of the strain itself. There are various measures which are able to represent large deformations but are restricted to small strains. Just a few measures are able to include large deformations as well as large strains. In general, the deformation process of tensile structures is characterized by large deformations but small strains, which allows the application of a wide range of strain measurements. In the following, different types of strain measurements which are appropriate for both small and large strains will be introduced. For all of the presented types the evaluation will be restricted to the in-plane parts, due to the assumption which were made for the numerical modeling of tensile structures (cf. section 2.1).

Green Lagrange Strain: The Green Lagrange strain tensor \mathbf{E} is a strain measurement which is defined in the reference configuration. It is able to represents large

deformations:

$$\begin{aligned}
 \mathbf{E} &= \frac{1}{2}(g_{\alpha\beta} - G_{\alpha\beta})\mathbf{G}^\alpha \otimes \mathbf{G}^\beta \\
 &= \frac{1}{2}(\mathbf{F}^T \mathbf{F} - \mathbf{I}) \\
 &= \frac{1}{2}(\mathbf{C} - \mathbf{I}) \\
 &= \frac{1}{2}(\lambda_\alpha^2 - 1)\mathbf{N}_\alpha \otimes \mathbf{N}_\beta
 \end{aligned} \tag{2.46}$$

Euler Almansi Strain: The Euler Almansi strain tensor \mathbf{e} is a strain measurement which is defined in the current configuration. Like the Green Lagrange strain it is able to represent large deformations:

$$\begin{aligned}
 \mathbf{e} &= \frac{1}{2}(g_{\alpha\beta} - G_{\alpha\beta})\mathbf{g}^\alpha \otimes \mathbf{g}^\beta \\
 &= \frac{1}{2}(\mathbf{I} - \mathbf{F}^{-T} \mathbf{F}^{-1}) \\
 &= \frac{1}{2}(\mathbf{I} - \mathbf{v}^{-2}) \\
 &= \frac{1}{2} \left(1 - \frac{1}{\lambda_\alpha^2} \right) \mathbf{n}_\alpha \otimes \mathbf{n}_\beta
 \end{aligned} \tag{2.47}$$

Hencky Strain: The Hencky strain tensor \mathbf{h} is a strain measurement which is defined in the current configuration. Due to the logarithm in the strain equation it can cause some numerical issues during the analysis of a certain body:

$$\begin{aligned}
 \mathbf{h} &= \ln \mathbf{U} \\
 &= \sum_{\alpha=1}^3 \ln(\lambda_\alpha) \mathbf{n}_\alpha \otimes \mathbf{n}_\beta
 \end{aligned} \tag{2.48}$$

The Green Lagrange and Euler Almansi strain measurements are not independent from each other. It is more the case that they are the same quantities from a different perspective, as they are defined w.r.t. different coordinate systems. This can also be seen by the identical coefficients of the two tensors:

$$E_{\alpha\beta} = e_{\alpha\beta} = \frac{1}{2}(g_{\alpha\beta} - G_{\alpha\beta}) \tag{2.49}$$

Due to this duality of the Green Lagrange and the Euler Almansi strain measurements, there exist transformation rules which can be used to transfer between the individual configuration descriptions. With a so-called *Push-Forward-Operation*, indicated by χ_* , the Euler Almansi strain tensor can be obtained from the Green Lagrange strain tensor:

$$\mathbf{e} = \chi_*(\mathbf{E}) = \mathbf{F}^{-T} \mathbf{E} \mathbf{F}^{-1} \tag{2.50}$$

Likewise the transformation of the Euler Almansi strain tensor into the Green Lagrange strain tensor can be done with the so-called *Pull-Back-Operation*, indicated by χ_*^{-1} :

$$\mathbf{E} = \chi_*^{-1}(\mathbf{e}) = \mathbf{F}^T \mathbf{e} \mathbf{F} \quad (2.51)$$

2.4.4 Stresses

As in case of strains, stresses can be also defined w.r.t. different coordinate or base vectors respectively. In the following, the derivation of different stress measurements will be given. Considering a continuum body which is subjected to external forces, by the definition of a sectional plane the body can be divided into two pieces. The same internal surface forces are acting on both sectional planes. It is possible to define a internal surface force $\Delta \mathbf{f}$ which acts on the area Δs . Furthermore, it is possible to define the surface normal \mathbf{n} and the in-plane vector \mathbf{m} in such a way that $\Delta \mathbf{f}$, \mathbf{n} and \mathbf{m} are defining a plane. With these surface quantities it is possible to split the force vector $\Delta \mathbf{f}$ into its components of \mathbf{n} and \mathbf{m} . Thus the force components $\Delta \mathbf{f}_n$ and $\Delta \mathbf{f}_m$ can be obtained as illustrated in figure 2.9. Based on the definitions

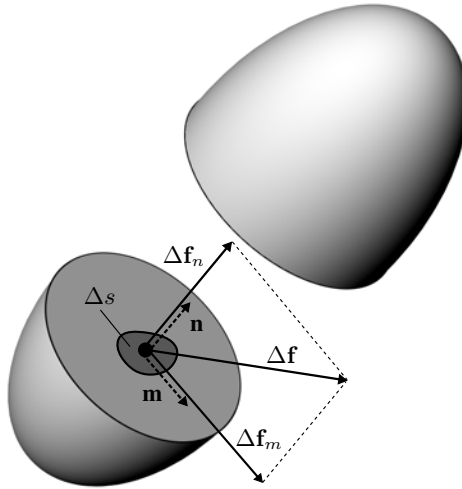


Figure 2.9: Force vector acting on a infinitesimal surface element

obtained from figure 2.9 it is also possible to define the ratio between the surface force vector $\Delta \mathbf{f}$ and the surface unit Δs :

$$\frac{\Delta \mathbf{f}}{\Delta s} \quad (2.52)$$

2.4 Continuum Mechanics

Considering the ratio from equation (2.52) in the limit state of vanishing surface unit $\lim_{\Delta s \rightarrow 0}$, the so called traction vector can be obtained [Man13]:

$$\mathbf{t} = \lim_{\Delta s \rightarrow 0} \frac{\Delta \mathbf{f}}{\Delta s} \quad (2.53)$$

Of course the limit state as described in equation (2.53) can be also applied to the individual directions $\Delta \mathbf{f}_n$ and $\Delta \mathbf{f}_m$ which then leads to the normal and shear traction vectors. An alternative evaluation of the traction vector can be obtained by applying *Cauchy's stress theorem* from a multiplication of the surface normal \mathbf{n} and a second-order tensor σ :

$$\mathbf{t} = \sigma \mathbf{n} \quad (2.54)$$

By applying the Cauchy's stress theorem to the current configuration the second-order tensor σ is defined as the symmetric *Cauchy Stress Tensor*:

$$\sigma = \sigma^{\alpha\beta} \mathbf{g}_\alpha \otimes \mathbf{g}_\beta \quad (2.55)$$

The Cauchy stress tensor is purely defined in the current configuration. Due to that it represents the "true" physical stresses in the continuum body. In general, the stress tensor includes stresses in all spatial directions, as it has to define the normal stresses as well as the shear stresses. Based on the assumptions for the numerical modeling of tensile structures, introduced in section 2.1, the Cauchy stress can be restricted to the in-plane components. From a mechanical point of view, this situation is known as the plane stress assumption, which includes the following:

- Normal stresses can be assumed to be constant throughout the thickness.
- The normal and shear stresses in the thickness direction (or perpendicular to the surface) are zero or negligible.
- The tensile structure is fabricated of the same material throughout the thickness.

Based on the plane stress assumption the stresses of the tensile structure can be restricted to the in-plane or tangential surface stresses. This restriction can be seen in equation (2.55) as the summation just includes the in-plane stress coefficients and the in-plane base vectors. Due to that, the Cauchy stress tensor includes 4 in-plane stress values. In figure 2.10 the remaining stresses for a tensile structure are illustrated for an infinitesimal surface element dA . It can be seen that the stress distribution purely acts w.r.t. the tangential directions of the surface. Due to that, this stress situation is also defined as the membrane stress situation. As a consequence tensile or membrane structures restrain external load situations, like dead or snow load, exclusively by in-plane stresses, which explains the necessity of deformation of the structure in order to align components of the internal stresses with the external load.

It is also possible to apply the Cauchy stress theorem to the force vectors in the reference configuration [Hol00]. For this purpose the transformation of the surface elements based on equation (2.40) has to be done. As a result of this transformation,

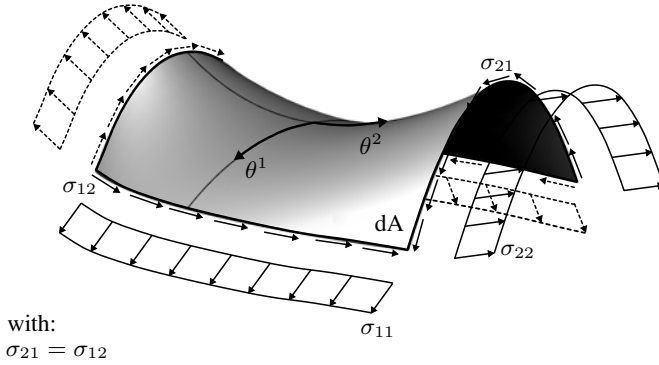


Figure 2.10: Tangential surface stresses

the 1. Piola Kirchoff stress tensor can be obtained. The 1. Piola Kirchoff stress tensor is a non-symmetric second order tensor which is defined in both reference and current configuration:

$$\mathbf{P} = \det \mathbf{F} \boldsymbol{\sigma} \mathbf{F}^{-T} = \det \mathbf{F} \sigma^{\alpha\beta} \mathbf{g}_\alpha \otimes \mathbf{G}_\beta = P^{\alpha\beta} \mathbf{g}_\alpha \otimes \mathbf{G}_\beta \quad (2.56)$$

For the 1. Piola Kirchoff stress tensor one of the base vectors are defined in current configuration. In the mechanical description of tensile structures it is advantageous when the stress quantity is just defined in the known and constant reference configuration. For this purpose the 2. Piola-Kirchhoff stress tensor is introduced. The symmetric second order tensor is purely defined in the reference configuration and can be obtained from the Cauchy stress tensor with the following transformation rule [Hol00]:

$$\mathbf{S} = \det \mathbf{F} \mathbf{F}^{-1} \boldsymbol{\sigma} \mathbf{F}^{-T} = \det \mathbf{F} \sigma^{\alpha\beta} \mathbf{G}_\alpha \otimes \mathbf{G}_\beta = S^{\alpha\beta} \mathbf{G}_\alpha \otimes \mathbf{G}_\beta \quad (2.57)$$

It is important to note that the 2. Piola-Kirchhoff stress tensor represents a mechanical quantity which is only introduced for the simplification of the governing equations and the robustness of the solution process. In contrast to the Cauchy stress tensor its value has no direct physical meaning.

2.4.5 Material Modeling

In the previous sections the governing equations for different types of strains and stresses are given. In general, these quantities are not independent from each other. A deformation of an elastic body is represented by the occurring strains. Of course due to the deformation, stresses will be occurring as well. The relation between the stresses and strains is described by the material model. As an example, a simple 1D

tension test is chosen for the illustration of the relation. If one takes a piece of fabric and stretches it, while the deformation and the applied force will be measured, the result will be a stress-strain diagram which is illustrated in figure 2.11. In case of

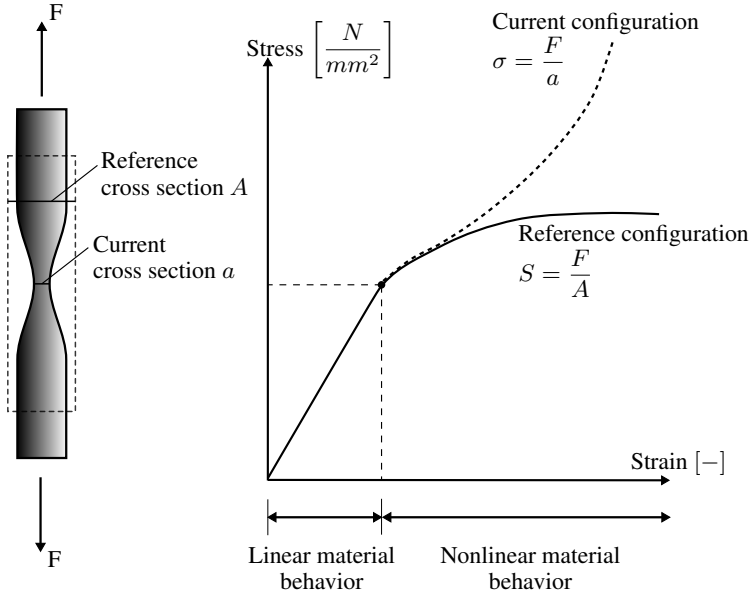


Figure 2.11: Stress-Strain-Diagram for a 1D tension test

a simple 1D tension test the stresses can be obtained by the ratio between the force and the cross section area as defined in equation (2.52). It can be seen that even for this simple example different possibilities in evaluating the stress are present. If the stress is evaluated w.r.t. the initial (or reference) cross section A the stress-strain diagram differs fundamentally from the case if the current cross section a is used. For simplicity, it is assumed in this example that in the beginning of the deformation the two curves of the individual stresses are coincident.

In general, in the stress-strain diagram two different regions can be identified. The linear part and the nonlinear part. In order to describe the relation between stresses and strains for both cases, linear and nonlinear, for the general case an incremental equation can be obtained [Hol00]:

$$d\mathbf{S} = \mathbf{C} : d\mathbf{E} \tag{2.58}$$

In equation (2.58) $d\mathbf{S}$ and $d\mathbf{E}$ are the increments in stresses and strains for the reference configuration. The link between them is done by the so-called *Elasticity Tensor* \mathbf{C} which is a fourth order tensor. In the case of linear material behavior, the

incremental relation between stresses and strains doesn't change during the overall deformation process. Due to that, the elasticity tensor doesn't change during the deformation, which leads to the integrated form of equation (2.58) for linear elasticity:

$$\mathbf{S} = \mathbf{C} : \mathbf{E} \quad (2.59)$$

It is obvious that the elasticity tensor can't remain constant for a nonlinear material behavior. Therefore, for nonlinear materials just the incremental representation is valid:

$$\mathbf{C} = \frac{\partial \mathbf{S}}{\partial \mathbf{E}} \quad (2.60)$$

In principle, for each hyperelastic material there exist a strain energy function W . Based on this function a more general approach to derive the elasticity tensor can be given. The second order derivative of the strain energy function w.r.t. the Green Lagrange strain tensor define the elasticity tensor \mathbf{C} :

$$\mathbf{C} = \frac{\partial^2 W}{\partial \mathbf{E} \partial \mathbf{E}} \quad (2.61)$$

A detailed discussion of the evaluation of the elasticity tensor based on a strain energy function is presented in [Cha14], [Par03], [Baş00], [Hol00].

A common representation of the elasticity tensor is based on the curvilinear base vectors in the reference configuration \mathbf{G}_i . In this thesis the elasticity tensor will always be defined based on the curvilinear coordinate system. Additionally, this representation allows the application of all derived continuum mechanical transformation rules. For example, to transform the elasticity tensor from the reference to the current configuration, a push-forward operation can be used as defined in [Hol00]. The elasticity tensor in the reference configuration in curvilinear coordinates can be given as:

$$\mathbf{C} = C^{ijkl} \mathbf{G}_i \otimes \mathbf{G}_j \otimes \mathbf{G}_k \otimes \mathbf{G}_l \quad (2.62)$$

Applying the push forward operation describes the elasticity tensor in the current configuration:

$$\mathbf{c} = \frac{1}{\det \mathbf{F}} C^{ijkl} \mathbf{g}_i \otimes \mathbf{g}_j \otimes \mathbf{g}_k \otimes \mathbf{g}_l \quad (2.63)$$

In the following, different material models will be discussed which are the most commonly used models for the numerical modeling of tensile structures. The description of the material models will be given in terms of the assumptions which were described in section 2.1, where the plane stress assumption is the most important one. Therefore, all of the stress components in the normal or thickness direction can be neglected, which reduces the needed summation index to two (\rightarrow indices from 1 to 2).

St. Venant-Kirchhoff: The St. Venant-Kirchhoff material model is the extension of the well known Hooke's law for large deformations with the limitation to small strains. It can be used for the modeling of linear elastic isotropic materials. An

application of the St. Venant-Kirchhoff material modeling is the simplified simulation of foils (e.g. ETFE-Foils) [Mor07], [Sch09], [MB02]. It is described by two individual numbers, the Young's modulus E and the Poisson's ratio ν . A detailed discussion on the two parameters can be found in [Man13]. The coefficients of the elasticity tensor for the St. Venant-Kirchhoff material law can be given by:

$$C^{\alpha\beta\gamma\delta} = \lambda G^{\alpha\beta} G^{\gamma\delta} + \mu \left(G^{\alpha\gamma} G^{\beta\delta} + G^{\alpha\delta} G^{\beta\gamma} \right) \quad (2.64)$$

$$\text{with } \lambda = \frac{E\nu}{1-\nu^2} \text{ and } \mu = \frac{E}{2(1+\nu)}$$

The constants λ and μ are defined as the *Lamé constants*.

Münsch-Reinhardt: The Münsch-Reinhardt material law is an extension of the St. Venant-Kirchhoff material law for orthotropic fabrics [MR95]. The assumption behind the material law, is that the different fiber directions are interact with each other but don't have an influence on the shear stiffness of the material. As it introduces fiber orientations in the governing equations, the material law is just valid in the defined fiber orientation \mathbf{F}_i . Due to that, a principle orientation has to be defined on the surface of the tensile structure. Additionally, the original form of the material law is given in Voigt notation w.r.t. the local cartesian coordinate system defined by the fiber directions. Due to that a transformation into the curvilinear coordinate system has to be done. In the following, the Münsch-Reinhardt Material law will be given in terms of the previously defined tensor notation. Herein, the material law is transformed into the fiber directions of the fabric based on the transformation principle defined in equation (2.17) applied for a fourth-order tensor:

$$C^{\alpha\beta\gamma\delta} = \bar{C}^{\varepsilon\zeta\eta\vartheta} (\mathbf{G}^\alpha \mathbf{F}_\varepsilon) (\mathbf{G}^\beta \mathbf{F}_\zeta) (\mathbf{G}^\gamma \mathbf{F}_\eta) (\mathbf{G}^\delta \mathbf{F}_\vartheta)$$

$$\bar{C}^{1111} = \frac{1}{1 - \mu_{ks}\mu_{sk}} E_k$$

$$\bar{C}^{2222} = \frac{1}{1 - \mu_{ks}\mu_{sk}} E_s \quad (2.65)$$

$$\bar{C}^{1122} = \bar{C}^{2211} = \frac{1}{1 - \mu_{ks}\mu_{sk}} \mu_{ks} E_k$$

$$\bar{C}^{1212} = \bar{C}^{2121} = \bar{C}^{1221} = \bar{C}^{2112} = G$$

$$\bar{C}^{\text{others}} = 0$$

The Münsch-Reinhardt material law is based on various individual parameters. The shear modulus G , the Young's modulus for the individual fiber directions E_k and E_s and the Poisson's ratios between the fiber directions μ_{ks} and μ_{sk} . Due to the forced symmetry in the material law the following condition holds:

$$\frac{\mu_{sk}}{E_k} = \frac{\mu_{ks}}{E_s} \quad (2.66)$$

The indices k and s are defining the individual fiber directions. In woven textiles a distinction between the warp (deutsch: Kette) and weft or fill (deutsch: Schuss)

direction is made. The warp direction is aligned with the straight fibers of the fabric. The weft fibers are woven around the warp fibers. Detailed discussions on the production of woven fabrics can be found in various literature focusing on the manufacturing of textiles. For a review focusing on architectural textiles, refer to [Koc04], [Sei08] and [Kni+11]. The Münsch-Reinhardt material law represents the basis for various methodologies for the case of orthotropic material properties. These extensions are trying to avoid the deficiencies of the original definitions of the Münsch-Reinhardt material law (e.g. [KWK07] and [GL09]).

Ogden: The Ogden material law was introduced for the simulation of rubber like materials [Ogd97]. It is appropriate to model large deformations in combination with large strains. Therefore, it can be used for the modeling of isotropic materials like foils. The Ogden material law is based on the assumption of hyperelasticity which enforces the formulation of a strain energy function W [Hol00]. By applying equation (2.61) the elasticity tensor can be obtained by the second order derivative of the strain energy function w.r.t. the Green Lagrange strain tensor.

There exist various applications and descriptions of the Ogden material law in engineering. The principal reference for the description of the material law can be found in [Ogd97]. The derived strain energy function of the Ogden material is based on the assumption of an incompressible body which doesn't change volume during the deformation. Based on this assumption in [Ogd97] the strain energy function is given by:

$$W(\lambda_\gamma) = \sum_r \frac{\mu_r}{\alpha_r} [\lambda_1^{\alpha_r} + \lambda_2^{\alpha_r} + \lambda_3^{\alpha_r} - 3] \quad (2.67)$$

In equation (2.67) the quantities μ_r and α_r represent the material constants which have to be defined for the application of the Ogden material law. The in-plane principal stretches λ_1 and λ_2 can be evaluated based on the Cauchy Green tensor given in equation (2.45). The third principal stretch λ_3 can be achieved by the formulation of the incompressibility condition:

$$\lambda_3 = (\lambda_1 \lambda_2)^{-1} \quad (2.68)$$

Substituting equation (2.68) into equation (2.67) the strain energy function for the Ogden material for the application of surfaces can be obtained by:

$$W(\lambda_\gamma) = \sum_r \frac{\mu_r}{\alpha_r} [\lambda_1^{\alpha_r} + \lambda_2^{\alpha_r} + (\lambda_1 \lambda_2)^{-\alpha_r} - 3] \quad (2.69)$$

In general, the elasticity tensor for the Ogden material can be achieved by taking the derivative of the derived strain energy function. In equation (2.69) the assumption for plane stress, which is done for tensile structures, still misses. In [GT92] the governing equations for the Ogden material for the application of tensile structures are given. The obtained elasticity tensor is defined in the principle directions. Due to that a transformation into the curvilinear coordinate system has to be made as already described for the Münsch-Reinhardt material model.

From the definition of the strain energy function it can be seen that the elasticity

2.4 Continuum Mechanics

tensor can't be constant during the deformation process as it is depending on the principal stretches. Due to that, the evaluation of the elasticity tensor has to be repeated in each time step of the deformation. Additionally, the relation between stresses and strains is just valid in the incremental form given in equation (2.58) or equation (2.60), which has to be considered in the derivation of the governing equation for the deformation process.

For the validation of the given material law for rubber-like materials in [Ogd97] a comparison with the experimental data from [Tre44] is proposed. In the following, the simple example of a membrane strip which is subjected to a tension force at the tip will be presented. Due to the boundary conditions of the example, a homogeneous stress distribution is achieved in the example. The investigated example is illustrated in figure 2.12. The material properties for this example are defined in

Material properties:
 $\mu_1 = 6.29947 \quad \alpha_1 = 1.3$
 $\mu_2 = 0.01267 \quad \alpha_2 = 5.0$
 $\mu_3 = -0.10013 \quad \alpha_3 = -2.0$

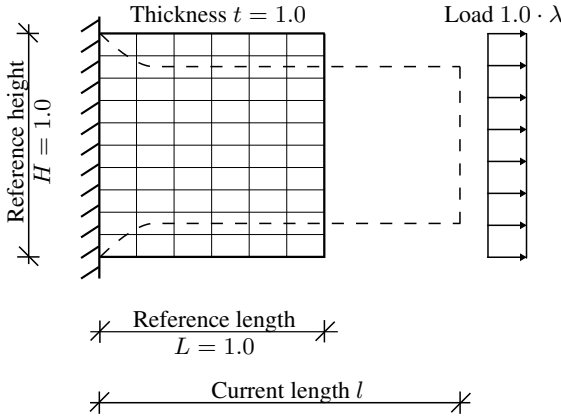


Figure 2.12: Example of a tension test described by Treloar in [Tre44]

[Ogd97] in order to fit the material model to the rubber used in the experiments. In the experiment of Treloar the membrane strip was stretched to approximately eight times the initial length. It is obvious that in this example large strains have to be included in the mechanical description of the experiment. In figure 2.13 the results of the described example are illustrated. It can be seen that the numerical results and the experimental data coincide, even for large strains.

The Ogden material offers an efficient and versatile material model for the appli-

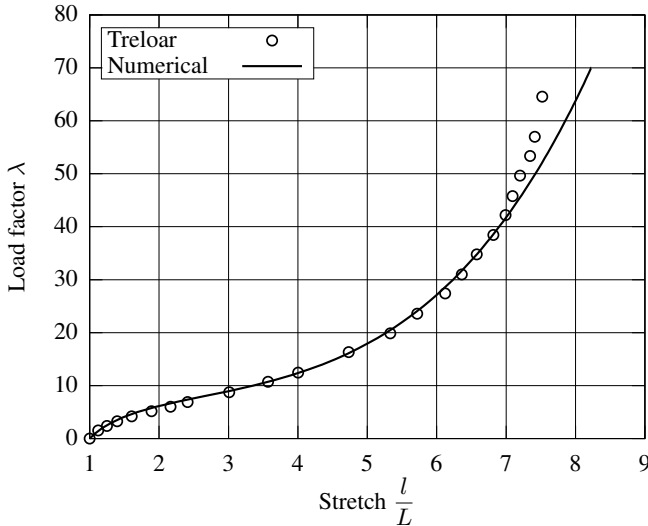


Figure 2.13: Tension test with an Ogden material model for the experimental data from Treloar

cation of isotropic fabrics. However, the Ogden material isn't widely used in the modeling of tensile structures. The reason for that can be identified by the missing material parameters for isotropic materials used in the context of tensile structures. The available material properties are more based on the well known and widely used linear isotropic approach based on the Young's modulus E and Poisson's ratio ν . Additional to the Ogden material model, there exists a number of related laws for the material modeling. The *Mooney-Rivlin* and the *Neo-Hooke* material model can also be used for the modeling of isotropic material and are special cases of the Ogden material law [Hol00].

Multi-linear elastic: The multi-linear elastic material model is trying to adopt the nonlinearity of the material by an extension of the linear elasticity defined in case of St. Venant-Kirchhoff. The basic idea of the material model is to evaluate an equivalent strain situation ε_e based on the current strains at a certain point in the tensile structure and the Poisson's ratio ν . Based on the assumption of plane stress, the equivalent strain can be obtained by the relation given in [Lin09]:

$$\varepsilon_e = \frac{1}{1 - \nu^2} \left[(1 - \nu + \nu^2) (\varepsilon_{11} + \varepsilon_{22})^2 - 3(1 - \nu)^2 (\varepsilon_{11}\varepsilon_{22} - (\varepsilon_{12})^2) \right]^{\frac{1}{2}} \quad (2.70)$$

Therefore, the 2 dimensional strain situation is reduced to a 1 dimensional representation of the strains. For the evaluation of the equivalent strain, the content of the Green Lagrange strain tensor has to be transformed from the curvilinear coordi-

nate system to a local Cartesian one, as equation (2.70) refers to the assumption of the Voigt notation. With this one-dimensional strain, the equivalent stresses can be evaluated on the basis of a monoaxial stress-strain diagram obtained by experiments for the certain material as illustrated in figure 2.14. In this stress-strain diagram the individual linear sections are defined by specific points σ_i and ε_i . For the individual sections a related Young's modulus E_i can be evaluated.

Based on the multi-linear elastic stress-strain diagram and the equivalent strain, it is possible to evaluate an equivalent stress σ_e . This can be done by the computation

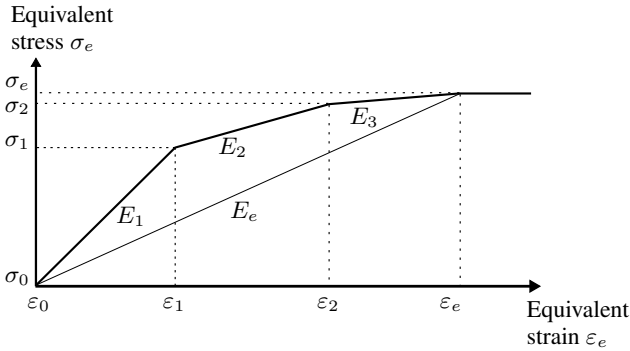


Figure 2.14: Multi-linear stress-strain curve

of an equivalent Young's modulus E_e as given by:

$$E_e(\varepsilon_e) = \frac{\sigma_e}{\varepsilon_e} = \frac{\sum_{i=1}^m [E_i (\varepsilon_i - \varepsilon_{i-1})] + E_{m+1} (\varepsilon_e - \varepsilon_m)}{\varepsilon_e} \quad \text{with } \varepsilon_e \geq \varepsilon_m \quad (2.71)$$

The equivalent Young's modulus describes the ratio between σ_e and ε_e . Based on the equivalent Young's modulus the current elasticity tensor $\hat{\mathbf{C}}$ can be evaluated by the scaling of the initial elasticity tensor $\mathbf{C}(E_1)$ with the ratio of the equivalent Young's modulus to the initial Young's modulus $\frac{E_e(\varepsilon_e)}{E_1}$. By applying this, the calculation of the 2. Piola-Kirchhoff stress from the Green-Lagrange strains can be obtained by:

$$\mathbf{S}(\varepsilon_e) = \frac{E_e(\varepsilon_e)}{E_1} \mathbf{C}(E_1) : \mathbf{E} = \hat{\mathbf{C}} : \mathbf{E} \quad (2.72)$$

To validate the presented multi-linear elastic material, the simulation of a burst test of an ETFE-foil membrane will be done. The experiments of the burst test are presented in [Sch09] and [Sch07]. In figure 2.15, the experiment is illustrated and defined in both top figures. In the experiment, the pressure of the membrane cushion was increased until the membrane burst. In order to quantify the deformations, which are occurring during the inflation, an optical measurement system

was applied. The obtained deformations are illustrated in figure 2.15. For the comparison of the numerical results with the experiments, two simulations were done. The first simulation is based on the introduced St. Venant-Kirchhoff material model with the material properties defined for the initial situation with the Young's modulus $E = E_1$ and the Poisson's ratio ν . The second simulation is based on the introduced multi-linear elastic material model. In figure 2.15 it can be seen that

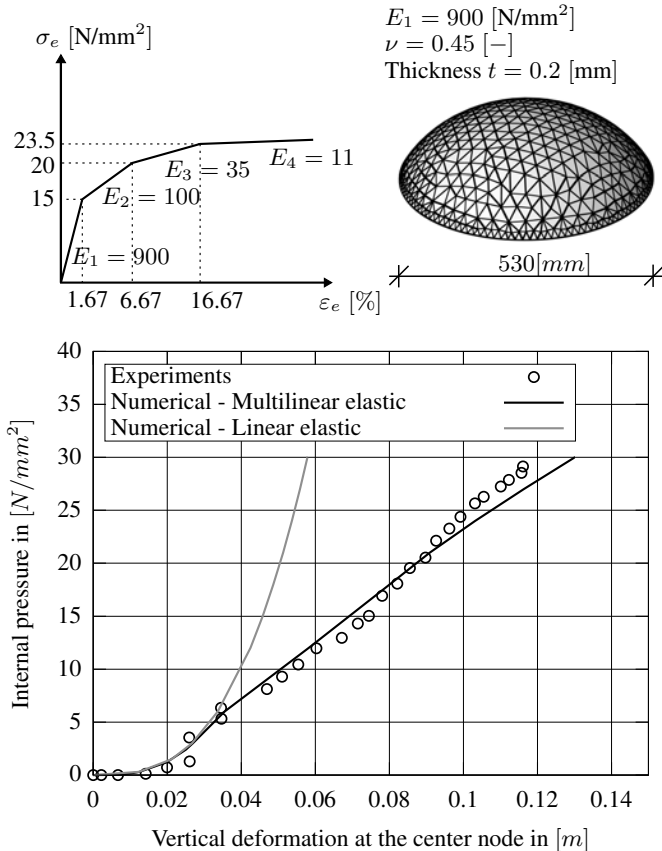


Figure 2.15: Example for a burst test with a ETFE foil

the results for the presented multi-linear elastic material model show a good agreement to the experimental data. Of course, the application of this material model is restricted to small strains in the structures as it is based on the Green Lagrange strains. Due to that, this material model isn't appropriate for the simulation of large strain situations.

Further material models: Summarizing the presented material models it can be stated that there are still limitations from the material modeling point of view for tensile structures (e.g. creep, plasticity, etc.). Currently, there are various number of new material models which have been developed for the application of tensile structures. One of the most interesting developments at the moment is the approximation of the stress-stain relation with non-uniform rational B-splines (NURBS) surfaces to create a response surface. For this purpose a defined set of experiments has to be done in order to ensure that a reasonable interpolation of the experimental data by the NURBS surfaces can be obtained. The basic idea behind this approach is to obtain a mathematically closed description of the stress-strain diagram to be able to evaluate the derivatives of the stresses w.r.t. to the strains. The derivatives of this surface are the individual values of the elasticity tensor. A detailed discussion of this approach can be found in [GB08], [Coe12] and [WWB12].

2.4.6 Equilibrium

The motion of a body can be described based on *Newton's Second law*. It states that the sum of all acting forces on a body has to be in equilibrium with the change of linear momentum. Taking into account as acting forces, the volume and surface forces, the *Cauchy first equation of motion* can be derived. Based on the Cauchy first equation the motion of a body can be described in a global and local form. In the local form it can be given by:

$$\operatorname{div} \boldsymbol{\sigma} + \rho \mathbf{b} - \rho \frac{d\mathbf{v}}{dt} = 0 \quad (2.73)$$

In equation (2.73) $\boldsymbol{\sigma}$ represents the stress state in the body, ρ the density, \mathbf{b} the applied body forces and \mathbf{v} defines the velocity of the body. Additionally, the derivative w.r.t. time, indicated by t , is introduced:

$$\frac{d(\bullet)}{dt} = (\dot{\bullet}) \quad (2.74)$$

The equilibrium given in equation (2.73) is known as the *strong form*, as the equilibrium has to be satisfied in each single point of the body. In general it is not possible to find a solution for the deformation \mathbf{u} which satisfies the equilibrium equation in the strong form. In order to solve the equilibrium equation, a Galerkin method (or weighted residual) is applied [Zie00], [Fin72]. Therefore, the original equilibrium equation will be multiplied with a weighting function $\boldsymbol{\eta}$ and will be integrated over the current volume v . By using the variation of the displacements as the weighting function $\boldsymbol{\eta} = \delta \mathbf{u}$ the known *Weak form of the equilibrium* is achieved:

$$\delta W = \int_v \left(\operatorname{div} \boldsymbol{\sigma} + \rho \mathbf{b} - \rho \frac{d\mathbf{v}}{dt} \right) \delta \mathbf{u} dv = 0 \quad (2.75)$$

The introduced variational or virtual displacements $\delta \mathbf{u}$ in equation (2.75) can be chosen arbitrarily, as at the solution of the equilibrium the equation in brackets will be equal to zero. The weak form given in equation (2.75) will be reformulated in

the following, in order to obtain the governing equation for the equilibrium.

With the identity introduced in [Par03]

$$(\operatorname{div}\boldsymbol{\sigma})\delta\mathbf{u} = (\operatorname{div}\boldsymbol{\sigma}\delta\mathbf{u}) - \boldsymbol{\sigma} : \nabla\delta\mathbf{u} \quad (2.76)$$

and using the Gaussian divergence theorem

$$\int_v (\operatorname{div}\boldsymbol{\sigma}\delta\mathbf{u}) dv = \int_a \mathbf{n}\boldsymbol{\sigma}\delta\mathbf{u} da \quad (2.77)$$

the negative weak form can be rewritten in a separated form:

$$-\delta W = - \int_a \mathbf{n}\boldsymbol{\sigma}\delta\mathbf{u} da + \int_v \boldsymbol{\sigma} : \nabla\delta\mathbf{u} dv - \int_v \rho\mathbf{b}\delta\mathbf{u} dv + \int_v \rho \frac{d\mathbf{v}}{dt} \delta\mathbf{u} dv = 0 \quad (2.78)$$

The relation from equation (2.78) is also known as the *Principle of virtual work*.

With the identity from [Mid02]:

$$\boldsymbol{\sigma} : \nabla\delta\mathbf{u} = \boldsymbol{\sigma} : \delta\mathbf{e} \quad (2.79)$$

the weak form of the equilibrium can be given in the individual parts related to the internal virtual work δW_{int} , the external virtual work δW_{ext} and the time related parts δW_{dyn} .

Internal virtual work:

$$-\delta W_{int} = \int_v \boldsymbol{\sigma} : \nabla\delta\mathbf{u} dv = \int_v \boldsymbol{\sigma} : \delta\mathbf{e} dv \quad (2.80)$$

External virtual work:

$$-\delta W_{ext} = - \int_a \mathbf{n}\boldsymbol{\sigma}\delta\mathbf{u} da - \int_v \rho\mathbf{b}\delta\mathbf{u} dv \quad (2.81)$$

Dynamical virtual work:

$$-\delta W_{dyn} = \int_v \rho \frac{d\mathbf{v}}{dt} \delta\mathbf{u} dv \quad (2.82)$$

Principle of virtual work:

$$-\delta W = -\delta W_{int} - \delta W_{dyn} - \delta W_{ext} = 0 \quad (2.83)$$

By considering the *Lie-Time derivative*, which can be derived from the equality of the principle of virtual work in the reference and the current configuration [Hol00], for the variation of the Euler-Almansi strain tensor

$$\delta\mathbf{e} = \mathbf{F}^{-T} \delta\mathbf{E} \mathbf{F}^{-1} \quad (2.84)$$

2.5 Discretization in Time and Space

and the relation for the transformation of the integration from current to reference configuration, defined in equation (2.42), the internal virtual work can be given in terms of the reference configuration:

$$\begin{aligned}
 -\delta W_{int} &= \int_v \boldsymbol{\sigma} : \delta \mathbf{e} dv \\
 &= \int_V \det \mathbf{F} \boldsymbol{\sigma} : \left(\mathbf{F}^{-T} \delta \mathbf{E} \mathbf{F}^{-1} \right) dV \\
 &= \int_V \det \mathbf{F} \left(\mathbf{F}^{-1} \boldsymbol{\sigma} \mathbf{F}^{-T} \right) : \delta \mathbf{E} dV \\
 &= \int_V \mathbf{S} : \delta \mathbf{E} dV
 \end{aligned} \tag{2.85}$$

In general, tensile structures are assumed to be thin. Due to this assumption, the part in the external virtual work w.r.t. the body forces \mathbf{b} can be neglected. Furthermore with the relation between the current density ρ and the reference density ρ_0 by

$$\rho = \det \mathbf{F} \rho_0 \tag{2.86}$$

the principle of virtual work defined in the reference configuration can be given in the well known form:

$$-\delta W = \int_V \mathbf{S} : \delta \mathbf{E} dV + \int_V \rho_0 \frac{dv}{dt} \delta \mathbf{u} dV - \int_a \mathbf{q}(\mathbf{n}) \delta \mathbf{u} da = 0 \tag{2.87}$$

In equation (2.87) the surface pressure $\mathbf{n}\boldsymbol{\sigma}$ is interpreted as an external surface loading $\mathbf{q}(\mathbf{n})$. In the analysis of tensile structures this part includes the external loading like dead, snow or wind load. A discussion on this part in the weak form of the equilibrium can be found in [Die09].

With the equilibrium representation from equation (2.87) it is possible to evaluate the motion of a tensile structure if a external load is applied or from a more general point of view, if a certain boundary condition is applied. As the equilibrium is still given in continuous form, for the solution a representation of the deformation for the complete structure should be achieved. It is obvious that for the general case such a description can't be found. Additionally, the included time dependency introduces a further complexity for the direct solution of the equilibrium equation. In order to be able to solve the equilibrium equation a discretization in time and space will be introduced in the following.

2.5 Discretization in Time and Space

The derived equation for the equilibrium from section 2.4.6 has the major variables space (in terms of the deformation \mathbf{u}) and time (in terms of time t). In general, it

is not possible to solve the equilibrium equation in a global sense, as the number of unknowns would be infinite. The problem is to find an appropriate deformation field which satisfies the equilibrium condition from equation (2.87) for all times t . In order to solve the equilibrium condition, the spatial and time fields are discretized. In the following the discretization for space and time are described.

2.5.1 Space discretization

The discretization in space is also known as the *Finite Element Method* [Bat96], [Bet97], [Hug00], [MM00], [Sch84], [Wri08], [Zie00], [AM88a], [AM88c], [AM88b], [Oña09], [Oña13]. Here, the unknown fields like deformation, stresses, geometry, etc. will be locally approximated by a patch of elements which provides a mathematical description of the unknowns for its region. The elements do not overlap each other and discretize the overall surface. In figure 2.16 an example for a surface is given, which is discretized by a certain number of elements. Here, for the explanation of the concept, one four-noded finite element is shown as an example. With

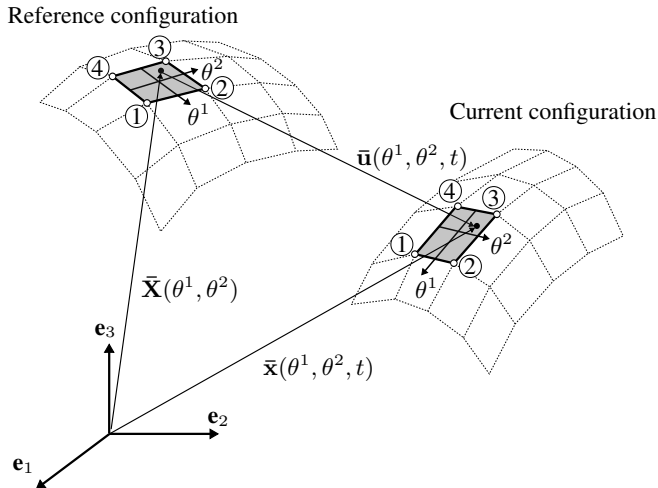


Figure 2.16: FEM discretization of a surface

the concept of the finite elements it is possible to reduce the set of unknowns to a finite number as the surface is described by the finite number of nodes and elements of the discretization. Using the finite elements, the unknown spatial fields can be given w.r.t. to the nodal deformations $\hat{\mathbf{u}}_i$ by using the shape functions N_i of the element. In general, the deformation in one element is a linear combination of the nodal deformations:

$$\mathbf{u}(\theta^1, \theta^2, t) \approx \bar{\mathbf{u}}(\theta^1, \theta^2, t) = \sum_{i=1}^{n_{\text{nodes}}} N_i \hat{\mathbf{u}}_i(\theta^1, \theta^2, t) \quad (2.88)$$

2.5 Discretization in Time and Space

If using the concept of isoparametric elements, the geometry will be discretized in the same way as the deformation. Due to that the geometry in reference and current configuration, can be given by:

$$\mathbf{X}(\theta^1, \theta^2) \approx \bar{\mathbf{X}}(\theta^1, \theta^2) = \sum_{i=1}^{n_{\text{nodes}}} N_i \hat{\mathbf{X}}_i(\theta^1, \theta^2) \quad (2.89)$$

$$\mathbf{x}(\theta^1, \theta^2, t) \approx \bar{\mathbf{x}}(\theta^1, \theta^2, t) = \sum_{i=1}^{n_{\text{nodes}}} N_i \hat{\mathbf{x}}_i(\theta^1, \theta^2, t) \quad (2.90)$$

For the four-noded element, the shape function can be formulated as follows:

$$\begin{aligned} N_1(\theta^1, \theta^2) &= \frac{1}{4} (1 + \theta^1) (1 + \theta^2) \\ N_2(\theta^1, \theta^2) &= \frac{1}{4} (1 - \theta^1) (1 + \theta^2) \\ N_3(\theta^1, \theta^2) &= \frac{1}{4} (1 - \theta^1) (1 - \theta^2) \\ N_4(\theta^1, \theta^2) &= \frac{1}{4} (1 + \theta^1) (1 - \theta^2) \end{aligned} \quad (2.91)$$

with $\theta^1 \in [-1; 1]$ and $\theta^2 \in [-1; 1]$

In general, the solution based on the FEM will result in an approximation of the correct results, due to the introduced discretization of the unknown fields. The exactness of the results can be improved by two approaches: (i) Increasing of the number of elements. This method is known as the h-method. (ii) Increasing of the polynomial degree of the applied finite elements. This method is called as the p-method. In this thesis, the applied finite elements will be limited to three- and four-noded elements based on linear shape functions, due to their advantage in the context of numerical effort for the governing equation.

2.5.2 Time discretization

For the discretization in time the *Newmark-Time-Integration* scheme is used [New59]. Therefore, the time relation of the deformation and the derivatives (e.g. velocity and acceleration) are approximated by the already known previous time step. The only remaining variable in the discretization is the deformation in the next time step. To discretize the time, the overall time integration is divided in certain time increments Δt . In general, the velocity and acceleration are quantities which can be derived from the deformation itself. So in classical dynamics the velocity and acceleration are given as the time derivatives of the deformation. Velocity \mathbf{v} can be given as the first order time derivative from the deformation \mathbf{u} :

$$\mathbf{v} = \frac{d\mathbf{u}}{dt} = \dot{\mathbf{u}} \quad (2.92)$$

Acceleration \mathbf{a} can be given as the first order time derivative from the velocity \mathbf{a} or as the second order time derivative of the deformation \mathbf{u} :

$$\mathbf{a} = \frac{d\mathbf{v}}{dt} = \ddot{\mathbf{u}} \quad (2.93)$$

The Newmark-Time-Integration uses approximated fields for velocity and acceleration which have at least the displacement from the next time step $n+1$ as unknowns:

$$\begin{aligned}\dot{\mathbf{u}}_{n+1} &= \frac{\gamma}{\beta\Delta t} [\mathbf{u}_{n+1} - \mathbf{u}_n] - \frac{\gamma - \beta}{\beta} \dot{\mathbf{u}}_n - \frac{\gamma - 2\beta}{2\beta} \Delta t \ddot{\mathbf{u}}_n \\ \ddot{\mathbf{u}}_{n+1} &= \frac{1}{\beta\Delta t^2} [\mathbf{u}_{n+1} - \mathbf{u}_n] - \frac{1}{\beta\Delta t} \dot{\mathbf{u}}_n - \frac{1 - 2\beta}{2\beta} \ddot{\mathbf{u}}_n\end{aligned}\quad (2.94)$$

A further approximation for the equilibrium equation is made by the midpoint approximation from Chung and Hulbert [CH93], where all quantities in the equilibrium equation are transformed to a certain intermediate time. This is achieved by the introduction of the approximation factors α_f and α_m :

$$\begin{aligned}\ddot{\mathbf{u}}_{n+1-\alpha_m} &= (1 - \alpha_m) \ddot{\mathbf{u}}_{n+1} + \alpha_m \ddot{\mathbf{u}}_n \\ \dot{\mathbf{u}}_{n+1-\alpha_f} &= (1 - \alpha_f) \dot{\mathbf{u}}_{n+1} + \alpha_f \dot{\mathbf{u}}_n \\ \mathbf{u}_{n+1-\alpha_f} &= (1 - \alpha_f) \mathbf{u}_{n+1} + \alpha_f \mathbf{u}_n \\ \mathbf{R}_{ext,n+1-\alpha_f} &= (1 - \alpha_f) \mathbf{R}_{ext,n+1} + \alpha_f \mathbf{R}_{ext,n}\end{aligned}\quad (2.95)$$

2.5.3 Linearization of the Equilibrium Equation

With the approximation in time and space from section 2.5 the equilibrium equation can be given in terms of the finite number of nodal deformations u_i for the next time step $n+1$. In order to solve the equilibrium equation, the virtual displacements can be linearized in terms of the nodal virtual displacements. The linearization can be given by:

$$\delta(\bullet) = \frac{\partial(\bullet)}{\partial u_r} \delta u_r \quad (2.96)$$

Therefore, the principle of virtual work can be evaluated in terms of the residual forces:

$$-\frac{\partial W}{\partial u_{r,n+1}} \delta u_{r,n+1} = R_{r,n+1} \delta u_{r,n+1} = 0 \quad (2.97)$$

As the virtual displacements are arbitrary, equilibrium is only satisfied if the residual forces $R_{i,n+1}$ are equal to zero. Due to that the equilibrium equation can be given in the residual form:

$$\begin{aligned}R_{r,n+1} &= \int_V \mathbf{S} : \frac{\partial \mathbf{E}(\mathbf{u}_{n+1})}{\partial u_{r,n+1}} dV + \int_V \rho_0 \ddot{\mathbf{u}}_{n+1-\alpha_m} \frac{\partial \mathbf{u}_{n+1}}{\partial u_{r,n+1}} dV \\ &\quad - \int_a \mathbf{q}(\mathbf{n}) \frac{\partial \mathbf{u}_{n+1}}{\partial u_{r,n+1}} da = 0\end{aligned}\quad (2.98)$$

In Order to solve the equilibrium equation, a *Newton Raphson* scheme is used. Therefore, the equilibrium equation is expand by a *Taylor-Series expansion* where just the first term is taken into account:

$$LIN(R_{r,n+1}) = R_{r,n+1} + \frac{\partial R_{r,n+1}}{\partial u_{s,n+1}} \Delta u_{s,n+1} = 0 \quad (2.99)$$

2.5 Discretization in Time and Space

When rearranging equation (2.99) the incremental nodal deformation $\Delta u_{s,n+1}$ can be computed by the linear system of equations, which is defined by the derivative of the residual forces $\frac{\partial R_{r,n+1}}{\partial u_{s,n+1}}$, also known as tangential stiffness matrix \mathbf{K}_T , and the actual residual forces $R_{r,n+1}$. With the incremental nodal deformation $\Delta u_{s,n+1}$ the overall nodal deformation $u_{i,n+1}$ can be updated:

$$u_{i,n+1} = u_{i,n} + \Delta u_{i,n+1} \quad (2.100)$$

The process of solving equation (2.99) and updating the overall deformations has to be repeated until the residual equation is fulfilled to a certain accuracy.

Form Finding

The first step in the numerical design and analysis of tensile structures is to find a shape which satisfies the requirements from an architectural and engineering point of view. For each structure, the choice of the shape has a fundamental influence on its structural behavior. Due to their special load carrying properties, tensile structures differ fundamentally from conventional structures in this process. The main difference between tensile and conventional structures is the absence of bending stiffness, due to the thin membrane material. As already described in section 2.1 the mechanical behavior can be characterized with the plane stress assumption, by neglecting the out-of-plane stresses. A tensile structure restrains external loads just based on the in-plane stresses. The limitation in the structural response on the in-plane stresses introduces special requirements into the design process. The shape can not be set arbitrarily as can be done within certain limits for conventional structures. The shape has to be found. The design steps of structural analysis and cutting pattern generation, as illustrated in figure 1.4, are based on the shape and the prestress evaluated in the process of form finding. Therefore, without form finding, as a center step, no closed design loop for tensile structures can be developed.

For the solution of the form finding, different methodologies have been developed in the past. They range from experimental to numerical methods, differing in the quality and exactness of their results. In the beginning of this chapter the principle question *What is form finding?* will be discussed. Here the discussion will be based on examples from everyday life to illustrate the underlying problem. From this intuitive explanation, the governing equations for the numerical description of the form finding problem will be derived and a solution technique presented in [BR99] will be introduced. The discussion on a general existence of a solution represents the basis for the description of various extensions to the originally developed method. Additionally, the effects of the inclusion of conventional structural elements in design process will be discussed in the end of this chapter.

3.1 What is form finding?

3.1 What is form finding?

The term form finding can be defined in various ways depending on the type of investigated structure. In case of tensile structures it can be defined as follows [DWB10]:

Form finding is the task to find the shape of equilibrium with respect to given surface stress state σ and natural (e.g. edge forces) or geometrical (e.g. clamped edges) boundary conditions.

In this definition it is implied that the surface stress state σ is given and the respective shape of equilibrium will be evaluated. The prescribed stress state is not naturally given for the process of form finding. Based on an example the principle necessity of prescribing a certain quantity will be discussed. Additionally, it will be shown that there are different possibilities in the choice of predefined parameters. As an result of this example it will be shown that the surface stresses are the most suitable quantity for the prescribed value.

Considering a clothesline which is assembled between two trees, the deformation illustrated in figure 3.1 when the laundry is put in place, will be obtained. For this

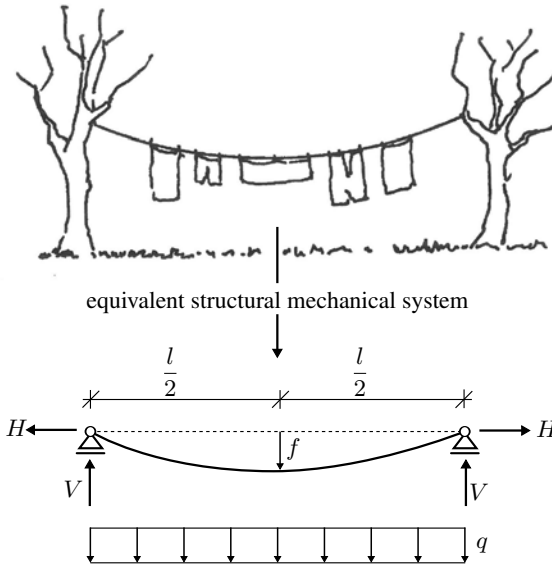


Figure 3.1: Equilibrium of a clothesline (top [Ber05])

example an equivalent structural model can be defined. The laundry is abstracted

by the distributed line load q and the stresses in the cable can be derived from the support forces V and H . The deformation in the center of the clothesline f can be evaluated by the equilibrium of forces. Based on experience it is well known that the deformation of the clothesline will be reduced if the intensity of the horizontal force H is increased. So from a general point of view this experience implies the answer to the question: *What is form finding?* The form of the shape of the tensile structure is related to the acting forces and stresses. This physical experience can also be expressed by means of equations.

For the evaluation of the governing equations, the equivalent structural model, illustrated in figure 3.1, has to be considered. The clothesline, or rod in terms of structural mechanics, is supported on both sides in the vertical direction which results in the vertical reaction forces V . These forces are purely dependent on the vertical acting forces q (or the laundry). The horizontal forces H have to be defined and they are dependent on the amount of prestress which can be applied to the rod. The maximum deformation in the middle of the rod is directly linked to the amount of applied horizontal forces, as the governing equation for the mid-deformation can be derived to be:

$$f = \frac{q \cdot l^2}{8 \cdot H} \quad (3.1)$$

It is also interesting to note, that the connection exists in both directions. If the prestress is fixed in the cable (so H has to be prescribed), the geometry can be directly evaluated. The other way around, if the geometry is fixed (so f has to be prescribed) the prestress can be obtained. It is obvious that prescribing the deformation (or geometry) can result in unphysical solutions. For instance, if one defines the deformation f to be zero, the prestress has to be infinite. Therefore, it is more appropriate to prescribe the prestress to ensure that the final solution remains physical. From a theoretical point of view, both approaches are feasible and can be applied in principle. From a practical point of view, the definition of the prestress is more suitable as it ensures that as long as state of the art technical solutions and materials are used, a feasible design will be achieved.

Another example is a bubble-like structure. Examples for bubbles can be found everywhere in reality (e.g. balloons, lather, soap bubbles, etc.) as illustrated in figure 3.2. Again an intuitive experience exists for such kinds of structures. In the following, the soap bubble example painted by Jean-Baptiste-Siméon Chardin will be discussed. The size of the bubble is directly connected to the intensity of the pressure inside the bubble. The phenomena of the bubble can also be expressed by a simple relation between forces and geometry. The *Young-Laplace Equation* can be used to describe the mechanical behavior of the bubble:

$$\frac{n_1}{R_1} + \frac{n_2}{R_2} = p_{\perp} \quad (3.2)$$

In equation (3.2) the principle relation of a curved surface at a certain point is described. Here, the equilibrium is given w.r.t. two principal directions on the surface. In general, at a certain point these two principal directions have individual unique principal radii R_1 and R_2 which can be evaluated by an eigenvalue analysis of the curvature tensor from equation (2.30). In the surface there exists a stress field n_1

3.1 What is form finding?

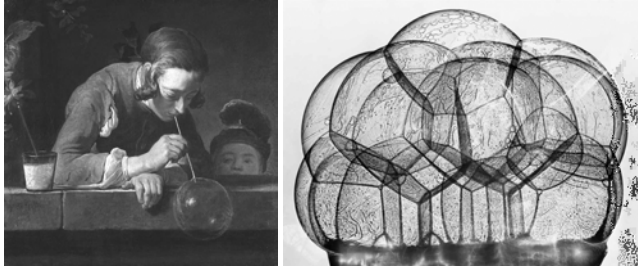


Figure 3.2: left: Jean-Baptiste-Siméon Chardin - The Soap Bubble [HT96]; right: Frei Otto - Soap films at the IL University Stuttgart [OR95]

and n_2 which corresponds with the principal directions. The pressure p_{\perp} inside the bubble is constant and perpendicular to the surface. The described relations from equation (3.2) are illustrated in figure 3.3. Here, the *Young-Laplace Equation* is shown on a segment of the sphere like bubble. With the assumption of isotropic

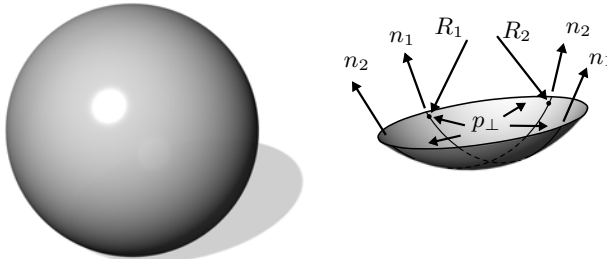


Figure 3.3: Equilibrium in a bubble like structure

prestress ($n_1 = n_2 = n$) and of an ideal sphere ($R_1 = R_2 = R$) equation (3.2) can be stated in the simplified form:

$$R = \frac{2 \cdot n}{p_{\perp}} \quad (3.3)$$

In equation (3.3) the relation between geometry and acting forces and stresses can be seen again. If one reduces the pressure inside the bubble, the radius (and in consequence the size of the bubble) will be increased and vice versa, if a constant prestress is assumed.

The discussed examples, the clothesline and the bubble-like structure, describe in terms of both experiences and equations the relation between the geometry and the acting stress state in the structure. Because of this coupling between geometry and mechanics, the shape of a tensile structure can't be defined as in case of conventional structures. The process of designing or finding the final form is known as the form finding analysis. In the following sections the principle mechanical description of the problem will be given and the solution for various applications is introduced.

3.2 Numerical form finding of tensile structures

In the previous section, a definition of the term form finding for tensile structures has been introduced. In this section the general description from a mechanical point of view will be given. As already described, the main shaping parameter for a tensile structure is the prestress. The relation between the defined prestress and the geometry can be given through the equilibrium equation as defined in equation (2.80) and equation (2.81). The dynamic part can be neglected as the form found shape is independent of any inertia effects. The equilibrium equation is formulated in the current configuration as the described prestress should satisfy the equilibrium in the final state. The starting point of the form finding process is the definition of the final prestress σ_0 . The geometry which satisfies the equilibrium condition w.r.t. the defined prestress field is stated as the *Shape of Equilibrium*. In order to find this shape, the equilibrium equation can be formulated based on the chosen prestress state:

$$-\delta W = t \int_a \sigma_0 : \delta e da - \int_a \mathbf{q}(\mathbf{n}) \delta u da = 0 \quad (3.4)$$

From equation (3.4) it can be seen that the numerical form finding problem is independent on any material property, as the surface stresses are predefined independent from the deformation. Additionally, external loads are considered as well, as $\mathbf{q}(\mathbf{n})$ defines the external load acting in a certain direction. Form finding is an inverse procedure compared to conventional structural analysis. In form finding first the final state of stresses is predefined and the related shape of equilibrium is determined. Material properties are introduced in a second step when the stresses are released to evaluate the cutting pattern. In contrast, with standard analyses, the undeformed geometry together with the material are given and the final geometry is determined by elastic deformations.

For the solution of the given problem in equation (3.4), the variation of the Euler-Almansi strain tensor δe has to be carried out in the internal virtual work. As the variation can't be straightforwardly evaluated, the Lie-Time derivative as introduced in equation (2.84) has to be applied. Additionally, with equation (2.42) the integration can be transferred into the reference configuration. The external part in the principle of virtual work will remain in the current configuration as the variation

3.2 Numerical form finding of tensile structures

can be made in a straightforward manner for the deformations:

$$-\delta W = t \int_A \det \mathbf{F} \boldsymbol{\sigma}_0 : \mathbf{F}^{-T} \delta \mathbf{E} \mathbf{F}^{-1} dA - \int_a \mathbf{q}(\mathbf{n}) \delta \mathbf{u} da = 0 \quad (3.5)$$

If introducing a discretization and linearization to equation (3.5), as described in section 2.5.1 and section 2.5.3, the residual form of the form finding problem can be given by:

$$R_r = t \int_A \det \mathbf{F} \boldsymbol{\sigma}_0 : \mathbf{F}^{-T} \frac{\partial \mathbf{E}}{\partial u_r} \mathbf{F}^{-1} dA - \int_a \mathbf{q}(\mathbf{n}) \frac{\partial \mathbf{u}}{\partial u_r} da = 0 \quad (3.6)$$

By substituting the second formulation of the Green-Lagrange strain tensor from equation (2.46) in equation (3.6) the residuum can be obtained by:

$$R_r = t \int_A \det \mathbf{F} \boldsymbol{\sigma}_0 : \left[\frac{1}{2} \left(\mathbf{F}^{-T} \frac{\partial \mathbf{F}^T}{\partial u_r} + \frac{\partial \mathbf{F}}{\partial u_r} \mathbf{F}^{-1} \right) \right] dA - \int_a \mathbf{q}(\mathbf{n}) \frac{\partial \mathbf{u}}{\partial u_r} da = 0 \quad (3.7)$$

Based on equation (2.15) and equation (2.14) the residuum can be reformulated as follows:

$$R_r = t \int_A \det \mathbf{F} \boldsymbol{\sigma}_0 : \left[\frac{1}{2} \left(\left(\mathbf{F}^{-T} \frac{\partial \mathbf{F}^T}{\partial u_r} \right)^T + \frac{\partial \mathbf{F}}{\partial u_r} \mathbf{F}^{-1} \right) \right] dA - \int_a \mathbf{q}(\mathbf{n}) \frac{\partial \mathbf{u}}{\partial u_r} da = 0 \quad (3.8)$$

By applying equation (2.12), the residuum equation can be given by:

$$R_r = t \int_A \det \mathbf{F} \boldsymbol{\sigma}_0 : \frac{\partial \mathbf{F}}{\partial u_r} \mathbf{F}^{-1} dA - \int_a \mathbf{q}(\mathbf{n}) \frac{\partial \mathbf{u}}{\partial u_r} da = 0 \quad (3.9)$$

In order to separate the derivative of the deformation gradient for the double contraction, based on equation (2.13) the residuum equation can be stated:

$$R_r = t \int_A \det \mathbf{F} \left(\boldsymbol{\sigma}_0 \mathbf{F}^{-T} \right) : \frac{\partial \mathbf{F}}{\partial u_r} dA - \int_a \mathbf{q}(\mathbf{n}) \frac{\partial \mathbf{u}}{\partial u_r} da = 0 \quad (3.10)$$

If evaluating the double contraction of the derivative of the deformation gradient and the transposition of the inverse deformation gradient, the residual forces can be given in components as follows:

$$R_r = t \int_A \det \mathbf{F} \sigma_0^{\alpha\beta} \left(\frac{\partial \mathbf{g}_\alpha}{\partial u_r} \mathbf{g}_\beta \right) dA - \int_a \mathbf{q}(\mathbf{n}) \frac{\partial \mathbf{u}}{\partial u_r} da = 0 \quad (3.11)$$

If applying a Newton-Raphson algorithm, as derived in section 2.5.3, the system matrix has to be evaluated. For this purpose, the first order derivative of the residuum equation has to be evaluated which gives the components of the stiffness matrix:

$$K_{rs} = t \int_A \frac{\partial}{\partial u_s} \left[\det \mathbf{F} \left(\boldsymbol{\sigma}_0 \mathbf{F}^{-T} \right) : \frac{\partial \mathbf{F}}{\partial u_r} dA \right] - \int_a \frac{\partial \mathbf{q}(\mathbf{n})}{\partial u_s} \frac{\partial \mathbf{u}}{\partial u_r} da \quad (3.12)$$

The second part of equation (3.12) is related to the external forces. In general, the second order derivative of the deformation should occur for the external forces as well, but if applying the space discretization described in section 2.5.1 the term $\frac{\partial^2 \mathbf{u}}{\partial u_r \partial u_s}$ will vanish. It is obvious that, if the load is independent from the deformations ($q = \text{const.}$) the remaining term will vanish from the system matrix as well. This part in the system matrix, related to the external load, is stated as the *Load Stiffness Matrix*. A detailed discussion on the evaluation of the load stiffness matrix can be found in [Jru09], [Mok+99] or [SR84]. The first part, which is related to the internal forces, can be given in components:

$$K_{rs} = t \int_A \left(\frac{\partial \det \mathbf{F}}{\partial u_s} \sigma_0^{\alpha\beta} \left(\frac{\partial \mathbf{g}_\alpha}{\partial u_r} \mathbf{g}_\beta \right) + \det \mathbf{F} \frac{\partial \sigma_0^{\alpha\beta}}{\partial u_s} \left(\frac{\partial \mathbf{g}_\alpha}{\partial u_r} \mathbf{g}_\beta \right) + \det \mathbf{F} \sigma_0^{\alpha\beta} \left(\frac{\partial \mathbf{g}_\alpha}{\partial u_r} \frac{\partial \mathbf{g}_\beta}{\partial u_s} \right) \right) dA \quad (3.13)$$

Trying to solve the given problem from equation (3.10) with the Newton-Raphson algorithm, it turns out that the system matrix from equation (3.13) is singular for deformations tangential to the surface. The reason for this deficiency originates from the inverse character of the given problem where stresses in the deformed configuration are given without considering material properties and strains. This inverse character can be understood in comparison to standard structural analysis, where the stresses can be evaluated from displacements by applying the material law. In contrast to that, form finding already implies the stress in order to determine the deformed geometry. From a continuum mechanical point of view that means that stresses and strains are not related anymore. As a consequence, it turns out that the position of the nodes on the surface can't be evaluated uniquely since it is possible to describe the same surface with differently shaped finite elements as illustrated in figure 3.4. In other words the nodes can float freely on the surface. Hence, the same surface can be described by an infinite number of discretizations, which results in the singular system matrix. It turns out that the solution for the form finding can't be achieved directly as there exists no unique numerical solution for this problem. Due to that, stabilization techniques have to be involved to solve the problem numerically.

3.3 Stabilization of the inverse problem

In the past, various methods for the stabilization of the inverse problem of form finding were developed. The methods applied by Frei Otto for the form finding on

3.3 Stabilization of the inverse problem

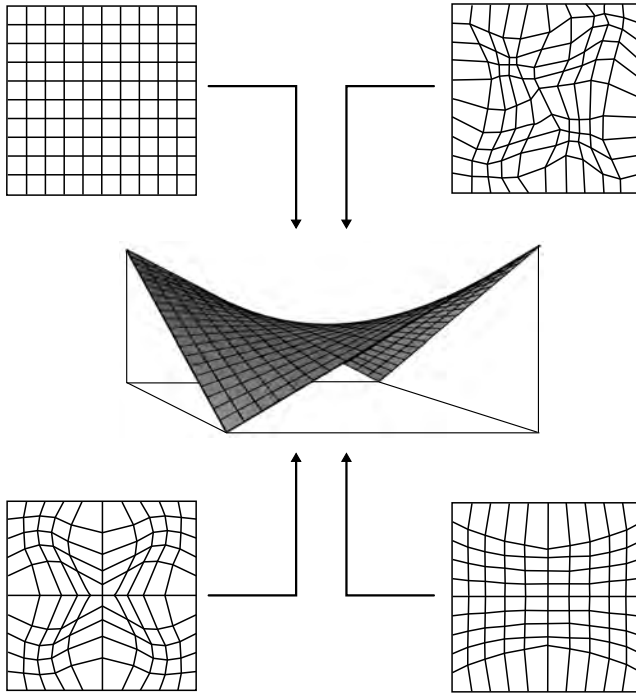


Figure 3.4: Arbitrarily deformed meshes for the same surface geometry

the basis of physical modeling like soap films or tulle models as illustrated in figure 3.5, can be understood as another approach for the stabilization (e.g. [WM95], [OT62], [OS66]). Of course, the application of physical models was not motivated from the knowledge of the inverse character in the numerical problem. Regardless, it represents a solution approach. From [HT96] the relation between soap film models and minimal surfaces is defined by the minimization of the elastic potential, which represents the equality of the governing equation from section 3.2 and the soap film models introduced by Frei Otto.

As previously described, the direct solution of the elastic potential based on the principle of virtual work results in a singular system matrix. The first numerical solution approaches which prevented the singularity, were motivated by geodesy. For the form finding of the roof of the Olympic stadium in Munich the well known *Force Density Method* was introduced by Linkwitz and co-workers [LS71],[Sch74], [Bub72], [Grü76] and [Sin95]. The original version of the force density method was limited to the form finding of cable net structures. The extension to triangular membranes was done by [Sin95], [MM98].

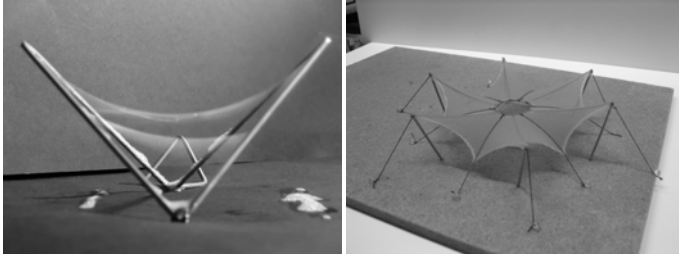


Figure 3.5: Soap film (left) and tulle model (right) [Wil11]

Based on the increasing relevance of tensile structures in modern architecture, more methods for the solution of the form finding problem were developed. The *Dynamic Relaxation Method* was first published by Day [Day65] from a general point of view and the application to tensile structures by [Bar74], [Bar88], [Bar99], [Wak99], [LL96]. Here, the stabilization of the inverse problem is achieved by applying the time dependent version of the equilibrium from equation (2.87) and introducing artificial mass and damping effects. Starting from an arbitrary initial configuration, the shape of equilibrium is achieved by a transient analysis. The drawback of this method is to choose appropriate mass and damping coefficients in order to stabilize the governing equation. Therefore, a high level of experience is needed for the robust application of the method. Nonetheless, the dynamic relaxation is successfully used for the form finding of a large number of structures.

A further method based on a modified Newton-Raphson iteration is proposed by [HP72], [Hau88a], [Hau88b], [HA82]. Here, the stabilization is achieved by a inconsistent linearization of the residual equation. This results in a stiffness matrix of full rank but as a consequence quadratic convergence is impossible.

In order to avoid the arbitrary choice of main quantities in the solution of the inverse problem in [BR99] a more general method is introduced based on a homotopy mapping. The main advantage of this method is that it is consistently derived from continuum mechanics. In the following section, principles of this method will be illustrated and extensions for the general application will be discussed.

3.3.1 Updated Reference Strategy

The *Updated Reference Strategy* (URS) was introduced by Bletzinger [BR99] at the University of Stuttgart. The URS introduces a mathematically based method to stabilize the inverse problem that was discussed in section 3.2. The idea for the URS is to apply a homotopy mapping [AG12] to stabilize the singular equation system. For the stabilization, a related problem will be added to the original one, which fades out the singularity. Therefore, equation (3.4) will be expanded by an additional term which describes an alternative formulation of the internal virtual

3.3 Stabilization of the inverse problem

work:

$$-\delta W = -(\lambda \delta W_{\text{orig}} + (1 - \lambda) \delta W_{\text{mod}}) \quad (3.14)$$

In equation (3.14) the first part of the equation is related to the singular original problem from equation (3.4). The second part is a solvable related problem, which stabilizes the overall equation. The homotopy factor λ ensures the solvability. If $\lambda = 1$ the original problem is solved and on the other hand if $\lambda = 0$ just the modified problem is solved.

The formulation of the stabilization term has to fulfill the requirement that it converges to the original problem if the correct solution is achieved. In order to define an appropriate related problem, the equilibrium equation will be formulated w.r.t. to a given reference configuration:

$$-\delta W_{\text{mod}} = t \int_A \mathbf{S}_0 : \delta \mathbf{E} dA \quad (3.15)$$

For the stabilization term, the same linearization w.r.t. the unknown deformation can be derived, which results in the residual form of the stabilization term:

$$R_{r,\text{mod}} = t \int_A \mathbf{S}_0 : \frac{\partial \mathbf{E}}{\partial u_r} dA = t \int_A S_0^{\alpha\beta} \left(\frac{\partial \mathbf{g}_\alpha}{\partial u_r} \cdot \mathbf{g}_\beta \right) dA \quad (3.16)$$

For the application of a Newton-Raphson algorithm for the solution, the system matrix for the stabilization term can be given by:

$$K_{rs,\text{mod}} = t \int_A \mathbf{S}_0 : \frac{\partial^2 \mathbf{E}}{\partial u_r \partial u_s} dA = t \int_A S_0^{\alpha\beta} \left(\frac{\partial \mathbf{g}_\alpha}{\partial u_r} \cdot \frac{\partial \mathbf{g}_\beta}{\partial u_s} \right) dA \quad (3.17)$$

For the evaluation of the governing equations for the stabilization term, the prestress state \mathbf{S}_0 has to be defined. From a continuum mechanical point of view, it would be possible to achieve the prestress in the reference configuration by a pull back operation as defined in equation (2.57). It is obvious, that if this would be applied to the form finding equations, the original and the stabilization term would be equivalent and the singularity still remains. To ensure the solvability of the modified internal virtual work the assumption is done that the coefficients in the reference and the current configuration are identical:

$$\sigma_0^{\alpha\beta} = S_0^{\alpha\beta} \quad (3.18)$$

Due to this modification the two parts in equation (3.14) will be different and the resulting system of equations can be solved. For the evaluation of the governing equation of the modified internal virtual work, both a reference and a current configuration have to be defined. The solution of the modified problem will correspond with the optimal shape if the reference is identical to the current configuration. Of course, this situation would result again in the singular state. From a mathematical point of view, the results from the homotopy method will never end up in the final solution, only an approximation can be achieved. This theoretical difference can be

neglected in the application of the URS as the error can be reduced to the chosen order of numerical accuracy.

It would seem that if it was possible to define an appropriate reference configuration, the solution of the form finding could be achieved in advance. In general, this is not the case. Therefore, in the URS the initial reference configuration will be chosen arbitrarily. For this choice the boundary conditions have to be considered (e.g. fixed points of the tensile structure). Based on this, the solution of the modified virtual work can be achieved by a Newton-Raphson method. It is obvious, that the stabilization term will not fade out as long as the reference and the current configuration will not coincide. Therefore, deformations at the nodes of the discretized surface will occur. To ensure that the procedure will converge to the final form of the tensile, the deformed shape is used as a new reference configuration. By updating the reference configuration after each solution step, the method will finally converge to the shape of equilibrium for an arbitrary choice of the homotopy factor $0 \leq \lambda < 1$.

As the choice of λ is arbitrary, it is also possible to choose a homotopy factor equal to zero for all carried out form finding steps as suggested in [Lin09]. Of course, this approach omits the need of predefining a computational quantity, but results in the necessity of more form finding steps. If applying the full URS, the homotopy factor has to be chosen for each form finding step. Depending on the quality of the initially chosen reference configuration, the solution in the first form finding step can be challenging for the applied solution algorithm by defining values for λ close to 1. Therefore, it is recommended to apply a small homotopy factor in the first form finding step and increase it for the next steps. The general process of the URS is illustrated in figure 3.6 for the form finding of the well known Scherk minimal surface [Sch35].

3.3.1.1 Membrane element

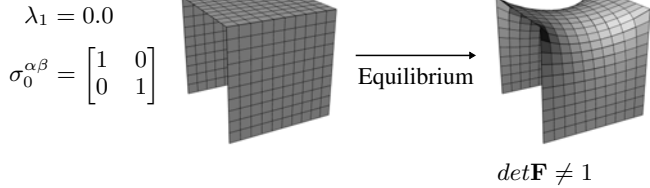
The governing equations for the membrane element are already defined in section 3.3.1. With the introduction of a discretization, finite elements for the form finding of membranes can be derived. In general, all types of 2D finite elements can be applied to discretize the governing equations.

For the evaluation of the residual forces and the system matrix for a membrane finite element, the definition of a required prestress σ_0 has to be made. As defined in equation (3.18) the coefficients for the Cauchy and the 2. Piola Kirchhoff stresses are assumed to be identical. The derived residual forces and the system matrix for the original and the stabilization term were based on the curvilinear form of the stress tensors, defined as follows:

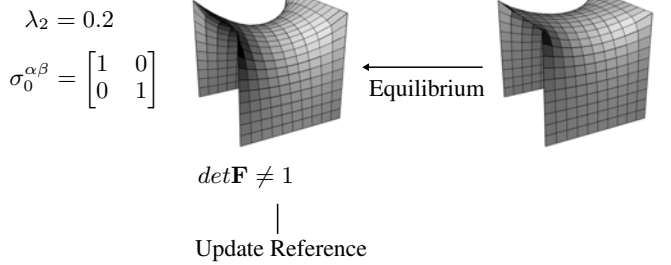
$$\begin{aligned}\sigma_0 &= \sigma_0^{\alpha\beta} \mathbf{g}_\alpha \otimes \mathbf{g}_\beta \\ \mathbf{S}_0 &= \mathbf{S}_0^{\alpha\beta} \mathbf{G}_\alpha \otimes \mathbf{G}_\beta \\ \text{with } \sigma_0^{\alpha\beta} &= S_0^{\alpha\beta}\end{aligned}\tag{3.19}$$

3.3 Stabilization of the inverse problem

Form finding step 1



Form finding step 2



Form finding step 3

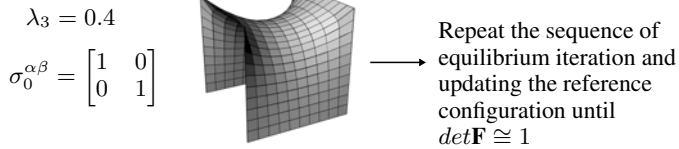


Figure 3.6: Form finding process using the URS applied to the Scherk minimal surface

From a practical point of view, the definition of the coefficients of the curvilinear prestress tensor is not straight forward, as the values have no direct physical meaning. Therefore, the prescribed prestress will be applied based on a local Cartesian coordinate system. If the derived equation for the form finding should be applied, the prestress has to be transformed into the curvilinear coordinate system. For this purpose various methods have been previously introduced. The main difference between the suggested methods is the geometrical part, where the local Cartesian coordinate system is defined on the curved 3D surface. In [Die09] a method limited to isotropic situations is introduced. A more general approach is presented in [Lin09] and [Wüc07], where based on the definition of approximative directions in a projection plane, the local Cartesian coordinate system is evaluated. In the following, the method described in [Wüc07] will be presented.

Consider a plane defined by the directions \mathbf{T}_1 and \mathbf{T}_2 as illustrated in figure 3.7. With the intersection of this plane area and the tangential plane on the surface defined by base vectors \mathbf{G}_1 and \mathbf{G}_2 , the first local cartesian direction $\hat{\mathbf{T}}_1$ can be defined. The line of intersection $\hat{\mathbf{T}}_1$ can be evaluated by the cross product of the surface normal \mathbf{T}_3 of the projection plane and the surface normal of the curved surface \mathbf{G}_3 :

$$\hat{\mathbf{T}}_1 = \frac{\mathbf{T}_3 \times \mathbf{G}_3}{\|\mathbf{T}_3 \times \mathbf{G}_3\|} \quad (3.20)$$

The direction $\hat{\mathbf{T}}_1$ can be interpreted as the first prestress direction. The second prestress direction can be obtained by the cross product of the surface normal \mathbf{G}_3 and the first prestress direction $\hat{\mathbf{T}}_1$:

$$\hat{\mathbf{T}}_2 = \frac{\hat{\mathbf{T}}_1 \times \mathbf{G}_3}{\|\hat{\mathbf{T}}_1 \times \mathbf{G}_3\|} \quad (3.21)$$

The resulting local Cartesian coordinate system $\hat{\mathbf{T}}_\alpha$ can be used to define the physical values of the prestress on the curved surface. In figure 3.7 this process of defining the prestress directions is illustrated. With the prestress directions defined by equation (3.20) and equation (3.21), the physical prestress values can be transformed into the curvilinear coordinate system based on equation (2.17). The resulting transformation rule from the local cartesian coefficients $\hat{S}_0^{\alpha\beta}$ into the curvilinear coefficients $S_0^{\delta\gamma}$ can be given for the 2. Piola Kirchhoff stresses by:

$$S_0^{\delta\gamma} = \hat{S}_0^{\alpha\beta} \left(\hat{\mathbf{T}}_\alpha \cdot \mathbf{G}^\delta \right) \left(\hat{\mathbf{T}}_\beta \cdot \mathbf{G}^\gamma \right) \quad (3.22)$$

This transformation can also be applied for the Cauchy stresses. But as the assumption is introduced that the components of both, the Cauchy and the 2. Piola Kirchhoff stresses are identical, this only has to be done for the reference configuration. Of course, the transformation of the prestress into the curved surface has to be done in each iteration step and for each integration point as the directions will change constantly. Based on the transformed prestress coefficients the residuum and the system matrix can be evaluated as already defined in equation (3.13) for the original part and in equation (3.17) for the stabilization part.

3.3 Stabilization of the inverse problem

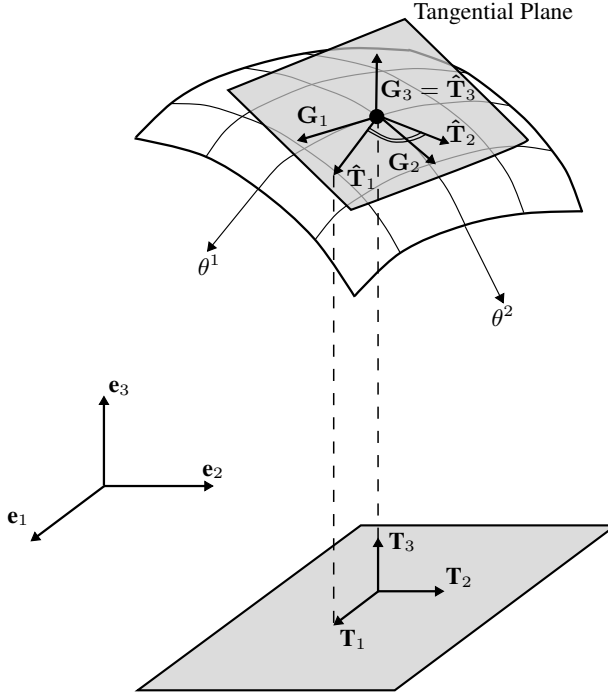


Figure 3.7: Local Cartesian coordinate system for the definition of the physical prestress values

3.3.1.2 Cable element

Cable elements are one dimensional elements which are applied to model all types of cables in the tensile structure. For this type of finite element, the local coordinate system is defined by the cable axis. Additionally, the derived equations can be simplified, as there is just one dimension to consider. The summation from the governing equations for the form finding problem can be reduced to a fixed version as just one base vector has to be considered. The residual forces for the original part can be given by:

$$R_{r,org} = A \int_L \det \mathbf{F} \sigma_0^{11} \left(\frac{\partial \mathbf{g}_1}{\partial u_r} \mathbf{g}_1 \right) dL - \int_l \mathbf{q}(\mathbf{n}) \frac{\partial \mathbf{u}}{\partial u_r} dl = 0 \quad (3.23)$$

Furthermore, the system matrix for the original part is obtained as follows:

$$K_{rs,org} = A \int_L \frac{\partial \det \mathbf{F}}{\partial u_s} \sigma_0^{11} \left(\frac{\partial \mathbf{g}_1}{\partial u_r} \cdot \mathbf{g}_1 \right) + \det \mathbf{F} \frac{\partial \sigma_0^{11}}{\partial u_s} \left(\frac{\partial \mathbf{g}_1}{\partial u_r} \cdot \mathbf{g}_1 \right) + \det \mathbf{F} \sigma_0^{11} \left(\frac{\partial \mathbf{g}_1}{\partial u_r} \cdot \frac{\partial \mathbf{g}_1}{\partial u_s} \right) dL - \int_l \frac{\partial \mathbf{q}(\mathbf{n})}{\partial u_r} \frac{\partial \mathbf{u}}{\partial u_r} dl \quad (3.24)$$

Of course, the stabilization part can also be reduced in case of cable elements. The residual forces can be evaluated by:

$$R_{r,mod} = A \int_L S_0^{11} \left(\frac{\partial \mathbf{g}_1}{\partial u_r} \cdot \mathbf{g}_1 \right) dL \quad (3.25)$$

Additionally, the system matrix in case of the stabilization part can be given as follows:

$$K_{rs,mod} = A \int_L S_0^{11} \left(\frac{\partial \mathbf{g}_1}{\partial u_r} \cdot \frac{\partial \mathbf{g}_1}{\partial u_s} \right) dL \quad (3.26)$$

In general, it is possible to introduce arbitrary 1D Finite Elements for the discretization of the described equations for the original and stabilization term. An interesting property of the stabilization term can be obtained in the case that finite elements with linear shape functions are applied as illustrated in figure 3.8. For a linear cable

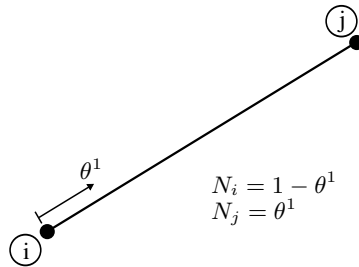


Figure 3.8: Linear cable Finite Element

element, the integration over the length can be reduced to a multiplication of the function by the overall length of the element:

$$\int_L (\dots) dL = (\dots) L \quad (3.27)$$

Additionally, taking into account that with the transformation of the prestress into the curvilinear coordinates by equation (3.22), applied for the one-dimensional case,

3.3 Stabilization of the inverse problem

the prestress in terms of the 2. Piola Kirchhoff stress can be given by:

$$\begin{aligned}
 \mathbf{S}_0 &= S_0^{11} \mathbf{G}_1 \otimes \mathbf{G}_1 = \hat{S}_0^{11} \mathbf{e}_1 \otimes \mathbf{e}_1 \\
 \Rightarrow S_0^{11} &= \hat{S}_0^{11} (\mathbf{e}_1 \mathbf{G}^1) (\mathbf{e}_1 \mathbf{G}^1) \\
 &= \hat{S}_0^{11} G^{11} = \frac{\hat{S}_0^{11}}{L^2}
 \end{aligned} \tag{3.28}$$

Substituting equation (3.28) into equation (3.25) the residual forces for the stabilization term can be given w.r.t. the cable forces N , which are assumed to act along the axial direction of the cable:

$$\begin{aligned}
 R_r &= AS_0^{11} L \left(\frac{\partial \mathbf{g}_1}{\partial u_r} \cdot \mathbf{g}_1 \right) \\
 &= \frac{A \hat{S}_0^{11}}{L} \left(\frac{\partial \mathbf{g}_1}{\partial u_r} \cdot \mathbf{g}_1 \right) \\
 &= \frac{N}{L} \left(\frac{\partial \mathbf{g}_1}{\partial u_r} \cdot \mathbf{g}_1 \right) = R_{r, \text{force density}}
 \end{aligned} \tag{3.29}$$

The last line in equation (3.29) includes the ratio between the cable force N and the cable length L which is well known from literature as the *Force Density* $q = N/L$ which was introduced by Linkwitz [LS71]. Therefore, it can be stated that the URS, for the special case of $\lambda = 0$, represents the generalization of the Force Density Method. In contrast to the Force Density Method, the URS is consistently defined for the 2-D states of stress as well and for arbitrary kinds of discretization of membrane and cable elements.

3.3.1.3 Existence of a solution for the form finding problem

In the previous sections the governing equations for the solution of the inverse problem of the form finding by the Updated Reference Strategy were described. Based on this, the formulation of appropriate Finite Elements was presented. It has been shown, that the main input parameter for the evaluation of the shape of equilibrium is the prestress distribution in the surface. In principle, the prestress can be defined arbitrarily for the individual directions, as the equations were not simplified in the description of the prestress. In fact, there is a discussion included in the description of the membrane finite element about how to define the prestress directions on a curved surface.

In general, there are three possible types of prestress definitions: (i) The prestress is equal in the individual directions and on the overall surface \rightarrow isotropic prestress; (ii) The prestress is unequal in the individual directions, but constant along the surface lines \rightarrow constant anisotropic prestress; (iii) The prestress is unequal in the individual directions and non-constant along the surface lines \rightarrow anisotropic prestress.

In the next sections there will be a discussion for which cases the individual prestress definitions are appropriate. In this section the existence of a solution for the

form finding based on different prestress definitions will be discussed from a mathematical point of view. The example which will be discussed in the following, on the solvability for the different prestress types, was first presented in [Lin09].

In figure 3.9 a surface of rotation is illustrated. It is defined by two fixed circles at the top and the bottom with the radii R_1 and R_2 . The distance between the radii is defined by the height H and it is assumed that both are fixed boundary conditions. In between there is a membrane surface which has the radial prestress σ_r and the meridian prestress σ_m . It is assumed that there are no shear stresses involved in the form finding.

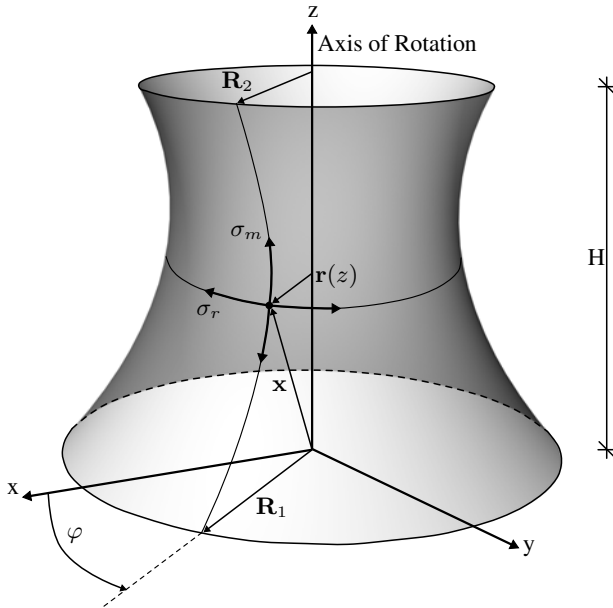


Figure 3.9: Surface of rotation with anisotropic prestress

The geometry of the surface of rotation can be uniquely defined by the varying radius along the rotation axis $r(z) = r$ and the rotation angle φ . Therefore, the two surface parameters can be identified by the angle of rotation $\varphi = \theta_1$ and the position along the rotation axis $z = \theta_2$. Based on this, the geometry given in terms of the position vector is defined as follows:

$$\mathbf{x} = \begin{bmatrix} r \cos(\varphi) \\ r \sin(\varphi) \\ z \end{bmatrix} \quad (3.30)$$

3.3 Stabilization of the inverse problem

The covariant base vectors can be evaluated by the partial derivative of the position vector w.r.t. the surface parameters:

$$\begin{aligned}\mathbf{g}_1 = \mathbf{g}_r &= \frac{\partial \mathbf{x}}{\partial \varphi} = \begin{bmatrix} -r \sin(\varphi) \\ r \cos(\varphi) \\ 0 \end{bmatrix} \\ \mathbf{g}_2 = \mathbf{g}_m &= \frac{\partial \mathbf{x}}{\partial z} = \begin{bmatrix} r_{,z} \cos(\varphi) \\ r_{,z} \sin(\varphi) \\ 1 \end{bmatrix}\end{aligned}\quad (3.31)$$

In equation (3.31) $r_{,z}$ indicates the derivative of the radius $r(z)$ w.r.t. to the coordinate z . For the evaluation of the solution of the form finding, the variation of the Euler Almansi strains is needed as defined in equation (2.84). The variation of the strains in the radial and the meridian direction can be obtained by:

$$\begin{aligned}\delta e_{11} = \delta e_r &= \frac{\delta \mathbf{g}_r \cdot \mathbf{g}_r}{\mathbf{g}_r \cdot \mathbf{g}_r} \\ \delta e_{22} = \delta e_m &= \frac{\delta \mathbf{g}_m \cdot \mathbf{g}_m}{\mathbf{g}_m \cdot \mathbf{g}_m}\end{aligned}\quad (3.32)$$

In equation (3.32) the variation of the covariant base vectors is included, which can be evaluated by:

$$\begin{aligned}\delta \mathbf{g}_1 = \delta \mathbf{g}_r &= \frac{\partial \delta \mathbf{x}}{\partial \varphi} = \begin{bmatrix} -\delta r \sin(\varphi) \\ \delta r \cos(\varphi) \\ 0 \end{bmatrix} \\ \delta \mathbf{g}_2 = \delta \mathbf{g}_m &= \frac{\partial \delta \mathbf{x}}{\partial z} = \begin{bmatrix} \delta r_{,z} \cos(\varphi) \\ \delta r_{,z} \sin(\varphi) \\ 0 \end{bmatrix}\end{aligned}\quad (3.33)$$

Based on the derived equations, the formulation of the principle of virtual work defined in equation (3.4) can be evaluated by:

$$\begin{aligned}-\delta W &= t \int_a \sigma_r \delta e_r + \sigma_m \delta e_m da \\ &= t \int_0^H \int_0^{2\pi} (\sigma_r \delta e_r + \sigma_m \delta e_m) \|\mathbf{g}_1 \times \mathbf{g}_2\| d\varphi dz \\ &= 2t\pi \int_0^H (\sigma_r \delta e_r + \sigma_m \delta e_m) r \sqrt{1 + r_{,z}^2} dz \\ &= 2t\pi \int_0^H \left(\sigma_r \frac{\delta r}{r} + \sigma_m \frac{r_{,z} \delta r_{,z}}{1 + r_{,z}^2} \right) r \sqrt{1 + r_{,z}^2} dz = 0\end{aligned}\quad (3.34)$$

By applying integration by parts and the assumption that the boundaries of the surface are fixed, the principle of virtual work can be rewritten as follows:

$$-\delta W = 2t\pi \int_0^H \left(\sigma_r \sqrt{1 + r_{,z}^2} - \left(\sigma_m \frac{r r_{,z}}{\sqrt{1 + r_{,z}^2}} \right)_{,z} \right) \delta r dz = 0 \quad (3.35)$$

It is obvious that equation (3.35) can only be fulfilled if the term in the brackets will be equal to zero. Therefore, the governing equation of the equilibrium of forces can be given by:

$$\sigma_r \sqrt{1 + r_{,z}^2} - \left(\sigma_m \frac{r r_{,z}}{\sqrt{1 + r_{,z}^2}} \right)_{,z} = 0 \quad (3.36)$$

By taking the derivative and doing some algebraic operations (e.g. dividing the equation by the radius r), the governing equation can be rewritten as follows:

$$\begin{aligned} (\sigma_r - \sigma_m) r_{,z}^2 \left(\frac{1}{r \sqrt{1 + r_{,z}^2}} \right) + \sigma_{m,z} \frac{r_{,z}}{\sqrt{1 + r_{,z}^2}} \\ + \sigma_r \underbrace{\left(-\frac{1}{r} \frac{1}{\sqrt{1 + r_{,z}^2}} \right)}_{k_r} - \sigma_m \underbrace{\left(\frac{r_{,zz}}{(1 + r_{,z}^2)} \right)}_{k_m} = 0 \end{aligned} \quad (3.37)$$

The first line of equation (3.37) can be identified as the equilibrium in the in-plane direction of the surface. The second line represents the out-of-plane equilibrium and is identical to the Young-Laplace equation as defined in equation (3.2) with the absence of an external pressure force. Due to that it is possible to formulate two individual equilibrium requirements. In the in-plane direction the following condition has to be satisfied:

$$(\sigma_r - \sigma_m) r_{,z}^2 \left(\frac{1}{r \sqrt{1 + r_{,z}^2}} \right) + \sigma_{m,z} \frac{r_{,z}}{\sqrt{1 + r_{,z}^2}} = 0 \quad (3.38)$$

In the out-of-plane the simplified Young-Laplace equation represents the equilibrium:

$$\sigma_r k_r + \sigma_m k_m = \frac{\sigma_r}{R_r} + \frac{\sigma_m}{R_m} = 0 \quad (3.39)$$

Based on the derived equations it is possible to discuss the individual prestress characteristics:

Isotropic prestress: $\sigma_r = \sigma_m = \text{const}$ and $\sigma_{m,z} = 0$

It can be seen that in case of isotropic prestress the in-plane equilibrium equation (3.38) is always fulfilled, independent of the shape of the surface. From the out-of-plane case the requirement is defined, that at each point of the surface the radii in radial and meridian direction have to be equal and of opposite sign. Due to that it can be concluded that in case of isotropic prestress definition, the resulting surface has to have an anticlastic curvature. This has the result that all spatial tensile

3.3 Stabilization of the inverse problem

structures with isotropic prestresses are non-developable, except of the special case of plane surfaces where one radius tends to infinity.

Constant anisotropic prestress: $\sigma_r \neq \sigma_m = \text{const}$ and $\sigma_{m,z} = 0$

By substituting the conditions for a constant anisotropic prestress definition into the governing equations it turns out that it is impossible to satisfy the in-plane equilibrium. The only exception is in the special case that the derivative of the radius is equal to zero $r_{,z} = 0$, which results in a surface with constant radius over the height (i.e. a cylinder). The out-of-plane equilibrium can be satisfied, as the radii in radial and meridian direction are unequal at each point of the surface. Hence, with the definition of a constant anisotropic prestress the shape of the surface can be modified in an effective way, but it is impossible to achieve equilibrium in the in-plane direction.

Anisotropic prestress: $\sigma_r \neq \sigma_m$ and $\sigma_{m,z} \neq 0$

With the definition of a non-constant prestress distribution along the surface lines it is possible to satisfy the in plane as well as the out of plane equilibrium. Due to that, as for the isotropic case, a unique solution for the form finding problem can be achieved. It is obvious, that the definition of such a prestress situation introduces some major difficulties, as the prestresses in the radial and meridian direction have to fit to the derivative of the meridian direction to satisfy the in plane equilibrium equation. Due to that, the general anisotropic case can't be used effectively for the definition of the prestress.

Summarizing the different effects from the prestress situations to the equilibrium equations, the conclusion can be made that only in the case of the isotropic prestress can a unique solution be achieved with an acceptable effort. In case of the constant anisotropic prestress there doesn't exist a solution for the form finding problem. With the choice of a well defined general anisotropic prestress, a unique solution could be found, but from a practical point of view this type of definition can't be applied in a straightforward fashion for the form finding. In the following, based on this discussion the individual prestress situations will be described with the effects on the governing equations as well as on the process of the URS. For anisotropic situations an alternative possibility in defining the prestress will be presented.

3.3.1.4 Isotropic prestress

In case of an isotropic prestress the coefficients of the stress tensor are identical in both local Cartesian directions. Additionally, the shear stresses are zero. Based on this, the prestress tensor σ_0 can be given in a simplified form:

$$\sigma_0 = \sigma_0^{\alpha\beta} \mathbf{g}_\alpha \otimes \mathbf{g}_\beta = \bar{\sigma} \mathbf{I} = \bar{\sigma} g^{\alpha\beta} \mathbf{g}_\alpha \otimes \mathbf{g}_\beta \quad (3.40)$$

In equation (3.40) the prestress tensor is defined as the product of the identity matrix \mathbf{I} and a scalar value $\bar{\sigma}$ which can be understood as a stress intensity factor. For this situation the assumption of equal prestress coefficients in the reference and the current configuration can be reduced to the assumption that in both configurations the stress intensity factors are equal $\bar{\sigma} = \bar{S}$. \bar{S} and $\bar{\sigma}$ represent the stress intensity factors in the reference and current configurations, respectively. Therefore, the

prestress for the stabilization part can be given by:

$$\mathbf{S}_0 = S_0^{\alpha\beta} \mathbf{G}_\alpha \otimes \mathbf{G}_\beta = \bar{S} \mathbf{I} = \bar{S} G^{\alpha\beta} \mathbf{G}_\alpha \otimes \mathbf{G}_\beta = \bar{\sigma} G^{\alpha\beta} \mathbf{G}_\alpha \otimes \mathbf{G}_\beta \quad (3.41)$$

For the case of isotropic prestress it is possible to validate the derived governing equations for the form finding problem. For the validation of this type of prestress, soap film models as described in section 3.1 can be applied. The surfaces which are found by soap film models will result in a minimal surface content within given boundaries. The connection between the pure geometrical and the mechanical model is the overall prestress in the surface, as minimal surfaces are characterized by an isotropic stress distribution. For centuries mathematicians have worked on the solution for minimal surfaces for different cases of boundary conditions [Die10]. The experimental work of Joseph Plateau in the 19th Century was one of the most important contributions to this research. Examples for minimal surfaces from mathematics are illustrated in figure 3.10.

From a mathematical point of view, the minimum of area content a can be derived by the vanishing variation δa :

$$\delta a = \delta \int_a da = 0 \quad (3.42)$$

By applying Nanson's relation defined in equation (2.40), the variation of the area content can be formulated as follows:

$$\delta a = \delta \int_A \det \mathbf{F} dA = 0 \quad (3.43)$$

The variation of the determinant of the deformation gradient can be given by [BR99]:

$$\delta (\det \mathbf{F}) = \det \mathbf{F} \mathbf{F}^{-T} : \delta \mathbf{F} \quad (3.44)$$

Substituting equation (3.44) into equation (3.43), the variation of the area content can be derived as follows:

$$\delta a = \int_A \det \mathbf{F} \mathbf{F}^{-T} : \delta \mathbf{F} dA = 0 \quad (3.45)$$

Applying the definitions for isotropic prestress from equation (3.40) to the derived equation for the original part of the URS defined in equation (3.10), the principle of virtual work can be given by:

$$\begin{aligned} -\delta W &= t \int_A \det \mathbf{F} \left(\boldsymbol{\sigma}_0 \mathbf{F}^{-T} \right) : \delta \mathbf{F} dA \\ &= t \int_A \det \mathbf{F} \left(\bar{\sigma} \mathbf{I} \mathbf{F}^{-T} \right) : \delta \mathbf{F} dA \\ &= t \bar{\sigma} \int_A \det \mathbf{F} \mathbf{F}^{-T} : \delta \mathbf{F} dA = 0 \end{aligned} \quad (3.46)$$

3.3 Stabilization of the inverse problem

The comparison of equation (3.45) and equation (3.46) illustrates that the mechanically motivated derived equations are identical to the geometrical equation except for the scalar factor $t\bar{\sigma}$. Therefore, the solution of the form finding problem with isotropic prestress, can be seen as identical to the solution for finding minimal surfaces. Of course, surfaces with an isotropic prestress definition aren't exclusively

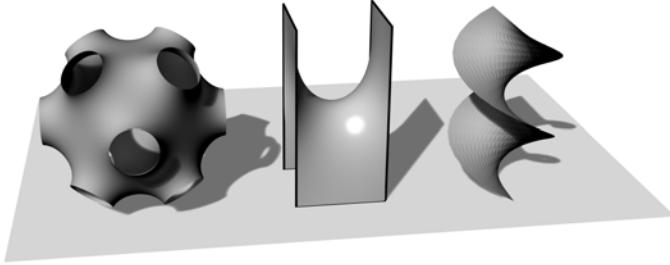


Figure 3.10: Minimal surfaces created by applying the URS (left: Schön minimal surface; center: Scherk minimal surface; right: Helicoid;)

restricted to the application for mathematically motivated surfaces. Various of existing tensile structures are based on the assumption of isotropic prestress fields. Certainly, one of the most prominent is the roof of the Olympic Stadium in Munich. Despite this structure being a cable net, the overall shape of the surface can be found by the application of membrane elements. In figure 3.11 the numerical recalculation of the form finding for the roof, based on the URS is illustrated.

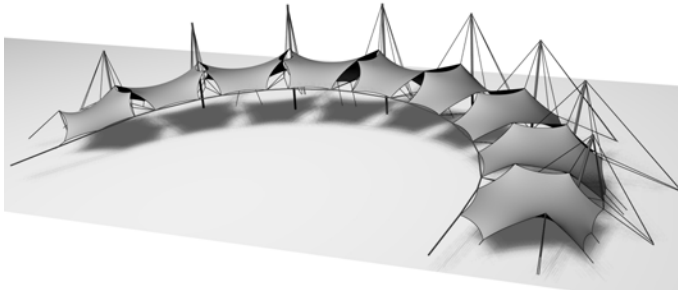


Figure 3.11: Form finding result for the roof of the Olympic Stadium in Munich (recalculation)

3.3.1.5 Anisotropic prestress

In section 3.3.1.3 it was discussed that in general, for a constant anisotropic prestress definition, there exists no solution for the form finding problem. From a

design point of view the restriction to isotropic prestress would result in a major drawback for the application of tensile structures. Due to the fact that the resulting minimal surfaces are characterized by slightly curved areas, the potential of ponding or snow accumulations is decisive. To prevent this surface characteristic in common practice, the definition of anisotropic prestress is applied to generate sufficiently curved shapes. As shown in section 3.3.1.3 the only possibility to achieve anisotropic prestress is to accept variations from the intended prestress state and to define a general anisotropic prestress.

To achieve the shape of equilibrium with a variation in the prestress field, various methodologies are available. One of simplest methods is to limit the form finding process to a fixed number of steps. This means that the process of solving the governing equations and the updating of the reference configuration will be defined in advance. Of course, in each form finding step, deformations will be evaluated, as the equilibrium can be never satisfied. Therefore, in each form finding step a difference between the predefined 2. Piola Kirchhoff stress \mathbf{S}_0 and the Cauchy stresses $\boldsymbol{\sigma}$ will remain. It is important to note that due to the solution of the equilibrium in the URS, the current configuration in each intermediate form finding step is in equilibrium w.r.t. the current Cauchy stresses $\boldsymbol{\sigma}_{cur}$. Based on this, the process for the form finding of anisotropic prestressed tensile structures can be applied as follows: (i) Define an anisotropic prestress and a maximum number of form finding steps; (ii) The current configuration in the last form finding step and the current stresses $\boldsymbol{\sigma}_{cur}$ represent the shape of equilibrium. The current Cauchy stresses can be evaluated based on equation (2.57) as given as follows:

$$\boldsymbol{\sigma}_{cur} = \frac{1}{\det \mathbf{F}} \mathbf{F} \mathbf{S}_0 \mathbf{F}^T \quad (3.47)$$

The approach of terminating the form finding after a certain number of steps will introduce the drawback that the resulting surface is weakly defined, as the result depends on the initial reference configuration and the number of form finding steps. In order to introduce a possibility to have an influence on the final shape, methods based on the results of the clothesline example in section 3.1 have been developed. In the clothesline example it was shown that in principle either the prestress or the final geometry can be predefined to solve the form finding problem. In [WB05], [Wüc07] and [LB10] a method is introduced which enables the control of the form finding for anisotropic prestress situations by geometrical constraints. Here, the control of the geometry is achieved by controlling the distortion of the finite elements.

Distortion Control Method: The main idea of the distortion control method is to control the mesh distortion of the finite elements. In principle, the method can be described on the basis of the example of the clothesline from figure 3.1. In the case of the clothesline, the maximum deformation f could be set to a fixed value. It is obvious that in the case of tensile structures the overall shape can't be defined in advance by prescribing a few selected parameters. Therefore, the method uses the maximum allowable deviation from the initial defined reference configuration. This is achieved by the measurement of the distortion in terms of the principal stretches which are defined in section 2.4.2.

3.3 Stabilization of the inverse problem

To control the distortion of the surface, a maximal allowable configuration of the deformation will be defined. With this definition and the initially defined reference configuration, the upper and lower bounds of the distortion are set. Based on these definitions, the distortion control can be formulated in terms of continuum mechanics by the maximum allowable deformation gradient \mathbf{F}_{\max} . In each form finding step the current total deformation gradient \mathbf{F}_{tot} can be compared to the maximum allowed deformation. The prestress values can be modified for the next step to ensure that the deformation will remain in the defined boundaries. In figure 3.12 the individual configurations are illustrated.

In the distortion control method in each form finding step the principal stretches λ_{α}^i

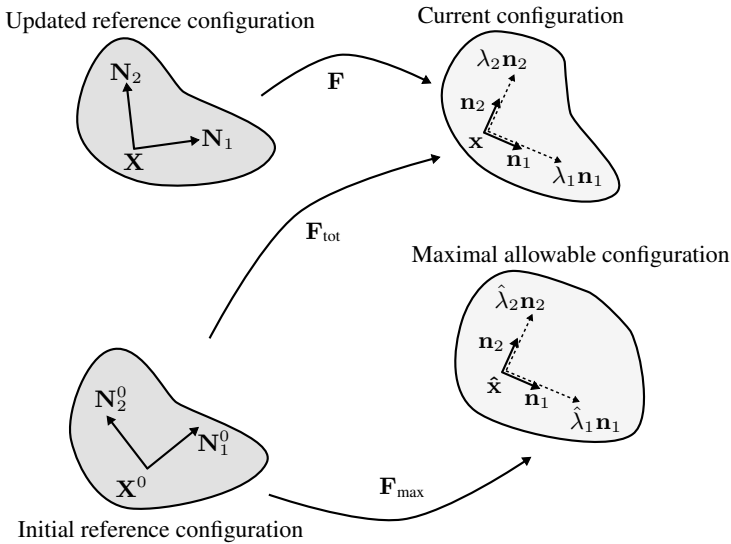


Figure 3.12: Configurations for the distortion control method [Lin09]

are evaluated. Subsequently, these stretches are compared to the allowed extremes. If one of them is violated, the prestress tensor has to be modified. The deformation in a form finding step i exceeds the allowed limits if:

$$\lambda_{\alpha}^i > \lambda_{\max} \quad \text{or} \quad \lambda_{\alpha}^i < \frac{1}{\lambda_{\max}} = \lambda_{\min} \quad (3.48)$$

If the principal stretch in a form finding step fulfills one of the conditions in equation (3.48), a modified prestress field for the next form finding step will be evaluated, which ensures that the distortion of the Finite Element will remain within the defined boundaries. In order to evaluate the modified prestress, the maximum allowable deformation gradient has to be computed. Therefore, the allowable de-

formation gradient can be given by:

$$\mathbf{F}_{\max}^i = \hat{\lambda}_{\alpha}^i \mathbf{n}_{\alpha}^i \otimes \mathbf{N}_{\alpha}^0$$

$$\text{with } \hat{\lambda}_{\alpha}^i = \begin{cases} \lambda_{\max} & \text{for } \lambda_{\alpha}^i > \lambda_{\max} \\ 1 & \text{for } \lambda_{\alpha}^i < \frac{1}{\lambda_{\max}} \\ \lambda_{\alpha}^i & \text{other cases} \end{cases} \quad (3.49)$$

Additionally, the total deformation gradient between the initial and the current configuration can be obtained by:

$$\mathbf{F}_{\text{tot}}^i = \lambda_{\alpha}^i \mathbf{n}_{\alpha}^i \otimes \mathbf{N}_{\alpha}^0 \quad (3.50)$$

Based on the deformation gradients, the modified prestress field can be evaluated as described in [WB05]:

$$\begin{aligned} \boldsymbol{\sigma}_{\text{mod}}^i &= \frac{\det \mathbf{F}_{\max}^i}{\det \mathbf{F}_{\text{tot}}^i} \mathbf{F}_{\text{tot}}^i \left(\mathbf{F}_{\max}^i \right)^{-1} \boldsymbol{\sigma}^i \left(\mathbf{F}_{\max}^i \right)^{-T} \left(\mathbf{F}_{\text{tot}}^i \right)^T \\ &= \frac{\hat{\lambda}_1 \hat{\lambda}_2 \lambda_{\alpha} \lambda_{\beta}}{\lambda_1 \lambda_2 \hat{\lambda}_{\alpha} \hat{\lambda}_{\beta}} \boldsymbol{\sigma}^{\alpha\beta,i} \mathbf{n}_{\alpha}^i \otimes \mathbf{n}_{\beta}^i \end{aligned} \quad (3.51)$$

The modified prestress will be applied for the next form finding step. It is obvious, that the modification of the prestress has to be made for each evaluation point of the governing equations (e.g. Gaussian integration points). Therefore, the resulting prestress distribution in the surface is highly nonlinear and deviates from the predefined one. Because of this, the initially defined prestress can be understood as an approximative guess of the resulting stresses. As the distortion control method switches the major input from the prestress to the geometry, the governing equations can be reduced to the stabilization term from equation (3.14). This means that the homotopy factor can be set to zero ($\lambda = 0$).

In principle, the distortion control can be described as a restriction of the possible geometrical design space. For example, if the maximum principal stretch is fixed to 1 ($\lambda_{\max} = 1$), the surface content has to remain equal as defined by the initial reference configuration. As a consequence, the final solution is now depending on the initial guess of the form finding problem which is not arbitrary anymore as it has a major influence on the final design. In figure 3.13 the result for different maximum allowable stretches is illustrated for the case of a simple cylindrical example. It can be seen that with decreasing λ_{\max} the resulting shape of equilibrium tends towards the initial reference configuration.

Since the prestress is indirectly controlled by the adapted geometry the final stress distribution has to be checked against allowable values concerning material properties and design practice.

For the discussion of the resulting prestress distribution the form finding for the well known *Chinese Hat* will be discussed in the following [MM98], [RW04]. In

3.4 eXtended Updated Reference Strategy (X-URS)

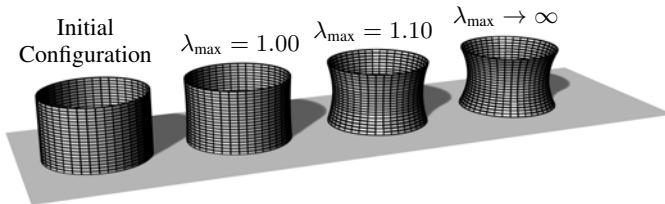


Figure 3.13: Catenoid for different values of λ_{\max}

this example a top ring and a bottom ring are defined. The radii of these two rings are different. The top ring has the radius $R_{\text{top}} = 4.0$ and the bottom radius is defined as $R_{\text{bottom}} = 20.0$. The initial reference configuration is defined as a cone between the two radii. The initial predefined prestress will be isotropic and has a unit value. The maximum allowable stretch is defined as 1.1. The resulting surface and the prestress distribution in warp and weft directions is illustrated in figure 3.14. It can be seen that the maximum stress ratio in radial and circumferential direction has a ratio of approximately $r = \sigma_{\text{warp}}/\sigma_{\text{weft}} \cong 4.5$. The resulting prestress distribution is purely based on the definition of the allowable stretch and for other values the result would differ from that illustrated. From a practical point of view it has to be discussed if such a stress distribution can be realized. The task of introducing such prestress values into the tensile structure has to be considered as well as the task of finding a material which has a long term behavior such that the prestress distribution can be kept over time. It has to be ensured that the material doesn't compensate the prestress towards an isotropic situation due to creep in time. The distortion control method enlarges the design space for tensile structures, but the practicability has to be discussed in each case.

3.4 eXtended Updated Reference Strategy (X-URS)

In the previous sections the Updated Reference Strategy was introduced. Additionally, different aspects of the solution process were included. The influence of isotropic and anisotropic prestress definitions were discussed as well as the introduction of the distortion control method to include geometrical constraints. In the discussion of the form finding problem it can be seen that just for isotropic prestress definitions a unique solution can be given and the application of the URS allows one to approximate the shape of equilibrium up to small numerical deviations. However, the homotopy factor has to be chosen for a defined number of form finding steps. In the following, a modified version of the URS will be presented which is able to evaluate the exact shape of equilibrium without defining a homotopy factor.

The *eXtended Updated Reference Strategy* (X-URS) modifies the singular problem in such a way, that the singular term is removed from the residual equation. The idea is to split the residual forces into parts in order to identify the singularity. Based on the separated form of the residuum it is possible to modify the governing

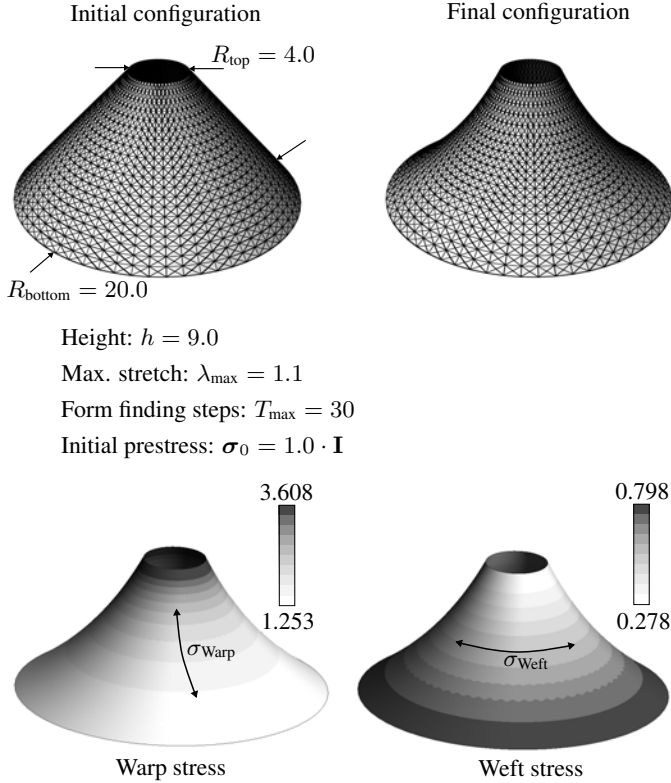


Figure 3.14: Warp and Weft stress for the Chinese Hat

equations to eliminate the problematic parts. Before the modification can be done, the principle structure of the residuum derived in equation (3.4) and equation (3.16) has to be discussed in detail. In the following the residual equation are discussed without the presence of external forces, as this part does not change in comparison to the original derivations. The overall residuum is given by:

$$\begin{aligned}
 R_r &= t\lambda \int_a \sigma_0 : \frac{\partial \mathbf{e}}{\partial u_r} da + t(1-\lambda) \int_A \mathbf{S}_0 : \frac{\partial \mathbf{E}}{\partial u_r} dA = 0 \\
 &= \lambda R_{r,\sigma_0} + (1-\lambda) R_{r,\mathbf{S}_0} = 0
 \end{aligned} \tag{3.52}$$

As already discussed in section 3.2 the singularity originates from the residual force based on the original term R_{r,σ_0} . In more detail, the part of the force which points in the tangential direction of the surface is responsible for the singularity in the governing equation. In order to identify this part, it is important to note that the

3.4 eXtended Updated Reference Strategy (X-URS)

residual force represents an unbalanced force at the node. As every other force, the residuum can be split in individual parts aligned with certain directions. In this case, the residuum will be split into components in the direction of the normal \mathbf{n} and the tangent \mathbf{t} to the surface. In figure 3.15 the described split is illustrated. From

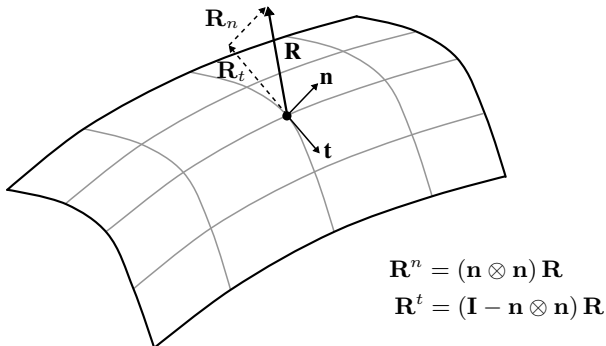


Figure 3.15: Separation of the residual force into normal and tangential direction

a mathematical point of view the split of the residuum force into certain directions can be made by the projection of a vector onto another vector. Based on this mathematical operation, the part of the residual force which is aligned with the normal direction can be obtained by:

$$\mathbf{R}^n = (\mathbf{n} \otimes \mathbf{n}) \mathbf{R} \quad (3.53)$$

With the same operation, the part of the residual force which is aligned with the tangential direction could be achieved. In order to avoid the direct evaluation of the tangential direction, this part is obtained by the difference of the actual force and by the one aligned to the normal:

$$\mathbf{R}^t = (\mathbf{I} - \mathbf{n} \otimes \mathbf{n}) \mathbf{R} \quad (3.54)$$

Based on the forces acting in normal and tangential direction the overall residual force can be represented by the summation of the two separated parts at a certain node of the finite element discretization. The rewritten governing equation of the URS, based on equation (3.52), for every node can be given by:

$$\mathbf{R} = \lambda (\mathbf{R}_{\sigma_0}^n + \mathbf{R}_{\sigma_0}^t) + (1 - \lambda) (\mathbf{R}_{S_0}^n + \mathbf{R}_{S_0}^t) = 0 \quad (3.55)$$

Note, that at every node the 3-dimensional vector \mathbf{R} is composed of the Cartesian components R_r as of equation (3.52) which refers to the spatial displacement parameters u_r . With the separated representation of the residual form, as given in equation (3.55), the part which causes the singularity in the system matrix can be identified. The force aligned with the tangential direction based on the original part $\mathbf{R}_{\sigma_0}^t$ can be identified as responsible for the singularity. As already introduced,

the second part in equation (3.55) is defined to stabilize the overall equation in the tangential direction. It can be seen, that the stabilization part also effects the non-singular normal force which defines the nodal position in space of the form found geometry. The influence of the stabilization part on the normal direction decreases the speed of convergence of the overall process. The separated form offers the possibility to only take into account the parts which are important in order to solve the form finding problem. It is obvious, that the normal part of the original problem $\mathbf{R}_{\sigma_0}^n$ is crucial as it defines the nodal position in space. The tangential part of the stabilization term $\mathbf{R}_{\mathbf{S}_0}^t$ is also needed in order to stabilize the overall problem. The parts which can be neglected are the tangential part of the original problem $\mathbf{R}_{\sigma_0}^t$ as it causes the singularity and introduces no additional information to the governing equation. The normal part of the stabilization problem $\mathbf{R}_{\mathbf{S}_0}^n$ can be neglected as well, as it just slows down the overall convergence and also introduces no additional information. Obviously, applying this modification would lead to a non-singular problem. Due to that, the homotopy mapping is not necessary anymore. This means, that the homotopy factor λ can be neglected and the nonlinear problem can be solved directly. Based on the described modifications, the governing equation for the *eXtended Updated Reference Strategy* can be given in the nodal form as follows:

$$\mathbf{R}_{\text{X-URS}} = \mathbf{R}_{\sigma_0}^n + \mathbf{R}_{\mathbf{S}_0}^t = (\mathbf{n} \otimes \mathbf{n}) \mathbf{R}_{\sigma_0} + (\mathbf{I} - \mathbf{n} \otimes \mathbf{n}) \mathbf{R}_{\mathbf{S}_0} = 0 \quad (3.56)$$

From a theoretical point of view, the solution of the form finding problem with the X-URS represents the analytical shape of equilibrium. It is important to note, that this property only holds if no tangential mesh deformations are needed to achieve the final solution. This is obvious, as the tangential part of the equation is purely based on the stabilization term. This can be summarized as follows: The X-URS solves the form finding problem in the normal direction exactly within the first form finding step and approximates the in plane deformation as it is done in the force density method.

The introduced split of the governing equations can also be found for other types of form finding methodologies. In the case of the dynamic relaxation in [BL03], a similar idea is discussed.

For the separation of the residual equation, the normal vector at each node is introduced. Of course, the normal vector of the current configuration has to be used in order to describe the shape of equilibrium at the end of the nonlinear process. By applying a Finite Element Method for the solution of the X-URS at each node, there are as many normals as elements. In order to compute one single normal vector for each node, an approximation of the true surface normal vector has to be made. For this, an averaging of the individual normal vectors of the surrounding finite elements at the node is necessary. In principle, the averaging can be done by just summing up the individual normals and doing a normalization to ensure a length of one for the normal vector. This basic idea of averaging doesn't take into account that the mesh size of adjacent elements could differ. In order to achieve a most fitted approximation of the true surface normal the influence of different mesh sizes has to be taken into account. In [LWB07] the idea of a weighting factor for the individual mesh normals is discussed. By multiplying the individual normals

3.4 eXtended Updated Reference Strategy (X-URS)

\mathbf{n}_k^i with a weighting factor w_{ki} the averaged surface normal at a certain node can be obtained as follows:

$$\mathbf{n}_k = \frac{\sum_{i=1}^{n_{\text{elem}}} w_{ki} \mathbf{n}_k^i}{\left\| \sum_{i=1}^{n_{\text{elem}}} w_{ki} \mathbf{n}_k^i \right\|} \quad (3.57)$$

There exist various possibilities in choosing the weighting factor for the individual nodal normals. In [Wak99] the weighting factor is given as the inverse of the area content of the considered element. Based on this in [Lin09] the difference between triangle and quadrilateral elements is additionally taken into account:

$$w_{ki,\text{tria}} = \frac{1}{\|\mathbf{g}_{ki,1} \times \mathbf{g}_{ki,2}\|} \quad (3.58)$$

$$w_{ki,\text{quad}} = \frac{1}{4 \cdot \|\mathbf{g}_{ki,1} \times \mathbf{g}_{ki,2}\|}$$

A detailed discussion on the influence of different weighting factors for triangular meshes is presented in [UEG13]. Of course, the influence of the weighting factor decreases if a regular mesh of the same element type is applied.

Due to the introduction of the mean normal vector in the governing equation, the number of degrees of freedom for the nodal residual force will change. The introduced mean normal depends on all degrees of freedom of the nodes which are included into its evaluation. Due to that, for the computation of the system matrix, in order to solve the nonlinear problem by a Newton-Raphson algorithm, the residual force at the node has to be derived w.r.t. to all nodes which are included in the patch of elements. In figure 3.16, the influence on the residual forces at the nodes of an element for the standard case and the patch case is illustrated. The residual forces

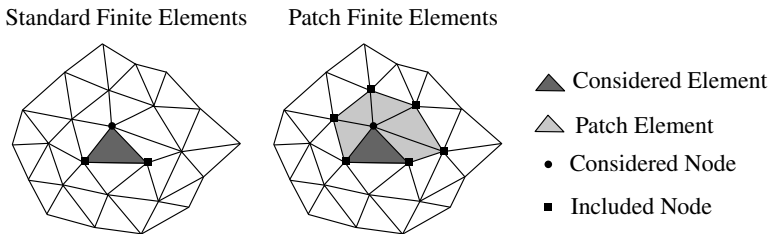


Figure 3.16: Patch of finite Elements to compute the mean surface normal

will be evaluated from the variation of the virtual work w.r.t. the nodal degrees of freedom, like in the standard Finite Element case from figure 3.16. Evaluating the elemental system matrix for the Newton Raphson method, the number of degrees of freedom will be changed to those included in the patch.

The simplest form of deriving the system matrix for the solution with a Newton-Raphson method is to stay in the form of nodal quantities. The resulting entities for

the system matrix of a certain node can be given by the derivative of the modified residual forces w.r.t. the patch's degrees of freedom:

$$\begin{aligned} \frac{\partial \mathbf{R}_{\text{X-URS}}}{\partial \bar{u}_j} &= \left(\frac{\partial \mathbf{n}}{\partial \bar{u}_j} \otimes \mathbf{n} + \mathbf{n} \otimes \frac{\partial \mathbf{n}}{\partial \bar{u}_j} \right) \mathbf{R}_{\sigma_0} + (\mathbf{n} \otimes \mathbf{n}) \frac{\partial \mathbf{R}_{\sigma_0}}{\partial \bar{u}_j} \\ &\quad - \left(\frac{\partial \mathbf{n}}{\partial \bar{u}_j} \otimes \mathbf{n} + \mathbf{n} \otimes \frac{\partial \mathbf{n}}{\partial \bar{u}_j} \right) \mathbf{R}_{\mathbf{S}_0} + (\mathbf{I} - \mathbf{n} \otimes \mathbf{n}) \frac{\partial \mathbf{R}_{\mathbf{S}_0}}{\partial \bar{u}_j} \end{aligned} \quad (3.59)$$

The resulting force vector has to be assembled into the system matrix. It is important to note, that the three components of the residual force vector have to be derived w.r.t. all nodal degrees of freedom in the patch. The resulting matrix has the dimension $3 \times n_{\text{dof,patch}}$. For each node of an element, this type of matrix is achieved. In principle it is possible to assemble all of the nodal matrices into a single matrix which can be interpreted as the "elemental system matrix". As the number of rows of the force vector and the nodal degrees of freedom are equal, the size of the resulting elemental system matrix is $n_{\text{dof,element}} \times n_{\text{dof,patch}}$. Of course, this characteristic of the elemental system matrix in the X-URS causes special assembling algorithms in the context of the Finite Element Method. Another characteristic for this formulation of the X-URS is w.r.t. to the symmetry of the system matrix. As the governing equation is modified during the linearization, the resulting global system matrix is non-symmetric. Due to that, special solvers, which are able to deal with non-symmetric matrices are needed for the solution of the linear system of equations. Of course, this characteristic originates from the choice of solution approach of the X-URS. An alternative formulation can be described, which keep the symmetry of the system matrix and make use of standard assembling routines. The modification of the URS can also be applied for the incremental form of the residual equation, which is defined as follows:

$$(\lambda \mathbf{K}_{\sigma_0} + (1 - \lambda) \mathbf{K}_{\mathbf{S}_0}) \Delta \mathbf{u} = -(\lambda \mathbf{R}_{\sigma_0} + (1 - \lambda) \mathbf{R}_{\mathbf{S}_0}) \quad (3.60)$$

The involved system matrices \mathbf{K}_{σ_0} and $\mathbf{K}_{\mathbf{S}_0}$ are symmetric. It is possible to transform equation (3.60) into the local directions defined by the surface normal \mathbf{n} and the tangential vectors \mathbf{t}_i . Related to this transformation the evaluated variables $\Delta \mathbf{u}$ are no longer aligned with the 3-dimensional spatial directions but with the local directions aligned with the normal and the tangential vectors. The changed variables will be indicated by $\Delta \bar{\mathbf{u}}$. The transformed equation system can be given such:

$$\left(\lambda \underbrace{\mathbf{T}^T \mathbf{K}_{\sigma_0} \mathbf{T}}_{\bar{\mathbf{K}}_{\sigma_0}} + (1 - \lambda) \underbrace{\mathbf{T}^T \mathbf{K}_{\mathbf{S}_0} \mathbf{T}}_{\bar{\mathbf{K}}_{\mathbf{S}_0}} \right) \Delta \bar{\mathbf{u}} = - \left(\lambda \underbrace{\mathbf{T}^T \mathbf{R}_{\sigma_0}}_{\bar{\mathbf{R}}_{\sigma_0}} + (1 - \lambda) \underbrace{\mathbf{T}^T \mathbf{R}_{\mathbf{S}_0}}_{\bar{\mathbf{R}}_{\mathbf{S}_0}} \right) \quad (3.61)$$

In equation (3.61) \mathbf{T} indicates the respective transformation matrix. Based on the resulting local versions of the system matrices $\bar{\mathbf{K}}_{\sigma_0}$ and $\bar{\mathbf{K}}_{\mathbf{S}_0}$, which are still symmetric, the parts which are aligned with the normal and tangential vectors can be again identified and separated. Therefore, it is possible to integrate the ideas from the X-URS again in the solution of the form finding problem. For the numerical process, the modified matrices can be transformed into the original spatial variables

3.4 eXtended Updated Reference Strategy (X-URS)

$\Delta \mathbf{u}$ for the integration in standard Finite Element software. As neither the transformations nor the modifications influences the symmetry of the system matrices the final equation system keeps symmetric as well. For the following examples the first, non-symmetric, version of the X-URS formulation will be used, as no modification on the matrix level has to be done.

As the X-URS solves the form finding problem without any compromises in the normal direction, the final solution for the shape of equilibrium can be found within one form finding step. To illustrate the principle behavior, the convergence of the method will be discussed on the basis of the Schwarz minimal surface (see figure 3.17). The surface is discretized with 4 finite elements in order to reduce the example to a single degree of freedom system, as for the middle node just vertical displacements occur. For the correct solution of the form finding problem, the residual equation should be zero for the final position of the middle node. In figure 3.17 the example for this investigation is illustrated. The final position of the

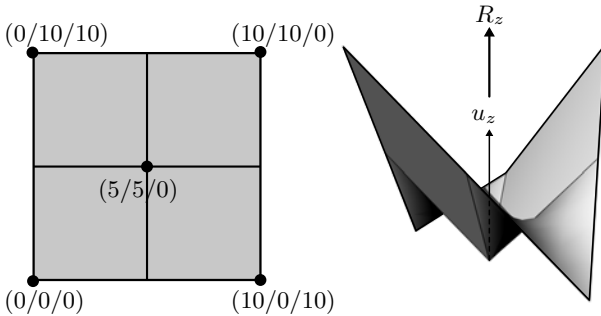


Figure 3.17: Schwarz minimal surface reference configuration; top view (left); isometric view (right)

middle node in the final configuration can be given at the height of 5, which is in the middle between the high and low points of the surface. This means for the displacement of 5, the residual equation should be 0 if it is able to represent the final solution. In figure 3.18 the residual forces for the Force Density Method (URS with the special choice of $\lambda = 0$), the Updated Reference Strategy for different choices of λ and the extended Updated Reference Strategy are illustrated. Here the individual residual forces are measured while varying the deformation. From figure 3.18 it can be seen that only the eXtended Updated Reference Strategy is able to obtain the correct solution within the first form finding step. As the residual forces are equal to zero for the analytical solution of $u_z = 5$. All other methods have zero values for the residual forces for a different displacement. Based on this, it is obvious why additional form finding steps are needed to converge to the final solution for these methods. The Force Density method shows the worst convergence within the first form finding step, while the URS convergences to the final solution with increasing

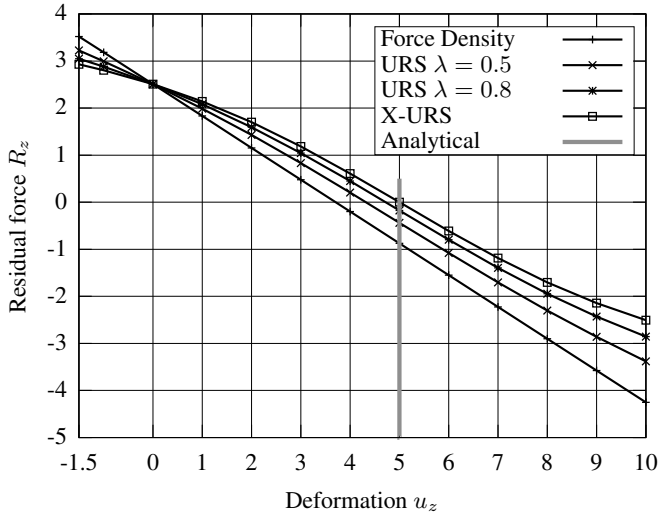


Figure 3.18: Residual forces for the Schwarz minimal surface with varying deformations for different form finding methods

homotopy factors λ . It should be stated at this point, that the nonlinearity increases from Force Density to X-URS. When applying the force density method to a form finding problem in each form finding step, only a linear system has to be solved. This advantage has the price of an increasing amount of form finding steps. In contrast the X-URS leads to a nonlinear problem in each form finding step but with a decreased number (in the best case, just one) of necessary form finding steps.

The performance of the X-URS can also be seen on the example of the Catenoid minimal surface illustrated in figure 3.19. For this example the convergence of the deformation with different form finding methods is compared. Again the Force Density Method and the Updated Reference Strategy are used for the comparison. As the Catenoid is a minimal surface, the prestress is defined as $\sigma_0 = \sigma_0 \mathbf{I}$ and a unit thickness is assumed. Based on the resulting convergence graphs in figure 3.20 it can be seen that the X-URS is able to solve the form finding problem within one form finding step. In this example, the first form finding step is done based on the force density method which ensures that all methods are going to start from the same configuration. The URS with an optimized homotopy mapping converges slower than the X-URS but still faster than the Force Density Method. Of course, it has to be discussed if the savings in form finding steps is canceled by the increased amount of iteration steps in one form finding step for the X-URS.

For this purpose in figure 3.21 the error for the individual analyses is shown w.r.t. the overall iteration steps. Here, the error is defined for a certain point, where the

3.4 eXtended Updated Reference Strategy (X-URS)

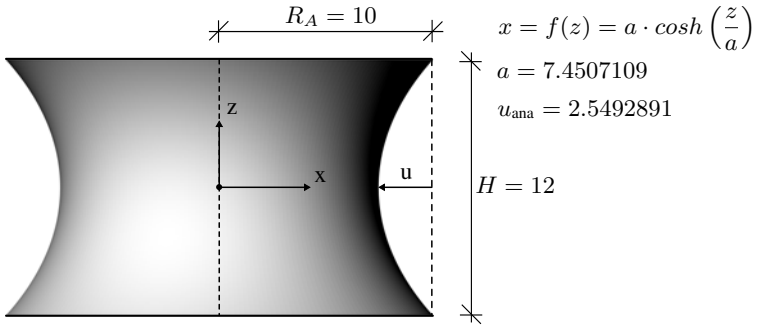


Figure 3.19: Catenoid minimal surface

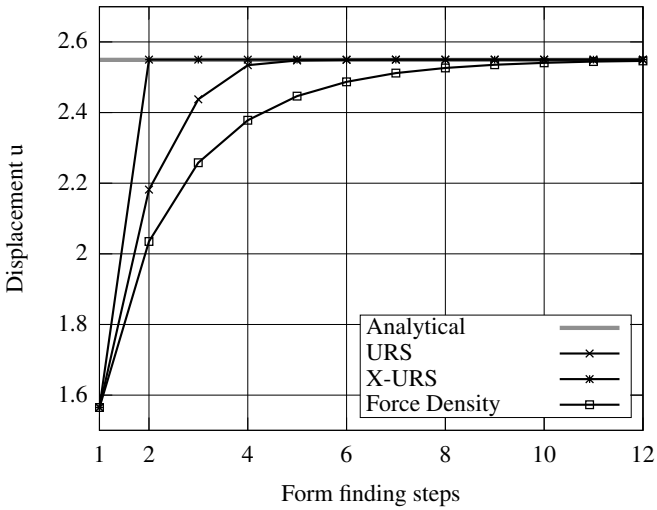


Figure 3.20: Displacement convergence for the Catenoid minimal surface

analytical deformation is known in advance. The error can be evaluated as follows:

$$\varepsilon = \frac{|u_{\text{analytical}} - u_{\text{numerical}}|}{u_{\text{analytical}}} \quad (3.62)$$

It can be seen, that the X-URS needs the least number of iteration steps and is able to achieve the analytical solution to machine precision. Both, the Force Density and the URS, are just able to approximate the exact solution. Based on the comparison of the Force Density and the URS it is interesting to note, that both methods need the same number of iteration steps to achieve the almost same exactness. Of course, the solution based on the URS can be optimized by modifying the choice of the homotopy factor. The sequence of solution and update the reference configuration are getting obvious in figure 3.21 for the URS.

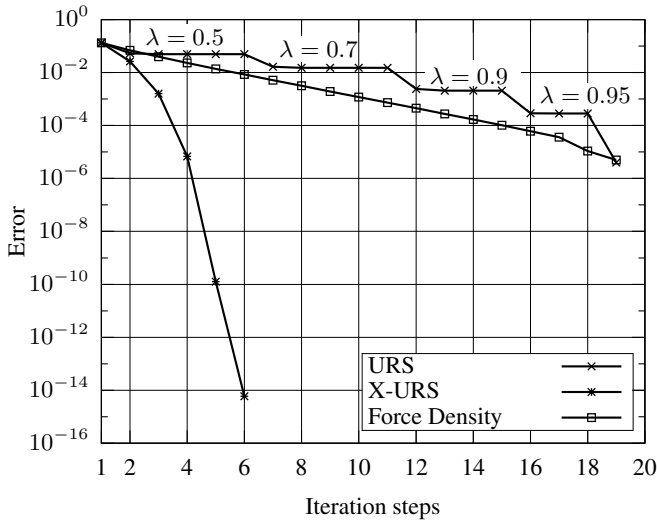


Figure 3.21: Error plot for the Catenoid minimal surface for the overall iteration steps

As a more practical motivated example a 4 point tent will be discussed. The 4 point tent has a base length of 10.0 by 10.0 and a height of 10.0 as illustrated in figure 3.22. The prestress in this case is again isotropic. The prestress in the edge cables and the membrane has to be defined appropriately. Based on equation (3.3), a relation for the prestress in the membrane and in the edge cable can be obtained:

$$R_{\text{cable}} = \frac{N_{\text{cable}}}{\sigma_0} \quad (3.63)$$

In equation (3.63) the cable forces N_{cable} and the membrane stresses σ_0 define the curvature radius of the edge cable R_{cable} . In this example, the thickness of the

3.5 Form finding of hybrid structures

membrane and the cross section area of the cable are set to unit values. In this case the ratio is chosen as 20, which means that the resulting radius of curvature of the edge cable is 20 as well. In figure 3.22 the example is illustrated. In figure 3.23 the

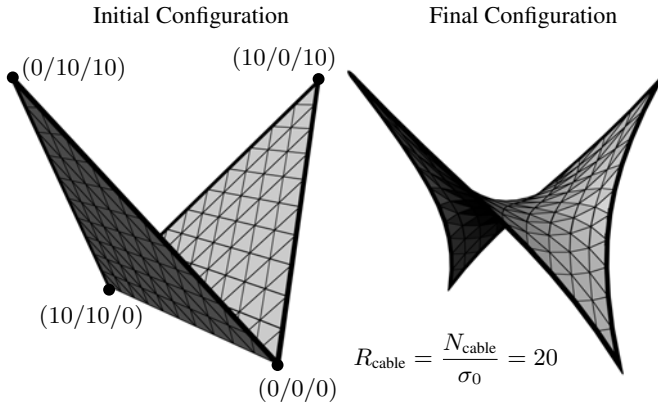


Figure 3.22: 4 point tent

resulting convergence of the X-URS and the Force Density is shown. It can be seen that the X-URS achieves a very good convergence behavior in comparison to the Force Density Method. Obviously, the X-URS is not able to achieve the analytical solution within the first form finding step. This can be explain by the needed mesh deformation in the tangential direction related to the edge cables. As the X-URS is restricted to the stabilization part in the tangential direction more form finding steps have to be done to achiev the analytical solution. As the tangential part of the X-URS is just related to the Force Density Method, the convergence is influenced in such a way that the method can't converge within the first form finding step. This characteristic will occur every time if tangential mesh adaption is needed in order to achieve the final solution.

3.5 Form finding of hybrid structures

In general, hybrid structures combine different structural elements with different types of materials. The main characteristic of hybrid structures is that the individual structural elements are combined in such a way that their involvement in the load bearing process happens in the most efficient manner. The best known example for a hybrid structure is reinforced concrete slabs, where the concrete acts in pure compression and the reinforcement acts in tension. As the concrete has a remarkable capability of restraining compression stresses, it will usually crack in case of tension stresses. Due to that, the tension stress will be restrained by the reinforcement where materials are used which are optimal for resisting tension stresses (e.g. steel, carbon or glass fiber, etc.).

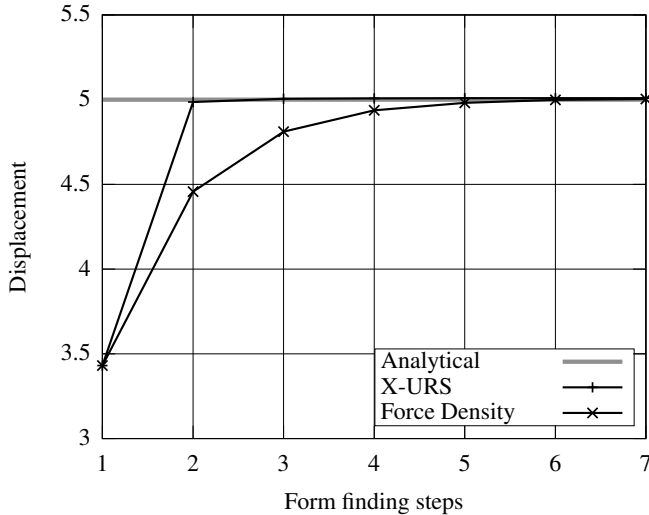


Figure 3.23: Displacement convergence for the 4 point tent

In the case of tensile structures, the combination of purely tensioned membrane or cable elements with elastic (or conventional) elements which can restrain all types of forces can be defined as a hybrid structure. The motivation for the combination of tensiles with conventional structural elements is that the resulting hybrid structures have an improved structural capability and the design space will be increased as new types of shapes can be achieved. Of course, the type of improvement differs from application to application. It could vary from the dynamical response up to more practical reasons like the overall area which can be covered by the tensile structure. In figure 3.24 the combination of a membrane with edge cables (as the tensile part) and a supporting arch (as the elastic part) is illustrated. A detailed discussion on the possible applications for hybrid structures can be found in [Lie+13].

The most obvious implementation of a hybrid tensile structure is if the elastic members are directly integrated in the surface. In the past, various structures have been build on the basis of this type of process. In figure 3.25 two examples for these types of structures are illustrated. In both cases the elastic elements are directly integrated in the membrane and influence the shape of the structure as well as modify the structural behavior. Another type of hybrid tensile structure can be defined if the elastic elements are outside of the tensile structure. For instance, flying masts or supporting framework are typical applications. In figure 3.26 two examples of these types of structures are illustrated. Here, the elastic elements are not directly integrated in the membrane, they are attached externally. The impact on the structural behavior is in principle the same for both types of structures. From a computational point of view, the combination of tensile and elastic elements in the form finding

3.5 Form finding of hybrid structures

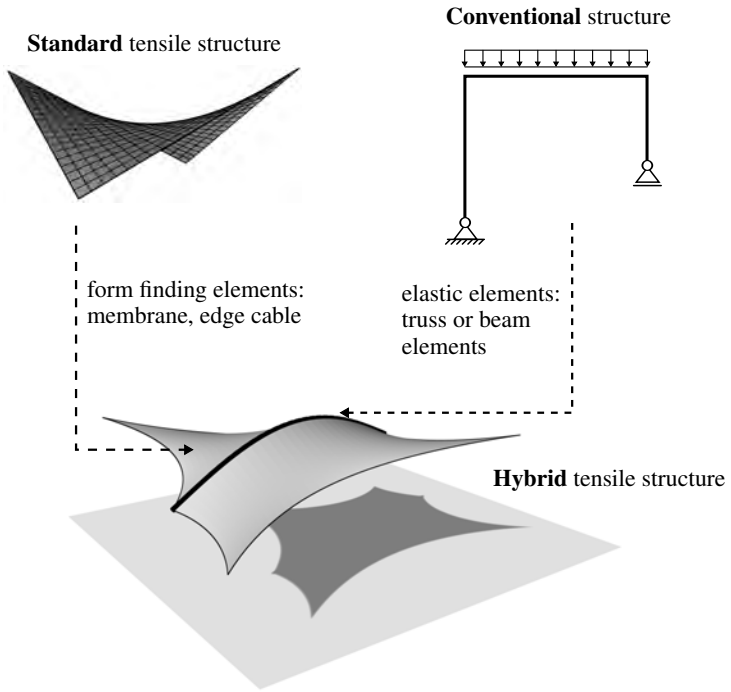


Figure 3.24: Hybrid tensile structures



Figure 3.25: Hybrid tensile structures with integrated elastic members (left [LK12]; right [Off10])



Figure 3.26: Hybrid tensile structures with external elastic members (left [Koc04]; right [Sei08])

introduces some special difficulties. For classical tensile structures, the process of form finding tries to find the shape equilibrium for the prescribed prestress. As the stresses are predefined, there is no relation between strains and stresses, which has already been explained in the previous sections. In contrast, for elastic elements the relation between stresses and strain are still valid as described in section 2.4.4. Due to that the combination of elastic elements and form finding elements is not straight forward from a mechanical point of view. The discussion of the effects on the numerical modeling for hybrid tensile structures is given in detail in [DWB12], [Die+13b] and [PB13].

For the form finding elements, the reference configuration is updated in each form finding step. The reference configuration for the elastic elements stays the initially defined configuration. In figure 3.27 the individual deformations for form finding and elastic elements are illustrated. Whereas as the goal for the form find-

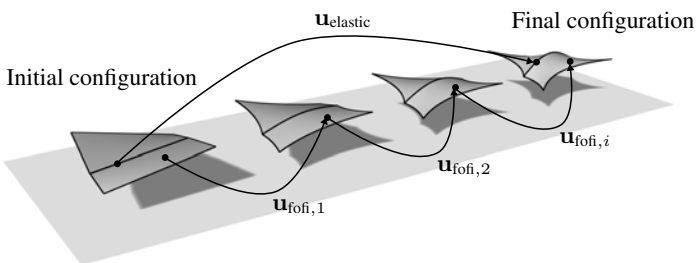


Figure 3.27: Configurations for form finding with integrated elastic elements

ing elements is that the deformation is equal to zero in the last form finding step, $\mathbf{u}_{\text{fofi},i} \rightarrow 0$, the deformation for the elastic elements has to be measured through the overall deformation process $\mathbf{u}_{\text{elastic}} \neq 0$. This characteristic is important, as the elastic and the form finding elements should be in a state of equilibrium in the final

3.5 Form finding of hybrid structures

configuration. Here, the stresses of the elastic elements can only be developed from deformations. Therefore, the stresses are evaluated from elasticity and additionally predefined stresses:

$$\mathbf{S} = \mathbf{S}(\mathbf{u}_{\text{elastic}}) + \mathbf{S}_0 \quad (3.64)$$

The elastic stresses $\mathbf{S}(\mathbf{u}_{\text{elastic}})$ originate from the deformations and in consequence from the strains. In general, this means that for the elastic elements the process of form finding is equivalent to the process of a standard structural analysis. Therefore, the residual forces for the elastic elements in the form finding process can be derived from the weak form given in equation (2.87). As there are no dynamical influences in the form finding process and the external influence is already concerned in the weak form of the tensile elements, the weak form for the elastic elements can be reduced to just the internal part. By substituting equation (3.64) in the internal virtual work, the residual forces can be given by:

$$R_r = \int_V (\mathbf{S}(\mathbf{u}_{\text{elastic}}) + \mathbf{S}_0) : \frac{\partial \mathbf{E}(\mathbf{u}_{\text{elastic}})}{\partial u_r} dV = 0 \quad (3.65)$$

As the form finding problem is solved by a Newton-Raphson algorithm, the system matrix for the elastic elements can be obtained as follows:

$$K_{rs} = \frac{\partial}{\partial u_s} \int_V (\mathbf{S}(\mathbf{u}_{\text{elastic}}) + \mathbf{S}_0) : \frac{\partial \mathbf{E}(\mathbf{u}_{\text{elastic}})}{\partial u_r} dV \quad (3.66)$$

Because of, the predefined prestress \mathbf{S}_0 for the elastic members is independent from the elastic deformation, the system matrix can be given by:

$$K_{rs} = \int_V \frac{\partial \mathbf{S}(\mathbf{u}_{\text{elastic}})}{\partial u_s} : \frac{\partial \mathbf{E}(\mathbf{u}_{\text{elastic}})}{\partial u_r} + (\mathbf{S}(\mathbf{u}_{\text{elastic}}) + \mathbf{S}_0) : \frac{\partial^2 \mathbf{E}(\mathbf{u}_{\text{elastic}})}{\partial u_r \partial u_s} dV \quad (3.67)$$

If comparing the system matrix of the elastic elements with that defined by the Force Density Method, given in equation (3.17), the difference between the individual elements is obvious. For the tensile elements, just the last part of the system matrix remains by fading out the elastic stresses. Of course, this difference is based on the update of the reference configuration as well as on the existence of the predefined stresses.

As the elastic elements keep their initial reference configuration and the strains are computed w.r.t. this geometry, it is obvious that the initial configuration is not just an arbitrary starting point. Therefore, the initial reference configuration for the elastic elements has to be aligned to the actual manufactured configuration. Due to that the choice of the stress free configuration is a crucial step in the form finding of hybrid tensile structures.

Conclusions

In the beginning of the numerical design and analysis process of tensile structures, a satisfying shape from an architectural and engineering point of view has to be found. In this chapter the inverse problem of form finding was described and appropriate solution approaches have been presented. Based on the discussion of the general solvability of the governing equations for different characteristic types of prestress distributions, adapted numerical methods for their solution have been developed. Additionally, the effects from conventional structural elements and their integration into the governing equations have been included in this chapter.

Based on the described numerical methods, the form finding for arbitrary prestress situations for the tensile, in combination with conventional structural elements, can be done. This provides the possibility to evaluate the shape of equilibrium for state of the art tensile structures, which is the basis for the following design steps, cutting pattern generation and structural analysis. The discussion of the integration of the presented form finding method in the individual design loops will be given in chapter 6.

Structural Analysis

In section 2.5 the equilibrium of a body has been derived. In general, for structural analysis the distinction in the transient and the steady state case is made. For a transient analysis, the change of the equilibrium in time is considered. Due to that, the inertia effects of the structure have to be considered as well. This effect to the structure can be identified in equation (2.83) by the dynamical part in the principle of virtual work $-\delta W_{\text{dyn}}$. If there is no time dependency involved in the structure (e.g. the external load is invariant in time), the equilibrium equation can be reduced to the steady state case. Then the dynamical part in the equilibrium can be neglected.

In this chapter, both cases of equilibrium, transient and steady state, will be discussed. The governing equations for the solution with a Newton-Raphson algorithm will be derived on the basis of a finite element discretization in space and the Newmark-Time-Integration for the time discretization. The derived equations will be validated on the basis of principal benchmark examples for large deformations. Based on these examples the principal properties and the solution behavior of non-linear problems will be discussed.

For the modeling and simulation of state of the art tensile structures, different structural elements such as cables or membranes are involved. As already discussed in the previous sections, for the modeling of recent tensile structures the number of different involved structural element types increase because of the complexity of the design. In this chapter the formulation of different finite elements will be presented which are needed in the design and analysis process of tensile structures. The description of the membrane and cable element will be a substantial content. Additionally, the discussion on special conditions originating from pressure loads, like wind loads, will be discussed at the end of this chapter.

4.1 Transient Analysis

In the transient analysis, all effects in the equilibrium equation, defined by the principle of virtual work in equation (2.83), will be considered. For the solution, dis-

4.1 Transient Analysis

cretization approaches were discussed in section 2.5 for time and space. With the introduced Newmark-Time-Integration approach it is possible to reduce the unknowns to the nodal deformations \mathbf{u}_{n+1} in the next time step $t_{i+1} = t_i + \Delta t_i$. Based on this, it is possible to define the equilibrium on the basis of the residuum equation, by a linearization of the principle of virtual work. In the following, the solution of the equilibrium for the transient case will be described.

The residuum equation defined in equation (2.98) can be enhanced by the structural damping of the system with the introduction of the damping coefficient c_0 . In general, in a dynamical system, the kinetic and potential energy is transformed into each other while the system is vibrating if no external energy input is included. From a theoretical point of view this process could proceed for an infinite time. During the vibration some part of the energy will be transformed into thermal energy. Due to this "loss" of energy, the vibration will be decreased in time until it results in a steady situation. This damping effect of the vibration in time is considered by the introduction of the damping coefficient in the governing equations. The enhanced residual equation considering the damping effects can be given by:

$$\begin{aligned}
 R_{r,n+1} = & \int_V \mathbf{S}(\mathbf{u}_{n+1-\alpha_f}) : \frac{\partial \mathbf{E}(\mathbf{u}_{n+1})}{\partial u_{r,n+1}} dV \\
 & + \int_V \rho_0 \ddot{\mathbf{u}}_{n+1-\alpha_m} \frac{\partial \mathbf{u}_{n+1}}{\partial u_{r,n+1}} dV \\
 & + \int_V c_0 \dot{\mathbf{u}}_{n+1-\alpha_f} \frac{\partial \mathbf{u}_{n+1}}{\partial u_{r,n+1}} dV \\
 & - \int_a \mathbf{q} \frac{\partial \mathbf{u}_{n+1}}{\partial u_{r,n+1}} da = 0
 \end{aligned} \tag{4.1}$$

The first line in equation (4.1) is assigned to the elasticity of the structure and can be interpreted as the internal residual forces. The second line contains the mass inertia of the structure which will be computed on the basis of the density ρ_0 of the structure. The third line describes the effects from structural damping based on the damping coefficient c_0 . The last line defines the external forces in the equilibrium equation by the external load \mathbf{q} . In the following the individual parts of the residual equation will be discussed. Additionally, the governing equations for the solution process based on a Newton-Raphson algorithm are going to be presented.

4.1.1 Internal Forces in the Transient Analysis

The internal forces are related to the elasticity of the structure. As the internal forces are dependent on the deformation at time $n + 1 - \alpha_f$, the derivative w.r.t. the unknown deformations \mathbf{u}_{n+1} is not straightforward. Due to that, the assumption introduced in equation (2.95) for the external forces is also applied for the internal ones. Here, the general formulation of the internal forces is replaced by a linear combination of the forces at current time step n and the next time step $n + 1$ by

the combination factor α_f . Based on this assumption the internal forces at the next time step $n + 1$ can be given by:

$$R_{int,r}(\mathbf{u}_{n+1-\alpha_f}) \approx (1 - \alpha_f) R_{int,r}(\mathbf{u}_{n+1}) + \alpha_f R_{int,r}(\mathbf{u}_n) \quad (4.2)$$

Based on this approximation the derivation of the internal forces w.r.t. the unknown nodal deformations \mathbf{u}_{n+1} is possible. The resulting components of the system matrix can be evaluated as follows:

$$K_{rs} = \frac{R_{int,r}(\mathbf{u}_{n+1-\alpha_f})}{\partial u_{s,n+1}} = \frac{\partial}{\partial u_{s,n+1}} \left[(1 - \alpha_f) \int_V \mathbf{S}(\mathbf{u}_{n+1}) : \frac{\partial \mathbf{E}(\mathbf{u}_{n+1})}{\partial u_{r,n+1}} dV \right] + \frac{\partial}{\partial u_{s,n+1}} \left[\alpha_f \int_V \mathbf{S}(\mathbf{u}_n) : \frac{\partial \mathbf{E}(\mathbf{u}_n)}{\partial u_{r,n}} dV \right] \quad (4.3)$$

The second part in equation (4.3) is independent from the unknown deformations at time $n + 1$. Due to that, this term will vanish in the derivation of the residual equation. The components of the resulting system matrix can be given by:

$$K_{rs} = (1 - \alpha_f) \int_V \frac{\partial \mathbf{S}(\mathbf{u}_{n+1})}{\partial u_{s,n+1}} : \frac{\partial \mathbf{E}(\mathbf{u}_{n+1})}{\partial u_{r,n+1}} + \mathbf{S}(\mathbf{u}_{n+1}) : \frac{\partial^2 \mathbf{E}(\mathbf{u}_{n+1})}{\partial u_{r,n+1} \partial u_{s,n+1}} dV \quad (4.4)$$

4.1.2 Mass Inertia in the Transient Analysis

The mass inertia is related to the mass of the structure defined by the density ρ_0 . Like the internal forces, the mass dependent part will have an influence on the system matrix in the Newton-Raphson algorithm. This effect can be evaluated by the first order derivative of the dynamical part in the residual equation, as derived in equation (2.98), w.r.t. the unknown deformations in the next time step $n + 1$. The derivative of the mass part can be obtained by:

$$\begin{aligned} M_{rs} &= \frac{\partial}{\partial u_{s,n+1}} \left[\int_V \rho_0 \ddot{\mathbf{u}}_{n+1-\alpha_m} \frac{\partial \mathbf{u}_{n+1}}{\partial u_{r,n+1}} dV \right] \\ &= \int_V \rho_0 \frac{\ddot{\mathbf{u}}_{n+1-\alpha_m}}{\partial \ddot{\mathbf{u}}_{n+1}} \frac{\partial \ddot{\mathbf{u}}_{n+1}}{\partial u_{s,n+1}} \frac{\partial \mathbf{u}_{n+1}}{\partial u_{r,n+1}} dV \\ &= \int_V \rho_0 (1 - \alpha_m) \frac{1}{\beta \cdot \Delta t^2} \frac{\partial \mathbf{u}_{n+1}}{\partial u_{s,n+1}} \frac{\partial \mathbf{u}_{n+1}}{\partial u_{r,n+1}} dV \end{aligned} \quad (4.5)$$

For the evaluation of the last line in equation (4.5) for the mass matrix, the Newmark time integration defined in equation (2.94) and the midpoint of approximation from Chung and Hulbert from equation (2.95) are introduced.

4.1 Transient Analysis

4.1.3 Damping in the Transient Analysis

From a mathematical point of view, the damping part differs from the mass part only in the constant factor in the integral (c_0 for the damping and ρ_0 for the mass). Therefore, this part can be treated as described for the mass part in the residual equation. So, the damping part in the system matrix can be formulated based on equation (2.98), equation (2.94) and equation (2.95) as follows:

$$\begin{aligned}
 C_{rs} &= \frac{\partial}{\partial u_{s,n+1}} \left[\int_V c_0 \dot{\mathbf{u}}_{n+1-\alpha_f} \frac{\partial \mathbf{u}_{n+1}}{\partial u_{r,n+1}} dV \right] \\
 &= \int_V c_0 \frac{\partial \dot{\mathbf{u}}_{n+1-\alpha_f}}{\partial \dot{\mathbf{u}}_{n+1}} \frac{\partial \dot{\mathbf{u}}_{n+1}}{\partial u_{s,n+1}} \frac{\partial \mathbf{u}_{n+1}}{\partial u_{r,n+1}} dV \quad (4.6) \\
 &= \int_V c_0 (1 - \alpha_f) \frac{\gamma}{\beta \cdot \Delta t} \frac{\partial \mathbf{u}_{n+1}}{\partial u_{s,n+1}} \frac{\partial \mathbf{u}_{n+1}}{\partial u_{r,n+1}} dV
 \end{aligned}$$

The definition of a damping coefficient which is able to represent the structural behavior in a correct way is a major difficulty for complex structures. For simple structures the damping coefficient can be defined by experiments. Here, the structure is subjected to a certain initial deformation. After releasing the structure, it will vibrate in the first eigenform of the system. Due to damping, the system will reduce the amplitude of the vibration in each oscillation. Based on this reduction of the maximum deformation, the damping coefficient can be evaluated. In [Wer83] an example for the determination of the damping coefficient can be found. It is obvious that this approach can't be applied for arbitrarily shaped structures, as the damping has to be known in advance. Therefore, the *Rayleigh damping* is introduced [Ray94]. It is assumed that the damping of the structure is proportional to the distribution of the mass and the elastic stiffness in the structure. Based on this the Rayleigh damping is formulated as a factorized summation of the system matrix w.r.t. the internal forces and the mass inertia:

$$C_{rs} = \alpha_0 M_{rs} + \alpha_1 K_{rs} \quad (4.7)$$

With the definition of the Rayleigh damping in equation (4.7) it is possible to define the damping by the two combination parameters α_0 and α_1 . A detailed discussion on the effects of the Rayleigh damping and the choice of the combination parameters can be found in [CP93], [Pet96], [CKC06].

4.1.4 Solution process for the Transient Analysis

Based on the derived residual forces and the related system matrices, the equation of motion can be solved on the basis of a Newton-Raphson algorithm. For the description of the solution process it is advantageous to formulate the equilibrium based on matrix notation. Here, the components from equation (4.4), equation (4.5) and equation (4.6) have to be assembled in their individual global matrices. The process of assembling the components in the global matrix is well known in finite

element applications. In the following, the mathematical operation of the assembly will be defined as given in [Wri08]:

$$\mathbf{A} = \bigcup_{e=1}^{n_{ele}} A_{r,s} \quad (4.8)$$

Based on the global matrices, the equilibrium can be written in terms of a matrix notation. With the mass matrix \mathbf{M} , the damping matrix \mathbf{D} and the stiffness matrix \mathbf{K} the well known equation of motion can be obtained by:

$$\left[\frac{1 - \alpha_m}{\beta \Delta t^2} \mathbf{M} + \frac{(1 - \alpha_f) \gamma}{\beta \Delta t} \mathbf{D} + (1 - \alpha_f) \mathbf{K} \right] \Delta \mathbf{u}_{n+1} = \mathbf{R}_{ext} - \mathbf{R}_{int} \quad (4.9)$$

Here, the mass matrix \mathbf{M} can be identified as

$$\mathbf{M} = \bigcup_{e=1}^{n_{ele}} \int_V \rho_0 \frac{\partial \mathbf{u}_{n+1}}{\partial u_{s,n+1}} \frac{\partial \mathbf{u}_{n+1}}{\partial u_{r,n+1}} dV \quad (4.10)$$

the damping matrix \mathbf{D} as

$$\mathbf{D} = \bigcup_{e=1}^{n_{ele}} \int_V c_0 \frac{\partial \mathbf{u}_{n+1}}{\partial u_{s,n+1}} \frac{\partial \mathbf{u}_{n+1}}{\partial u_{r,n+1}} dV \quad (4.11)$$

and the stiffness matrix \mathbf{K} as

$$\mathbf{K} = \bigcup_{e=1}^{n_{ele}} \int_V \frac{\partial \mathbf{S}(\mathbf{u}_{n+1})}{\partial u_{s,n+1}} : \frac{\partial \mathbf{E}(\mathbf{u}_{n+1})}{\partial u_{r,n+1}} + \mathbf{S}(\mathbf{u}_{n+1}) : \frac{\partial^2 \mathbf{E}(\mathbf{u}_{n+1})}{\partial u_{r,n+1} \partial u_{s,n+1}} dV \quad (4.12)$$

With equation (4.9) an incremental solution process for the unknown deformation \mathbf{u}_{n+1} for the time step $n + 1$ is defined. Therefore, the incremental deformation $\Delta \mathbf{u}_{n+1}$ has to be evaluated and the overall deformation can be updated until the residuum equation is fulfilled for the current time step. After convergence, the next time increment can be solved.

The derived equation of motion defined in equation (4.9) can also be given in a simplified form. The term in brackets can be defined as the effective stiffness matrix \mathbf{K}_{eff} . The structure of the simplified form of the equation of motion is given by:

$$\mathbf{K}_{eff} \Delta \mathbf{u}_{n+1} = \mathbf{R}_{ext} - \mathbf{R}_{int} \quad (4.13)$$

Here, the effective stiffness matrix \mathbf{K}_{eff} is defined by:

$$\mathbf{K}_{eff} = \left[\frac{1 - \alpha_m}{\beta \Delta t^2} \mathbf{M} + \frac{(1 - \alpha_f) \gamma}{\beta \Delta t} \mathbf{D} + (1 - \alpha_f) \mathbf{K} \right] \quad (4.14)$$

One of the main challenges in the solution of transient problems is the choice of the process parameters α_m , α_f , β and γ as well as the choice of an appropriate time step

4.1 Transient Analysis

Δt . In the past, various choices for these parameters have been made, which results in different published time integration methods. In [KC99] an overview of the different possible choices is given with a discussion of their influence and properties. For the application to tensile structures the most commonly used time integration scheme is used in the following. In [New59] the *Newmark- β* time integration was introduced by defining certain values for the process parameters:

$$\begin{aligned}\beta &= \frac{1}{4} & \text{and} & & \gamma &= \frac{1}{2} \\ \alpha_f &= 0 & \text{and} & & \alpha_m &= 0\end{aligned}\tag{4.15}$$

In [New59] it is shown that for this choice of the process parameters, the time integration of the Newmark- β method is always stable, independent of the choice of the time step Δt . Of course, Δt has to be chosen in a way that the applied load and vibration characteristic are discretized in an appropriate way.

One of the most popular benchmarks for the non-linear transient problem is the *Duffing Oscillator* first published in [Duf18]. In figure 4.1 the free vibration of the Duffing Oscillator is illustrated in the middle of the figure. At time $t = 0$ an initial deformation u_0 is applied to the structure. For the illustrated structure different initial deformations u_0 are defined. The introduced initial deformations have such a size, that the consideration of large deformations in the governing equations is required. The initial velocity and acceleration are assumed to be zero $v_0 = a_0 = 0$. The time increment for the Newmark- β method is set to be $\Delta t = 0.1$ and the process parameters are chosen as given in equation (4.15). For the evaluation of the Duffing Oscillator a geometrical nonlinear spring finite element has to be derived. The governing equations for this type of element are depicted in section 4.3.3. The example of the Duffing Oscillator is widely discussed. In [Kuh96] a review of the Duffing Oscillator can be found. The phase diagram at the bottom of figure 4.1 shows the periodic behavior for the defined initial deformations.

Based on the example of the Duffing Oscillator it can be seen that with the derived equations it is possible to describe the vibration of structures subjected to large deformations. Due to this the applicability for tensile structures is given. Additionally to the solution of the equation of motion, an important modeling aspect has to be considered in case of tensile structures. In general, these types of structures are light due to their thinness which, of course, is one of their most important advantages. For the modeling, this property results in an additional discussion of the input parameters for the analysis. Due to the lightness of the structure, during the vibration the surrounding air has to be considered for a realistic result of the analysis. The air around the tensile structure will vibrate in the same sense as the surface vibrates. Therefore, additional mass and damping effects, resulting from the added air, have to be considered. The added mass and the aerodynamic damping have to be included into the evaluation of the mass and damping matrices for the transient analysis. The definition of the added mass and aerodynamic damping is not straightforward as the measurement of how much air will be moved based on the vibration of the tensile structure is not straightforward. In [Hol07] an introduction and discussion related to the effects of the surrounding air of a vibrating system is given. Nevertheless, the inclusion of these effects in the derived governing equations is possible without any

modification. Due to that a further discussion on this topic is not included in this thesis.

4.2 Steady State Analysis

The steady state case of the equilibrium describes the situation if all quantities (e.g. loads) are invariant in time. Due to this property of the problem, the governing equations can be reduced to the time independent parts. From a mathematical point of view this reduction can be justified since the time derivatives of the related quantities will be zero. Because of that the mass and damping do not occur in the residual equation for the steady state case. It can be formulated by the internal and external forces in the principle of virtual work as follows:

$$-\delta W = \int_V \mathbf{S} : \delta \mathbf{E} dV - \int_a \mathbf{q} \delta \mathbf{u} da = 0 \quad (4.16)$$

For the solution of the equilibrium equation in steady state, a discretization in space has to be applied as described in section 2.5.1. Due to the absence of a time dependency the discretization of time can be neglected. As a result, the residual form of the equilibrium can be given by:

$$R_r = \int_V \mathbf{S} : \frac{\partial \mathbf{E}(\mathbf{u})}{\partial u_r} dV - \int_a \mathbf{q} \frac{\partial \mathbf{u}}{\partial u_r} da = R_{r,int} - R_{r,ext} = 0 \quad (4.17)$$

In equation (4.17) the first part is defined as the internal residual forces and the second part as the external residual forces. The external forces depend on the load intensity \mathbf{q} , which is defined as a distributed load over the surface. The definition of this quantity can be given by a certain direction and a respective value which defines the intensity. The external load can have certain properties as based on the definitions of the direction and the intensity. If the load is invariant w.r.t. the deformation of the structure, this part will vanish in the derivation of the system matrix. The independence of the deformations can be assumed for dead or snow loads. If the external load depends on the deformation of the structure it will affect the system matrix, which can be assumed for wind loads. The discussion of the influence on the solution process of such load conditions will be given in section 4.4.

If a Newton-Raphson algorithm is applied for the solution of the nonlinear residual equation, the system matrix can be evaluated by the first order derivative of the residuum as described in equation (2.99). The resulting system matrix can be given by:

$$K_{rs} = \frac{\partial R_r}{\partial u_s} = \int_V \frac{\partial \mathbf{S}(\mathbf{u})}{\partial u_s} : \frac{\partial \mathbf{E}(\mathbf{u})}{\partial u_r} + \mathbf{S}(\mathbf{u}) : \frac{\partial^2 \mathbf{E}(\mathbf{u})}{\partial u_r \partial u_s} dV - \frac{\partial}{\partial u_s} \int_a \mathbf{q} \frac{\partial \mathbf{u}}{\partial u_r} da \quad (4.18)$$

4.2 Steady State Analysis

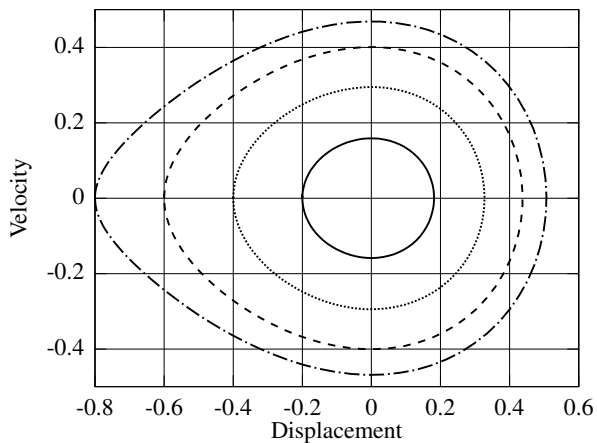
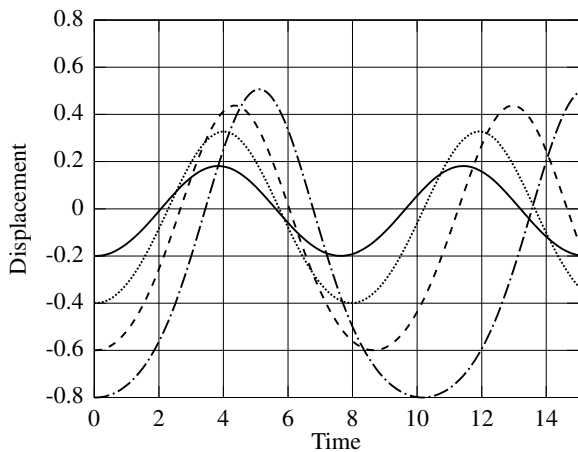
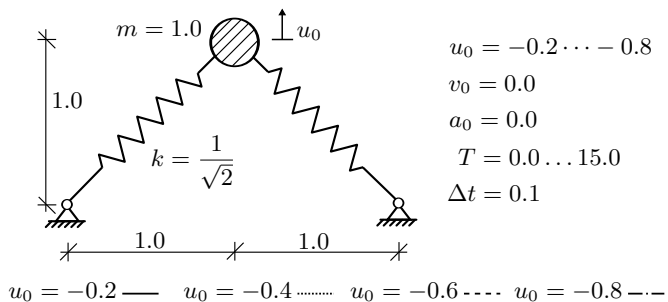


Figure 4.1: Results for the Duffing Oscillator; top: Definition of the structure; middle: Time-displacement diagram; bottom: Displacement-velocity diagram

Based on the governing equations defined in equation (4.17) and equation (4.18) all types of steady state problems can be solved. For the discussion of the solution process the well known *von Mises* truss example, illustrated in figure 4.2, is used as a benchmark example for the nonlinear steady state analysis. A detailed discussion on the example can be found in [Cri91]. The main advantage of this example is, that it can be formulated on the basis of one single degree of freedom. Due to that the governing equations can directly be derived and it is possible to describe the results in a clear form. For the discretization of the von Mises truss example the

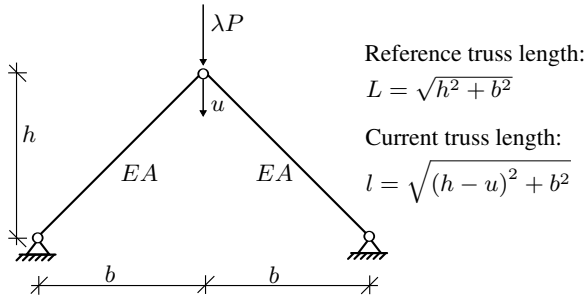


Figure 4.2: von Mises truss example

equations from a truss finite element, derived in section 4.3.1, will be applied. For this example the assumption of linear elastic isotropic material is applied and the prestress is set to be zero. Due to these simplifications it is possible to derive the residual equation for the von Mises truss w.r.t. the unknown deformation u by:

$$-\frac{EA}{L^3} (h - u) (u^2 - 2hu) = \lambda P \quad (4.19)$$

In equation (4.19) the Young's modulus E and the cross section area A of the trusses are assumed to be known. The external nodal force P will be controlled by the load factor λ . With the residual equation from equation (4.19) a $\lambda - u$ diagram can be constructed as illustrated in figure 4.3.

It is obvious, that only for a single degree of freedom example it is possible to derive a equation where the construction of the $\lambda - u$ diagram is directly possible. In general, the nonlinear residual equation has to be solved. Due to the fact that the relation between the applied load and the deformation is nonlinear, the load should not be applied at once. In fact, the definition of a varying load factor is equivalent to a pseudo time representing the load history as a sequence of steady state analyses. A detailed discussion on the inclusion of a pseudo time in the steady state case of the equilibrium can be found in [Wri08].

Additionally, in a general sense the introduction of the load factor λ defines another degree of freedom for the governing equations. Due to that an additional equation has to be defined in order to be able to solve the equilibrium equation. There are

4.2 Steady State Analysis

various methods to describe this additional equation. The simplest method is to prescribe the value of the load factor λ w.r.t. the pseudo time directly. That means for each pseudo time step, an increment for the load factor has to be defined, which is known as the force control method. As a consequence, it is not generally possible to trace the λ - u or load-displacement curve in detail. From figure 4.3 it can be seen that after the first buckling point (at point B in figure 4.3) of the structure, the load should be decreased if the overall load-displacement curve should be evaluated. If the load is increased constantly in case of the force control method, the next equilibrium point E will be found when the structure has recovered after snapping through. In general, for tensile structures the evaluation of the exact load-displacement curve is not of such an importance as only the first buckling point is of interest in the design and analysis. If the complete curve should be evaluated, more advanced methods like displacement control or the arc length method can be applied. A detailed discussion on different solution strategies for such cases can be found in [Rei94], [Ram82], [WS90].

With the described method it is possible to analyze the deformation of a tensile structure subjected to time invariant loads. The application of these methods for systems with large deformations has been discussed on the basis of the von Mises truss example. It can be seen that, as for the transient analysis, appropriate finite elements have to be available for a geometrical nonlinear steady state analysis. In the following, the most important elements for the analysis of tensile structures will be discussed.

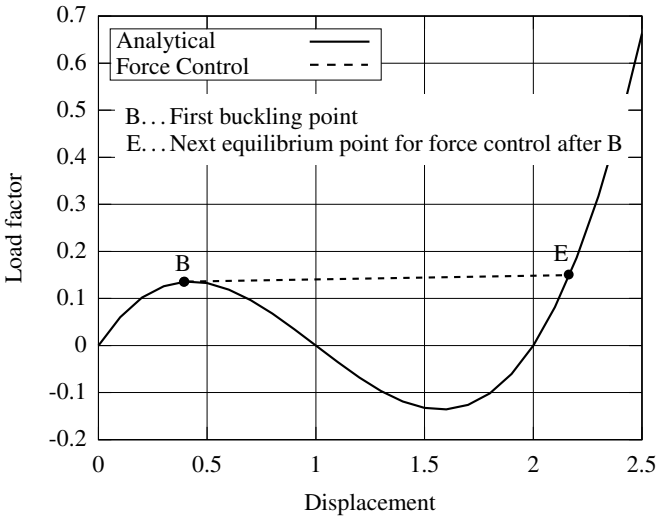


Figure 4.3: λ - u diagram for the von Mises truss example (with $P = 1$; $EA = 1$; $h = 1$; $b = 1$)

4.3 Finite Element Formulations

In the previous sections the governing equations and the process of the structural analysis of tensile structures in case of transient and steady state conditions were discussed. The necessity of appropriate finite element formulations for the modeling and simulation of state of the art applications became obvious. In this section the most important finite elements will be introduced. For a collection of elements, the governing equations will be derived, as they are adapted for the special applications for tensile structures. For the elements which are applied for the modeling of conventional structures, a wide discussion on the individual finite elements is available in literature. For those, which are also applied for the modeling of tensile structures, the relevant references will be given. The important step of introducing the discretization in the governing equations was already described in section 2.5.1.

4.3.1 Truss or Cable Element

The presented truss or cable element connects two nodes in space as shown in figure 3.8. It is assumed that the element has a constant axial stiffness EA , a distributed mass over length m and an initial prestress S_0 which is constant over the length of the element. The element is a 1D element, which has the consequence that the summation over the components in the governing equations can be reduced to a scalar equation. Due to that the overall stress in the element is the summation of the elastic and the prestress, based on a local Cartesian coordinate system:

$$S^{11} = S_{el}^{11} + S_0^{11} \quad (4.20)$$

One possibility is to derive the equation w.r.t. the curvilinear coordinate system as done for the cable element in section 3.3.1.2. Here, an alternative approach is shown where the governing equation will be given in terms of a local Cartesian coordinate system. This approach is restricted to elements which remain straight during the deformation. Based on this, the Green-Lagrange strain tensor can be transferred into the local Cartesian coordinate system as given by:

$$\begin{aligned} \mathbf{E} &= E_{11} \mathbf{G}^1 \otimes \mathbf{G}^1 = \hat{E}_{11} \mathbf{e}^1 \otimes \mathbf{e}^1 \\ \Rightarrow \hat{E}_{11} &= E_{11} (\mathbf{G}^1 \cdot \mathbf{e}_1) (\mathbf{G}^1 \cdot \mathbf{e}_1) = \frac{E_{11}}{L^2} = \frac{1}{2} \frac{l^2 - L^2}{L^2} \end{aligned} \quad (4.21)$$

In equation (4.21) the length of the element in the reference configuration is defined by L and with l in the current configuration. With the relation for the Green-Lagrange strains in equation (4.21) the internal forces can be formulated as follows, where S^{11} is identified as the 2. Piola-Kirchhoff stresses:

$$R_r = A \int_L S^{11} \cdot \frac{\partial \hat{E}_{11}}{\partial u_r} dL \quad (4.22)$$

The system matrix can be given with the derivative of the internal forces w.r.t. the nodal deformations. Here, the independence of the prestress w.r.t. the deformations

4.3 Finite Element Formulations

is assumed:

$$K_{rs} = A \int_L \frac{\partial S_{el}^{11}}{\partial u_r} \cdot \frac{\partial \hat{E}_{11}}{\partial u_r} + S^{11} \cdot \frac{\partial^2 \hat{E}_{11}}{\partial u_r \partial u_s} dL \quad (4.23)$$

For the mass matrix, the formulation from equation (4.5) can be applied for the truss element. For the evaluation of the volume integral the fact is used that the cross section area is already defined in advance. Therefore, the volume integral can be reduced to the integral over the length and a multiplication by the cross section area A . Based on this the components of the mass matrix can be obtained by:

$$M_{rs} = A \int_L \rho_0 \frac{\partial \mathbf{u}_{n+1}}{\partial u_{s,n+1}} \frac{\partial \mathbf{u}_{n+1}}{\partial u_{r,n+1}} dL \quad (4.24)$$

4.3.2 Membrane Element

The most important elements for the design and analysis of tensile structures are membrane elements. The main requirements are: (i) Large deformation in the kinematics; (ii) Possibility to define additional prestress in the surface; (iii) Possibility to define the warp and weft direction aligned to the fiber directions. In the following, the description of an appropriate membrane finite element will be given on the basis of the formulated requirements. The presented governing equations are based on the description given in [Die09] and [Lin09].

Membrane finite elements are surface elements which can be either triangles or quadrilateral elements as shown in section 2.5.1. For the description of the kinematic of the membrane finite element, the Green-Lagrange strains are used as introduced in section 2.4.3. Based on this strain measurement, the simulation of large deformations is possible.

The definition of the warp and weft directions on the surface can be given by the approach presented in section 3.3.1.1. By defining a local Cartesian coordinate system where the prestress is defined, it has to be decided if the element is formulated w.r.t. the local or curvilinear coordinate system. Most of the available derivations are done w.r.t. the local Cartesian coordinate system as the material definition is given in the Voigt notation and the prestress is defined in the same coordinate system. From a continuum mechanical point of view it is more appropriate to derive the governing equations in the curvilinear coordinate system. If the element is derived in the curvilinear coordinate system the prestress has to be transformed from the local coordinate system. This can be done as described in equation (3.22) for the 2. Piola-Kirchhoff stresses. The overall stress for the membrane element is a summation of the elastic stresses \mathbf{S}_{el} and the prestress \mathbf{S}_0 considering the plane membrane state of stresses:

$$\mathbf{S} = \mathbf{S}_{el} + \mathbf{S}_0 \quad (4.25)$$

With the definition of the stresses the internal forces can be given with the assumption of constant thickness by:

$$R_r = t \int_A \mathbf{S} : \frac{\partial \mathbf{E}}{\partial u_r} dV \quad (4.26)$$

The system matrix for a Newton-Raphson algorithm can be given by the first order derivative of the internal forces:

$$K_{rs} = t \int_A \frac{\partial \mathbf{S}}{\partial u_s} : \frac{\partial \mathbf{E}}{\partial u_r} + \mathbf{S} : \frac{\partial^2 \mathbf{E}}{\partial u_r \partial u_s} dA \quad (4.27)$$

In case of a transient analysis the required components of the mass matrix can be evaluated by equation (4.5) with the assumption of a constant thickness:

$$M_{rs} = t \int_A \rho_0 \frac{\partial \mathbf{u}_{n+1}}{\partial u_{s,n+1}} \frac{\partial \mathbf{u}_{n+1}}{\partial u_{r,n+1}} dA \quad (4.28)$$

4.3.3 Spring-Damper Element

In state-of-the-art tensile structures, different applications are used to reduce the vibration due to transient load conditions. The introduction of damper elements in bridge design is well known. Similar applications can be found in recent designs of tensile structures. For the simulation of most bridge designs, spring-damper elements based on linear kinematics are sufficient, as the deformations of the structure remains small. In case of tensile structures this assumption, of small deformations for the spring-damper elements does not hold. Due to that, an appropriate element has to be derived. In figure 4.4 the reference and the current configuration of this element is illustrated. The spring-damper element is defined by a stiffness in

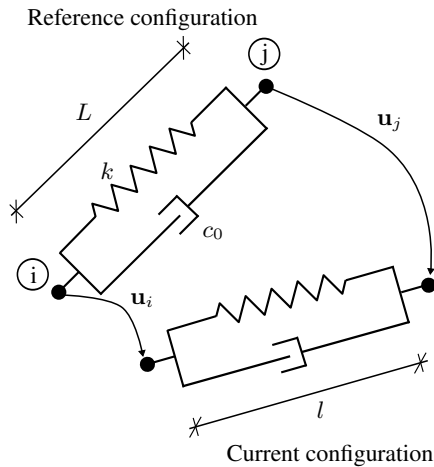


Figure 4.4: Spring Damper Finite Element

the spring k and a damping coefficient in the damper element c_0 . In general, the residual forces can be formulated in different ways for the geometrical nonlinear

4.3 Finite Element Formulations

spring-damper element. Here, the governing equation for the internal forces will be derived from the assumption of a potential energy of the spring. The potential energy can be formulated based on the stiffness and the axial deformation \mathbf{u} of the spring as follows:

$$\Pi = \frac{1}{2}k \cdot \mathbf{u}^2 \quad (4.29)$$

For the potential energy of the spring just the axial deformations are needed. Therefore, the vector of the deformations can be reduced to the axial deformation $\mathbf{u} = u_{\text{axial}}$. Substituting the relation between the current and the reference length for the axial deformation $u_{\text{axial}} = (l - L)$, the potential energy can be rewritten as follows:

$$\Pi = \frac{1}{2}k \cdot (l - L)^2 \quad (4.30)$$

From the condition that the residuum of the spring-damper element is the first order derivative of the potential energy the residuum can be given by:

$$\frac{\partial \Pi}{\partial u_r} = R_r = k \cdot (l - L) \frac{\partial l}{\partial u_r} \quad (4.31)$$

With the derivative of the residual force, the components of the system matrix can be obtained by:

$$K_{rs} = \frac{\partial R_r}{\partial u_s} = k \frac{\partial l}{\partial u_s} \frac{\partial l}{\partial u_r} + k \cdot (l - L) \frac{\partial^2 l}{\partial u_r \partial u_s} \quad (4.32)$$

For the components of the damping matrix, equation (4.11) can be applied directly. With the assumption of a constant distributed damping coefficient over the length $c(s) = \text{const} = c_0$, the volume integral can be reduced to an integration over length. As the function in the integral is independent of the length, the integral can be reduced to a multiplication with the reference length:

$$C_{rs} = c_0 \cdot L \frac{\partial \mathbf{u}_{n+1}}{\partial u_{s,n+1}} \frac{\partial \mathbf{u}_{n+1}}{\partial u_{r,n+1}} \quad (4.33)$$

The resulting damping matrix is a consistent system matrix, which also have components outside the main diagonal. For some applications it can be useful to be able to define the damping effects just on the main diagonal. This means a certain damping definition only affects the related degree of freedom. This type of description of the damping matrix is also known as a lumped damping matrix. In this case the components on the main diagonal of the damping matrix have to be directly defined.

The derived spring-damper element can be applied for the modeling of state of the art tensile structures, as it includes large deformations in the governing equations. A restriction for the element is that a linear stiffness is assumed, which can be understood as a linear material definition. Another restriction originates from the assumption of a constant damping coefficient. As for the spring stiffness, this assumption can be interpreted as a material property.

4.3.4 Further Finite Elements

In the previous sections, the finite elements for the simulation of tensile structures were described for transient and steady state analysis. Of course, for state of the art applications more elements are necessary to satisfy the requirements of the models. Certainly, beam finite elements have to be available for the simulation of recent tensile structures. With the inclusion of the supporting structures in the design, this type of element became more important in the simulation of recent designs. Additionally, the applications where the beam elements are also subjected to large deformation is growing. Due to that, the necessity of beam finite elements, which are able to describe large deformations is obvious. Certainly, the formulation of appropriate beam elements is one of the most complex tasks in the context of finite elements. This is due to the description of the rotational degrees of freedom at the nodes. There exist various approaches to describe the full kinematic of the nodal deformation. Based on this, different element formulations for beam elements are available. A detailed review of different methods to describe beam finite elements can be found in [Rom08]. Based on the concept of *Co-rotational deformation* description in [Kre09] a recent derivation of a geometrical nonlinear beam element is introduced.

Another important type of finite elements for the state-of-the-art modeling of tensile structures are shell elements. As for beam elements, there exists a wide range of available formulations based on different theoretical assumptions. A detailed discussion on different shell finite elements can be found in [CB98], [KJ03], [Bis+04]. Most recently, shell elements which are free of rotational degree of freedoms were developed [LWB07], [OF05]. These elements have the advantage that the governing equations only depend on the translational degrees of freedom. Due to that, the problematic rotational parts do not appear in the formulation. An interesting development in this direction is made by the introduction of non-rational B-Splines (NURBS) as shape functions for the finite elements. NURBS are successfully applied in Computer Aided Design (CAD) for the advanced modeling of curves and surfaces on the basis of well defined and flexible mathematical equations [Pie97]. Due to the mathematical description it is possible to formulate shell (or beam) elements without introducing rotational degrees of freedom. The formulation of appropriate shell finite elements based on NURBS surfaces for different mechanical assumptions can be found in [CHB09], [EB10], [Kie11]. As well as for the beam elements there exist some formulations for shell elements which are based on the co-rotational concept. A promising formulation has been recently made by [FH05], [Hau94]. An extension of the formulated element by an in plane prestress is made in [Kök13].

With the described finite elements, recent designs of tensile structures can be modeled. It can be seen that a wide range of element types have to be available for the numerical modeling of an appropriate design and analysis process. In addition to the finite elements, the modeling of the external loads introduce a further complexity to the numerical process. In the following section the discussion of special loading conditions will be given.

4.4 External Loads

For invariant loads, like snow or dead load, neither the direction nor the load value will change due to deformation. Based on this the load \mathbf{q} can be obtained by the multiplication of the intensity q and the direction \mathbf{v} .

$$\mathbf{q} = q\mathbf{v} \quad (4.34)$$

Based on equation (4.34) the external virtual work can be given by:

$$\delta W_{\text{ext}} = - \int_A \mathbf{q} \delta \mathbf{u} dA \quad (4.35)$$

The description in equation (4.35) is appropriate to describe dead loads, where the direction is defined as the gravity and the intensity can be evaluated from the density of the structure. Furthermore, snow loads can be described on this basis in an appropriate way as they are also gravity dependent. From a numerical point of view these types of loads do not need a special discussion as they do not affect the structural stiffness.

For other load conditions the assumption of the invariance of the load definition w.r.t. the deformation does not hold. In case of wind loads, or more general pressure loads, the direction always is perpendicular to the surface in direction of the surface normal \mathbf{n} . Since the load will follow the surface as it deforms, this type of load is called follower load. The final load can be given by the multiplication of the intensity of the wind load and the normal direction of the surface:

$$\mathbf{q}(\mathbf{n}) = q \frac{\mathbf{g}_1 \times \mathbf{g}_2}{\|\mathbf{g}_1 \times \mathbf{g}_2\|} \quad (4.36)$$

Substituting equation (4.36) into the external virtual work and introducing equation (2.27) to describe the surface integral by the surface parameters, the external residual forces can be given by, where θ^1 and θ^2 are the surface parameters:

$$R_{r,\text{ext}} = \int_{\theta^1} \int_{\theta^2} q (\mathbf{g}_1 \times \mathbf{g}_2) \frac{\partial \mathbf{u}}{\partial u_r} d\theta^1 d\theta^2 \quad (4.37)$$

It is obvious that due to the introduction of the normal vector of the surface the derivative of the external forces will not vanish in the system matrix. The remaining load stiffness matrix can be given by the first order derivative of the residual forces:

$$K_{r,s,\text{ext}} = \int_{\theta^1} \int_{\theta^2} q \frac{\partial (\mathbf{g}_1 \times \mathbf{g}_2)}{\partial u_s} \frac{\partial \mathbf{u}}{\partial u_r} d\theta^1 d\theta^2 \quad (4.38)$$

The governing equations for the load stiffness matrix do not result in a symmetric matrix in all cases depending on the type of boundary conditions. In [SR84] the discussion of the symmetric and non-symmetric cases can be found. The described

modeling of follower forces for a pressure load is appropriate for free constant pressure. That means that the intensity of the load is independent from the deformations. Additionally, it can be the case that the intensity of the load changes as the structure is deformed. In case of tensile structures, this has certainly to be considered for enclosed cushions. Recently, this type of structures is applied for roofs and facades as illustrated in figure 4.5. Additionally, the pressure intensity is depending on the cur-



Figure 4.5: Examples for ETFE cushions; top: Casino Macao; bottom: Lyon Confluence (copyright: Seele Cover GmbH)

rent volume of the structure. For the description of the change in pressure intensity w.r.t. the current volume, various methods exist. According to the adiabatic state of thermodynamics the current pressure can be defined on the basis of a reference pressure q_0 , the reference volume V and the current volume v as follows:

$$q = q_0 \left(\frac{V}{v} \right)^\kappa \quad (4.39)$$

In equation (4.39) κ defines the isentropic exponent, which can be used to define different behaviors of the enclosed gas. For $\kappa = 1$ an isothermal behavior of an ideal gas is mentioned, which is defined as the Boyle's law [Bon+00]. For the choice of $\kappa = 1.4$ a two-atomic gas is modeled, as mentioned in [SH08]. It is obvious, that if the relation of the pressure as defined in equation (4.39) is considered, the derivative of the pressure intensity w.r.t. to the degrees of freedom has to be taken into account for the system matrix as well. As the volume depends on all defined unknowns of the system, the special characteristic of the load stiffness is that the system matrix

4.4 External Loads

is fully populated. Most of the available numerical solvers for a system of equations are assuming a sparse matrix. Due to this, special strategies for the solution of the resulting system of equations have to be considered. For a numerical efficient solution of the fully populated nonlinear problem, the *Woodbury's formula* can be applied [Woo50]. A detailed discussion on the topic of enclosed cushions can be found in [Jru09].

Conclusions

For state of the art tensile structures the requirements on the modeling with the FEM increase constantly. Therefore, it is necessary to derive appropriate simulation methods to ensure a high quality in the results. Hence, in this chapter methods for the structural analysis for transient and steady state conditions were presented.

For the modeling of tensile structures, different finite elements have to be available to describe the structural model in an appropriate way. In this chapter the individual elements were described. For the most important ones, the governing equations are derived. For elements which are published in a satisfying manner, the related literature is discussed.

Due to the large deformation of tensile structures, the discussion of follower forces is essential. Based on the description of external loads in the principle of virtual work, the special characteristic of this type of load is discussed. The governing equations for the modeling of direction and intensity depending loads were derived. This type of loading condition has to be available for the state of the art modeling of cushions with enclosed pressure.

With the described methods for the structural analysis it is possible to simulate the behavior of all types of tensile structures subjected to external loads. The evaluation of the deformation in this process is based on the definition of an appropriate reference configuration. In general, this reference configuration of the tensile structure will be computed in the form finding process. The discussion of the introduction of the results of the form finding in the structural analysis will be presented in chapter 6.

Cutting Pattern Generation

Due to their large scale, architectural tensile structures can't be manufactured out of a single piece of fabric. To realize the design, the surface will be divided into a number of patterns which will be assembled together to form the final shape. The fabric, which will be used for the production of the individual patterns, is available on rolls of material with a certain width. For the production, a blueprint has to be provided which defines the shape of the pattern on the flat fabric. The process of defining the form of the flat patterns is called the *Cutting Pattern Generation*.

The cutting pattern generation involves a great deal of experience from the designer. The architectural effect and the structural behavior are substantially affected by the shape of the patterns. The process is defined by the creative part of designing a pattern layout which satisfies the architectural concept and the pure mathematical problem of the evaluation of the flattened patterns.

The architectural requirements on the cutting pattern generation can't be solved in a general numerical way. Here still, the experience of the designer and the manufacturer is the most important component in the definitions concerning the cutting patterns.

In this chapter the principal mathematical problem of the cutting pattern generation will be described. Subsequently, different existing solution strategies, which have been developed in the past, will be discussed. Based on this review of the existing methods improvements will be introduced which are motivated from the application in practice. Additionally, the discussion of the main influence parameters for the cutting pattern problem will be made. As the resulting method is consequently derived from continuum mechanics, the definitions introduced in chapter 2 can be applied for the solution process. Based on the general formulation, it is possible to include all types of mechanical and practical requirements in the governing equations. Therefore, it is possible to achieve high quality cutting patterns and thus enlarge the design space for tensile structures.

5.1 Cutting Pattern Generation for Tensile Structures

In the process of cutting pattern generation, the flat patterns for the manufacturing of the tensile structure are computed. The underlying mathematical problem originates from the doubly curvature of the surface. In general, double curved surfaces can't be developed into a plane as already discussed in section 2.3. The non-developability can be illustrated on the basis of the two examples shown in figure 5.1. Here, for the discussion of the developability of a surface the examples of a cylinder and a sphere are introduced. In both cases the surface should be covered with a simple flat piece of fabric. In the case of the cylinder, it can be seen that the structure can be covered by the fabric without any elastic deformations in the cover. For the example of the sphere, it is obvious that elastic deformations are needed for covering the overall surface. The occurring wrinkles visualize the elastic deformations for the observer, which illustrates the non-developability of the surfaces.

The described example shows that in the case of the manufacturing of tensile structures, the final shape will differ from the intended one due to the non-developability of the structure. Additionally, elastic deformations are needed to shape the final surface from the flat patterns. In general, the prestress in the tensile structure is achieved through these elastic deformations. However, the elastic deformations are not constant over the overall surface. Due to that, the final stress distribution will vary around the defined prestress introduced in form finding. If the elastic stress state remains in tension, no wrinkles will occur in the surface. If large elastic deformations are needed to shape the surface from the patterns, compression stresses can occur, which will result in wrinkles in the surface. From a theoretical point of view, the best result for the surface and stress distribution can be achieved if the width of the patterns will tend to zero, which results in the recommendation to divide the tensile structure into as many individual patterns as possible. Of course, the number of patterns is limited from practical and architectural point of view. Therefore, in the design of the pattern layout a compromise between minimization of stress deviation and architectural or practical aspects has to be made.

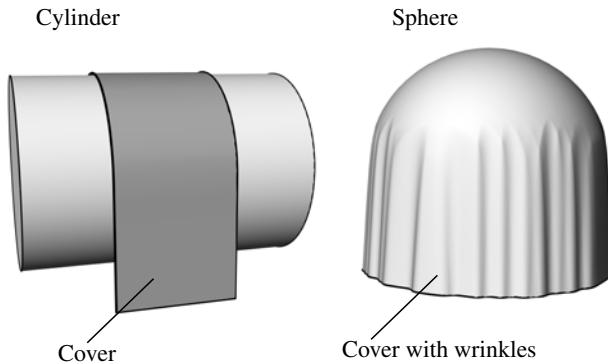


Figure 5.1: Cylinder and Sphere covered by an initially flat plane

In figure 5.2 the principal process of the cutting pattern generation for tensile structures is illustrated. Based on an intended surface from form finding, the pattern layout will be defined by the designer with the decision about the number of patterns and the shape of the cutting lines. Subsequently, the computation of the cutting patterns will be made. For each of these steps, various experimental and numerical methods have been developed in the past. In the following, a brief discussion on these methods will be given.

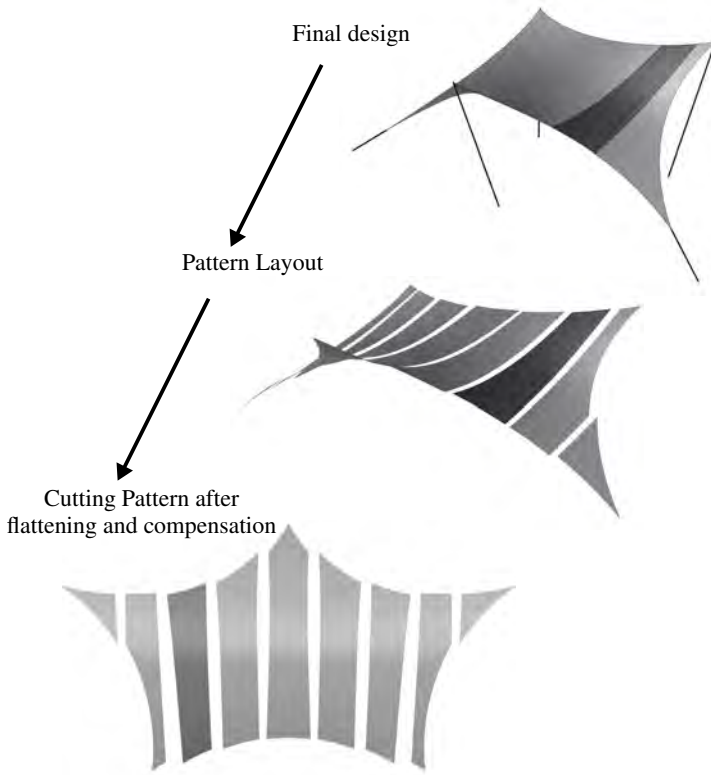


Figure 5.2: Principal steps for the cutting pattern generation

Pattern Layout: The definition of the pattern layout is influenced by deterministic and non-deterministic aspects. The maximum available width of the applied material is an example of a deterministic influence. The architectural appearance can't be formulated and due to that, it can be characterized as non-deterministic.

5.1 Cutting Pattern Generation for Tensile Structures

Therefore, the process of the definition of the pattern layout can't be formulated in a closed numerical method, but for different aspects in this process numerical methods can be applied. The definition of the cutting lines to divide the overall surface into the individual patterns is typically done based on numerical methods. In principle, the cutting line between two defined points on the structure can be described arbitrarily. In [FM04] the advantage of geodesic lines is discussed. The main advantage is that the cutting patterns will show the straightest boundaries in the flattened configuration, which provides the most economical material use of all possibilities.

In general, the surface of the tensile structure will be discretized by finite elements in order to solve the governing equations. Therefore, the surface isn't described in a closed mathematical form. The evaluation of the geodesic lines on a discrete surface can't be done directly as it is defined by nodes in space and the topology of the finite elements. The solution for the definition of geodesic lines on the discretized surface can be solved in a two step approach: (i) Evaluate an approximation of the geodesic line along the edges of the finite elements. (ii) Optimize the approximative geodesic line by moving the position of the involved nodes of the finite elements on the surface. The optimization process can be done with a mechanical approach. If a cable is taut on a fixed surface it will deform in the position where the potential energy is minimized. From a geometrical point of view this position will connect the start and end point by the shortest distance. As the geodesic line is defined as the shortest distance between two points, the analogy of the prestressed cable and the geodesic line is obvious. In figure 5.3 the principal process is illustrated.

For the evaluation of the approximation of the geodesic line, various methods exist. From a general point of view, the problem to find the shortest path of a start and end point through a defined set of nodes can be found in different applications like navigation, optimized data storage or computer graphics. Most of the available algorithms are based on the idea of *wave propagation*. Here, the approximation of the geodesic line is computed in two steps. (i) Evaluate, starting from the end point of the geodesic line, the shortest distance to all other nodes in the mesh: (ii) From the start node evaluate step by step the next node which is characterized by the minimal path length to the end node. This step is repeated until the end node is reached. The first publication based on this approach is by Dijkstra [Dij59]. The presented algorithm includes the disadvantage that for regular meshes there is no unique result. This drawback was overcome by the method published in [KS98]. Here, the process of computing the minimal distances of the individual nodes to the end node is modified to ensure a unique approximation of the geodesic line. A description of an algorithm based on this method is presented in [NK02].

Along the approximation of the geodesic line, highly prestressed cables will be introduced in the surface. The position of the nodes, where the potential energy is minimized, can be evaluated by form finding as introduced in chapter 3. Of course, if the cable will be prestressed and can deform freely in space, kinks will occur in the surface. Due to that, the cables have to be limited in their possible deformation to the in-plane direction. This can be achieved by the modification of the residual force vector of the cable element. As described in section 3.4 it is possible to

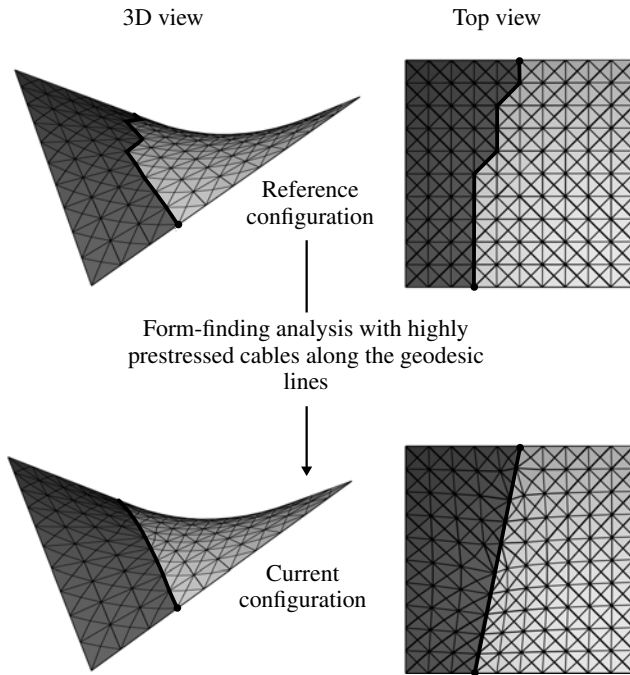


Figure 5.3: Discrete geodesic line computation

split the residual force vector into its individual parts. For the geodesic line finite element, the in-plane part of the residual vector will be taken into account and the out-of-plane part will be neglected. With this modification, the deformations of the nodes are restricted to the in-plane direction of the surface. Additionally, all components of the residual force at the start and end node of the geodesic line have to be neglected as well. This approach defines a flexible and adapted method to determine geodesic lines on discretized surfaces. Of course, there are various disadvantages related to this approach. One major disadvantage is that through the in-plane deformation of the nodes, the mesh in the vicinity of the geodesic line will be distorted. It is obvious, that the mesh distortion depends on the quality of the approximation of the geodesic line, which is in general related to the element size.

Another interesting possibility for the evaluation of geodesic lines can be introduced if non-rational B-splines (NURBS) are applied for the discretization in space of the structure. The application of NURBS as shape functions was already mentioned in section 4.3.4 for a shell type finite element. The introduction of this type of function for tensile structures can be found in [Phi+14]. By applying NURBS

5.1 Cutting Pattern Generation for Tensile Structures

surfaces, a mathematically closed form of the surface is achieved and the geodesic lines can directly be evaluated as defined in [BZ13]. The resulting geodesic line is of course the same as evaluated with standard finite elements for the discretization. The comparison of the two approaches is illustrated in figure 5.4.

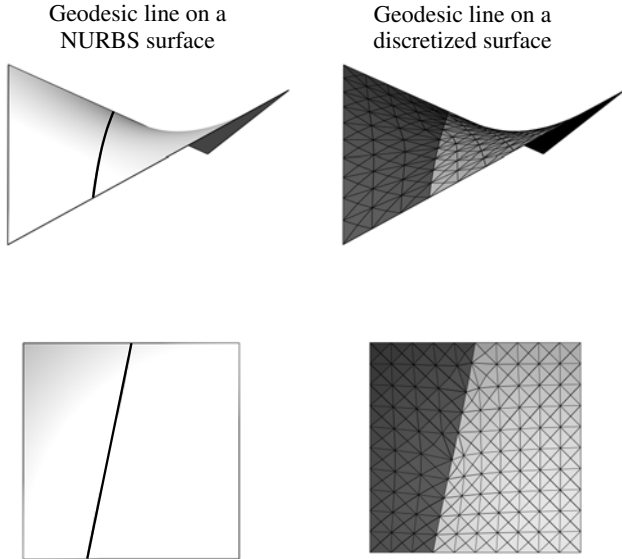


Figure 5.4: Geodesic line on a NURBS and discretized surface

Cutting Pattern Generation: The task in the evaluation of the cutting patterns is to develop the individual 3D shaped strips of the tensile structure into a flat, 2D configuration. Historically, this task is well known from cartography where a plane representation of the sphere-like surface of the earth is going to be evaluated. The methods applied for this task are adapted for the needs in the generation of maps. Mostly, the *Mercator-Projection* is used as a projection method. With this method it is ensured that the angles are unchanged through the projection, but the area content of an object may change. There exist various methods which are based on the idea of unchanged surface angles for the unfolding of general kinds of surfaces, e.g. [SS01].

One of the simplest methods for the unfolding of a tensile structure is described in [MT90]. Here, the discretization of a general non-developable strip of the tensile will be modified in order to be able to unfold it. This can be achieved, if the strip is discretized by triangle elements which cover the whole width. This special surface discretization enables the unfolding of the strip along the individual edges of the

triangles. Of course, the resulting cutting patterns do not have a high quality, as the surface representation is not detailed enough and depends extremely on the choice of discretization. In [Sch78] an improvement of the idea of triangulation is made.

It is obvious that with the purely geometrical based formulations, some major drawbacks are introduced. The most important one is the independence of the cutting pattern of the applied material. Due to that in [OH79] a method is presented where the material properties are included. Here, the cutting patterns are achieved based on a finite element simulation, where the nodes of the individual strips are forced into a plane. The method can be described as two plates which compress the strip into the flat configuration while no friction is present between the plates and the strip.

In [MM99] and [KL02] the *Stress Composition Method* is introduced. Here, the cutting pattern generation is formulated w.r.t. the defined prestress. In this method, a 2D configuration is defined. Based on this configuration the resulting stresses can be evaluated which occur while assembling the 2D to the 3D configuration. Of course, the resulting stresses will not fit the defined prestresses, but with an optimization of the 2D configuration the difference between the resulting and the predefined stresses can be achieved. The main advantages of this method is that all kinds of mechanical properties can be included and it is possible to formulate the governing equations in a continuum mechanical framework.

There exist more than the described methods for the solution of the cutting pattern generation problem. In [Top07] and [Bäu95] a review of the existing methods from a methodological and historical perspective can be found. In the following, existing methods on the basis of the stress composition method will be discussed, which are purely derived from continuum mechanics and numerical optimization.

5.2 Solution approach for the Cutting Pattern Generation

In this section, the principle objective for the cutting pattern generation will be discussed, which is based on the idea of the stress composition method and will be used in the following sections when the solution approaches will be discussed. As previously described, the stress composition method evaluates a 2D plane configuration which results in a stress distribution with a minimal difference to the intended prestress after the assembly. To find this 2D configuration, optimization methods can be applied. For the solution of an appropriate optimization problem, the formulation of the objective function is essential. For this purpose the process of the optimization is illustrated in figure 5.5. Here, the 3D configuration of the tensile structure is defined as Ω_{3D} . From a manufacturing point of view, the 3D surface will be achieved by assembling the cutting pattern in the final position. Transforming this process to the continuum mechanical description of the cutting pattern problem, the 3D surface can be understood as the current configuration in this process. Introducing the cutting pattern as well to the governing equations, it can be defined as the reference configuration. As the cutting patterns are placed in the 2D domain, the surface will be indicated by Ω_{2D} . The process of optimization can be

5.2 Solution approach for the Cutting Pattern Generation

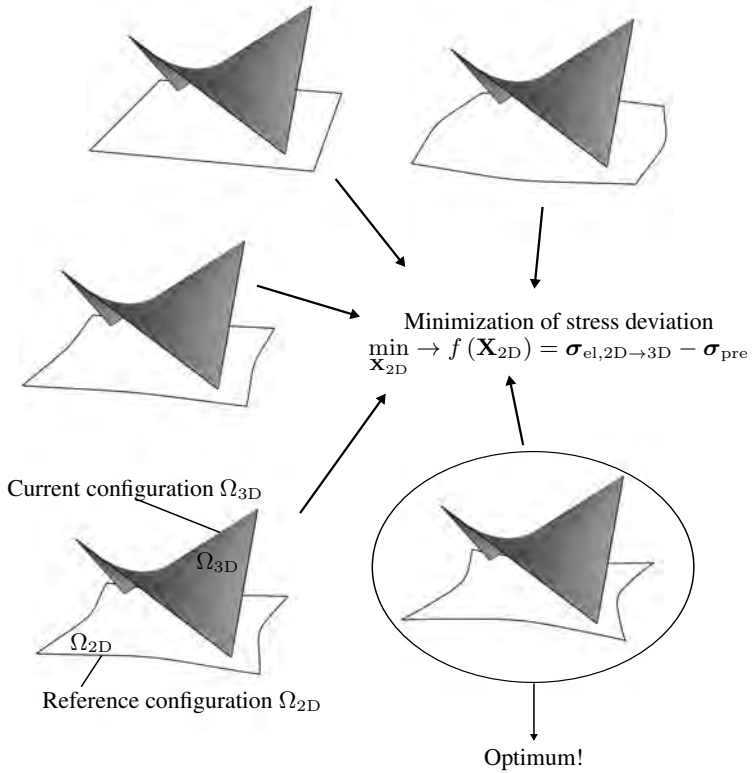


Figure 5.5: Optimization problem for cutting pattern generation

understood as a guess of different cutting patterns and testing them w.r.t. the objective function. In the end, the cutting pattern which results in the minimal value for the objective function will represent the optimum. As mentioned before, the crucial point in the formulation of the cutting pattern is the appropriate objective function, as it is responsible for the quality of the final patterns. Based on the idea of the stress composition method the objective function can be formulated as follows:

$$\min_{\mathbf{X}_{2D}} \rightarrow f(\mathbf{X}_{2D}) = \sigma_{el,2D \rightarrow 3D} - \sigma_{pre} \quad (5.1)$$

In equation (5.1) the definition of the stress difference is defined by the stresses resulting from the assembling of the 2D to the 3D surface $\sigma_{el,2D \rightarrow 3D}$ and the intended prestress σ_{pre} . The related design variables or unknowns is the geometry \mathbf{X}_{2D} in the 2D reference configuration Ω_{2D} . Based on this objective function the cutting pattern generation can be solved with numerical optimization methods.

The principal continuum mechanical definitions are already made by assigning the 2D and 3D surfaces to the reference and the current configuration, respectively. This definition reflects the true process of manufacturing in the numerical approach. Most of the available methods for the cutting pattern generation are defining the configurations the other way around, so that the 3D surface is assigned to be the reference configuration and the 2D surface to be the current configuration. As this approach introduces a misinterpretation of the configurations in the governing equations, the quality of the resulting stresses and patterns is not as precise as for the adjusted definition. In principle, both ways would fit to the concept of the stress composition method.

By defining the 2D surface as the geometry of the reference configuration, the underlying kinematic of the cutting pattern generation can be described as illustrated in figure 5.6. Here, the 2D configuration Ω_{2D} is defined as the reference and the 3D configuration Ω_{3D} as the current one. The difference between the geometry of the two configurations defines the overall deformation $\mathbf{u}_{2D \rightarrow 3D}$. Based on these defini-

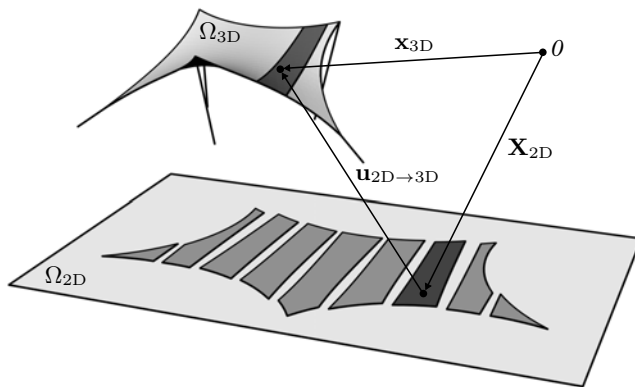


Figure 5.6: Configurations for Cutting Pattern Generation

tions, the unusual situation occurs that the geometry of the reference configuration is unknown. In standard problems of structural mechanics, the current configuration is intended to be unknown. As for the cutting pattern analysis the unknowns are "inverted", thus, the idea of inverse engineering is introduced. If gradient based methods, like the Newton Raphson method, are applied for the solution of the defined objective function, the variation of the reference configuration has to be made. Due to that in [WWB12] the method is introduced as the *Variation of Reference Strategy* (VaReS).

In the following, different existing solution approaches for the VaReS are discussed.

5.2 Solution approach for the Cutting Pattern Generation

Additionally, general statements for the solution process are introduced as well as further extensions to the method. The discussion of the sensitivity of the method w.r.t. the individual input parameters is also included in the subsequent sections.

5.2.1 Minimization of the Work of Stress Differences

In [BLW10], [Lin09] and [BLW09] a solution approach for the defined objective function from equation (5.1) is suggested based on the method of weighted residuals [Fin72], [Zie00]. For this purpose, the objective function is multiplied with a so-called test or weighting function and will be integrated over the 3D domain. In general, the weighting function can be chosen arbitrarily. In this approach, the virtual Euler-Almansi strains will be chosen, as they are energetically conjugated to the used Cauchy stresses. The solution for the optimization problem is achieved if the first variation is equal to zero. As the formulated governing equation is similar to the internal virtual work, defined in equation (2.80), it is introduced as the minimization of the work of stress differences. The resulting governing equation can be given by:

$$\delta W = \int_{\Omega_{3D}} (\boldsymbol{\sigma}_{\text{el},2D \rightarrow 3D} - \boldsymbol{\sigma}_{\text{pre}}) : \delta \mathbf{e}_{2D \rightarrow 3D} d\Omega_{3D} = 0 \quad (5.2)$$

For the solution of equation (5.2) a linearization w.r.t. the unknown parameters has to be done. In the original discussion of the introduced method (e.g. [BLW10]), artificial deformations \mathbf{U}_{2D} in the 2D configuration are introduced. This means, that the overall deformation process is divided into a purely geometrical projection of the 3D surface in the 2D domain and the deformation w.r.t. this intermediate configuration. In [Die+13a] the linearization w.r.t. the unknown geometry \mathbf{X}_{2D} of the reference configuration Ω_{2D} is done. By applying this to equation (5.2) the residual form of the governing equation can be given in terms of the individual components as follows:

$$R_r = \int_{\Omega_{3D}} (\boldsymbol{\sigma}_{\text{el},2D \rightarrow 3D} - \boldsymbol{\sigma}_{\text{pre}}) : \frac{\partial \mathbf{e}_{2D \rightarrow 3D}}{\partial X_r} d\Omega_{3D} = 0 \quad (5.3)$$

For the solution of equation (5.3) the Newton Raphson method can be applied. As a consequence of the derivative of the residuum, the resulting system matrix becomes non-symmetric. Most available numerical solvers assume that the involved matrices are symmetric. In order to fit to the widely used solution strategies, the system matrix will be modified to ensure the symmetry. It is obvious that this results in the loss of the quadratic convergence of the Newton Raphson algorithm. The modified version of the system matrix can be given by:

$$\begin{aligned} K_{rs}^{\text{sym}} = & \int_{\Omega_{3D}} \frac{1}{2} \left(\frac{\partial \boldsymbol{\sigma}_{\text{el},2D \rightarrow 3D}}{\partial X_r} : \frac{\partial \mathbf{e}_{2D \rightarrow 3D}}{\partial X_s} + \frac{\partial \boldsymbol{\sigma}_{\text{el},2D \rightarrow 3D}}{\partial X_s} : \frac{\partial \mathbf{e}_{2D \rightarrow 3D}}{\partial X_r} \right) d\Omega_{3D} \\ & + \int_{\Omega_{3D}} (\boldsymbol{\sigma}_{\text{el},2D \rightarrow 3D} - \boldsymbol{\sigma}_{\text{pre}}) : \frac{\partial^2 \mathbf{e}_{2D \rightarrow 3D}}{\partial X_r \partial X_s} d\Omega_{3D} \end{aligned} \quad (5.4)$$

The solution process based on the modified system matrix shows a robust convergence behavior, even for complex cutting patterns as discussed in [Lin09] and [BLW10]. However, the non-symmetry of the system matrix has to be discussed. The reason for this can be explained in the misinterpretation of the variation of the Euler Almansi strains in equation (5.3). In the original presentation of the approach, the variation of the strains is evaluated straightforward w.r.t. the unknown reference configuration. The misinterpretation becomes obvious when equation (5.2) is transformed into the reference configuration:

$$\begin{aligned}
\delta W^{\text{ref}} &= \int_{\Omega_{3D}} (\boldsymbol{\sigma}_{\text{el},2D \rightarrow 3D} - \boldsymbol{\sigma}_{\text{pre}}) : \delta \mathbf{e}_{2D \rightarrow 3D} d\Omega_{3D} \\
&= \int_{\Omega_{2D}} \frac{1}{\det \mathbf{F}} \mathbf{F} (\mathbf{S}_{\text{el},2D \rightarrow 3D} - \mathbf{S}_{\text{pre}}) \mathbf{F}^T : \delta \mathbf{e}_{2D \rightarrow 3D} \det \mathbf{F} d\Omega_{2D} \\
&= \int_{\Omega_{2D}} (\mathbf{S}_{\text{el},2D \rightarrow 3D} - \mathbf{S}_{\text{pre}}) : \mathbf{F}^T \delta \mathbf{e}_{2D \rightarrow 3D} \mathbf{F} d\Omega_{2D} \\
&= \int_{\Omega_{2D}} (\mathbf{S}_{\text{el},2D \rightarrow 3D} - \mathbf{S}_{\text{pre}}) : \delta \mathbf{E}_{2D \rightarrow 3D} d\Omega_{2D}
\end{aligned} \tag{5.5}$$

In equation (5.5) it can be seen that the previously introduced Lie-Time-Derivative from equation (2.84) has to be applied to calculate the variation of the Euler Almansi strains. Additionally, the description of the cutting pattern generation problem w.r.t. the reference configuration is introduced in the last line of equation (5.5). If this formulation is used instead of the original one given in equation (5.3), the resulting system matrix stays symmetric. The application of this idea is presented in [WWB12]. Here, the cutting pattern generation is formulated in the reference configuration. In the next section, the governing equations for this approach will be discussed.

5.2.2 Minimization of Potential Energy

In contrast to the minimization of work from stress difference in the approach suggested in [WWB12], the minimization here is done w.r.t. the difference of the elastic potential introduced by the resulting stresses from assembling $\Pi_{\text{el},2D \rightarrow 3D}$ and the elastic potential from prestresses Π_{pre} . Based on this, the minimization problem will be reformulated in terms of the difference in the potentials:

$$\min_{\mathbf{X}_{2D}} \rightarrow \Pi_{\text{Total}} = \Pi_{\text{el},2D \rightarrow 3D} - \Pi_{\text{pre}} \tag{5.6}$$

For both parts, the elastic and the prestress, the elastic potential will be evaluated by a strain energy function Ψ . In general, it is possible to formulate the strain energy function on the basis of the Right Cauchy Green tensor or the Green Lagrange strain tensor [Hol00]. In the following, the Green Lagrange strains are used to formulate the strain energy. For the elastic stress and the prestress, the strain energy function

5.2 Solution approach for the Cutting Pattern Generation

can be given for the general case by:

$$\begin{aligned}\Pi_{\text{el},2\text{D}\rightarrow 3\text{D}} &= \int_{\Omega_{2\text{D}}} \Psi_{2\text{D}\rightarrow 3\text{D}}(\mathbf{E}_{2\text{D}\rightarrow 3\text{D}}) d\Omega_{2\text{D}} \\ \Pi_{\text{pre}} &= \int_{\Omega_{2\text{D}}} \Psi_{\text{pre}}(\mathbf{E}_{2\text{D}\rightarrow 3\text{D}}) d\Omega_{2\text{D}}\end{aligned}\quad (5.7)$$

In case of linear elastic material the strain energy function can be given on the basis of the individual stress contributions and the strains:

$$\begin{aligned}\Psi_{2\text{D}\rightarrow 3\text{D}} &= \frac{1}{2} \mathbf{S}_{\text{el},2\text{D}\rightarrow 3\text{D}} : \mathbf{E}_{2\text{D}\rightarrow 3\text{D}} \\ \Psi_{\text{pre}} &= \frac{1}{2} \mathbf{S}_{\text{pre}} : \mathbf{E}_{2\text{D}\rightarrow 3\text{D}}\end{aligned}\quad (5.8)$$

A necessary condition for a minimum in the potential energy, is a stationary point in the functional Π_{Total} w.r.t. a variation in the reference geometry. This results in the following variation of the optimization problem:

$$\delta \Pi_{\text{Total}} = \delta \Pi_{\text{el},2\text{D}\rightarrow 3\text{D}} - \delta \Pi_{\text{pre}} = 0 \quad (5.9)$$

The variation can be done by a linearization as defined in equation (2.96). By substituting the linearization to equation (5.9) and formulating the strain energy in the reference configuration as given in equation (5.8), the residual forces for the individual terms can be obtained. For the elastic part

$$\begin{aligned}\frac{\partial \Pi_{\text{el},2\text{D}\rightarrow 3\text{D}}}{\partial X_r} &= \frac{1}{2} \int_{-1}^1 \int_{-1}^1 \left(\left(\frac{\partial \mathbf{S}_{\text{el},2\text{D}\rightarrow 3\text{D}}}{\partial X_r} : \mathbf{E}_{2\text{D}\rightarrow 3\text{D}} \right) \|\mathbf{G}_1 \times \mathbf{G}_2\| \right. \\ &\quad + \left(\mathbf{S}_{\text{el},2\text{D}\rightarrow 3\text{D}} : \frac{\partial \mathbf{E}_{2\text{D}\rightarrow 3\text{D}}}{\partial X_r} \right) \|\mathbf{G}_1 \times \mathbf{G}_2\| \\ &\quad \left. + (\mathbf{S}_{\text{el},2\text{D}\rightarrow 3\text{D}} : \mathbf{E}_{2\text{D}\rightarrow 3\text{D}}) \frac{\partial \|\mathbf{G}_1 \times \mathbf{G}_2\|}{\partial X_r} \right) d\theta^1 d\theta^2\end{aligned}\quad (5.10)$$

and for the prestress part

$$\begin{aligned}\frac{\partial \Pi_{\text{pre}}}{\partial X_r} &= \frac{1}{2} \int_{-1}^1 \int_{-1}^1 \left(\left(\frac{\partial \mathbf{S}_{\text{pre}}}{\partial X_r} : \mathbf{E}_{2\text{D}\rightarrow 3\text{D}} + \mathbf{S}_{\text{pre}} : \frac{\partial \mathbf{E}_{2\text{D}\rightarrow 3\text{D}}}{\partial X_r} \right) \|\mathbf{G}_1 \times \mathbf{G}_2\| \right. \\ &\quad \left. + (\mathbf{S}_{\text{pre}} : \mathbf{E}_{2\text{D}\rightarrow 3\text{D}}) \frac{\partial \|\mathbf{G}_1 \times \mathbf{G}_2\|}{\partial X_r} \right) d\theta^1 d\theta^2\end{aligned}\quad (5.11)$$

In equation (5.10) and equation (5.11) the integration is transformed to the surface parameters, as the integration domain has to be derived as well. The evaluation

of the individual derivatives is straightforward except for the prestress contribution $\frac{\partial \mathbf{S}_{\text{pre}}}{\partial X_r}$ in equation (5.11). Due to the definition of the prestress as Cauchy stress in the form finding process, it has to be transformed to the reference configuration by applying the pull back operation from equation (2.57). Due to the dependency of the prestress in the reference configuration on the Deformation Gradient, the derivative of the prestress will not vanish.

The solution of the discussed optimization problem can be achieved by various methods known from numerical optimization. In [WWB12] the solution is achieved by the application of a Newton Raphson method, while the resulting system matrices will be symmetric in each case.

5.2.3 Least Square Approach

An alternative way of evaluating the minimum of the objective function is based on methodologies which are known from numerical optimization and was introduced in [LWB08] and [Die+13a]. A standard approach for the formulation of an appropriate objective function is the *Least Square approach*. The stress difference is multiplied by itself and integrated over the overall 3D surface. The objective function based on the Least Square approach can be formulated as follows:

$$\min_{\mathbf{X}_{2D}} \rightarrow f(\mathbf{X}_{2D}) = \frac{1}{2} \int_{\Omega_{3D}} (\boldsymbol{\sigma}_{\text{el},2D \rightarrow 3D} - \boldsymbol{\sigma}_{\text{pre}}) : (\boldsymbol{\sigma}_{\text{el},2D \rightarrow 3D} - \boldsymbol{\sigma}_{\text{pre}}) d\Omega_{3D} \quad (5.12)$$

As equation (5.12) represents a standard optimization task, all solution methods for this type of numerical problem can be applied. If a gradient based optimization algorithm is used, like the steepest descent or conjugate gradient [HG92], the gradient of the objective function w.r.t. the design variables has to be evaluated. From a mathematical point of view, this is equivalent to a stationary point in the functional. In this case the design variables of the optimization problem are defined as coordinates in the 2D reference configuration. Based on this, the gradient of the objective function can be given by:

$$\nabla_{\mathbf{X}_{2D}} f(\mathbf{X}_{2D}) = \frac{\partial f(\mathbf{X}_{2D})}{\partial X_r} = R_r = 0 \quad \text{with } r = 1, \dots, n_{\text{dof}} \quad (5.13)$$

Based on equation (5.13) the residuum of the cutting pattern generation can be formulated as follows:

$$R_r = \int_{\Omega_{3D}} (\boldsymbol{\sigma}_{\text{el},2D \rightarrow 3D} - \boldsymbol{\sigma}_{\text{pre}}) : \frac{\partial \boldsymbol{\sigma}_{\text{el},2D \rightarrow 3D}}{\partial X_r} d\Omega_{3D} \quad (5.14)$$

It is obvious that the resulting residual equation can be solved efficiently by a Newton Raphson algorithm. Therefore, the system matrix has to be evaluated. This can

5.2 Solution approach for the Cutting Pattern Generation

be achieved by the first order derivate of the residual equation:

$$K_{rs} = \int_{\Omega_{3D}} \left(\frac{\partial \sigma_{el,2D \rightarrow 3D}}{\partial X_s} : \frac{\partial \sigma_{el,2D \rightarrow 3D}}{\partial X_r} \right) + (\sigma_{el,2D \rightarrow 3D} - \sigma_{pre}) : \frac{\partial^2 \sigma_{el,2D \rightarrow 3D}}{\partial X_r \partial X_s} d\Omega_{3D} \quad (5.15)$$

Based on equation (5.14) and equation (5.15) it is possible to solve the minimization problem for the cutting pattern generation effectively. In contrast to the methods discussed in the beginning of this section, the formulation of the objective function allows the application of standard solution techniques from numerical optimization. Moreover, it enables the addition of constraints to the objective function to include additional requirements to the problem. This characteristic will be used in section 5.2.6 to formulate an extended version of the described optimization problem.

5.2.4 Summary of the Cutting Pattern Methods

Form section 5.2.1 to 5.2.3 it can be seen, that the principal objective function of the cutting pattern generation problem can be solved differently. All of the methods have advantages and disadvantages which can be found in the respective literature. For the following enhancements the least square approach from section 5.2.3 will be used. Here, it is possible to include all types of state-of-the-art material models for the modeling of tensile structures as well as the respective formulation of the objective function allows the integration of constraints. Before the enhancements to the method will be introduced, in the following section general statements to the chosen method will be given. Here, the investigation on the sensitivity w.r.t. to different input parameters (e.g. material properties, pattern layout, etc.) is included as well as remarks to the numerical implementation.

5.2.5 General Statements

The process of VaReS for the evaluation of the cutting patterns includes different process steps and mathematical operations which differ from standard computational mechanics. In the following, the most important steps will be discussed. The effect on the cutting pattern w.r.t. the resulting stress distribution in the tensile structure will be discussed as well.

General process and boundary conditions: With the previously described methods, it is possible to evaluate the cutting patterns for tensile structures. The overall simulation process is divided into individual steps. For the application of numerical optimization approaches for the minimization of the objective function, an initial guess has to be provided. This is required since the optimization algorithm needs a first evaluation of the objective function, which then can be improved. Of course, the convergence depends crucially on the quality of the initial guess. This first guess can be achieved by different methods like simple projection techniques as discussed in section 5.1. The process of cutting pattern generation can be divided into two steps as illustrated in figure 5.7: (i) Choose an initial guess and (ii) Perform

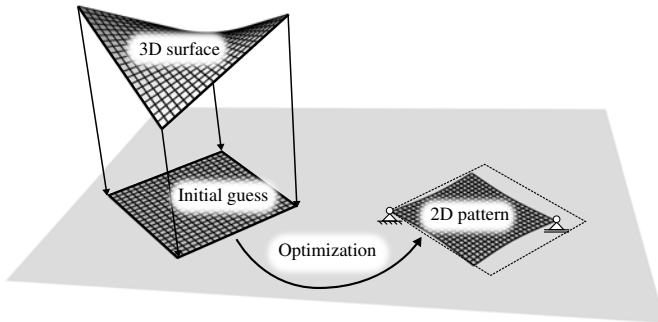


Figure 5.7: Process for cutting pattern generation

the optimization. Since projection and compensation come together with large displacements and, eventually, large strains as well, the procedure is highly nonlinear. Consequently, the problem might be solved using intermediate analysis steps. For example, the method of minimization of the work from stress difference as introduced in [BLW09] has a robust convergence behavior in the solution process. This property can be used to increase the overall robustness of cutting pattern generation, by introducing this approach as an intermediate process step.

If the optimization problem is solved with the Newton Raphson method, it is important to introduce appropriate boundary conditions as otherwise the system matrix will be singular. This can be explained by the rigid body rotation of the cutting pattern if there are no boundary conditions defined. In order to prevent this, a statically determined boundary condition has to be defined as illustrated in figure 5.7. If other optimization techniques are used, where no system matrix is involved (e.g. steepest descent, conjugate gradient), the definition of appropriate boundary conditions is not necessary, as there is no system matrix involved which can become singular. From a general point of view the singular system matrix can be prevented by methods introduced to solve a pure Neumann problem as described in [BL05].

Fiber orientation in the patterns: In the beginning of the computation of a tensile structure, the fiber orientation will be defined on the 3D surface. In the process of cutting pattern generation, this orientation has to be included in the computation. In general, the fiber orientation in the applied fabric is orthogonal. After assembly of the pattern in the final position, the resulting fiber orientation should align with the predefined one. Therefore, besides the evaluation of the cutting pattern, which minimizes the objective function, the fiber orientation in the pattern which results in the predefined fiber orientation must be found. To include the fiber orientation in the computation, a continuum mechanical relation between the fiber orientation in the reference and the current configuration has to be defined. Based on the kinematics, illustrated in figure 5.8, this relation can be derived. Of course, it can't be ensured

5.2 Solution approach for the Cutting Pattern Generation

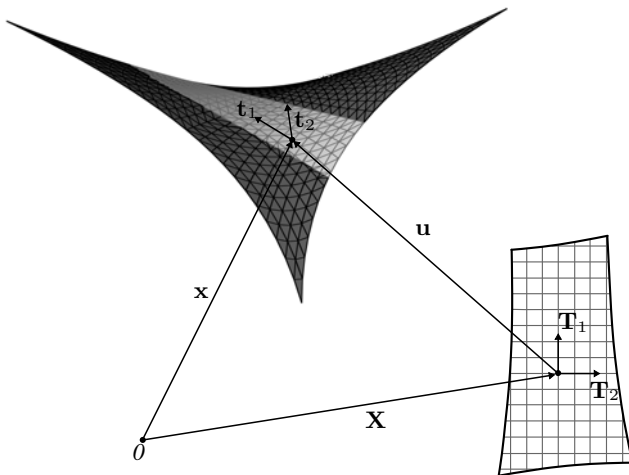


Figure 5.8: Computation of the fiber directions in the cutting pattern generation

that the predefined fiber orientation on the 3D surface can be achieved from the orthogonal fibers in the cutting pattern. Therefore, the suggested approach attempts to fit the warp direction as closely as possible.

In general, the fiber directions can be transformed from the 2D reference to the 3D current configuration by applying the deformation gradient. As the weft direction \mathbf{t}_1 is predefined in the current configuration, it will be transformed into the reference configuration by the inverse of the deformation gradient:

$$\mathbf{T}_1 = \mathbf{F}^{-1} \cdot \mathbf{t}_1 \quad (5.16)$$

It is obvious that based on the relation defined in equation (5.16) the resulting warp direction \mathbf{T}_1 in the cutting pattern will differ in the orientation at each point in the surface. In general, the fabric material has a unique fiber orientation. Due to that, the approach from equation (5.16) has to be modified to achieve a mean warp direction. For this purpose, an averaging of the individual warp directions will be introduced. Therefore, the projected warp directions in the 2D surface are summed up at each point and will be normalized. The summation can be realized by an integration over the 2D surface. Based on this, the mean warp direction can be given by:

$$\mathbf{T}_1 = \frac{\int_{\Omega_{2D}} \mathbf{F}^{-1} \cdot \mathbf{t}_1 d\Omega_{2D}}{\left\| \int_{\Omega_{2D}} \mathbf{F}^{-1} \cdot \mathbf{t}_1 d\Omega_{2D} \right\|} \quad (5.17)$$

With the assumption of equation (5.17) the optimization approach for the cutting pattern generation will result in an optimized stress difference by finding the optimal fiber orientation for the warp direction.

The evaluated warp direction is excluded from the variation and is assumed to be invariant due to small variations in the reference configuration. Of course, after each optimization step, the fiber directions have to be adjusted. Based on the averaged warp orientation, the weft direction can be evaluated by the cross product with the normal vector \mathbf{T}_3 of the pattern:

$$\mathbf{T}_2 = \mathbf{T}_3 \times \mathbf{T}_1 \quad (5.18)$$

Derivative of the Cauchy stresses for linear and nonlinear materials: In the Least Square optimization approach introduced in section 5.2.3, the derivative of the Cauchy stress tensor has to be evaluated w.r.t. the nodal position in the reference configuration. For linear elasticity this can be done easily as there exists a relation between strains and stresses in the current configuration. Based on the definition of the material tensor in the current configuration in equation (2.63) the gradient of the Cauchy stresses can be given by

$$\frac{\partial \boldsymbol{\sigma}}{\partial X_r} = \frac{\partial \mathbf{c}}{\partial X_r} : \mathbf{e} + \mathbf{c} : \frac{\partial \mathbf{e}}{\partial X_r} \quad (5.19)$$

where the derivative of the Euler-Almansi-strain tensor can be obtained by:

$$\frac{\partial \mathbf{e}}{\partial X_r} = -\frac{1}{2} \left(\frac{\partial \mathbf{G}_\alpha}{\partial X_r} \cdot \mathbf{G}_\beta + \mathbf{G}_\alpha \cdot \frac{\partial \mathbf{G}_\beta}{\partial X_r} \right) \mathbf{g}^\alpha \otimes \mathbf{g}^\beta \quad (5.20)$$

In the case of linear elasticity, equation (2.64) defines an analytical representation of the coefficients of the material tensor in the reference configuration w.r.t. the curvilinear coordinate system. Based on this representation, the derivative of the elasticity tensor in the current configuration can be obtained by:

$$\frac{\partial \mathbf{c}}{\partial X_r} = \left(\frac{\partial}{\partial X_r} \left(\frac{1}{\det \mathbf{F}} \right) C^{\alpha\beta\gamma\delta} + \frac{1}{\det \mathbf{F}} \frac{\partial C^{\alpha\beta\gamma\delta}}{\partial X_r} \right) \mathbf{g}^\alpha \otimes \mathbf{g}^\beta \otimes \mathbf{g}^\gamma \otimes \mathbf{g}^\delta \quad (5.21)$$

In the case that a material model is introduced, where linear elasticity is no longer valid the relation between stresses and strains have to be defined in the incremental form as introduced in equation (2.60). As for such materials there is no linear relation between the strains and stress, the derivative of the Cauchy stresses can be formulated as follows:

$$\begin{aligned} \frac{\partial \boldsymbol{\sigma}}{\partial X_r} &= \frac{\partial}{\partial X_r} \left(\frac{1}{\det \mathbf{F}} \mathbf{F} \mathbf{S} \mathbf{F}^T \right) \\ &= \frac{\partial}{\partial X_r} \left(\frac{1}{\det \mathbf{F}} \right) \mathbf{F} \mathbf{S} \mathbf{F}^T + \frac{1}{\det \mathbf{F}} \frac{\partial \mathbf{F}}{\partial X_r} \mathbf{S} \mathbf{F}^T \\ &\quad + \frac{1}{\det \mathbf{F}} \mathbf{F} \frac{\partial \mathbf{S}}{\partial X_r} \mathbf{F}^T + \frac{1}{\det \mathbf{F}} \mathbf{F} \mathbf{S} \frac{\partial \mathbf{F}^T}{\partial X_r} \end{aligned} \quad (5.22)$$

5.2 Solution approach for the Cutting Pattern Generation

The derivatives in equation (5.22) are straightforward except for the derivative of the 2. Piola-Kirchhoff stresses w.r.t. the nodal position in the reference configuration. To evaluate this derivation, the chain rule has to be applied:

$$\frac{\partial \mathbf{S}}{\partial X_r} = \frac{\partial \mathbf{S}}{\partial \mathbf{E}} : \frac{\partial \mathbf{E}}{\partial X_r} \quad (5.23)$$

In equation (5.23) the derivative of the 2. Piola-Kirchhoff stresses w.r.t. to the Green Lagrange strain tensor is equal to the elasticity tensor in terms of the reference configuration, which is defined in equation (2.60).

Residual stresses in the tensile structure: In the previous section it was discussed, that due to their double curvature, tensile structures can't be developed into a plane without compromises. Based on the governing equation derived in section 5.2, the difference of elastic and predefined stresses is minimized. This means that the resulting stress can't be identical to the intended one at each point on the surface. This shall be illustrated with the example shown in figure 5.9. If the resulting cutting pattern is introduced as the reference configuration of the elastic deformations of the assembling process in absence of external loads, the compromise can be seen in the resulting stress distribution. For the process of the structural analysis, the distance between the 2D pattern and the 3D current configuration is defined as an initial deformation. The 3D surface is in equilibrium w.r.t. the predefined stresses, as it was evaluated in form finding. Of course, if the cutting pattern is deformed to this configuration, the resulting stresses are not identical to the prestress. Due to that, this situation does not fulfill equilibrium. The resulting deformations to satisfy the equilibrium condition will result in a deviation of the current stress situation. The current stress distribution is illustrated in figure 5.9. It can be seen that the stresses deviate considerably from the indented prestress, which illustrates the compromise due to the non-developability of the doubly curved surface.

The compromise which has to be accepted in the cutting pattern of a doubly curved surface depends on different aspects. The first one is related to the material properties, or more precisely to the shear stiffness. The second influence parameter is the number of strips into which the tensile structure is divided. The last influence originates from the curvature of the tensile structure. In the following, the sensitivity of the cutting pattern w.r.t. the influence parameters is discussed.

The example illustrated in figure 5.10 will be used. The geometry of the hyperbolic kind of surface is defined in [Gos+13]. The length and width of the structure is defined to be $10.0[m]$ and the prestress to be $3.0[kN/m]$. In the following three different aspects will be discussed: (i) The change of area content of the cutting pattern w.r.t. a variation in the material parameters. Here, a linear elastic isotropic material is assumed with Young's modulus E and Poisson's ratio ν . In this case the cutting pattern of the surface will be evaluated in one piece, which means that the surface won't be divided into strips. The height is defined as $H = 5.0[m]$. (ii) The next investigation is done w.r.t. to the change in the maximum surface stress based on the variation of the number of introduced strips n . For this discussion the height is defined to be $H = 5.0[m]$ and the material parameters are fixed as $E = 250.0[kN/m]$ and $\nu = 0.3$. (iii) The third investigation will be done w.r.t. the

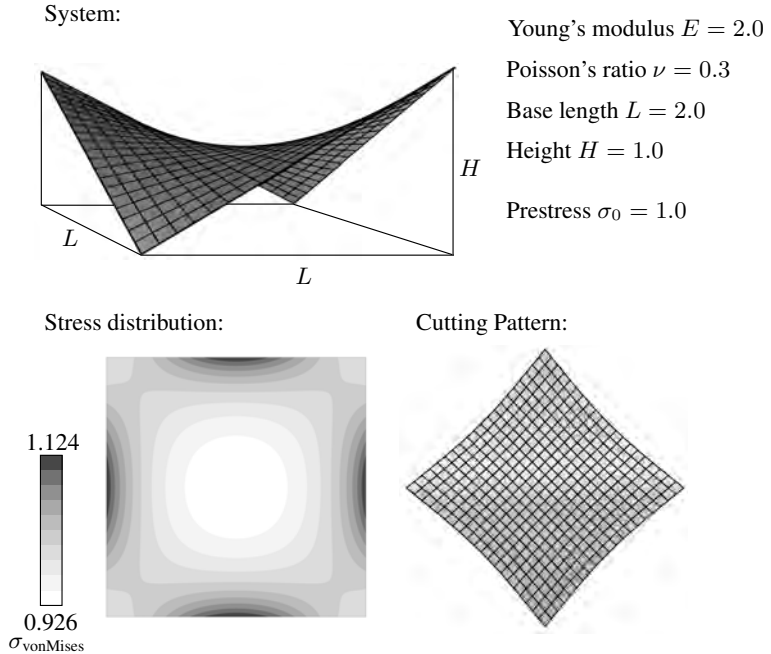


Figure 5.9: Residual stresses based on the optimized cutting pattern

change of maximum surface stress based on a variation in the Gaussian curvature if the surface is flattened in one piece. In order to modify the Gaussian curvature, the height of the structure is changing as $H = 0 \dots 10.0[m]$. It is obvious that for the case of zero height, the structure can be developed as it is already a plane surface. In this case the resulting stresses have to be the intended ones. Here, the material parameters again are defined as $E = 250.0[kN/m]$ and $\nu = 0.3$.

Sensitivity of the cutting pattern w.r.t. the material properties: In figure 5.11 the area content of the resulting cutting pattern for different material parameters is illustrated. As previously described, for the evaluation Young's modulus is varied from $E = 1.0 \dots 1000[kN/m]$ and Poisson's ratio from $\nu = 0.05 \dots 0.45$. The height and the number of strips are fixed. It can be seen that there is a large change in the area content for smaller values of Young's modulus and the influence of the Poisson's ratio is almost negligible. For a Young's modulus $E > 200.0$ the change in area content decreases substantially. The Young's modulus for architectural tensile structures is larger than 200.0 in general. Due to that it can be concluded that the influence of the material properties on the cutting pattern for architectural tensile

5.2 Solution approach for the Cutting Pattern Generation

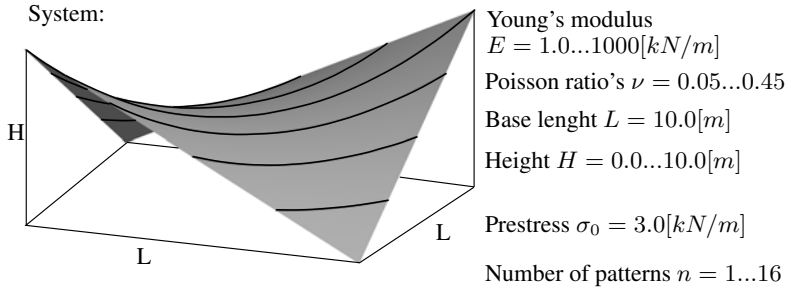


Figure 5.10: Hypar example for sensitivity of the residual stresses

structures is not overly critical. Of course, this conclusion only holds if a linear elastic material model is valid. If this is the case, for the evaluation of the cutting patterns the exact values of the parameters do not have such a vital influence since the overall shapes of the resulting patterns do not change that much. In the case of highly deformable materials, such as with furniture or car seats, the definition of the material parameters has to be precise. In this discussion only the influence from the elastic deformation in the cutting pattern is concerned. Of course, there will be an additional influence from the pre-stretch in the material, which will be discussed in the following.

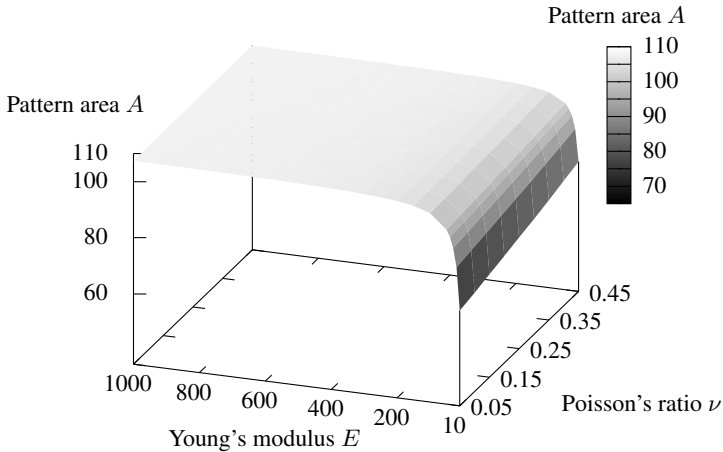


Figure 5.11: Sensitivity of residual stress w.r.t. material properties

Include the pre-stretch in the governing equations: In general the cutting pattern generation consist of the flattening of the doubly curved strips into a plane, compensate the elastic deformations which will occur during the assembly process and compensate the deformations which are related to the pre-stretch of the material. In the previous introduced governing equations this initial strain hasn't been discussed. In general the integration of the pre-stretch in the governing equation can be made by a various number of methods. One possibility is to modify the deformation gradient as formulated in equation (2.44). Here, the deformation is defined by the stretches λ_k . Therefore, the overall stretch consist of the elastic part $\lambda_{k,elastic}$ and the pre-stretched part $\lambda_{k,pre}$. Based on this, the modified deformation gradient can be given such:

$$\mathbf{F}_{mod} = \sum_{k=1}^3 (\lambda_{k,elastic} + \lambda_{k,pre}) \mathbf{n}_k \otimes \mathbf{N}_k \quad (5.24)$$

The integration of the pre-stretch $\lambda_{k,pre}$ in the deformation gradient can be done straightforward as these stretches are known from experiments. In the following examples the pre-stretch isn't considered, as it would not change the principal statement of the investigations.

Sensitivity of the cutting pattern w.r.t. the number of patterns: In figure 5.12 the result for the maximum von Mises stresses is illustrated, if the number of strips for the cutting pattern generation is varied. In this case the example defined in figure 5.10 will be divided into different numbers of patterns $n = 1 \dots 16$. The material parameters are fixed at $E = 250.0[kN/m]$ and at $\nu = 0.3$. The height of the structure is defined to be $H = 5.0[m]$ and the prestress to $\sigma_0 = 3.0[kN/m]$. It can be seen that by increasing the number of patterns, the maximum stresses in the surface will converge to the predefined stresses. Of course, this can be explained by the fact that as the strips get smaller the needed deformation to develop the individual strip decreases. In the limit case, if the width of the strips will tend to zero, the resulting stresses would be identical to the prestress at each point on the surface. In this example it can be seen that already for 8 strips the stresses will be close to the intended stresses. Of course, the resulting width of the patterns, approximately $1.25[m]$, is too small from a practical point of view, but the general conclusion can be made that with more strips the resulting stresses will converge to the intended stresses.

Sensitivity of the cutting patterns w.r.t. the Gaussian curvature of a tensile structure: In figure 5.13 the change in the maximum von Mises stresses w.r.t. a variation of the Gaussian curvature as defined in equation (2.32) is illustrated. Here, the Gaussian curvature is investigated in the center of the surface and the maximum values of the stresses are used. Based on the example defined in figure 5.10 the number of patterns is fixed at $n = 1$, which means that the surface isn't divided into parts, and the material parameters are defined as $E = 250.0[kN/m]$ and $\nu = 0.3$. For the variation of the curvature the height is changed as $H = 0 \dots 10.0[m]$. It can be seen that with increasing curvature the stress will increase as well. Therefore,

5.2 Solution approach for the Cutting Pattern Generation

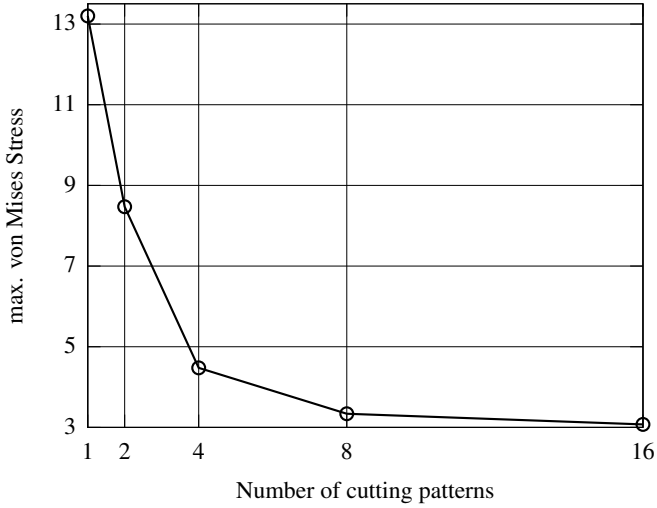


Figure 5.12: Sensitivity of residual stress w.r.t. number of cutting patterns

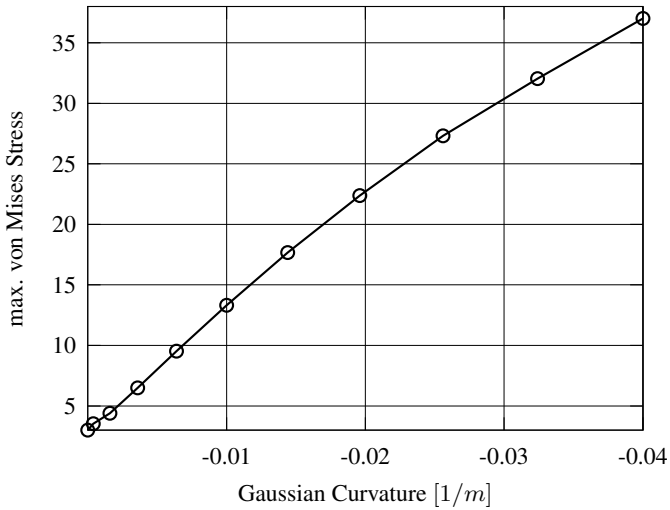


Figure 5.13: Sensitivity of maximum w.r.t. the change in curvature

it can be concluded that if the structure is characterized by a slight curvature, the width of the individual strips can be larger than in case of a high curvature. This discussion holds as well for certain regions of the structure. If a tensile structure is characterized by reasonable changes in curvature in the overall surface, the layout of the cutting patterns should be adapted to achieve a homogeneous stress distribution. Of course, it can be argued that if the curvature at a certain point is investigated, it won't change if the surface is considered as a whole or if it is divided into patterns. This argument is valid, but the deformation of a certain point from the plane 2D to the curved 3D configuration depends on the curvature and the distance of the point from the center of the pattern.

5.2.6 Ensure equal seam length of multi-strip cutting patterns

If the surface of the tensile structure is divided into more than one strip, the cutting patterns will be evaluated individually for each single strip. Because of this process it is obvious that the edge length of adjacent patterns do not fit to each other. From a practical point of view this characteristic introduces major difficulties in the manufacturing process, as the patterns will be welded together in order to assemble them in the final situation.

For the discussion of this characteristic, the example illustrated in figure 5.14 will be introduced. The geometry of the 6 point tent is defined with the base lengths $L = 10.0[m]$ and $B = 10.0[m]$, as well as by the height $H = 4.42[m]$. The prestress is defined as constant anisotropic. In section 3.3.1.3 it was discussed that for such a prestress distribution there exists no unique solution for the form finding problem. Based on the shape of equilibrium, the cutting pattern is evaluated. The surface of the given structure is divided into 5 strips.

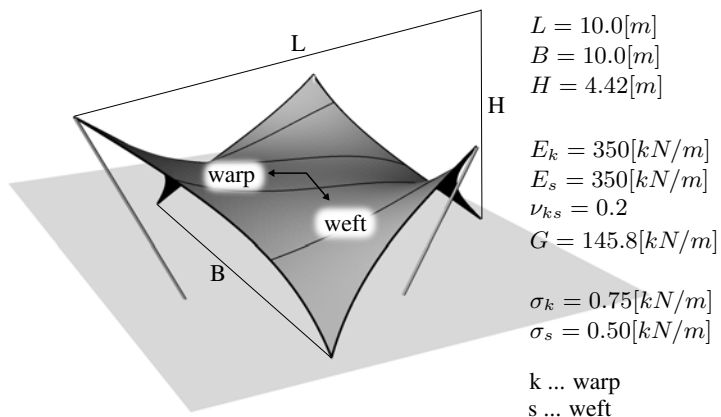


Figure 5.14: 6 point tent consisting of 5 patterns

5.2 Solution approach for the Cutting Pattern Generation

Table 5.1: Unconstrained seam lengths

No. seam line	L_i [m]	L_j [m]	ΔL_n [m]
1	4.69	4.74	0.05
2	7.08	7.07	0.01
3	7.08	7.07	0.01
4	4.69	4.74	0.05

The resulting cutting patterns for this example will be evaluated with the method of Least Squares as introduced in section 5.2.3 based on the discussion in section 5.2.4. For the case that the optimization is solved as previously defined, the shape, and therefore the seam lengths, are evaluated with the goal of minimizing the stress difference for the individual pattern. Based on this, it is obvious that the equality of the seam length of adjacent patterns can't be ensured. In figure 5.15 the individual lengths are illustrated and the resulting differences are given in table 5.1. However, an optimal cutting pattern is characterized by equal lengths of adjacent

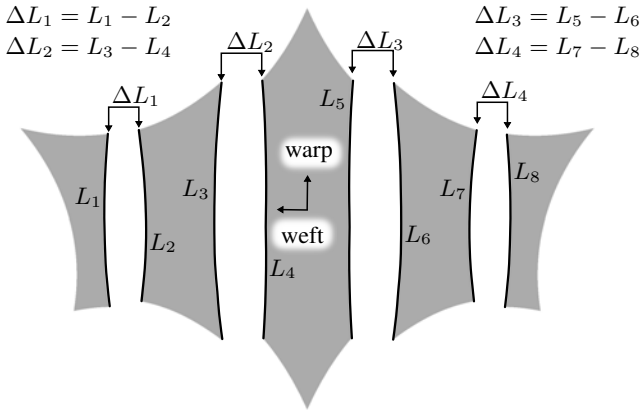


Figure 5.15: Cutting patterns of a 6 point tent and seam line lengths

patterns from a practical point of view.

The described result from the solution of the cutting pattern problem can be also explained on the basis of the governing equation. For the solution process, a discretization in terms of the Finite Element Method is introduced. In figure 5.16 some of the introduced degrees of freedom (dofs) at the nodes of the discretization are illustrated for the patterns in the middle of the surface. As illustrated, the dofs of

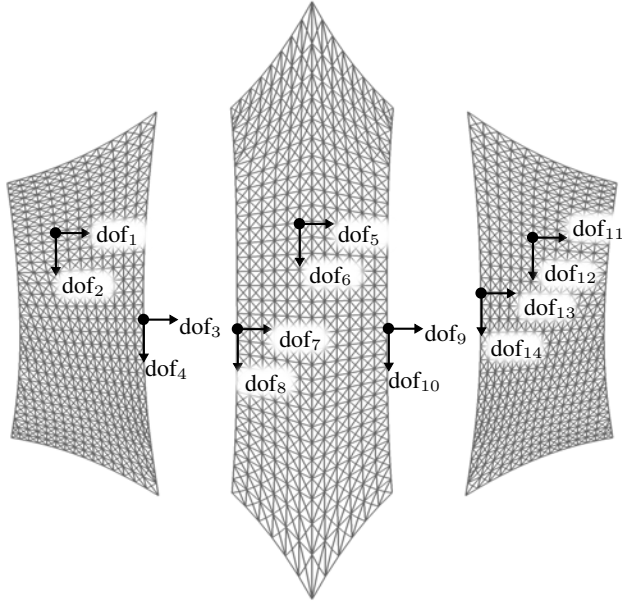


Figure 5.16: Degrees of freedom (dof) for the middle patterns

each individual pattern are restricted to a certain pattern. From a numerical point of view, this means that if the gradient of the objective function for a certain pattern is evaluated w.r.t. to a dof which belongs to another pattern, the resulting gradient will always be equal to zero. This can be understood as a decoupling of the individual patterns in the solution process. Of course this can also be seen in the resulting system of equations when applying a Newton Raphson method. Based on the objective function $f(\mathbf{X}_{2D})$, the resulting system of equations can be formulated as follows:

$$\begin{bmatrix} \nabla_{\mathbf{X}_{2D,1}}^2 f(\mathbf{X}_{2D}) & 0 & \dots & 0 \\ 0 & \nabla_{\mathbf{X}_{2D,2}}^2 f(\mathbf{X}_{2D}) & & 0 \\ \vdots & \vdots & & \vdots \\ 0 & 0 & \dots & \nabla_{\mathbf{X}_{2D,n}}^2 f(\mathbf{X}_{2D}) \end{bmatrix} \cdot \begin{bmatrix} \Delta \mathbf{X}_{2D,1} \\ \Delta \mathbf{X}_{2D,2} \\ \vdots \\ \Delta \mathbf{X}_{2D,n} \end{bmatrix} = \begin{bmatrix} \nabla_{\mathbf{X}_{2D,1}} f(\mathbf{X}_{2D}) \\ \nabla_{\mathbf{X}_{2D,2}} f(\mathbf{X}_{2D}) \\ \vdots \\ \nabla_{\mathbf{X}_{2D,n}} f(\mathbf{X}_{2D}) \end{bmatrix} \quad (5.25)$$

5.2 Solution approach for the Cutting Pattern Generation

In equation (5.25) $\mathbf{X}_{2D,n}$ are the unknown nodal coordinates in the 2D reference configuration w.r.t. the n^{th} cutting pattern. Based on the special structure of the resulting system matrix, it is possible to solve the cutting pattern problem separately for each strip. Therefore, the decoupling of the individual patterns also becomes visible from a mathematical point of view.

From an optimization point of view, the most direct way to ensure equal seam lengths is to introduce an appropriate constraint to the governing equation. In the case of the cutting pattern generation, the formulation of such a constraint can be achieved easily. As it should be ensured that the lengths of adjacent patterns are the same, the difference between them must be equal to zero. This type of constraint, where the equation has to be equal to zero, is introduced as an equality constraint in numerical optimization. Based on this idea the equality constraint can be formulated as follows:

$$\Delta L_i = L_{\text{left}} - L_{\text{right}} = 0 \quad (5.26)$$

To ensure equal seam lengths of adjacent cutting patterns, the introduced constraint from equation (5.26) has to be added to the optimization problem. There are various methods for the introduction of constraints in an optimization problem [BSS94], [Ber96], [HG92], [Van01]. Here, the *Augmented Lagrange Multiplier* (ALM) method will be applied. In principle this method represents a combination of a Lagrange Multiplier and a Penalty Method. The constraints ΔL_i are added to the objective function \mathbf{X}_{2D} and multiplied by the Lagrange parameter μ as well as the squared constraint multiplied with the penalty factor r . The *Augmented Lagrange Multiplier* was initially developed for the application of optimization problems with equality constraints. Therefore, the method is well suited for the given problem of cutting pattern generation. Based on the ALM the augmented Lagrange function L_A can be given by:

$$\min_{\mathbf{X}_{2D}} \rightarrow L_A(\mathbf{X}_{2D}, \mu_i) = f(\mathbf{X}_{2D}) + \sum_{i=1}^{n_{\text{seams}}} \mu_i \Delta L_i(\mathbf{X}_{2D}) + r \sum_{i=1}^{n_{\text{seams}}} \Delta L_i(\mathbf{X}_{2D})^2 \quad (5.27)$$

For the solution of the modified optimization problem given in equation (5.27) the *Karush-Kuhn-Tucker* (KKT) conditions are applied. The KKT conditions describe the stationary point condition for a constrained optimization problem. The resulting residual equations can be given as follows:

$$\begin{aligned} \nabla_{\mathbf{X}_{2D}} L_A(\mathbf{X}_{2D}, \mu_i) &= \nabla_{\mathbf{X}_{2D}} f(\mathbf{X}_{2D}) + \sum_{i=1}^{n_{\text{seams}}} \mu_i \nabla_{\mathbf{X}_{2D}} \Delta L_i(\mathbf{X}_{2D}) \\ &+ 2r \sum_{i=1}^{n_{\text{seams}}} \Delta L_i(\mathbf{X}_{2D}) \nabla_{\mathbf{X}_{2D}} \Delta L_i(\mathbf{X}_{2D}) = 0 \quad (5.28) \\ \nabla_{\mu_i} L_A(\mathbf{X}_{2D}, \mu_i) &= \sum_{i=1}^{n_{\text{seams}}} \Delta L_i(\mathbf{X}_{2D}) = 0 \end{aligned}$$

There are various solution techniques for constrained optimization problems. Here, a Newton Raphson algorithm will be applied. For the evaluation of the system matrix, the linearization of the KKT w.r.t. the nodal coordinates in the 2D reference

configuration and the Lagrangian parameters has to be done. The number of unknowns for the introduced governing equation are the number of nodal degrees of freedom plus the number of seam lines, as for each seam line i a Lagrangian parameter μ_i is defined ($\rightarrow \text{dof} + n_{\text{seams}}$). The resulting system of equations for the incremental solution of the minimization problem can be obtained by:

$$\begin{bmatrix} \nabla_{\mathbf{X}_{2D}}^2 L_A(\mathbf{X}_{2D}, \mu_i) & \sum_{i=1}^{n_{\text{seams}}} \nabla_{\mathbf{X}_{2D}} \Delta L_i(\mathbf{X}_{2D}) \\ \sum_{i=1}^{n_{\text{seams}}} \nabla_{\mathbf{X}_{2D}} \Delta L_i(\mathbf{X}_{2D}) & 0 \end{bmatrix} \cdot \begin{bmatrix} \Delta \mathbf{X}_{2D} \\ \Delta \mu_i \end{bmatrix} = \begin{bmatrix} \nabla_{\mathbf{X}_{2D}} L_A(\mathbf{X}_{2D}, \mu_i) \\ \sum_{i=1}^{n_{\text{seams}}} \Delta L_i(\mathbf{X}_{2D}) \end{bmatrix} \quad (5.29)$$

The component $\nabla_{\mathbf{X}_{2D}}^2 L_A(\mathbf{X}_{2D}, \mu_i)$ is again a decoupled matrix as in the unconstrained case. The off-diagonal terms of the system matrix $\sum_{i=1}^{n_{\text{seams}}} \nabla_{\mathbf{X}_{2D}} \Delta L_i(\mathbf{X}_{2D})$ are realizing the coupling in the system of equations, or in other words the gradients of the equality constraints are responsible for the coupling of the individual cutting patterns. From a numerical point of view the property of the decoupled system of equations in the unconstrained case allows an advantageous solution process, as the resulting system matrices can be solved individually for each strip in a certain iteration step. This characteristic introduces a time and storage saving potential in the numerical solution process. It is obvious that for the modified objective function the time saving potential will be lost. To overcome this drawback, a method will be introduced to exclude the Lagrangian parameters from the system of equations. For this purpose, an appropriate update method of the Lagrange parameters in the iteration steps has to be found. In [HG92] and [Hes69] a method to update the parameters is presented which can be derived from the equality of the Augmented Lagrangian and the Lagrangian function at the optimum $L_{\Lambda}^* = L^*$. The update method can be formulated as follows:

$$\mu_i^{(k+1)} = \mu_i^{(k)} + 2r \Delta L_i(\mathbf{X}_{2D}^{(k)}) \quad (5.30)$$

In equation (5.30) k represents the iteration counter for the optimization steps. Based on this update method the system of equations can be reduced to the nodal coordinates in the 2D reference configuration as remaining degrees of freedom. The

5.2 Solution approach for the Cutting Pattern Generation

Table 5.2: Constrained seam lengths

No. seam line	L_i [m]	L_j [m]	ΔL_n [m]
1	4.71	4.71	0.00
2	7.08	7.08	0.00
3	7.08	7.08	0.00
4	4.71	4.71	0.00

reduced system of equations can be given by:

$$\begin{bmatrix} \nabla_{\mathbf{X}_{2D,1}}^2 L_A(\mathbf{X}_{2D}, \mu_i) & 0 & \dots & 0 \\ 0 & \nabla_{\mathbf{X}_{2D,2}}^2 L_A(\mathbf{X}_{2D}, \mu_i) & & 0 \\ \vdots & \vdots & & \vdots \\ 0 & 0 & \dots & \nabla_{\mathbf{X}_{2D,n}}^2 L_A(\mathbf{X}_{2D}, \mu_i) \end{bmatrix} \cdot \begin{bmatrix} \Delta \mathbf{X}_{2D,1} \\ \Delta \mathbf{X}_{2D,2} \\ \vdots \\ \Delta \mathbf{X}_{2D,n} \end{bmatrix} = \begin{bmatrix} \nabla_{\mathbf{X}_{2D,1}} L_A(\mathbf{X}_{2D}, \mu_i) \\ \nabla_{\mathbf{X}_{2D,2}} L_A(\mathbf{X}_{2D}, \mu_i) \\ \vdots \\ \nabla_{\mathbf{X}_{2D,n}} L_A(\mathbf{X}_{2D}, \mu_i) \end{bmatrix} \quad (5.31)$$

Of course, with the update approach from equation (5.30) no quadratic convergence can be achieved in the Newton Raphson algorithm. Due to that, a further simplification for the process of the constrained optimization can be done. The gradient $\nabla_{\mathbf{X}_{2D,n}}^2 L_A(\mathbf{X}_{2D}, \mu_i)$ includes the derivative of the objective function and the constraints. The evaluation of the gradient of the constraints introduces additional effort from a numerical point of view and might be complex in the computation. Therefore, a *Modified Newton Method* can be used for the solution of the optimization problem. Therefore, the system matrix is replaced by the definition given in equation (5.25), as this version of the system matrix has to be computed in each case.

If the derived method is applied to the mentioned example, the resulting seam lines will be equalized. The overall patterns are just slightly effected and the difference can be seen only when looking in detail. In table 5.2 the equalized lengths for the constrained optimization problem are given.

The described extensions to the Least Square approach for the cutting patterns combines the general derived governing equations with the practical needs for the design of a tensile structure. As the governing equations are based on continuum mechanics and numerical optimization, it is possible to describe this behavior in a most general framework.

5.2.7 Influence of the Seams

In the manufacturing of a tensile structure, the individual cutting patterns will be assembled. In general, the strips will be welded along the seam lines. For the process of welding, the adjacent patterns have to overlap each other to enable the connection between them. The overlap can be realized in a simple way, in which just the two strips are overlapping. In this case, along the seam the material will be doubled and might be considered in the analysis. Additionally, the width of the overlap is important for the behavior of the seam. In [FM04] recommendations for the width of the overlap of the seams are given. From a mechanical point of view, the seam will introduce additional stiffness as the thickness is increased in these regions of the surface. Due to the increase of the stiffness along the seam lines, the stress distribution will be influenced. The effect of the seam line on the stress distribution is mainly controlled by the cross section area, as a product of the number of layers, the seam width and thickness of the membrane. Additionally, the density of the seams in the surface is an influence parameter. In the following, the influence of the seams on the resulting stress distribution will be discussed by varying the number of layers in the seam and the density of the seam lines in the surface. Here, the seam lines are modeled by cable elements as derived in section 4.3.1. It is important to consider that the thickness of the seam is defined by the number of layers minus 1, multiplied with the thickness of the membranes, as one layer is already included in the model of the membrane surface. The example illustrated in figure 5.17 will be used. The geometry of the hyper kind of surface is defined by the base length $L = 10.0[m]$ and the height $H = 5.0[m]$. The seam width is defined to be $b = 0.1[m]$ and the material is assumed to be linear elastic isotropic with the parameters $E = 250.0[kN/m]$ and Poisson's ratio $\nu = 0.3$. The prestress in the structure is defined to be $\sigma_0 = 3.0[kN/m]$.

Density of the seam lines in the surface: In figure 5.18 the ratio between the current maximum stress σ_{cur} in the surface for the individual pattern layouts w.r.t. the maximum stress σ_{max} for the single strip case is illustrated. In the following, the number of cutting patterns will be increased from 2 to 16. In this case the number of layers in the seams is fixed to 2. From figure 5.18 it can be seen that the number of seams effectively influences the stress distribution. Of course, this effect has to be seen in combination with the improvements regarding the developability of the individual strips for a low numbers of patterns as illustrated in figure 5.12. But in case of higher number of patterns $n > 4$ the stress reduction in the surface can be explained by the increased rearrangement of the stresses towards the seams.

Number of layers in the seam: In figure 5.19 the stresses in the membrane surface and the forces in the seam in relation to the individual maximum values are illustrated w.r.t. the number of layers in the seam. The computations for the given diagram are done on the basis of 8 patterns. As expected, the influence of the seam lines increases with the number of layers which are defined for the seam. While the stresses in the membrane decrease, the forces in the seam increase. This behavior can be explained purely by the introduced additional stiffness along the seam. Usually, in standard tensile structures, the number of layers does not exceed 4. From the

5.2 Solution approach for the Cutting Pattern Generation

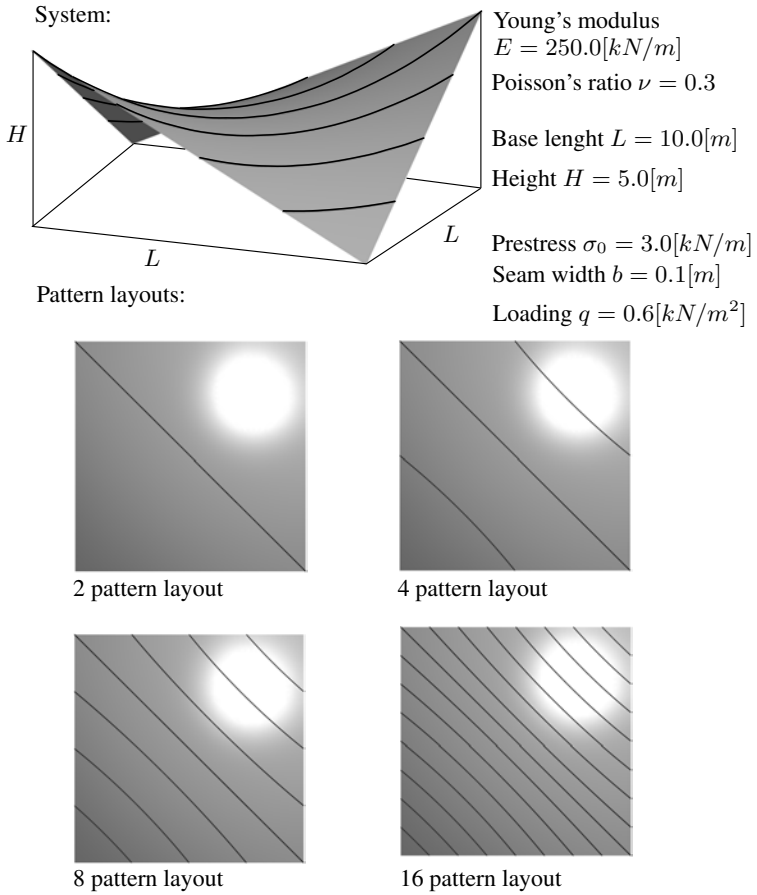


Figure 5.17: Different seam layouts for a hyper

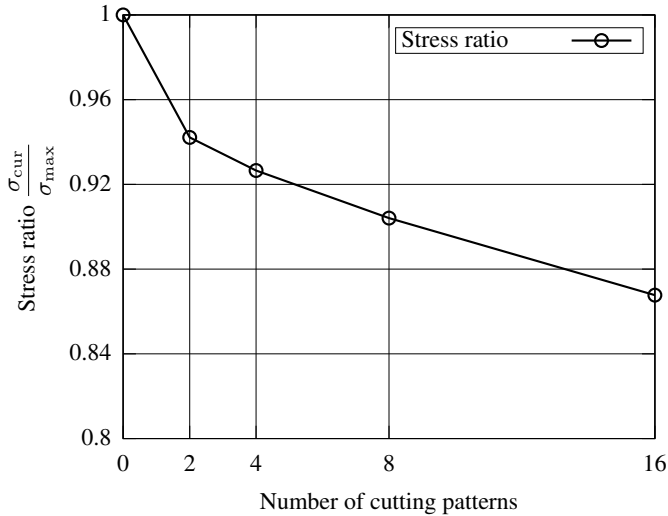


Figure 5.18: Stress ratio $\frac{\sigma_{cur}}{\sigma_{max}}$ w.r.t. the pattern layout

diagram it can be seen that in this case the surface stresses are reduced to 80% of the maximum value. Even for the simplest case of 2 layers the stresses are reduced by approximately 10%.

Based on the investigations described above, the question of whether the seam lines have to be modeled can't be answered uniquely. Of course, it can be seen that the seam lines have an influence on the final stress distribution, but it has to be decided in each case if the influence needs to be considered. It is obvious that it will never be a mistake if the seams are modeled, but in an early state of the design of a tensile structure, the exact layout of the seams is often not defined. In these cases it has to be decided on the basis of the pattern layout if the density and the possible number of layers are such that it will result in a major influence on the seams. If it is concluded that the seam will be influenced, an appropriate reserve in the stress design has to be considered.

5.2 Solution approach for the Cutting Pattern Generation

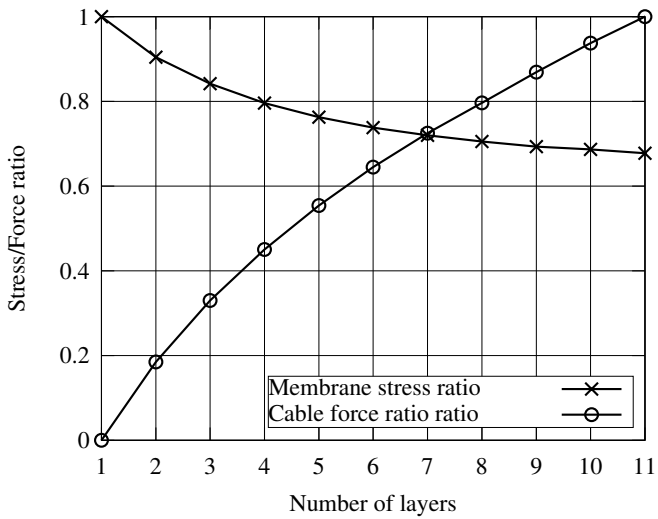


Figure 5.19: Stress $\frac{\sigma_{max}}{\sigma_0}$ and force $\frac{F_{max}}{F_0}$ ratio w.r.t. the seam layers

Conclusions

In general, tensile structures are doubly curved surfaces as the equilibrium, based on the in plane prestress, can just be satisfied by this type of shape. Therefore, the surfaces are non-developable. The process of cutting pattern generation defines the task of evaluating the plane 2D reference configuration which enables the manufacturing of the non-developable structure with the least compromises as possible. The evaluation of the cutting pattern can be made on the basis of different approaches. The compromise which has been accepted in this process becomes visible as the resulting deviation from the desired stresses when the assembly of the 2D reference to the 3D current configuration is done.

In this chapter, existing solution methods based on the *Variation of Reference Strategy* (VaReS) has been discussed. For a certain method the discussion of the sensitivity w.r.t. the individual input parameters has been included in this chapter. It was illustrated, that the derived method for the cutting pattern generation is able to evaluate high quality patterns. It is possible to include anisotropic material models, the compensation of the elastic and the pre-stretch deformations. Still, there are open questions as the influence and integration of creep and temperature, for example.

In addition to the discussion of the principles of the method, an extension that addresses practical issues is introduced to the method. The issue of equal seam lengths of adjacent strips is a crucial point to evaluate feasible cutting patterns. At the end of this chapter the influence of the welded seam lines has been included.

The process which has been introduced in this chapter consists of a continuum mechanical based method which is able to solve the problem of the non-developability of the structure. Additionally, the requirements to cutting patterns from a practical point of view have been included.

Design Loops and Interfaces

The design process of tensile structures can be divided into separate steps. The form finding, as discussed in chapter 3, is concerned with the evaluation of the shape of equilibrium w.r.t. a given prestress state in a given boundary. Based on this shape the following design steps, such as cutting pattern and structural analysis, will be carried out. In the step of structural analysis, the response of the structure w.r.t. external loads is evaluated. In chapter 4 this process has been discussed in detail. In order to manufacture the final shape of the tensile structure, a number of strips generally have to be assembled together to form the final shape. These strips for the manufacturing of the structure are defined in a 2D plane configuration. In the design step of cutting pattern generation, as discussed in chapter 5, the process of developing the individual 3D curved strips of the structure in the prescribed 2D domain is described.

In this chapter the individual steps will be connected in order to define appropriate design loops for the numerical simulation of tensile structures. Based on figure 1.4 it can be seen that it is possible to define two principal design loops. The standard design approach connects the individual design steps as *Form finding-Structural Analysis-Cutting Pattern Generation*. In contrast, the extended design approach switches the order to *Form finding-Cutting Pattern Generation-Structural Analysis*. In the following, the effects and the quality of the individual design loops will be discussed. Additionally, the effects of elastic members in the overall design process will be described.

For the connection of the individual design steps, interfaces are required which enable the transformation of the structural model between the design steps. At the end of this chapter the principal requirements of these interfaces will be discussed.

In the previous chapters the definition of the configurations from a continuum mechanical point of view could be done straightforward within each design step. In this chapter the definition of the reference configuration can't be done uniquely, as the reference point for the deformations may change for the individual design

6.1 Standard Design Approach

loops. In the following discussion of the different design loops the definition of the respective reference configuration will be done. The current configuration can be defined uniquely as it is the deformed geometry based on the external loads. To ensure consistent terms for the different geometry stages through the design loops the following naming will be introduced:

- Initial Configuration: The initial guess of the geometry in form finding
- Form Found Configuration: The shape of equilibrium which is determined in form finding
- Pattern Configuration: The geometry of the flat cutting pattern
- Assembled Configuration: The shape of the tensile structure after the assembling based on the cutting patterns
- Current Configuration: Deformed geometry based on the external loads

6.1 Standard Design Approach

The standard design approach, as illustrated in figure 1.4, starts with the evaluation of the shape of equilibrium by the form finding which represents the form found configuration. Based on the external load, the resulting deformations in a transient or steady state situation will be evaluated. The final stresses in the process of structural analysis will be used in order to decide about the ultimate and serviceability limit state of the design. If one of the structural requirements is not fulfilled, the overall design has to be changed. In the case that all requirements are fulfilled, the last step in this design loop is the evaluation of the cutting patterns for the manufacturing. In the standard design loop, this step is often done by the actual manufacturer of the structure instead of the designer. Due to that, the evaluation of the cutting patterns is usually located in a late phase of the overall design process.

From a continuum mechanical point of view, the steps in the standard design loop have to be assigned to the related configurations. In figure 6.1, it can be seen, that the form found configuration is introduced to be the reference configuration \mathbf{X} for the structural analysis. Here, the deformations $\mathbf{u}_{\text{Loading}}$ related to the external loads will lead to the current configuration \mathbf{x} .

In chapter 5 it was already discussed that the general non-developability of the shapes of tensile structures introduces variations in the resulting prestress. In the standard design approach, this effect, based on the deformations $\mathbf{u}_{2D \rightarrow 3D}$ from the cutting pattern on the resulting stress distribution, is neglected. The structural analysis is carried out on the assumption that the stresses in the surface are equal to the prescribed prestresses. The examples given in chapter 5 have shown that the difference in the resulting stresses from the assembling process and the prestresses can vary substantially. From an engineering point of view this means that with the application of the standard design approach a non quantifiable uncertainty remains in the design.

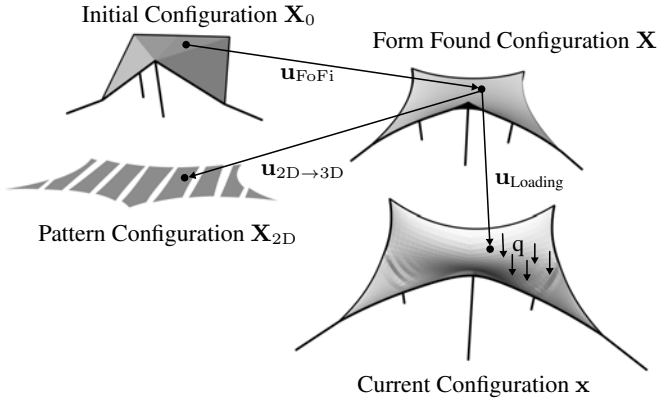


Figure 6.1: Standard Design Approach

In the following, the standard design approach will be applied for the evaluation of the final stresses for the example illustrated in figure 6.2. The given 4 point tent is defined referring to an example given in [Gos+13]. The form finding of the structure is carried out w.r.t. the given isotropic prestress values for the membrane and the edge cables. Subsequently, the resulting shape of equilibrium is interpreted as the reference configuration and the prescribed prestresses are considered in the formulation of the related finite elements as given in section 4.3. The load for the structural analysis is defined as a snow-type load, which is invariant in time. Therefore, a steady state analysis is applied in order to evaluate the stresses in warp and weft direction as illustrated in figure 6.2.

It can be seen that the final stress distribution is as expected. The stresses at the high points of the 4 point increase as the stresses at the low points decrease. From a design point of view, this stress distribution and the related deformations would be used in the design of the ultimate and serviceability limit state.

Based on the given example, it can be seen, that the standard design approach can be applied easily with a minimum of complexity in the interfaces to transfer the numerical model between the individual design steps. This approach is based on the simplified assumption that the cutting patterns have no influence on the final stress distribution. In the next section, the variations in the prescribed stresses based on the cutting pattern will be discussed, which will increase the quality of the evaluated stress distribution.

6.2 Extended Design Approach

The standard design approach described in the previous section includes the drawback that the influence of the cutting pattern on the final stress distribution is ne-

6.2 Extended Design Approach

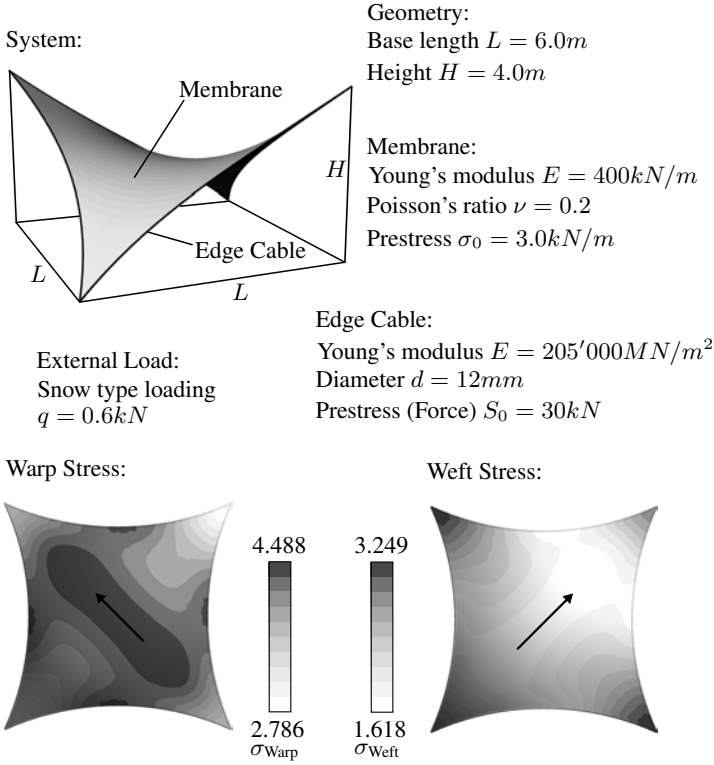


Figure 6.2: 4 point tent example with standard design approach

glected. In order to overcome this, the extended design approach will be introduced. Based on figure 6.3 the principal change in the definitions of the configurations can be described. The inclusion of the cutting pattern is realized by the definition of the assembled configuration $\bar{\mathbf{X}}$. Therefore, the deformations $\mathbf{u}_{2D \rightarrow 3D}$, evaluated in the cutting pattern process, are added to the pattern configuration \mathbf{X}_{2D} . The deformations w.r.t. the external load will be computed based on this assembled configuration $\bar{\mathbf{X}}$. Due to that, it is possible to introduce the exact stress distribution from the assembling process as already discussed in chapter 5.

In principle, there are two methods to introduce the assembled configuration in the numerical modeling process [Die+13b]. The obvious approach would be to include the deformations from the cutting pattern to the assembled configuration into the structural analysis as an initial deformation. Based on this, the overall deformation can be obtained by:

$$\mathbf{u}_{final} = \mathbf{u}_{2D \rightarrow 3D} + \mathbf{u}_{Loading} \quad (6.1)$$

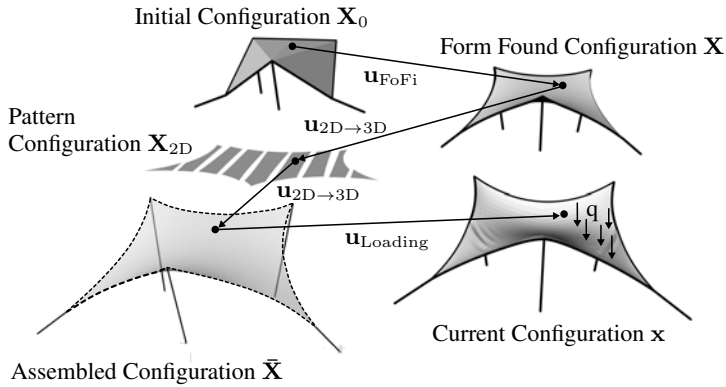


Figure 6.3: Extended Design Approach

Therefore, the cutting pattern will be introduced as the reference configuration for the evaluation of the continuum mechanical quantities. In the case of the application of external loads which are defined w.r.t. the built structure, like dead or snow load, the assembled configuration has to be introduced for the evaluation of the load related parts in the governing equations.

The second possibility, for the introduction of the cutting pattern in the structural analysis, is to evaluate the stress state resulting from the assembly process and define it as the prestress in the surface. This can be understood such that the prescribed stresses will represent the cutting patterns in the computation. Therefore, the assembled configuration can be introduced as the reference configuration. In this approach there is no need to introduce the cutting patterns in the governing equations. Of course, the main advantage of this approach is that all continuum mechanical quantities are related to the same reference configuration.

On the first glance it seems that the two approaches are identical. In [Die+13b] a discussion of the two methods is given on the basis of the previously introduced von Mises framework as illustrated in figure 4.2. Here, the first approach, where the deformation from the cutting pattern to the assembled configuration is considered as an initial deformation, is described as the modeling of the full deformation. The second approach, where the initial deformations are considered as a predefined stress distribution and the further deformations are defined w.r.t. the assembled configuration, is introduced as the incremental deformation description. In the following, the same example will be used in order to discuss the differences in the approaches. The example is illustrated in figure 6.4. In this example the cutting patterns are represented by the undeformed shape of the trusses defined by the height h and the base length b . The deformation between the cutting pattern and the assembled configuration is given by u_0 . The further deformation is defined by Δu . Here, the

6.2 Extended Design Approach

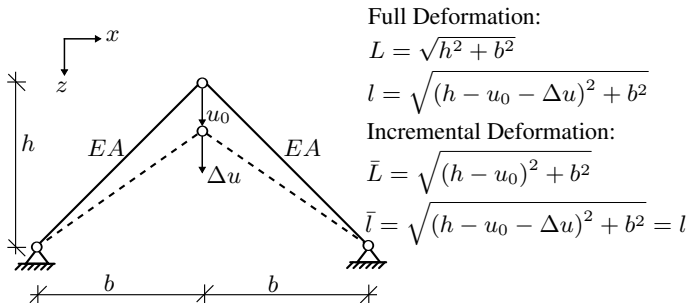


Figure 6.4: von Mises example for the configuration update

additional deformation is assumed to be prescribed, which is generally related to an external load of varying magnitude. For both cases, the full and the incremental description, the respective length in the reference and the current configuration is given. It can be seen that for both descriptions of the deformation process, u_0 and Δu are included in the current configuration. In the case of the incremental description u_0 is considered in the reference configuration as well. From this definition, the different interpretation of the reference configuration becomes obvious.

The formulation of the equilibrium equation can be done for both cases based on the governing equations which are derived in section 4.3.1. Here, the Green Lagrange strains are formulated w.r.t. a local coordinate system given in equation (4.21). Using this, the strains can be given in terms of the initial and the additional deformation. In case of the consideration of the full deformation process, the strain $\varepsilon_{GL}(l, L)$ dependent on the overall deformation $u_0 + \Delta u$. Due to that, the residual equation for this case can be given by:

$$\begin{aligned}
 R_z &= EA\varepsilon_{GL}(l, L) \frac{\partial \varepsilon_{GL}(l, L)}{\partial \Delta u} L \\
 &= EA \left(\frac{1}{2} \frac{l^2 - L^2}{L^2} \right) \frac{l}{L} \frac{\partial l}{\partial \Delta u} L
 \end{aligned} \tag{6.2}$$

In the case of the incremental modeling of the deformation process, the initial state u_0 is transferred to a prestress $S_0(\bar{L}, L)$ in the truss members. With the assumption of a linear elastic isotropic material, this prestress can be evaluated by the multiplication of the Green Lagrange strains $\varepsilon(\bar{L}, L)$ with the respective Young's modulus E :

$$S_0(\bar{L}, L) = E\varepsilon(\bar{L}, L) = E \left(\frac{1}{2} \frac{\bar{L}^2 - L^2}{L^2} \right) \tag{6.3}$$

With equation (6.3) the equilibrium equation for the incremental approach for the deformation process can be given by:

$$\begin{aligned}\bar{R}_z &= (EA\varepsilon_{GL}(\bar{l}, \bar{L}) + AS_0(\bar{L}, L)) \frac{\partial \varepsilon_{GL}(\bar{l}, \bar{L})}{\partial \Delta u} \bar{L} \\ &= EA \left(\frac{1}{2} \frac{\bar{l}^2 - \bar{L}^2}{\bar{L}^2} + \frac{1}{2} \frac{\bar{L}^2 - L^2}{L^2} \right) \frac{\bar{l}}{\bar{L}} \frac{\partial \bar{l}}{\partial \Delta u} \bar{L}\end{aligned}\quad (6.4)$$

Comparing equation (6.2) and equation (6.4) it can be seen that due to the different consideration of the initial deformation, the equilibrium equations are not equal. In particular, the value in brackets exemplifies the difference in the governing equations. The values around the brackets are equal in both cases as the derivative of the respective current lengths and the axial stiffness are identical. Due to the nonlinear nature of the strains, the different interpretation of the initial state the equilibrium equations differ from each other. The difference can be illustrated by a plot of the residual force R_z as well as the related first order derivative for the stiffness K for both cases. In figure 6.5 the difference in the solution can be seen. The diagram is achieved for an axial stiffness $EA = 1$, an initial deformation $u_0 = 0.2$ and the geometry $b = h = 1$. The resulting system behavior will differ fundamentally for

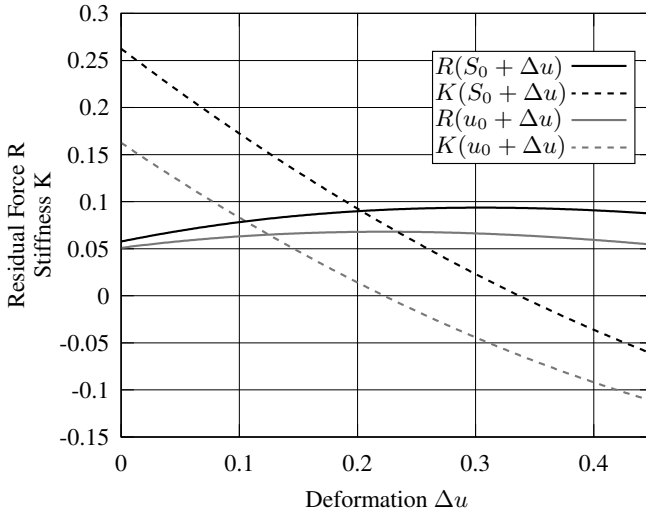


Figure 6.5: Results for the von Mises truss with an initial deformation

both modeling approaches. The different characteristics can be discussed based on the location of the critical point for the individual methods (i.e. where the stiffness is equal to zero $K = 0$). As for the full deformation approach, the critical point is located at $\Delta u \approx 0.22$. In contrast, for the incremental approach this point is

6.2 Extended Design Approach

located at $\Delta u \approx 0.34$. This substantial shift illustrates, the different structural behavior, only based on the individual modeling approaches.

The example of the von Mises framework can be easily transferred to the modeling of tensile structures. If the cutting pattern is introduced as the reference configuration in the strains, the initial deformations will occur which can be understood as equivalent to the full deformation description for the simple truss example. For the case that the stresses, resulting from the initial deformation from the cutting pattern to the assembled configuration, are introduced in the governing equation for the equilibrium, the incremental deformation formulation will be applied.

For the example of the 4 point tent given in section 6.1, the two modeling approaches will be applied. The cutting patterns are based on a 5 strip layout and the constraint of equal seam lengths is applied. The resulting cutting patterns are illustrated in figure 6.6 as well. The structural properties for the membrane, cable as well as for the loading are the same as in the discussion of the standard design loop.

The resulting stresses of the structural analysis w.r.t. to the defined snow-type loading are illustrated in figure 6.7. It can be seen that the principal characteristic of the stresses are the same for both modeling approaches. Even the maximum stresses in the warp direction are almost identical. The difference becomes visible by comparing the minimum warp stresses. For this example, the maximum stresses are almost equal. The difference in the minimum stresses is substantial. From a design point of view this result would not change the ultimate limit state design, but the interpretation of the possibility for wrinkles in the surface would differ. Based on this, it can be seen that the choice of the modeling approach influences the final stress distribution substantially.

Of course, from a continuum mechanical point of view, the full deformation approach seems to be preferable. However, for the modeling of the tensile structure this introduces additional effort in the numerical description. In general, the tensile structure will be divided into several cutting patterns. Additionally, structural elements, like edge cables or arches, will be involved in the simulation process. If the cutting patterns are introduced in the structural analysis as the reference configuration of the membranes, the individual elements are no longer attached to each other. The gap between the individual patterns as well as between the resulting membrane surface and the edge cable or other structural elements has to be closed. From a continuum mechanical point of view, this means that in this approach each structural element in the analysis has its own reference configuration which is not attached to the others. From a numerical point of view, this introduces the challenge that in the beginning of the computation the individual members have to be assembled together and the equilibrium of the resulting internal forces has to be evaluated before an external load can be applied. This additional modeling effort can be disadvantageous for various applications. However, this modeling approach should be preferred as it describes the "true" deformation process.

The discussion so far only addresses how the deformation from the cutting pat-

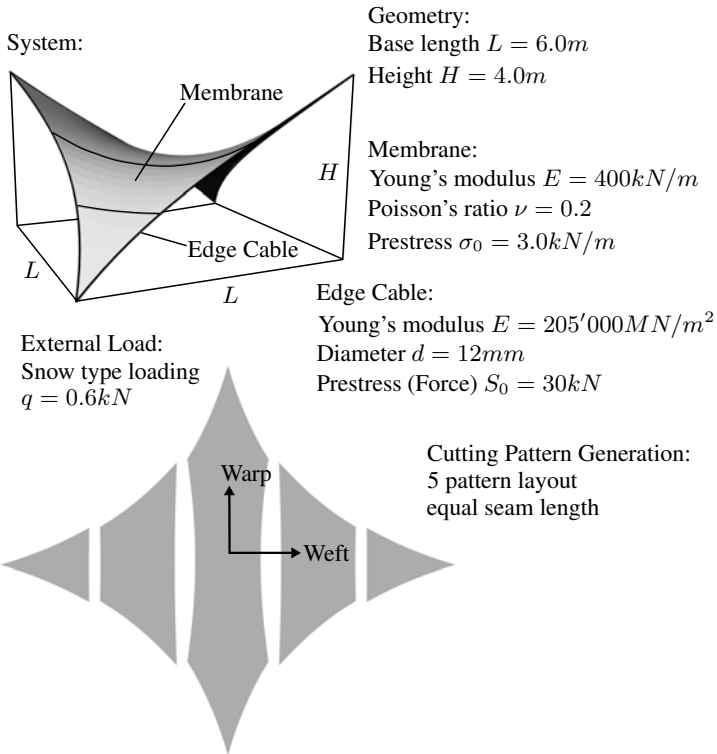


Figure 6.6: 4 point tent example with extended design approach - cutting pattern layout

tern to the assembled configuration can be introduced in the structural analysis. Of course, the actual comparison of the standard and the extended design approach is of major importance. For this comparison the final stresses will be evaluated on the basis of the full deformation modeling approach as illustrated in figure 6.8. Comparing figure 6.2 and figure 6.8 shows that there is a substantial difference in the final stresses. With the standard design approach, the maximum final stress in the warp direction has a value of $\sigma_{warp} = 4.498$, whereas the extended approach results in $\sigma_{warp} = 7.592$. Based on this comparison it can be seen that the decision of the design approach introduces substantial consequences to the final stress distribution, which have to be considered by the designer. Of course, the difference for the individual application is influenced by the choice of the material properties and the cutting pattern layout.

Based on this comparison, the extended design approach can be characterized as

6.2 Extended Design Approach

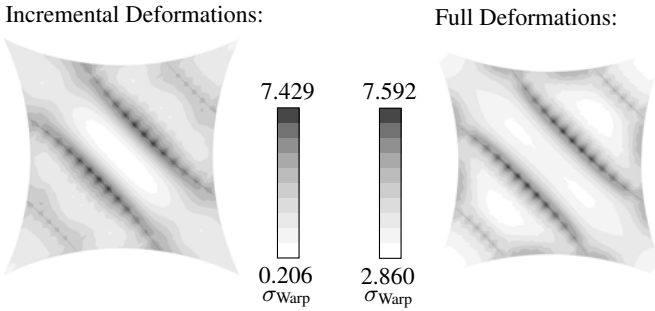


Figure 6.7: Residual stress for the 4 point tent w.r.t. the different modeling approaches

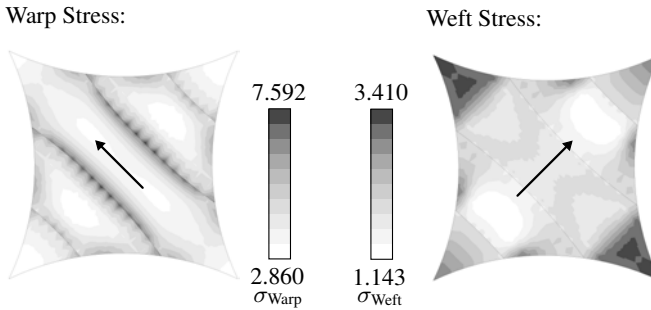


Figure 6.8: Residual stress for the 4 point tent for full modeling approach

the more exact and reliable modeling method. Of course, the introduction of the cutting patterns in the structural analysis requires the definition of the layout in an early stage of the design process and introduces new challenges to the designer. On the other hand, based on the extended approach the designer is able to come up with more effective and reliable designs. Additionally, the application of the extended design approach introduces the demand of high accuracy in the manufacturing process if the resulting potentials for a efficient design will be exploit. If the assembled cutting patterns deviate from those introduced in the numerical simulations, the final stress distribution will differ from the evaluated values. This will result in an uncertainty in the ultimate limit state design.

6.3 Elastic Members in the Design Process

In state-of-the-art tensile structures, elastic elements are introduced in order to enlarge the design space. From an engineering point of view, these elements can be applied to improve the structural capacity, such as the dynamic or buckling behaviors. From an architectural point of view, these elements can be used to design new types of shapes based on the elasticity of the elements. If elastic elements are introduced to tensile structures, they have to be considered in the overall design process. Therefore, the discussion of the effects of these elements was already included for the process of form finding in section 3.5. Here, it was shown that for the evaluation of the shape of equilibrium, elastic deformations are going to occur in the elastic elements. At the end of the form finding process the prestress in the tensile structure and the evaluated stresses in the elastic elements, based on the deformation in the form finding process, are in equilibrium. In order to transfer this shape of equilibrium to the structural analysis, two principal methods exist.

The first method is to introduce the deformation of the elastic elements from form finding as an initial deformation \mathbf{u}_0 and keep the initial configuration $\mathbf{X}_{\text{elastic}}$ as the reference configuration. For the tensile members, the reference configuration is updated in each form finding step by applying the URS in order to achieve the shape of equilibrium. Therefore, the reference configuration $\mathbf{X}_{\text{tensile}}$ for tensile elements is well defined by this shape. In figure 6.9 the process of the full description of the deformation for the elastic members is illustrated. It is obvious that for

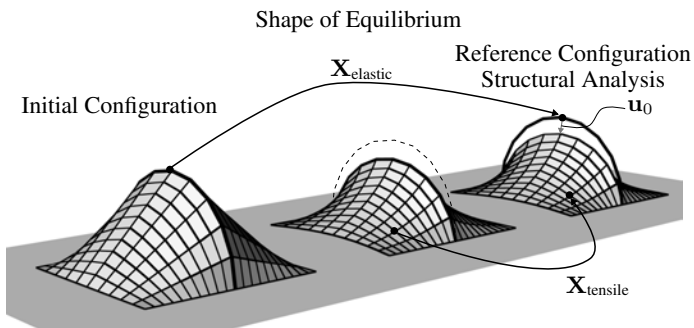


Figure 6.9: Configuration update in the case of the full description of the deformation process

this modeling approach it is implied, that the elastic and the tensile elements are not attached to each other anymore. Due to that, in the beginning of the structural analysis, the initial deformation has to be applied for the elastic elements in order to describe the actual shape of equilibrium. From a numerical point of view, this approach introduces additional effort as further nodes for the elastic elements have to be modeled and the coupling of these nodes with the related ones on the tensile after the application of the initial deformations have to be realized. In [DWB12] the

6.3 Elastic Members in the Design Process

effects on the numerical modeling by this approach were first discussed. In order to overcome this additional effort in the numerical modeling, a second method to transfer the shape of equilibrium to the structural analysis can be discussed.

The main idea for the second method to describe the shape of equilibrium is to keep the elastic and tensile elements attached. This can be realized by prescribing the stresses which are occurring due to the deformation of the elastic elements in the form finding process as predefined stresses $S_0 = S_{\text{elastic}}$. Due to this, the reference configurations for the elastic elements $\mathbf{X}_{\text{elastic}}$ and for the tensile members $\mathbf{X}_{\text{tensile}}$ are equal and aligned with the updated geometry. With this approach it is possible to describe the deformations w.r.t. external loads in an incremental method, based on the updated reference configuration. In figure 6.10 the process of the incremental description of the deformation for the elastic members is illustrated.

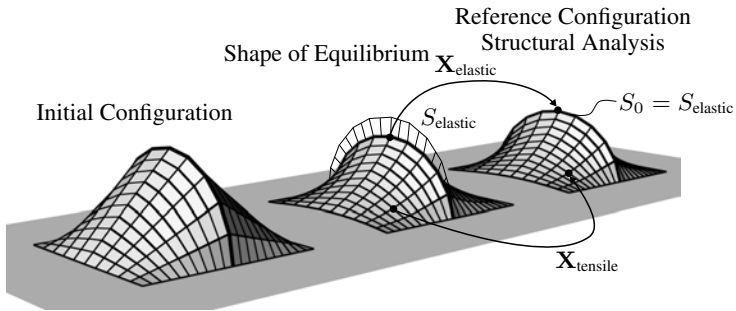


Figure 6.10: Configuration update in the case of the incremental description of the deformation process

For both methods the elastic deformations are assumed to be evaluated in the form finding process. These deformations are transferred to the structural analysis in order to describe the shape of equilibrium. If the cutting pattern of the membrane is designed such that the variation in the final stress distribution in the membrane can be assumed to be the intended stresses, the initial configuration of the elastic elements can be understood as the actual cutting pattern of these elements. Based on this idea it is obvious, that the discussion of the elastic elements in the structural analysis is the same as for the introduction of the cutting pattern for the tensile elements as they also are introducing elastic stresses in the assembly process.

In section 6.2 the individual methods for the introduction of the cutting pattern in the structural analysis are discussed for tensile elements. Here, the possibilities to model the full deformation of the structure w.r.t. an external load based on the cutting pattern as well as an incremental approach have been discussed. Obviously, these approaches requires that the cutting pattern of the elastic element is known. In contrast to the tensile elements, so far there exists no method for the evaluation

of the cutting pattern for the elastic elements similar to the presented ones. Therefore they can only be assumed. In the previous discussion, the initial configuration has been accepted as the cutting patterns for the elastic elements. Of course, the methods introduced in chapter 5 can be applied for elastic elements as well, but the related kinematic must be included in the governing equations.

From the discussion of the individual methods for the introduction of the initial deformations of the elastic elements in the structural analysis it could be concluded that the full deformation approach should be preferred in each case. This conclusion would be valid if the elastic elements were subjected to large deformations in each case, like tensile elements. However, for most architectural tensile structures the deformations of the elastic members remain small as they form the supporting structure which is required to keep its shape. Due to this, the formulation of the kinematic for the elastic elements can be linearized in most cases. In the following, the von Mises truss example given in section 6.2 will be discussed by applying linearized strain measurements to the governing equations.

For the formulation of the residual equations, the linearized strains for the initial deformation can be formulated as follows:

$$\varepsilon^{\text{lin}}(u_0) = \frac{u_0}{\sqrt{2}L} \quad (6.5)$$

The additional strains w.r.t. an incremental deformation based on the assumption of a linearized kinematic can be given by:

$$\varepsilon^{\text{lin}}(\Delta u) = \frac{\Delta u}{\sqrt{2}L} \quad (6.6)$$

Finally, the strains for the full modeling of the deformations can be achieved by the summation of the strains from equation (6.5) and equation (6.6):

$$\varepsilon^{\text{lin}}(\Delta u + u_0) = \frac{\Delta u + u_0}{\sqrt{2}L} \quad (6.7)$$

For the formulation of the residual forces, the derivative w.r.t. the incremental deformation Δu of the individual strain equations has to be calculated. In the case of the full deformation process, the residual equation can be obtained by substituting equation (6.7) and the related derivative in equation (6.2). Hence, the resulting residual equation can be formulated as follows:

$$R_z = \left(EA \frac{\Delta u + u_0}{\sqrt{2}L} \right) \frac{1}{\sqrt{2}} \quad (6.8)$$

For the incremental approach to the deformation modeling, the predefined stresses have to be evaluated. Based on the assumption of a linear elastic isotropic material, the prestress can be given by the multiplication of the strains w.r.t. the initial deformation and the related Young's modulus E :

$$S_0^{\text{lin}}(u_0) = E\varepsilon^{\text{lin}}(u_0) = E \frac{u_0}{\sqrt{2}L} \quad (6.9)$$

6.3 Elastic Members in the Design Process

Substituting equation (6.9) in equation (6.4), the residual equation can be formulated as follows:

$$\bar{R}_z = \left(EA \frac{\Delta u}{\sqrt{2L}} + AS_0^{\text{lin}}(u_0) \right) \frac{1}{\sqrt{2}} = \left(EA \frac{\Delta u + u_0}{\sqrt{2L}} \right) \frac{1}{\sqrt{2}} \quad (6.10)$$

From equation (6.8) and equation (6.10) it can be seen that the two approaches result in the almost identical residual equation beside the reference length. Therefore, it can be concluded that for the cases where the elastic element is subjected to small deformations, both introduced approaches for the inclusion of the initial state in the structural members will result in a similar or almost identical behavior as the reference length tends to be equal. In order to illustrate the correlation between the two individual methods in the case of small deformations, the example shown in the bottom figure of figure 6.11 will be discussed. The given arch hall is based on a design done at the Chair of Structural Design at the TU München, shown in the top figure of figure 6.11.

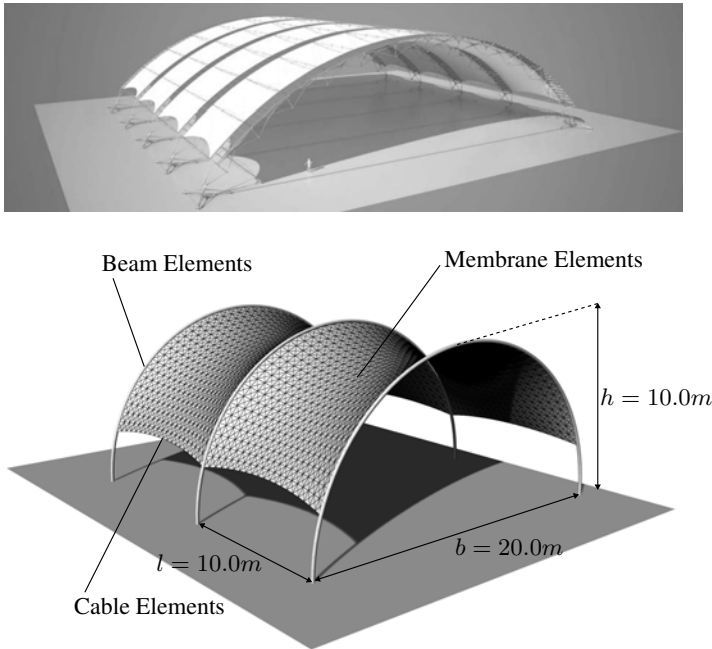


Figure 6.11: Arch Hall example

For the defined example, a form finding is evaluated in order to achieve the shape of equilibrium. The resulting maximum deformations of the elastic beam elements are

$u_{\max} = -0.1811[m]$. For the modeling of the beam elements the theory of second order is applied in order to be able to model the moderate deformations. It can be seen that the deformations remain small in contrast to the geometry, which allows the application of the theory of second order.

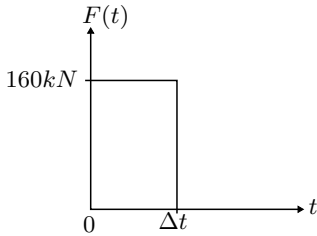
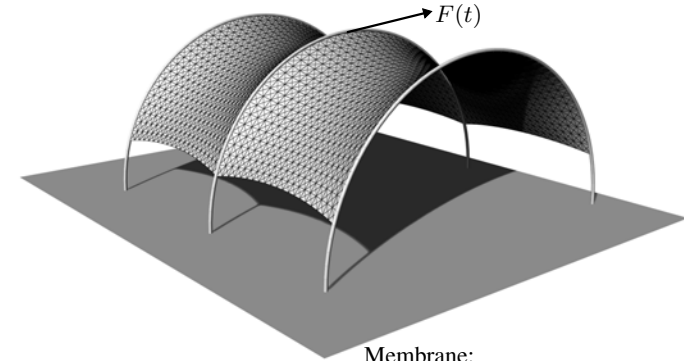
Based on the resulting shape of equilibrium a dynamic computation is evaluated, where a single force is applied to the top of the middle arch as illustrated in figure 6.12. The applied force only acts in the first time step, which results in a free vibration in the following time steps. For this simulation the damping effects of the structure are neglected. Based on this example it will be shown that for small deformations the applied methods for the initial state will result in the same structural behavior. Both methods will be compared to the approach where the initial state is neglected and the reference configuration of the elastic elements are defined on the shape of equilibrium by neglecting the initial deformations or stresses. This approach is indicated by "None" in the following.

From figure 6.12 it can be seen that the results for the full and incremental deformation modeling show the same structural behavior. The difference to the approach where the initial state is neglected becomes obvious. This can be seen in the substantial shift of the eigenfrequency of the system. The given example illustrates the general importance of the inclusion of the initial state even in cases of small deformations. However, the choice between these two approaches depends on preference or the numerical framework available. The effects of the modeling approach on the quality of the final results are not exclusively a discussion for the assessment of the ultimate and serviceability limit state. For numerical applications where the structural model can be interpreted as an input, the quality becomes essential for the related results. An example for such a simulation is given by the exact evaluation of the wind load behavior of the structure.

For the definition of the wind load which acts on a tensile structure, the available national codes are insufficient in most cases. Therefore, the wind loads are defined by performing wind tunnel experiments for small scale models of the tensile structure. As the thickness of the applied membrane material is thin in general, the scaling of the real structure to a small scale model introduces additional complexity to the process of experimental evaluation of the wind loads. Based on this scaling issue, the actual flexibility of the structure is difficult to adjust with the experimental model. To overcome this problem, the possibility to model the wind load situation on the tensile structure numerically has been introduced. For this, the characteristic of the wind is modeled as a fluid in a computational fluid dynamic simulation (CFD). If the structural model is introduced to the wind simulation, the effects from the deformation of the structure on the wind characteristic can be evaluated. The achieved numerical framework is defined as a Fluid-Structure-Interaction (FSI) simulation. For a discussion of this kind of simulation for tensile structures, refer to [Kup09], [Mic10], [Wüc07].

For the given example of the arch hall, the FSI simulation was done in [Gal10]. The results from this computation for a certain time step are illustrated in figure 6.13. Here, the structural model and the resulting stream lines of the wind are shown.

6.3 Elastic Members in the Design Process



Membrane:
 Young's modulus $E = 500kN/m$
 Poisson's ratio $\nu = 0.2$
 Prestress $\sigma_0 = 5.0kN/m$

Edge Cable:
 Young's modulus $E = 210.000MN/m^2$
 Cross Section $A = 236mm^2$
 Prestress (Force) $S_0 = 100kN$

Beam:
 Young's modulus $E = 210.000MN/m^2$
 Cross Section $A = 90mm^2$
 Moment of Inertia $I_y = I_z = 1200cm^4$

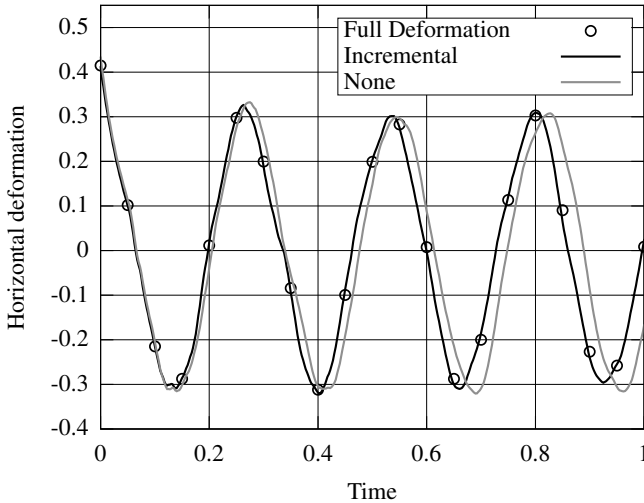
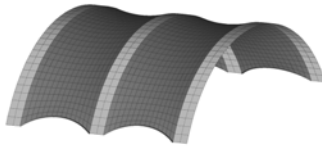


Figure 6.12: Arch Hall example results

Structural model:



Stream lines of the wind:

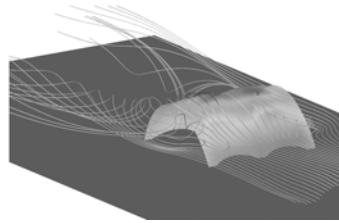


Figure 6.13: Arch Hall example FSI [DWB10], left: structural model; right: stream lines

Based on this numerical approach, for the evaluation of the wind effects on the tensile structure, arbitrarily shaped structures can be simulated without introducing an error from the scaling effect. It is obvious that for such challenging numerical simulations, the exactness of the introduced structural model has an essential effect on the final results achieved by the FSI simulation.

6.4 Requirements for the Interfaces

In the previous sections, two different design loops have been discussed. For both the transition between the individual design steps has to be realized. For the application, specific interfaces between the individual design steps have to be defined. In general, the requirements for the interfaces are to transfer stresses or deformations from the current design step to the following one. At a first glance it seems that based on this requirement the interfaces are well defined. It could be interpreted that the transition of the prestress state from the current design step to the next one would be enough to ensure a correct transition between the design steps. The discussion for the extended design loop, where either the initial deformations or the related stresses are introduced in the structural analysis, illustrates that there are more possible ways to realize the transition and the results in general differ based on the individual choice. Additionally, the introduction of elastic elements in the simulation of the tensile structure enlarge the appropriate definition of the interface, as the individual structural elements have to be processed in a specific manner. In general, it can be defined that the interface has to be able to transfer the state of equilibrium from one design step to the other. From a continuum mechanical point of view, this can be realized easily since the equilibrium is uniquely defined by the reference and the current configurations. For conventional structures, this definition is enough to realize the transition between the related design steps since the reference configuration can be defined in advance. In the case of tensile structures, the reference configuration is found by the form finding process or defined by the cutting pattern generation. As the result of this process defines the shape of equilibrium the transition is also well formulated. To ensure the correct transition from form finding to structural analysis in terms of the continuum mechanics, the form found shape and the related stresses have to be transferred. This means that if the

6.4 Requirements for the Interfaces

prestress is not identical to the intended one, e.g. due to stress adoption methods (e.g. distortion control from section 3.3.1.5), the current stress distribution in the surface has to be used. In this case, by the application of the Finite Element Method for the discretization of the governing equations, in combination with a Gaussian integration, at each evaluation or Gaussian point the prestress has to be defined.

For the individual structural elements, the requirements for the interfaces are well defined with the given discussion. It is obvious that the different situations for elastic and tensile elements introduce the special discussion on this topic, as from a continuum mechanical point of view the reference configurations are no longer attached to each other. In section 6.2 and section 6.3, the effects on the individual model approaches have been discussed. It was shown that by avoiding the issue of different reference configurations, by introducing initial stresses in the elastic elements, the resulting structural response is changed. The preference of the introduction of the "true" reference configurations for the tensile and elastic elements is obvious. For the interfaces, this introduces special requirements for the numerical modeling. After the form finding, the model has to be separated for the definition of the individual reference configurations. Of course, the connectivity of the structure has to be preserved. Due to that, the interfaces have to realize the coupling of the individual nodes. This way of simulating the structure is well known from bridge design, where it is common practice to simulate the full assembly process.

From this discussion it can be seen that from a numerical point of view the interfaces have to be able to prescribe stresses for each element and define initial deformations at each node in the case of a Finite Element Method for the discretization of the governing equations. Additionally, the topology of the numerical model has to be modified if the individual reference configurations will be introduced. The implementation of the interfaces showed that it is important to have the access to all data of the numerical model. Therefore, the modification of the source code of the used program has to be possible. Finally, it is important to note that from a continuum mechanical point of view, all of the discussed methods try to transfer the state of equilibrium from one design step to the other, which is the primary requirement.

Conclusions

In this chapter the individual design loops introduced in figure 1.4 have been discussed in detail. The differences for the standard and extended design loop have been illustrated. It became obvious that with the extended design loop, where the cutting patterns are introduced in the analysis, the quality of the structural response can be improved. The extended design approach defines a major complexity in the simulation process, as the structural models are no longer attached to each other. The discussion of the requirements for the interfaces between the individual design loops has addressed this issue and strategies for how to achieve a feasible simulation have been given.

The introduction of elastic elements in the modeling of tensile structures can be processed in the same way as for the cutting pattern for the tensile elements. This can be explained because the initial configuration of the elastic elements is interpreted as their cutting pattern. Therefore, it becomes obvious that the definition of the initial configuration for the elastic elements can't be made arbitrarily.

Based on the discussion of the different design loops it becomes obvious that the final results for a tensile structure can vary essentially. If the designer applies the standard design approach, he must be aware of the uncertainties in the final results. The extended design approach offers the possibility to improve the quality substantially. Hence, an simulation approach is presented which enables the designer to create more effective and efficient structures.

Projects

In the previous chapters, methods for the numerical design and analysis of tensile structures have been derived. For the individual steps of form finding, structural analysis and cutting pattern generation, detailed discussions were given regarding the solution possibilities and applied approaches. In chapter 6, the individual steps were connected to describe two different design loops which can be applied for the numerical design and analysis.

In this chapter, different projects will be presented where the introduced methods and design loops have been applied. The first project which will be presented is a realization of a student project developed in an annual workshop held at the Technical University in Munich. The second project is a simulation of a wide-span umbrella structure which is used to shadow piazzas in Medina. The third project describes the results from a research project where the validation of the presented methods against experimental data was the objective.

In the following, brief introductions to the projects will be given. The principal objectives, the background and the achieved results will be presented. The detailed discussion of the individual projects can be found in the related literature, which will be given for each project.

7.1 Student Project

The present student project is the result of an annual workshop held at the Technische Universität München. This workshop is part of the curriculum of the master program in civil engineering and architecture. Each year the students have to elaborate a design of a tensile structure in teams. The individual teams consist of students from architecture and civil engineering which introduces the challenge to combine the aesthetic of a design with the engineering needs.

In 2011 the task for the students was to design a pavilion which covers an area of approximately $100m^2$. The objective was to design a structure which is flexible

7.1 Student Project

and mobile, as it should be assembled in various places for different occasions. The individual teams developed different designs and in the end one was chosen to be realized in real scale. In the beginning the teams started to realize design studies on the basis of tulle models to get an idea of their final design. Based on these models the teams were starting to apply the introduced numerical methods to simulate their chosen design. In this case the standard design loop, as introduced in section 6.1, has been applied for the numerical modeling of the design process.

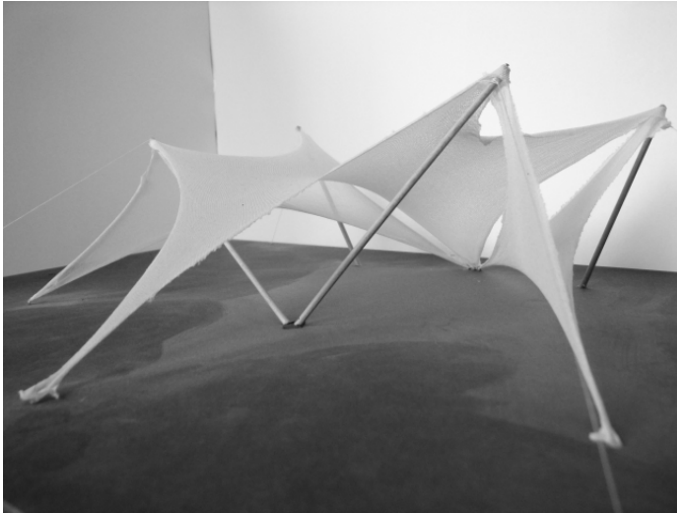


Figure 7.1: Tulle model for the student project

In figure 7.1 the tulle model of the design chosen for the realization is shown. It consists of a 6-point tent in the middle to which two 4-point tents are attached. The main idea for connecting the three tents is to join them at the adjacent high points. The detailed report on this design can be found in [Gre11].

It can be seen that at this stage of the design a first idea of the final shape of the structure is given by the tulle model. The actual shape will be determined in the form fining process. The process of getting ideas from tulle models and computing the related shape of equilibrium has to be repeated several times until a satisfying result from an architectural point of view can be achieved. In figure 7.2 the rendering of the final shape of equilibrium is illustrated.

The individual steps for the standard design approach are introduced as *Form finding-Structural Analysis-Cutting Pattern Generation*. For the presented design, the structural analysis was evaluated for the steady state case for a certain snow and wind load applied to the structure.

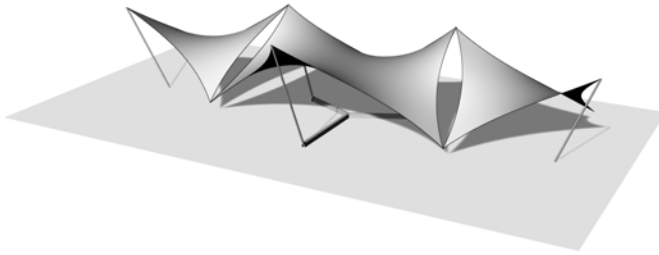


Figure 7.2: Rendering of the form found tensile structure

The final design of the tensile structure was supposed to be realized. This has been possible based on the support of CARPRO in Belgium, which is a company realizing tensile structures all over the world. They provided their knowledge, time and facilities to enable the students to manufacture their design of the structure.

The most important input from the students in this process was to provide appropriate cutting patterns for the tents. For this purpose, the methods discussed in chapter 5 were applied. The resulting patterns for the 6-point tent are illustrated in figure 7.3. Here, the numerically evaluated patterns and those that were manufactured can be seen. The real scale of the overall tent becomes obvious by comparing the illustrated cutting patterns with the team of students beside.

The cutting patterns for the 6-point tent have been industrially manufactured to ensure a high accuracy for the resulting structure. In case of the 4-point tent it was possible to produce the patterns for one tent industrially and one manually. The resulting difference in the quality in the patterns was remarkable. The designed patterns and the manufactured ones for the 4-point tent are illustrated in figure 7.4.

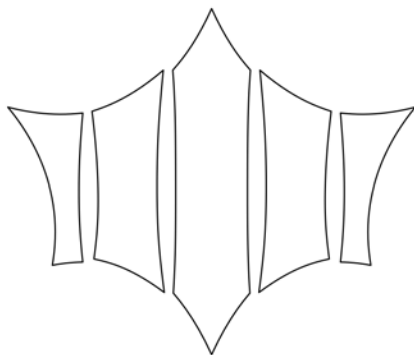
Based on the manufactured cutting patterns, the individual strips were welded together. For this purpose, a high frequency welding machine was used. Here, the coating and the fibers of the adjacent strips will be heated and under the acting pressure they will be connected while the welding area is cooling down. This process has to be done along the overall seams as illustrated in figure 7.5.

The welded cutting patterns will form the final shape of the structure when it will be assembled into the boundary conditions defined by the high and low points as well as by the edge cables. For the assembly of the membrane, the edge cables will be attached to the surface in pockets along the edges. The inlying cable is going to form a loop at the end. This loop enables the connection of the structure at the high and low points to the supporting structure. In figure 7.6 the realization of the end points of the edge cables is illustrated.

The manufactured tensile structures can be erected with a minimum of effort. The

7.1 Student Project

Cutting Pattern Layout:



Cutting Pattern:

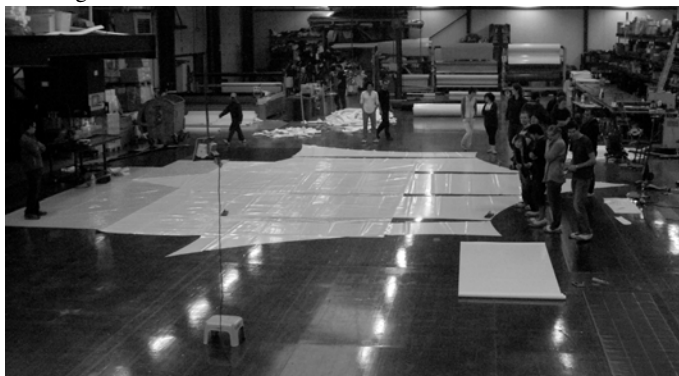
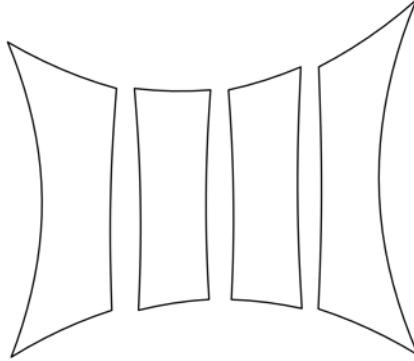


Figure 7.3: Cutting pattern for the 6-point sail

assembled 6-point tent is illustrated in figure 7.7. It can be seen that the resulting structure and the rendering are in accordance from a visual point of view. The experience from the erection process shows, that the most important aspect for the realization is the exactly positioned and appropriately designed high and low points. For assembly of the tensile structure to its final position, the high points will be put in place first. For the final positioning of the tensile structure the low points have to be pulled into their final location, which introduces the prestress in the cables. By prestressing the cables, the stresses in the surface will be introduced as well. In the case of a highly accurate manufacturing, the resulting structure and stresses should be identical to the indented ones. Of course, based on variations in the quality of the simulation or manufacturing the resulting structure will vary from the designed one. In the case of the student project, the exact measuring of the resulting surface and stresses has not been done.

Cutting Pattern Layout:



Cutting Pattern:



Figure 7.4: Cutting pattern for the 4-point sail



Figure 7.5: Welding process

7.1 Student Project



Figure 7.6: Assembling of the edge cables

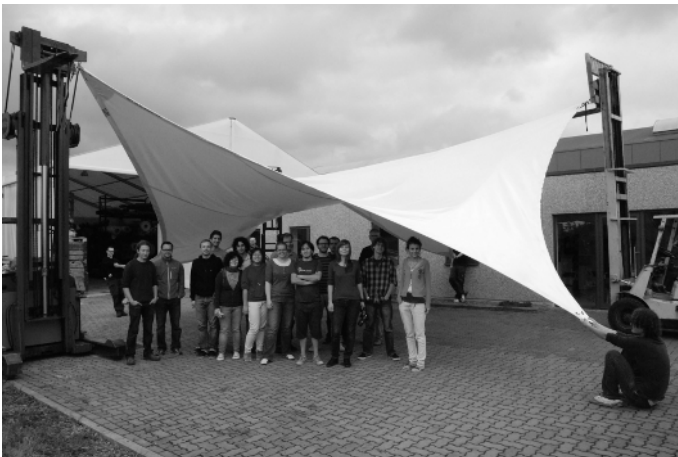


Figure 7.7: Final 6-point tent of the student project

7.2 Wide-span Umbrella Structure

The wide-span umbrella structure described below is part of an on-going research project as a cooperation of the SL-Rasch GmbH and the Chair of Structural Analysis at the Technische Universität München. The actual design of the umbrella structures is done by the architectural office SL-Rasch and the manufacturing is done by Liebherr. The motivation for this project is to shadow the places of prayer at holy cities in the Islamic culture. Because of the considerable temperatures and solar radiation during the time of pilgrimage, Saudi Arabia has started to shadow this piazzas with wide-span umbrella structures as illustrated in figure 7.8. In order



Figure 7.8: Umbrellas in Medina, Saudi Arabia (copyright SL-Rasch GmbH)

to cover the overall area of the piazzas, the edge length of the individual umbrellas increased to $29m$ and in the latest version up to $53m$. One of the main challenges for the engineering of the umbrellas was related to the external loads. In Saudi Arabia the main load condition originates from wind. For the simulation of the overall structure, the wind loads have to be defined. For such complex structures, the wind load is not defined in the available design codes. The wind situation for the umbrellas is influenced by the local wind intensity, the shape of the structure itself and of course the surrounding building conditions. The surrounding conditions are complex, since groups of umbrellas are placed in a certain piazza. Due to that, the evaluation of the wind conditions for one umbrella isn't straightforward. In order to define the wind conditions for the umbrellas in the piazza, sophisticated numerical simulations and wind tunnel experiments of the individual local conditions have been performed, which are presented in [Mic10] and [Mic+11]. Here, a real scale prototype of the $29m$ umbrella was build in Ehingen (Germany) as illustrated in figure 7.9. For this prototype the wind intensity and the deformations was monitored so that the structural behavior of the umbrella for specific wind situations can be investigated. In order to compare the in-situ measurements with the wind tunnel experiments, it was attempted to model the same conditions in the wind tunnel as illustrated in figure 7.10. In addition to the complexity of the evaluation of the wind loads, the structure itself also introduces a major challenge based on the external wind loads. Due to the lightness of the overall structure, the deformations at the edges of the umbrella can't be assumed to be small, which introduces an interaction between the wind loads and the structure. In order to study this *Wind-Structure-Interaction*, an on-going research project was initiated by SL-Rasch and the Chair of Structural Analysis. For the detailed study of the behavior of the umbrella in

7.2 Wide-span Umbrella Structure

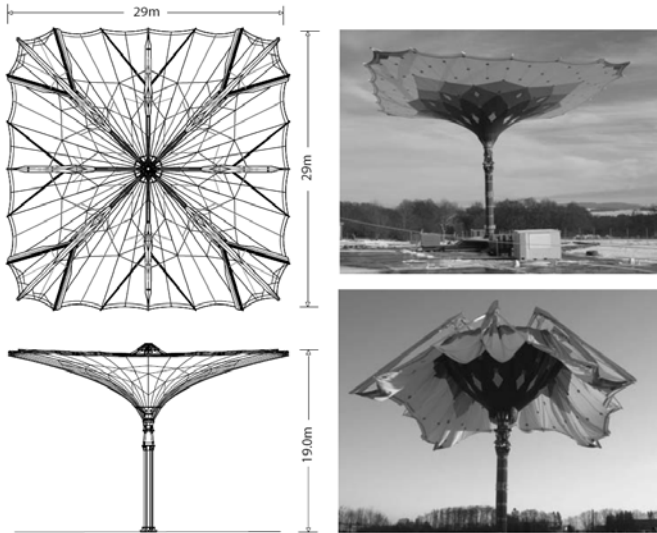


Figure 7.9: Umbrella-prototype in Ehingen, Germany [Mic10]

wind, different disciplines are involved in numerical simulations in transient and steady state, Fluid-Structure-Interaction simulations (FSI), wind tunnel tests and in-situ real scale experiments.

In [Mic10] and [Mic+11], as the first work in this cooperation, it was attempted to achieve the results from the in-situ experiments and from the wind tunnel by a numerical FSI simulation. Based on a three dimensional turbulent wind flow simulation, the interaction with the structural model is evaluated in a FSI simulation. Here, satisfying accordance of the results from the in-situ and the wind tunnel experiments with the numerical simulation have been achieved.

In order to validate the commercial software used for the simulation of the structural behavior, in [Deg12] a comparison with the methods presented and implemented in this thesis has been made. Therefore, the simulation was re-run with an independent numerical model as illustrated in figure 7.11. For the comparison of the different simulations for the umbrella, the load situations evaluated from the wind tunnel experiments have been applied. Here, the surface of the umbrella is divided into individual wind pressure areas as illustrated in figure 7.10. For these areas the wind load is defined for the overall measuring time. It is obvious, that the wind loads are not invariant in time, which introduces that a transient structural analysis has to be performed as described in section 4.1.

For the simulation of the umbrella structure, various modeling decisions are nec-

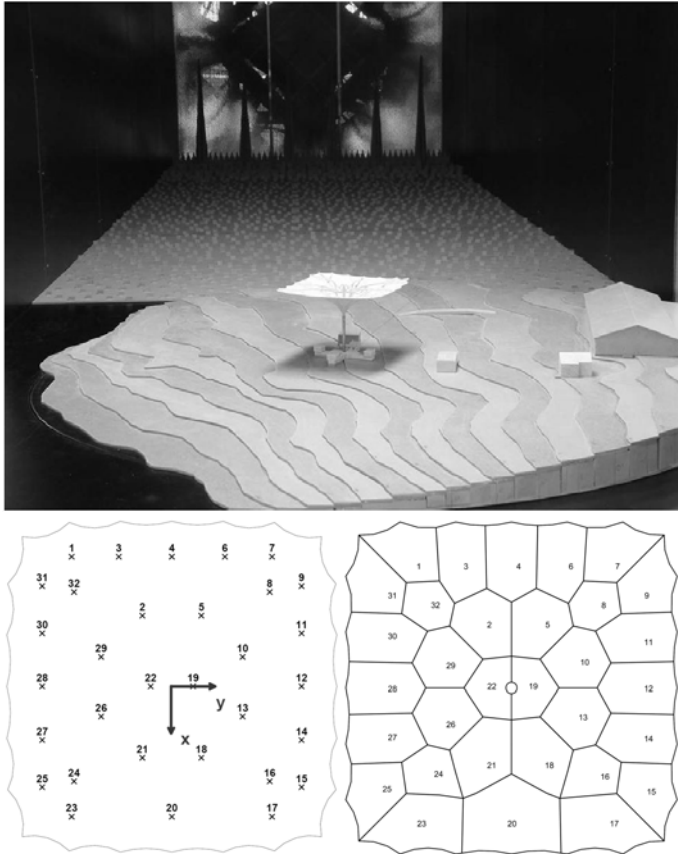


Figure 7.10: Wind tunnel test of the Umbrella; top: Model for the experiment; bottom: Position of the measurement points and the resulting pressure areas [Deg12]

7.2 Wide-span Umbrella Structure

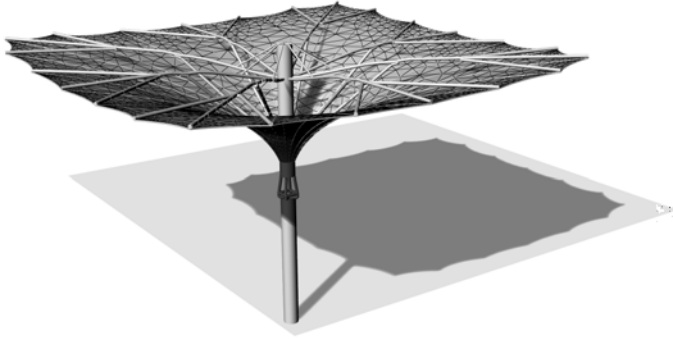


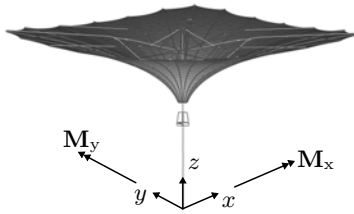
Figure 7.11: Numerical model of the Umbrella with its FE-mesh

essary. Since the commercial code does not provide the possibility to include the cutting patterns in the process of structural analysis, the standard design approach has been applied. Furthermore, the umbrella structure consists of membrane, cable and beam elements. With the integration of the elastic elements in all design steps of the numerical simulation at the interface between form finding and structural analysis the decision regarding the transition of the shape of equilibrium has to be taken. In section 6.3 the possibilities of prescribing the deformations or the stresses in the elastic elements have been discussed. In order to simplify the modeling effort, the stresses have been prescribed for this simulation.

For the comparison of the different simulations, the resulting bending moment at the mast foot for the commercial and presented approaches was chosen. In figure 7.12 the results for a certain period of time are illustrated. It can be seen that in principal the results have the same characteristics. Of course, there are still small variations for individual time steps, but this has no major influence on the overall design.

The presented research project is part of the efforts which are made for the development of a virtual wind tunnel. Therefore, validated numerical methods for the computational fluid dynamics and the structural analysis have to be available. In order to achieve a validated simulation framework for the coupled analysis of lightweight tensile structures in realistic wind conditions, further research is presented in [Fis+12], [Hoj+11], [Šar+12], [Sic+11], [WKB07], etc.

Numerical Model:



Resulting bending moment:

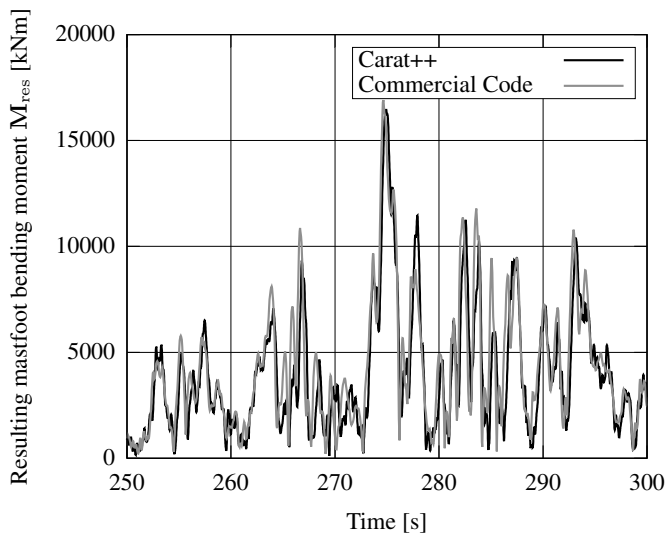
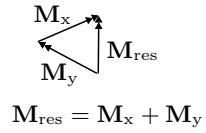


Figure 7.12: Resulting mastfoot bending moment for the umbrella

7.3 Cushions

In the following, the extract of the results from a research project funded by the German Research Foundation will be presented. The project is designed to be processed together with a partner from industry (here: Seele Cover GmbH, Obing, Germany) to ensure the transfer of the research results into practice. The objective of this research project was the simulation and experimental validation of cushions. Here, the contribution of the industry partner is their knowledge of the manufacturing process of the cushions as well as providing the overall experimental set-up.

In section 4.4, the special characteristic of the simulation of enclosed cushions was already discussed. In general, cushions are applied for roofs or facades as illustrated in figure 4.5. It is common practice to neglect the effects from the enclosed volume for the overall structural behavior in the simulation process. Additionally, most cushions have dimensions which can be realized without the division of the surface into individual strips. Therefore, the application of appropriate cutting patterns is mostly neglected. If it is necessary to assemble the surface of the cushion from individual cutting patterns, this is often done by simplified approaches (e.g. the projected area is used as the cutting pattern).

In this research project the exactness of the presented simulation methods should be validated with experimental data. For this purpose a set of different cushions has been investigated. In order to execute the experiments, an appropriate set-up has to be developed. The main decision was to define the results which should be compared. Of course, the overall deformation of the cushion is an important quantity which has to be measured. Additionally, the pressure inside the cushion is of interest, as this quantity is constantly evaluated in the simulation process.

The principal experimental set-up is illustrated in figure 7.13. For the experiment, a rectangular cushion was chosen since similar shapes are most commonly built in practical applications. The dimensions of the cushions were chosen according to the available experimental facility as $70/105[cm]$, based on different cutting pattern layouts. The cushions consist of a single chamber, which means there is an upper and lower membrane layer which encloses the air. In the initial step, the chamber of the cushion is inflated up to a defined pressure p_i . For the modeling of an external load, the chamber is assembled in an airtight wooden box, which will be pressurized. The pressure in the box p_e will simulate the situation in which the cushion is subjected to a constant wind load. The pressure in the cushion and the airtight box can be measured by a U-tube manometer. Both pressures have been introduced by a compressor.

During the experiments different load levels were measured. The main goal was to simulate realistic wind scenarios. The available design codes for wind loads define a maximum wind load for roofs and facades of approximately $2.0[kN/m^2]$. Due to that, for the experiment the maximum applied pressure was defined to be twice as large. The process of pressuring the cushion and the box was realized in 6 steps and in each step a deformation measurement was made. The first two steps were done to pressurize the cushion and in the next four steps the pressure in the

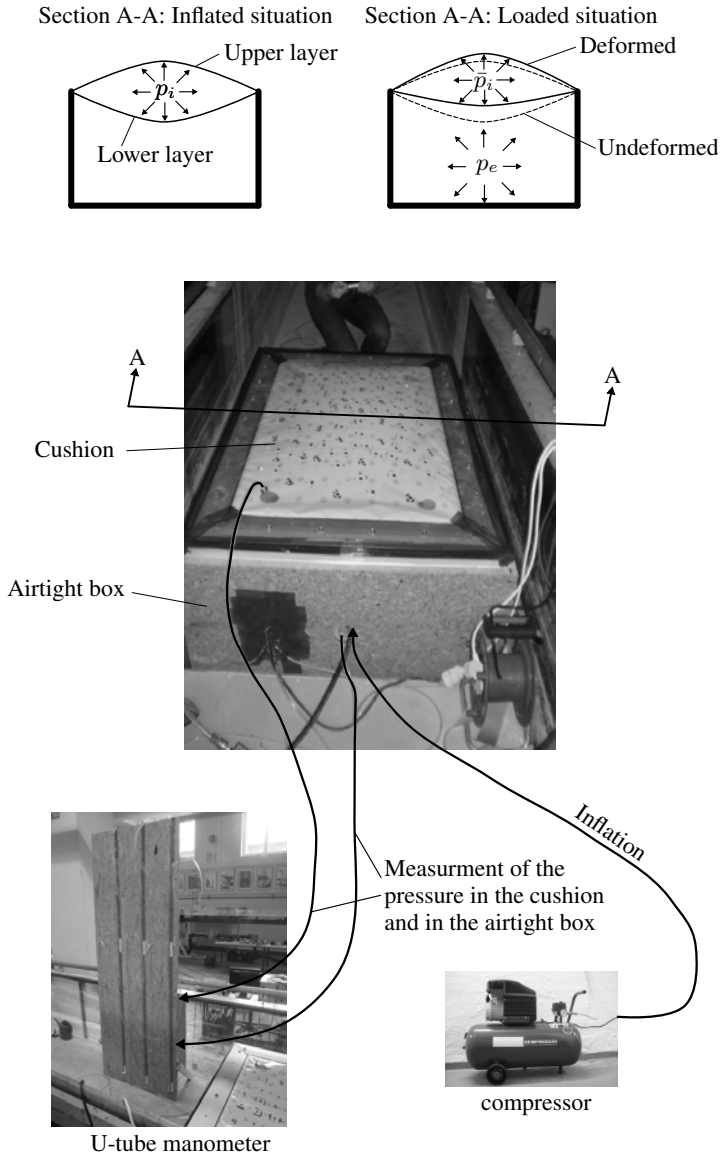


Figure 7.13: Experiment set up for the cushions; top: Different situations for the cushions; bottom: Experimental set-up

7.3 Cushions

airtight box was increased. The measured pressures in the cushion and the box is listed in table 7.1.

Table 7.1: Measured Pressures in Cushion 1-SO-4

Load Case	Chamber [kN/m^2]	Airtight Box [kN/m^2]
-1	0.00	0.00
0	0.34	0.00
1	1.00	0.00
2	1.42	1.00
3	2.04	1.96
4	2.92	2.98
5	3.90	4.00
6	3.98	4.06

For the comparison of the experiments and the simulations, detailed deformation measurements had to be made. These have been done by Konrad Eder, Carsten Götz, Sebastian Tuttas and Berit Cantzler from the Institute of Photogrammetry and Cartography at the Technische Universität München. In [Can13] the overall process is discussed. In order to measure the deformation of the upper and lower layer of the cushion, two cameras at each side are needed as illustrated in figure 7.14.

Additionally, appropriate measuring points have to be assembled on the cushion. For the manufacturing of the cushions it is important that an airtight material is used. For this purpose ETFE-foils are used in most applications. In this research project, this type of material was used as well to align the experiment to the practical applications. The disadvantage of ETFE is that the measured points can't be applied by standard paint. The first challenge in this project was to find an appropriate paint which keeps its shape during the deformation process. A detailed discussion on that can be found in [Can13].

The result from the measuring of the deformation process are point clouds for each individual pressure step of the lower and upper layer of the cushion. With base points on the airtight box it was possible to combine the measurements from the lower and upper cameras to one point cloud as illustrated in figure 7.14. Based on these point clouds it was possible to compare the results from the experiment to the simulation.

For the discussion of the exactness of the presented simulation methods and the influence of the cutting patterns to the final results, different cushions were defined for the experiments. In figure 7.15 the different cutting pattern layouts are illustrated. The first experiment was defined to be aligned with common practice, where the cutting pattern is defined to be a flat rectangle shape with the actual dimensions of the supporting framework (1-FG-1). For the other cushions, the cutting patterns have been introduced. The patterns for the individual specimen have been deter-

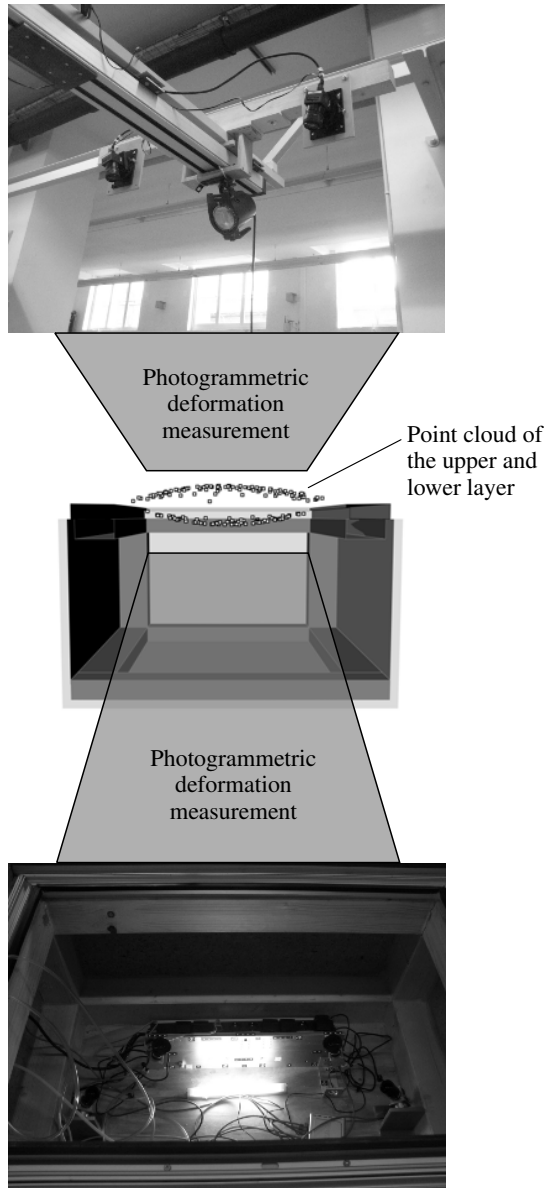


Figure 7.14: Photogrammetric deformation measurement

7.3 Cushions


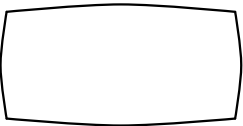
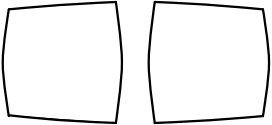
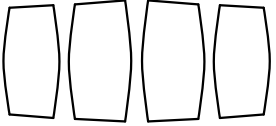
Name	Patterning type	Cutting pattern layout
1-FG-1	Flat geometry 1 strip	
1-SO-1	Stress optimized 1 strip	
1-SO-2	Stress optimized 2 strips	
1-SO-4	Stress optimized 4 strips	

Figure 7.15: Experiment types of cutting patterns

mined by the Variation of Reference Strategy as introduced in section 5.2.3. The stress optimized cutting patterns consist of 1 (1-SO-1) to 4 strips (1-SO-4). For these cutting patterns, equal seam lengths are ensured by the methods described in section 5.2.6, if applicable.

In the following, results for the cushion based on the 4-strip layout will be presented. A detailed discussion of the overall simulation process and the comparison with the experimental data can be found in [Kos14]. For the simulation of the cushions, the extended design approach is applied as the cutting patterns should be included in the structural analysis. In figure 7.16 and figure 7.17 the deformations for the cushion at a section in the middle of the length of the cushion are illustrated.

Here, the deformations from the simulations and from the experiments are shown. In figure 7.16 the results for the case that just the cushion is pressurized is shown. In figure 7.17 the deformation is shown were the pressure in the cushion is equal to the half of the final load situation. In both figures it can be seen that the deformations in the simulation are too small in comparison to the one evaluated in the experiments. Based on various investigations it turned out that the manufactured cushions have

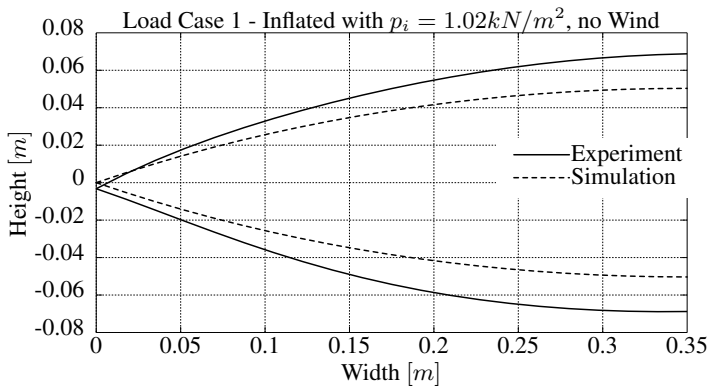


Figure 7.16: Deformation comparison for pressure in the cushion and without external load

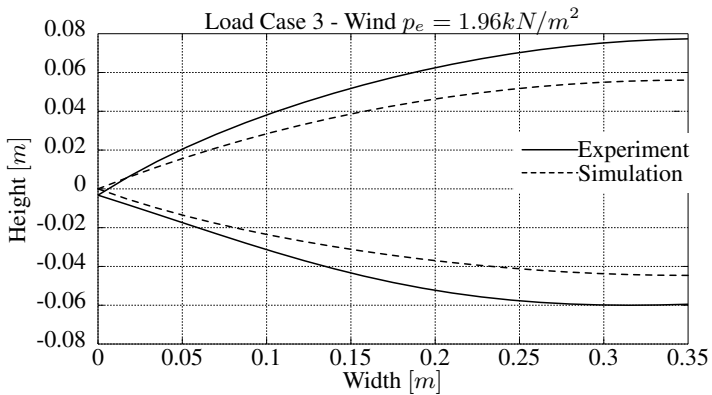


Figure 7.17: Deformation comparison for pressure in the cushion and with external load

7.3 Cushions

had an imperfection w.r.t. to the defined cutting patterns as illustrated in figure 7.18. Based on the evaluated cutting patterns, the initial surface should be straighter in the

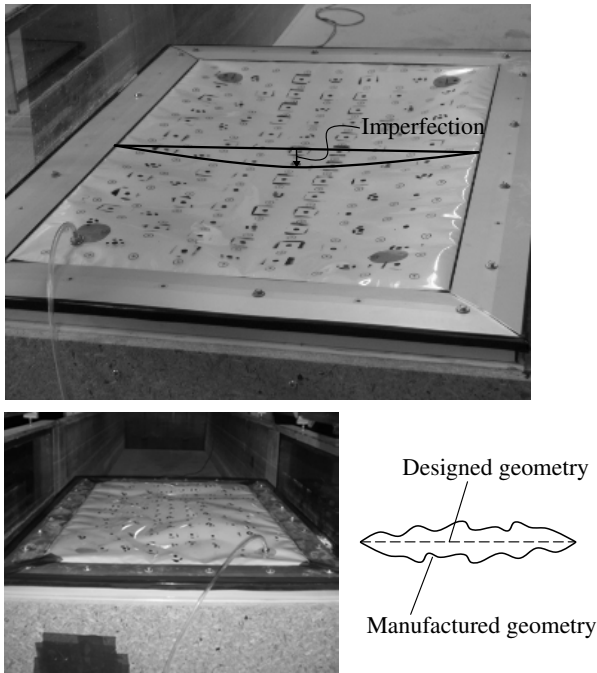


Figure 7.18: Imperfections of the cushion geometry

supporting frames. In order to introduce these imperfections in the simulation process, the geometry of the cutting patterns as starting point of the simulation has been modified accordingly. Of course, this introduces the disadvantage that it is impossible to discuss the effects of the cutting patterns on the final result as the imperfections overlap this influence. In figure 7.19 and figure 7.20, the results with the modified cutting patterns are illustrated. It can be seen that the deformations after inflation of the cushion are equal for the simulation and the experiment. For the situation where the external load is applied, the deformations for the lower layer are equal as well. In the upper layer there are still small variations in the results. The discussion of whether this variation originates from the governing equations or from the introduced imperfections can't be solved as the individual effects overlap each other. At first glance it seems that the derived simulation methods are able to predict the overall structural behavior as the lower layer can be evaluated exactly. In order to finally discuss the exactness of the developed simulation methods, further experiments would be necessary where the manufactured and simulated cushions are compared in order to ensure the accordance between the two reference situations.

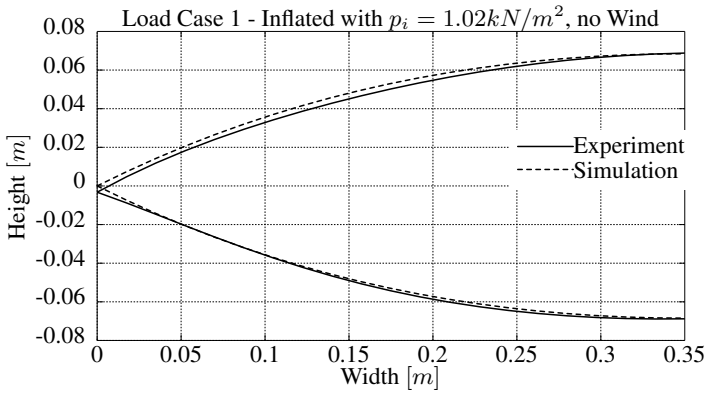


Figure 7.19: Deformation comparison for pressure in the imperfect cushion and without external load

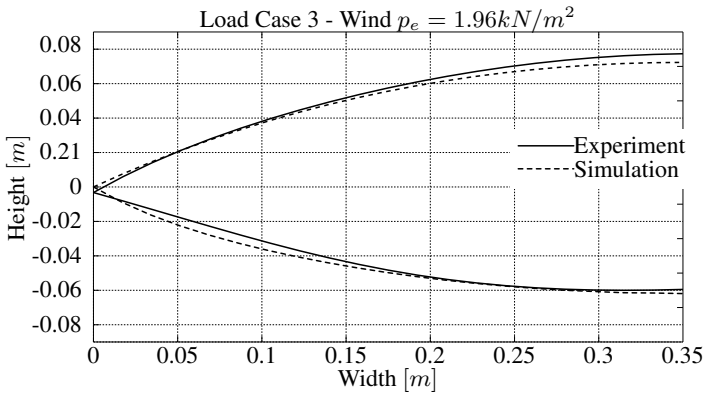


Figure 7.20: Deformation comparison for pressure in the imperfect cushion and with external load

Conclusion

In this chapter, the application of the presented numerical methods for the design and analysis of tensile structures was shown for different projects. It can be seen that the individual methods and the defined design approaches are suitable to simulate state of the art tensile structures. The student project illustrates the application for classical tensiles, whereas the simulation of the wide-span umbrella shows the possibilities for complex hybrid structures. In this example, the comparison to a commercial software proves the applicability to modern structural systems. The example of comparing experimental data with simulation results for cushions illustrates that the numerical modeling and final manufacturing interacts strongly for the final results.

Based on the discussed examples it can be seen, that the presented methods define an appropriate framework for the simulation of tensile structures. Additionally, the necessity of highly accurate manufacturing processes in order to take advantage of the possibilities offered by the advanced simulation methods have been depicted. Only if all steps from the first idea to the completed structure are at the same level of quality the most efficient structures can be built.

Concluding Remarks

The design and analysis process for tensile structures differs fundamentally from conventional structures as the overall shape and the structural capacity are strongly coupled. The lightness and the characteristic that external loads are only restrained by in-plane stresses introduces the requirement of adapted simulation and modeling techniques. For a successful design of a tensile structure, the influences of the special demands in the simulation process have to be considered.

Due to the special connection between acting forces and overall form of the tensile structure, the design step of *Form Finding* has to be introduced at the beginning of the overall design process. Here, the shape of equilibrium w.r.t. to a given pre-stress and certain boundary conditions will be evaluated. The resulting shape of this design step represents the input for all following analyses.

Based on the results from form finding, different analyses have to be made to achieve a feasible design. Certainly, a *Structural Analysis* has to be made in order to ensure that the tensile structure is able to restrain the external loads. Comparing this analysis for a conventional and a tensile structure, the least differences of all will be recognized. The difference, most likely, is that tensile structures are subjected to large deformations in general, especially in the assembly process. In contrast, for conventional structures this is rarely the case for applications in civil engineering.

Besides this more mechanical based discussion, the manufacturing process of the tensile structure also introduces a considerable influence to the overall design process. In general, *Cutting Pattern Generation* describes the process of evaluating the individual plane strips for the manufacturing of the tensile structure. Additionally, this design step is concerned with the task of minimizing the effects from the doubly curved shapes regarding the final stress distribution.

The design steps of form finding and cutting pattern generation introduce the main difference to the design and analysis process of conventional structures. Additionally, the interaction between them has to be considered in the simulations. There-

8 Concluding Remarks

fore, a substantial level of experience regarding the structural behavior of tensile structures is required for a feasible design.

In the present thesis, the individual design steps of form finding, structural analysis and cutting pattern generation have been discussed in detail. The derivation of the individual governing equations is done on the basis of continuum mechanics. This way of formulating the actual underlying mechanical problem allows the application of efficient numerical solution methods. Here, the concept of the Finite Element Method is introduced to the solution process.

In the case of the form finding, the inverse nature of the problem has been discussed. The stabilization of the governing equations based on the Updated Reference Strategy has been described. Based on the discussion of the general existence of a solution w.r.t. different prestress situations, respective numerical solution approaches are included in the discussion as well. In case of an isotropic prestress in the surface, a unique solution for the form finding can be achieved. From a mathematical point of view, all of the existent methods converge iteratively to an approximated solution. In this thesis the eXtended Updated Reference Strategy is introduced which is able to describe the exact solution in a nonlinear equation. Due to that, it is possible to evaluate the analytical shapes for the tensile structure without introducing an iterative form finding process. In addition to the pure discussion of the form finding problem, the introduction of elastic elements in this design step has been discussed. It can be seen that for the correct description of the resulting hybrid structure w.r.t. continuum mechanics, adapted interpretations of the individual reference configurations have to be considered.

For the design step of structural analysis, a detailed review of the transient and steady state case has been discussed from a continuum mechanical point of view. The special focus in this discussion is on the large deformations of tensile structures in cases of external load. This characteristic introduces special needs in the mechanical description of the external loads as well. If the load depends on the deformation of the structure, the respective influence has to be considered in the governing equations. The application of cushions has been discussed as an example for these effects.

The cutting pattern generation introduces special requirements to the formulation of the governing equations as it is influenced by mechanical and manufacturing arguments. In this thesis, different methods have been discussed which address the mechanical problem of minimizing the stress difference between the intended prestress and the resulting stress distribution from the assembly process. With the introduction of the Variation of Reference Strategy a continuum mechanical based method is described which enables the inclusion of the manufacturing requirements. Here, the need of equal seam lengths of adjacent cutting patterns has been introduced as a constraint motivated from practice. The mathematical inclusion has been realized in the formulation of an equality constraint in the optimization problem. Additionally, the influence of the seams w.r.t. the stress distribution in the overall membrane has been discussed.

Based on the discussion of the individual design steps, the interaction between them has been discussed in detail. With the definition of a standard and an extended design approach, the difference in the results from the simulation of the tensile structures becomes obvious. The structural behavior strongly depends on the choice of design approach and can be interpreted as a fundamental design decision. The extended design approach offers the possibility to analyze the structure in a more realistic way and so more efficient structures can be achieved. Of course, the accuracy of the manufacturing has to be as precise as the simulation to ensure that the evaluated and real stress distribution are as equal as possible. In this case it is possible to reduce the considered safety factors between the ultimate and the actual stress state to achieve more efficient designs.

Based on the numerical design and analysis methods introduced in this thesis, the overall simulation process has been adapted to the requirements formulated by the realization of a state of the art tensile structure. Of course, the present thesis does not give an answer to all of the open questions in the numerical simulation of such structures.

Certainly, the cutting pattern generation of elastic elements can be addressed as one of the major tasks which have to be added in order to enhance the presented design approaches. Here, the main issue is the introduction of the kinematic description of the elastic elements in the governing equations of the Variation of Reference Strategy. Furthermore, an appropriate material law which covers all design steps has to be developed. This would lead to an improvement in the accuracy of the simulation results. It must be investigated how the material behaves during the short term assembling process and the long term period of usage, especially for the extended design loop.

For conventional structures made of wood, steel or concrete a wide range of experimental data is available. Due to that, it is possible to compare the developed simulation techniques w.r.t. the realistic results. In the case of tensile structures, such experimental data is not available so far. In order to improve the reliability of the simulation results, the validation of the available numerical methods w.r.t. experimental results should be intended. This would also introduce the possibility to discuss the applied modeling techniques introduced for the simulation of tensile structures. Here, the question regarding the level of detail in the modeling could be discussed (e.g. wrinkling models, effects from bending stiffness, etc.). The different investigations should lead to the definition of requirements for the numerical simulation of tensile structures which could be defined in a design code.

It can be concluded that for an efficient and effective design and analysis process of tensile structures, numerical simulation methods are essential. In the present thesis a contribution to the improvement of existing methods is made. Particularly, the entanglement of the numerical simulation approaches and the requirements from the manufacturing process has been addressed in this thesis. Through the continuum mechanical description of the governing equations and the detailed discussion of the solution process, the introduced methods can be applied by those who are involved in the numerical modeling of tensile structures.

List of Figures

1.1	Early tensile structures (top left: Canopy on a bazaar in Bahrain [Koc04]; top right: Sail ship [Ber05]; bottom left: Nomad tent [Rob96]; bottom right: Figure of roman military tents [Koc04])	2
1.2	Tensile structures designed by <i>Frei Otto</i> (left: Tanzbrunnen in Cologne 1957 [Sch90]; right: Roof of the Olympic stadium in Munich 1972 (Architect: Behnisch & Partners) [Sch90])	3
1.3	Modern tensile structures (left: Expo axis in Shanghai (<i>copyright: Knippers Helbig - Advanced Engineering</i>); right: Bangkok international airport (<i>copyright: Werner Sobek Group GmbH</i>))	4
1.4	Design process for tensile structures	6
2.1	Length-to-Thickness ratio for a tensile structure	10
2.2	Numerical modeling steps for a tensile structure	11
2.3	Position vector \mathbf{r} of point \mathbf{P} in a cartesian coordinate system	16
2.4	Parametric description of a surface	17
2.5	Co- and contravariant base vectors	18
2.6	Example for the calculation of the area content of a rectangle surface	20
2.7	Example for the calculation of the curvature of a sphere	22
2.8	Reference and current configuration in continuum mechanics	24
2.9	Force vector acting on a infinitesimal surface element	29
2.10	Tangential surface stresses	31
2.11	Stress-Strain-Diagram for a 1D tension test	32
2.12	Example of a tension test described by Treloar in [Tre44]	36
2.13	Tension test with an Odgen material model for the experimental data from Treloar	37
2.14	Multi-linear stress-strain curve	38
2.15	Example for a burst test with a ETFE foil	39
2.16	FEM discretization of a surface	43
3.1	Equilibrium of a clothesline (top [Ber05])	48

3.2	left: Jean-Baptiste-Siméon Chardin - The Soap Bubble [HT96]; right: Frei Otto - Soap films at the IL University Stuttgart [OR95]	50
3.3	Equilibrium in a bubble like structure	50
3.4	Arbitrarily deformed meshes for the same surface geometry	54
3.5	Soap film (left) and tulle model (right) [Wil11]	55
3.6	Form finding process using the URS applied to the Scherk minimal surface	58
3.7	Local Cartesian coordinate system for the definition of the physical prestress values	60
3.8	Linear cable Finite Element	61
3.9	Surface of rotation with anisotropic prestress	63
3.10	Minimal surfaces created by applying the URS (left: Schön minimal surface; center: Scherk minimal surface; right: Helicoid;)	68
3.11	Form finding result for the roof of the Olympic Stadium in Munich (recalculation)	68
3.12	Configurations for the distortion control method [Lin09]	70
3.13	Catenoid for different values of λ_{\max}	72
3.14	Warp and Weft stress for the Chinese Hat	73
3.15	Separation of the residual force into normal and tangential direction	74
3.16	Patch of finite Elements to compute the mean surface normal	76
3.17	Schwarz minimal surface reference configuration; top view (left); isometric view (right)	78
3.18	Residual forces for the Schwarz minimal surface with varying deformations for different form finding methods	79
3.19	Catenoid minimal surface	80
3.20	Displacement convergence for the Catenoid minimal surface	80
3.21	Error plot for the Catenoid minimal surface for the overall iteration steps	81
3.22	4 point tent	82
3.23	Displacement convergence for the 4 point tent	83
3.24	Hybrid tensile structures	84
3.25	Hybrid tensile structures with integrated elastic members (left [LK12]; right [Off10])	84
3.26	Hybrid tensile structures with external elastic members (left [Koc04]; right [Sei08])	85
3.27	Configurations for form finding with integrated elastic elements	85
4.1	Results for the Duffing Oscillator; top: Definition of the structure; middle: Time-displacement diagram; bottom: Displacement-velocity diagram	96
4.2	von Mises truss example	97
4.3	λ - u diagram for the von Mises truss example (with $P = 1$; $EA = 1$; $h = 1$; $b = 1$)	98
4.4	Spring Damper Finite Element	101
4.5	Examples for ETFE cushions; top: Casino Macao; bottom: Lyon Confluence (copyright: Seele Cover GmbH)	105
5.1	Cylinder and Sphere covered by an initially flat plane	110
5.2	Principal steps for the cutting pattern generation	111

List of Figures

5.3	Discrete geodesic line computation	113
5.4	Geodesic line on a NURBS and discretized surface	114
5.5	Optimization problem for cutting pattern generation	116
5.6	Configurations for Cutting Pattern Generation	117
5.7	Process for cutting pattern generation	123
5.8	Computation of the fiber directions in the cutting pattern generation	124
5.9	Residual stresses based on the optimized cutting pattern	127
5.10	Hypar example for sensitivity of the residual stresses	128
5.11	Sensitivity of residual stress w.r.t. material properties	128
5.12	Sensitivity of residual stress w.r.t. number of cutting patterns	130
5.13	Sensitivity of maximum w.r.t. the change in curvature	130
5.14	6 point tent consisting of 5 patterns	131
5.15	Cutting patterns of a 6 point tent and seam line lengths	132
5.16	Degrees of freedom (dof) for the middle patterns	133
5.17	Different seam layouts for a hypar	138
5.18	Stress ratio $\frac{\sigma_{cur}}{\sigma_{max}}$ w.r.t. the pattern layout	139
5.19	Stress $\frac{\sigma_{max}}{\sigma_0}$ and force $\frac{F_{max}}{F_0}$ ratio w.r.t. the seam layers	140
6.1	Standard Design Approach	145
6.2	4 point tent example with standard design approach	146
6.3	Extended Design Approach	147
6.4	von Mises example for the configuration update	148
6.5	Results for the von Mises truss with an initial deformation	149
6.6	4 point tent example with extended design approach - cutting pattern layout	151
6.7	Residual stress for the 4 point tent w.r.t. the different modeling approaches	152
6.8	Residual stress for the 4 point tent for full modeling approach	152
6.9	Configuration update in the case of the full description of the deformation process	153
6.10	Configuration update in the case of the incremental description of the deformation process	154
6.11	Arch Hall example	156
6.12	Arch Hall example results	158
6.13	Arch Hall example FSI [DWB10], left: structural model; right: stream lines	159
7.1	Tulle model for the student project	164
7.2	Rendering of the form found tensile structure	165
7.3	Cutting pattern for the 6-point sail	166
7.4	Cutting pattern for the 4-point sail	167
7.5	Welding process	167
7.6	Assembling of the edge cables	168
7.7	Final 6-point tent of the student project	168
7.8	Umbrellas in Medina, Saudi Arabia (<i>copyright SL-Rasch GmbH</i>)	169
7.9	Umbrella-prototype in Ehingen, Germany [Mic10]	170

7.10	Wind tunnel test of the Umbrella; top: Model for the experiment; bottom: Position of the measurement points and the resulting pressure areas [Deg12]	171
7.11	Numerical model of the Umbrella with its FE-mesh	172
7.12	Resulting mastfoot bending moment for the umbrella	173
7.13	Experiment set up for the cushions; top: Different situations for the cushions; bottom: Experimental set-up	175
7.14	Photogrammetric deformation measurement	177
7.15	Experiment types of cutting patterns	178
7.16	Deformation comparison for pressure in the cushion and without external load	179
7.17	Deformation comparison for pressure in the cushion and with external load	179
7.18	Imperfections of the cushion geometry	180
7.19	Deformation comparison for pressure in the imperfect cushion and without external load	181
7.20	Deformation comparison for pressure in the imperfect cushion and with external load	181

Bibliography

- [AG12] E. L. Allgower and K. Georg. *Numerical continuation methods: An introduction*. Berlin, Heidelberg, New York: Springer, 2012.
- [Alt12] Holm Altenbach. *Kontinuumsmechanik Einführung in die materialunabhängigen und materialabhängigen Gleichungen*. Berlin: Springer, 2012.
- [AM88a] J. Argyris and H.-P. Mlejnek. *Die Methode der Finiten Elemente - Band I: Verschiebungsmethode in der Statik*. Braunschweig: Vieweg & Sohn, 1988.
- [AM88b] J. Argyris and H.-P. Mlejnek. *Die Methode der Finiten Elemente - Band II: Kraft- und gemischte Methoden, Nichtlinearitäten*. Braunschweig: Vieweg & Sohn, 1988.
- [AM88c] J. Argyris and H.-P. Mlejnek. *Die Methode der Finiten Elemente - Band III: Einführung in die Dynamik*. Braunschweig: Vieweg & Sohn, 1988.
- [Bär10] Christian Bär. *Elementary differential geometry*. New York: Cambridge University Press, 2010. 317 pp.
- [Bar74] M. R. Barnes. “Dynamic relaxation analysis of tension networks.” In: *Proceedings of the International Conference on Tension Roof Structures*. London, 1974.
- [Bar88] M. R. Barnes. “Form-finding and analysis of prestressed nets and membranes.” In: *Computers & Structures* 30.3 (1988), pp. 685–695.
- [Bar99] M. Barnes. “Form finding and analysis of tension structures by dynamic relaxation.” In: *International Journal of Space Structures* 14 (1999), pp. 89–104.
- [Baş00] Yavuz Başar. *Nonlinear continuum mechanics of solids: fundamental mathematical and physical concepts*. In collab. with Dieter Weichert. Berlin ; New York: Springer, 2000. 193 pp.
- [Bat96] Klaus-Jürgen Bathe. *Finite element procedures*. In collab. with Klaus-Jürgen Bathe. Englewood Cliffs, N.J.: Prentice Hall, 1996. 1037 pp.

Bibliography

- [Bäu95] Jochen Bäuerle. “Ein Beitrag zur Berechnung des Zuschnitts von vorgespannten Membranen.” PhD thesis. München: Beck, 1995.
- [Ber05] Horst Berger. *Light structures, structures of light: the art and engineering of tensile architecture*. 2nd ed. Bloomington, Ind: AuthorHouse, 2005. 228 pp.
- [Ber96] Dimitri P. Bertsekas. *Constrained optimization and Lagrange multiplier methods*. Optimization and neural computation series. Belmont, Mass: Athena Scientific, 1996. 395 pp.
- [Bet01] Josef Betten. *Kontinuumsmechanik - Elastisches und inelastisches Verhalten isotroper und anisotroper Stoffe*. Berlin, Heidelberg: Springer Berlin Heidelberg, 2001.
- [Bet87] J. Betten. *Tensorrechnung für Ingenieure*. LAMM Leitfäden der Angewandten Mathematik und Mechanik. Teubner B.G. GmbH, 1987.
- [Bet97] J Betten. *Finite Elemente für Ingenieure*. Berlin: Springer, 1997.
- [Bis+04] M. Bischoff et al. “Models and Finite Elements for Thin-Walled Structures.” In: *Encyclopedia of Computational Mechanics*. Ed. by Erwin Stein, Rene de Borst, and Thomas J. R. Hughes. Chichester, UK: John Wiley & Sons, Ltd, Nov. 15, 2004.
- [BK85] Y Basar and W. B Krätzig. *Mechanik der Flächentragwerke. Theorie, Berechnungsmethoden, Anwendungsbeispiele*. Braunschweig: Vieweg, 1985.
- [BL03] J. S. Brew and W. J. Lewis. “Computational form-finding of tension membrane structures—Non-finite element approaches: Part 2. Triangular mesh discretization and control of mesh distortion in modelling minimal surface membranes.” In: *International journal for numerical methods in engineering* 56.5 (2003), pp. 669–684.
- [BL05] Pavel Bochev and R. B. Lehoucq. “On the Finite Element Solution of the Pure Neumann Problem.” In: *SIAM Review* 47.1 (2005), pp. 50–66.
- [BLW09] K.-U. Bletzinger, J. Linhard, and R. Wüchner. “Extended and Integrated Numerical Form Finding and Patterning of Membrane Structures.” In: *Journal of the International Association for Shell and Spatial Structures* 1.50 (2009), pp. 35–49.
- [BLW10] Kai-Uwe Bletzinger, Johannes Linhard, and Roland Wüchner. “Advanced numerical methods for the form finding and patterning of membrane structures.” In: *New Trends in Thin Structures: Formulation, Optimization and Coupled Problems*. Springer, 2010, pp. 133–154.
- [Bon+00] J. Bonet et al. “Finite element analysis of air supported membrane structures.” In: *Computer Methods in Applied Mechanics and Engineering* 190.5 (2000), pp. 579–595.
- [BR99] Kai-Uwe Bletzinger and Ekkehard Ramm. “A General Finite Element Approach to the Form Finding of Tensile Structures by the Updated Reference Strategy.” In: *International Journal of Space Structures* 14.2 (June 1, 1999), pp. 131–145.

- [BSS94] Horst Baier, Christoph Seesselberg, and Bernhard Specht. *Optimierung in der Strukturmechanik*. Braunschweig; Wiesbaden: Vieweg, 1994.
- [Bub72] E. Bubner. *Zum Problem der Formfindung vorgespannter Seilnetzflächen*. IGMA Dissertationen. Krämer, 1972.
- [BZ13] Ilja Bronstein and Eberhard Zeidler. *Springer-Taschenbuch der Mathematik*. Wiesbaden: Vieweg+Teubner Springer Fachmedien, 2013.
- [Can13] B. Cantzler. *Photogrammetrische Verformungsmessung eines Pneus zur experimentellen Validierung*. Bachelorthesis. München: Technische Universität München, 2013.
- [Car76] Manfredo Perdigão do Carmo. *Differential geometry of curves and surfaces*. Englewood Cliffs, N.J: Prentice-Hall, 1976. 503 pp.
- [CB98] D. Chapelle and K. J. Bathe. “Fundamental considerations for the finite element analysis of shell structures.” In: *Computers & Structures* 66.1 (1998), pp. 19–36.
- [CH93] J. Chung and G. M. Hulbert. “A Time Integration Algorithm for Structural Dynamics With Improved Numerical Dissipation: The Generalized-alpha Method.” In: *Journal of Applied Mechanics* 60.2 (1993), pp. 371–375.
- [Cha14] Eduardo W. V Chaves. *Continuum mechanics: fundamental concepts and constitutive equations*. Dordrecht: Springer, 2014.
- [CHB09] J. Austin Cottrell, Thomas J. R. Hughes, and Yuri Bazilevs. *Isogeometric analysis: toward integration of CAD and FEA*. Chichester, West Sussex, U.K. ; Hoboken, NJ: Wiley, 2009. 335 pp.
- [CKC06] Roy R. Craig, Andrew Kurdila, and Roy R. Craig. *Fundamentals of structural dynamics*. 2nd ed. Hoboken, N.J: John Wiley, 2006. 728 pp.
- [Coe12] Marianna Coelho. “Analysis of pneumatic structures considering non-linear material models and pressure–volume coupling.” PhD thesis. Rio de Janeiro: Pontifical Catholic University of Rio de Janeiro, 2012.
- [CP93] R. W. Clough and J. Penzien. *Dynamics of Structures*. New York: McGraw, 1993.
- [Cri91] M. A. Crisfield. *Non-linear finite element analysis of solids and structures*. Chichester ; New York: Wiley, 1991. 2 pp.
- [Day65] A. S. Day. “An introduction to dynamic relaxation.” In: *The Engineer* (1965), pp. 220–221.
- [Deg12] Atis Degro. *Simulation of widespan umbrella structures under transient wind loads*. Masterthesis. Technische Universität München: Lehrstuhl für Statik, 2012.
- [Die+13a] Falko Dieringer et al. “Computational Cutting Pattern Generation for Membrane Structures.” In: *Proceedings of the Tensinet Symposium 2013*. Tensinet Symposium 2013 [RE] THINKING Lightweight Structures. Istanbul, May 2013.
- [Die+13b] F. Dieringer et al. “Numerical Methods for the Design and Analysis of Hybrid Structures.” In: *International Journal of Space Structures* 3&4.28 (2013), pp. 149–160.

Bibliography

- [Die09] Falko Dieringer. *Implementierung eines geometrisch nichtlinearen Membranelements in einer objektorientierten Programmierumgebung*. Diploma Thesis. München: TU München, 2009.
- [Die10] Ulrich Dierkes. *Minimal surfaces*. In collab. with Stefan Hildebrandt and Friedrich Sauvigny. Rev. and enl. 2nd ed. Grundlehren der mathematischen Wissenschaften 339. Heidelberg ; New York: Springer, 2010. 688 pp.
- [Dij59] E. W. Dijkstra. "A note on two problems in connexion with graphs." In: *Numerische Mathematik* 1.1 (Dec. 1959), pp. 269–271.
- [Duf18] G. Duffing. *Erzwungene Schwingungen bei veränderlicher Eigenfrequenz und ihre Technische Bedeutung*. Sammlung Vieweg. R. Vieweg & Sohn, 1918.
- [DWB10] F. Dieringer, R. Wüchner, and K.-U. Bletzinger. "Computational design and analysis of membrane structures: Teaching, research and practice." In: *Proceedings of the International Association for Shell and Spatial Structures Symposium 2010*. International Association for Shell and Spatial Structures Symposium 2010: Spatial Structures – Permanent and Temporary. Shanghai, 2010.
- [DWB12] F. Dieringer, R. Wüchner, and K.-U. Bletzinger. "Practical Advances in Numerical Form Finding and Cutting Pattern Generation for Membrane Structures." In: *Journal of the International Association for Shell and Spatial Structures* 3.53 (2012), pp. 147–156.
- [EB10] Ralph Echter and Manfred Bischoff. "Numerical efficiency, locking and unlocking of NURBS finite elements." In: *Computer Methods in Applied Mechanics and Engineering* 199.5 (2010), pp. 374–382.
- [FH05] C.A. Felippa and B. Haugen. "A unified formulation of small-strain corotational finite elements: I. Theory." In: *Computer Methods in Applied Mechanics and Engineering* 194.21 (June 2005), pp. 2285–2335.
- [Fin72] B.A. Finlayson. *The Method of Weighted Residuals and Variational Principles: With Application in Fluid Mechanics, Heat and Mass Transfer*. Educational Psychology. Academic Press, 1972.
- [Fis+12] Rupert Fisch et al. "Towards the establishment of a numerical wind tunnel." In: *Forschungskolloquium Baustatik-Baupraxis 2012*. 2012.
- [FM04] Brian Forster and Marijke Mollaert. *The European design guide for tensile surface structures*. Brussels: Tensinet, 2004.
- [Gal10] Thomas Georg Gallinger. "Effiziente Algorithmen zur partitionierten Lösung stark gekoppelter Probleme der Fluid-Struktur-Wechselwirkung." PhD thesis. Aachen: Shaker, 2010.
- [GB08] P. D. Gosling and B. N. Bridgens. "Material Testing & Computational Mechanics-A New Philosophy For Architectural Fabrics." In: *International Journal of Space Structures* 23.4 (2008), pp. 215–232.
- [GB09] Knut Göppert and Markus Balz. "Membrantragwerke." In: *Stahlbau-Kalender 2009*. Ed. by Ulrike Kuhlmann. Berlin, Germany: Ernst & Sohn Verlag für Architektur und technische Wissenschaften GmbH & Co. KG, 2009, pp. 707–759.

- [GL09] C. Galliot and R.H. Luchsinger. “A simple model describing the non-linear biaxial tensile behaviour of PVC-coated polyester fabrics for use in finite element analysis.” In: *Composite Structures* 90.4 (Oct. 2009), pp. 438–447.
- [Gos+13] P. D. Gosling et al. “Analysis and design of membrane structures: Results of a round robin exercise.” In: *Engineering Structures* 48 (2013), pp. 313–328.
- [Gre11] A. Greim. *Numerical Design and Analysis of a Membrane Structure*. Workshop Report. München: Technische Universität München, 2011.
- [Grü76] Lothar Gründig. “Die Berechnung vorgespannter Seil- und Hängenetze unter Berücksichtigung ihrer topologischen und physikalischen Eigenschaften und der Ausgleichsrechnung.” PhD thesis. München: Verlag der Bayerischen Akademie der Wissenschaften : In Kommission bei C.H. Beck, 1976.
- [GT92] F. Gruttmann and R. L. Taylor. “Theory and finite element formulation of rubberlike membrane shells using principal stretches.” In: *International Journal for Numerical Methods in Engineering* 35.5 (1992), pp. 1111–1126.
- [HA82] R. B. Haber and J. F. Abel. “Initial equilibrium solution methods for cable reinforced membranes part II.” In: *Computer Methods in Applied Mechanics and Engineering* 30.3 (1982), pp. 285–306.
- [Hau72] E. Haug. “Finite element analysis of nonlinear membrane structures.” PhD thesis. California: University of California Berkley, 1972.
- [Hau88a] E. Haug. *Numerical Form-Finding of Membranes*. 18. Stuttgart: University of Stuttgart, 1988, pp. 340–347.
- [Hau88b] E. Haug. *Numerical Simulation of Soap Films*. 18. Stuttgart: University of Stuttgart, 1988, pp. 376–380, 393–394.
- [Hau94] B. Haugen. “Buckling and Stability Problems for Thin Shell Structures Using High Performance Finite Elements.” PhD thesis. Colorado: University of Colorado, 1994.
- [Haz88] Michiel Hazewinkel. *Encyclopaedia of mathematics: an updated and annotated translation of the Soviet "Mathematical encyclopaedia"*. Dordrecht: Reidel, 1988.
- [Hel01] Peter Helnwein. “Some remarks on the compressed matrix representation of symmetric second-order and fourth-order tensors.” In: *Computer Methods in Applied Mechanics and Engineering* 190.22 (2001), pp. 2753–2770.
- [Hes69] Magnus R. Hestenes. “Multiplier and gradient methods.” In: *Journal of optimization theory and applications* 4.5 (1969), pp. 303–320.
- [HG92] Raphael T Haftka and Zafer Gürdal. *Elements of structural optimization*. Dordrecht; Boston: Kluwer Academic Publishers, 1992.
- [HO76] C E Hildebrand and R T Okinaka. “A rapid method for preparation of nuclear membranes from mammalian cells.” In: *Analytical biochemistry* 75.1 (Sept. 1976). PMID: 9015, pp. 290–300.

Bibliography

- [Hoj+11] M. Hojjat et al. "Fluid-Structure Interaction in the Context of Shape Optimization and Computational Wind Engineering." In: *Fluid Structure Interaction II*. Ed. by Hans-Joachim Bungartz, Miriam Mehl, and Michael Schäfer. Vol. 73. Berlin, Heidelberg: Springer Berlin Heidelberg, 2011, pp. 351–381.
- [Hol00] Gerhard A. Holzapfel. *Nonlinear solid mechanics: a continuum approach for engineering*. Chichester ; New York: Wiley, 2000. 455 pp.
- [Hol07] J. D. Holmes. *Wind loading of structures*. 2nd ed. London ; New York: Taylor & Francis, 2007. 379 pp.
- [Hop07] Diether S Hoppe. *Freigespannte textile Membrankonstruktionen: geschichtliche, materialtechnische, konstruktive und gegenwärtige Entwicklungen*. Wien: Böhlau, 2007.
- [HP72] E. Haug and G.H. Powell. "Finite Element Analysis of Nonlinear Membrane Structures." In: *Proceedings of the 1971 IASS Pacific Symposium*. Proceedings of the 1971 IASS Pacific Symposium. SESM report. Tokyo and Kyoto, 1972, pp. 165–175.
- [Hsi97] Chuan-Chih Hsiung. *A first course in differential geometry*. Cambridge, MA: International Press, 1997. 343 pp.
- [HT96] Stefan Hildebrandt and Anthony J Tromba. *Kugel, Kreis und Seifenblasen: optimale Formen in Geometrie und Natur*. Basel [u.a.]: Birkhäuser, 1996.
- [Hug00] Thomas J. R. Hughes. *The finite element method: linear static and dynamic finite element analysis*. Mineola, NY: Dover Publications, 2000. 682 pp.
- [Jru09] Amphon Jrusjungkiat. "Nonlinear analysis of pneumatic membranes:" from subgrid to interface". PhD thesis. München, Techn. Univ., Diss., 2009, 2009.
- [Käs64] S. Kästner. *Vektoren, Tensoren, Spinoren*: Akademie-Verlag, 1964.
- [KC99] D. Kuhl and M. A. Crisfield. "Energy-conserving and decaying algorithms in non-linear structural dynamics." In: *International journal for numerical methods in engineering* 45.5 (1999), pp. 569–599.
- [Kie11] Josef M Kiendl. "Isogeometric analysis and shape optimal design of shell structures." PhD thesis. Aachen: Shaker, 2011.
- [KJ03] W. B. Krätzig and D. Jun. "On 'best' shell models - From classical shells, degenerated and multi-layered concepts to 3D." In: *Archive of Applied Mechanics (Ingenieur Archiv)* 73.1 (Aug. 1, 2003), pp. 1–25.
- [KJS05] M.J. King, P. Jearanaisilawong, and S. Socrate. "A continuum constitutive model for the mechanical behavior of woven fabrics." In: *International Journal of Solids and Structures* 42.13 (June 2005), pp. 3867–3896.
- [KL02] Jae-Yeol Kim and Jang-Bog Lee. "A new technique for optimum cutting pattern generation of membrane structures." In: *Engineering Structures* 24.6 (2002), pp. 745–756.

- [Kli93] Eberhard Klingbeil. *Tensorrechnung für Ingenieure*. Mannheim [u.a.: BI-Wiss.-Verl., 1993.
- [Kni+11] Jan Knippers et al. *Construction manual for polymers + membranes: materials, semi-finished products, form-finding design*. 2011.
- [Koc04] Klaus-Michael Koch. *Membrane structures: innovative building with film and fabric*. In collab. with Karl J. Habermann and Brian Forster. Munich ; New York: Prestel, 2004. 263 pp.
- [Kök13] E.C. Kökan. *Implementation and validation of a co-rotational shell element in the FEM-software Carat++*. Masterthesis. München: Technische Universität München, 2013.
- [Kos14] V. Koslowski. *Implementation of the Pressure Volume Coupling of Pneumatic Structures in the FE-Code CARAT++ and its Experimental Validation*. Masterthesis. München: Technische Universität München, 2014.
- [Kre09] S. Krenk. *Non-linear modeling and analysis of solids and structures*. Cambridge, UK ; New York: Cambridge University Press, 2009. 349 pp.
- [Kre91] Erwin Kreyszig. *Differential geometry*. New York: Dover Publications, 1991. 352 pp.
- [KS98] R. Kimmel and J. A. Sethian. "Computing geodesic paths on manifolds." In: *Proceedings of the National Academy of Sciences* 95.15 (July 21, 1998), pp. 8431–8435.
- [Küh06] Wolfgang Kühnel. *Differential geometry: curves - surfaces - manifolds*. 2nd ed. Student mathematical library v. 16. Providence, R.I: American Mathematical Society, 2006. 380 pp.
- [Kuh96] Detlef Kuhl. "Stabile Zeitintegrationsalgorithmen in der nichtlinearen Elastodynamik dünnwandiger Querschnitte." PhD thesis. Stuttgart: Universität Stuttgart, 1996.
- [Kup09] Alexander Kupzok. "Modeling the Interaction of Wind and Membrane Structures by Numerical Simulation." Dissertation. München: Technische Universität München, 2009.
- [KWK07] Michael Karwath, Rosemarie Wagner, and Bernd Kröplin. "Ein orthotropes Werkstoffgesetz für Folien." In: *Stahlbau* 76.5 (May 2007), pp. 297–304.
- [LB10] Johannes Linhard and Kai-Uwe Bletzinger. "'Tracing" the Equilibrium-Recent Advances in Numerical Form Finding." In: *International Journal of Space Structures* 25.2 (2010), pp. 107–116.
- [LB73] Kurt Leichtweiß and Wilhelm Blaschke. *Elementare Differentialgeometrie*. Göttingen: Niedersächsische Staats- und Universitätsbibliothek, 1973.
- [Leo40] Fritz Leonhardt. "Leichtbau – eine Forderung unserer Zeit. Anregungen für den Hoch- und Brückenbau." In: *Die Bautechnik* 18 (Nr. 36/37 1940), pp. 413–423.

Bibliography

- [Lie+13] J. Lienhard et al. “Extending the Functional and Formal vocabulary of tensile membrane structures through the interaction with bending-active elements.” In: *Proceedings of the Tensinet Symposium 2013*. Tensinet Symposium 2013 [RE] THINKING Lightweight Structures. Istanbul, May 2013.
- [Lin09] Johannes Linhard. “Numerisch-mechanische Betrachtung des Entwurfsprozesses von Membrantragwerken.” PhD thesis. München, Techn. Univ., Diss., 2009, 2009.
- [LK12] Julian Lienhard and Jan Knippers. “Permanent and convertible membrane structures with intricate bending-active support systems.” In: *Proceedings of the International IASS-APCS Symposium 2012*. International IASS-APCS Symposium 2012. Seoul, 2012.
- [LL96] W.J Lewis and T.S. Lewis. “Application of formian and dynamic relaxation to the form finding of minimal surfaces.” In: *Journal of the International Association For Shell and Spatial Structures* 37.3 (1996), pp. 165–186.
- [LS71] Klaus Linkwitz and H.-J. Scheck. “Einige Bemerkungen zur Berechnung vorgespannter Seilnetzkonstruktionen.” In: *Ingenieurarchiv* 40 (1971), pp. 145–158.
- [LWB07] Johannes Linhard, Roland Wüchner, and Kai-Uwe Bletzinger. ““Upgrading” membranes to shells—The CEG rotation free shell element and its application in structural analysis.” In: *Finite Elements in Analysis and Design* 44.1 (Dec. 2007), pp. 63–74.
- [LWB08] Johannes Linhard, Roland Wüchner, and Kai-Uwe Bletzinger. “Introducing Cutting Patterns in Form Finding and Structural Analysis.” In: *Textile Composites and Inflatable Structures II*. Ed. by Eugenio Oñate and Bernhard Kröplin. Springer, 2008, pp. 69–84.
- [Man13] Herbert A Mang. *Festigkeitslehre*. Berlin, Heidelberg: Imprint: Springer Vieweg, 2013.
- [Mar94] Jerrold E. Marsden. *Mathematical foundations of elasticity*. In collab. with Thomas J. R. Hughes. New York: Dover, 1994. 556 pp.
- [MB02] Karsten Moritz and Rainer Barthel. “Transparente Architektur - Bauen mit ETFE-Folien.” In: *Detail* 12 (2002), pp. 1616–1620.
- [Meh97] Gerhard Mehlhorn. *Werkstoffe, Elastizitätstheorie*. Berlin: Ernst, 1997.
- [Mic+11] A. Michalski et al. “Validation of the computational fluid–structure interaction simulation at real-scale tests of a flexible 29m umbrella in natural wind flow.” In: *Journal of Wind Engineering and Industrial Aerodynamics* 99.4 (Apr. 2011), pp. 400–413.
- [Mic10] Alexander Michalski. “Simulation leichter Flächentragwerke in einer numerisch generierten atmosphärischen Grenzschicht.” PhD thesis. München, Techn. Univ., Diss., 2010, 2010.
- [Mid02] P. Middendorf. *Viskoelastisches Verhalten von Polymersystemen: Materialmodellierung und Finite-Elemente-Implementierung bei kleinen und finiten Deformationen*. Fortschritt-Berichte VDI: Reihe 5, Grund- und Werkstoffe, Kunststoffe. VDI-Verlag, 2002.

- [MM00] Udo F Meißner and Andreas Maurial. *Die Methode der finiten Elemente: eine Einführung in die Grundlagen*. Berlin [u.a.]: Springer, 2000.
- [MM98] Bernard Maurin and Rene Motro. “The surface stress density method as a form-finding tool for tensile membranes.” In: *Engineering Structures* 20.8 (Aug. 1998), pp. 712–719.
- [MM99] Bernard Maurin and Rene Motro. “Cutting pattern of fabric membranes with the stress composition method.” In: *International Journal of Space Structures* 14.2 (1999), pp. 121–129.
- [Mok+99] D.P. Mok et al. “Algorithmic aspects of deformation dependent loads in non-linear static finite element analysis.” In: *Engineering Computations* 16.5 (1999), pp. 601–618.
- [Mor00] Karsten Moritz. “Membranwerkstoffe im Hochbau.” In: *Detail* 6 (2000), pp. 1050–1054.
- [Mor07] Karsten Moritz. “ETFE-Folie als Tragelement.” Dissertation. München: Technische Universität München, 2007.
- [MR95] R. Münsch and H.-W. Reinhardt. “Zur Berechnung von Membrantragwerken aus beschichteten Geweben.” In: *Bauingenieur* 70 (1995), pp. 271–275.
- [MT90] E. Moncrieff and B. H. V. Topping. “Computer methods for the generation of membrane cutting patterns.” In: *Computers & Structures* 37.4 (1990), pp. 441–450.
- [New59] N.M. Newmark. *A Method of Computation for Structural Dynamics*. American Society of Civil Engineers, 1959.
- [NK02] M. Novotni and R. Klein. “Computing Geodesic Distances on Triangular Meshes.” In: *Proceedings of the 10-th International Conference in Central Europe on Computer Graphics, Visualization and Computer Vision’2002 (WSCG’2002)*. The 10-th International Conference in Central Europe on Computer Graphics, Visualization and Computer Vision’2002 (WSCG’2002). Universität Bonn, 2002.
- [Oel11] Stefan Oelkuch. *Formfindungsanalyse von Membrantragwerken mit der Updated Reference Strategy und Elementen mit quadratischen Ansatzfunktionen*. Masterthesis. Technische Universität München: Lehrstuhl für Statik, 2011.
- [OF05] Eugenio Oñate and Fernando G. Flores. “Advances in the formulation of the rotation-free basic shell triangle.” In: *Computer Methods in Applied Mechanics and Engineering* 194.21 (June 2005), pp. 2406–2443.
- [Off10] R Off. “New trends on membrane and shell structures—Examples of bat-sail and cushion-belt technologies.” In: *Structures & Architecture*. Ed. by Paulo Cruz. CRC Press, July 2, 2010, pp. 25–28.
- [Ogd97] R. W. Ogden. *Non-linear elastic deformations*. Mineola, N.Y.: Dover Publications, 1997. 532 pp.

Bibliography

- [OH79] J. Oelbermann and E. Haug. "Berechnung des Zuschnittes einer Membran mit Hilfe der Finiten-Elemente-Methode." In: 2. *Internationales Symposium Weitgespannte Flächentragwerke Sonderforschungsbereich 64*. 2. Internationales Symposium Weitgespannte Flächentragwerke Sonderforschungsbereich 64. Vol. Heft 1. Stuttgart, 1979, pages.
- [Oña09] Eugenio Oñate. *Structural analysis with the finite element method: linear statics: volume 1: basis and solids*. Barcelona: CIMNE, International Center for Numerical Methods in Engineering, 2009.
- [Oña13] E Oñate. *Structural analysis with the finite element method: linear statics: volume 2: beams, plates and shells*. Dordrecht; London: Springer, 2013.
- [OR95] Frei Otto and Bodo Rasch. *finding form: towards an architecture of the minimal*. Stuttgart: Axel Menges, 1995.
- [OS66] F. Otto and F.-K. Schleyer. *Zugbeanspruchte Konstruktionen*. Vol. 2. 2 vols. Frankfurt, Berlin: Ullstein, 1966.
- [OT62] F. Otto and R. Trostel. *Zugbeanspruchte Konstruktionen*. Vol. 1. 2 vols. Frankfurt, Berlin: Ullstein, 1962.
- [Par03] Horst Parisch. *Festkörper-Kontinuumsmechanik: von den Grundgleichungen zur Lösung mit finiten Elementen*. Stuttgart; Leipzig; Wiesbaden: Teubner, 2003.
- [PB13] Benedikt Philipp and K.-U. Bletzinger. "Hybrid Structures - Enlarging the Design Space of Architectural Membranes." In: *Jornal of the International Association for Shell and Spatial Structures* 4.54 (2013), pp. 281–291.
- [Pet96] Christian Petersen. *Dynamik der Baukonstruktionen*. Wiesbaden: Vieweg, 1996.
- [Phi+14] B. Philipp et al. "From-finding with the Isogeometric B-Reps Analysis." In: *Computer Methods in Applied Mechanics and Engineering* submitted (2014).
- [Pie97] Les A. Piegl. *The NURBS book*. In collab. with Wayne Tiller. 2nd ed. Monographs in visual communications. Berlin ; New York: Springer, 1997. 646 pp.
- [Ram82] E. Ramm. "The Riks/Wempner approach - An extension of the displacement control method in non-linear analysis." In: E. Hinton, D.R.J. Owen, and C. Taylor. *Non-linear computational mechanics*. UK: Pineridge Press, 1982, pp. 63–86.
- [Ray94] J.W.S.B. Rayleigh. *The Theory of Sound*. The Theory of Sound Bd. 1. Macmillan, 1894.
- [Rei94] R. Reitinger. "Stabilität und Optimierung imperfektionsempfindlicher Tragwerke." PhD thesis. Stuttgart: Universität Stuttgart, 1994.
- [Rob96] Tony Robbin. *Engineering a new architecture*. New Haven: Yale University Press, 1996. 138 pp.

- [Rom08] Ignacio Romero. "A comparison of finite elements for nonlinear beams: the absolute nodal coordinate and geometrically exact formulations." In: *Multibody System Dynamics* 20.1 (Mar. 7, 2008), pp. 51–68.
- [RW04] E. Ramm and W. A. Wall. "Shell structures - a sensitive interrelation between physics and numerics." In: *International Journal for Numerical Methods in Engineering* 60.1 (May 7, 2004), pp. 381–427.
- [Šar+12] Anina Šarkić et al. "Bridge flutter derivatives based on computed, validated pressure fields." In: *Journal of Wind Engineering and Industrial Aerodynamics* 104-106 (May 2012), pp. 141–151.
- [Sch+07] Lars Schiemman et al. "Bursting tests of ETFE-foil." In: *Proceedings of the III International Conference on Textile Composites and Inflatable Structures*. International Conference on Textile Composites and Inflatable Structures. Barcelona, 2007.
- [Sch09] Lars Schiemann. "Tragverhalten von ETFE-Folien unter biaxialer Beanspruchung." Dissertation. München: Technische Universität München, 2009.
- [Sch35] H.F. Scherk. "Bemerkungen über die kleinste Fläche innerhalb gegebener Grenzen." In: *Journal für die reine und angewandte Mathematik* 13 (1835), pp. 185–208.
- [Sch74] H.-J. Scheck. "The force density method for form finding and computation of general networks." In: *Computer Methods in Applied Mechanics and Engineering* 3 (1974), pp. 115–134.
- [Sch78] D. Schwenkel. "Mathematisch-numerische Methoden zur Approximation und Abbildung der Systemgeometrie weitgespannter Flächen-Tragwerke." PhD thesis. München: Verlag der Bayerischen Akademie der Wissenschaften in Kommission bei der C.H. Beck, 1978.
- [Sch84] Hans Rudolf Schwarz. *Methode der finiten Elemente: eine Einführung unter besonderer Berücksichtigung der Rechenpraxis; mit 57 Tab. und zahlr. Beisp.* Stuttgart: Teubner, 1984.
- [Sch90] Martina Schneider. *Der Umgekehrte Weg: Frei Otto zum 65. Geburtstag*. Arcus 10. Köln: R. Müller, 1990. 80 pp.
- [Sch97] Hans-Joachim Schock. *Segel, Folien und Membranen: innovative Konstruktionen in der textilen Architektur*. Basel [u.a.: Birkhäuser, 1997.
- [Sei08] Michael Seidel. *Textile Hüllen: Bauen mit biegeweichen Tragelementen ; Materialien, Konstruktion, Montage*. Berlin: Ernst, 2008.
- [SH08] K. Schweizerhof and M. Haßler. "On the Static Interaction of Fluid and Gas loaded Multi-Chamber Systems in a Large Deformation Finite Element Analysis." In: *Computer Methods in Applied Mechanics and Engineering* 197 (2008), pp. 1725–1749.
- [Sic+11] S. Sicklinger et al. "Verification Examples for Computational Fluid-Structure Interaction." In: *4th GACM Colloquium*. 2011.
- [Sin95] Peter Singer. "Die Berechnung von Minimalflächen, Seifenblasen, Membrane und Pneus aus geodätischer Sicht." PhD thesis. München: Beck, 1995.

Bibliography

- [SR84] Karl Schweizerhof and Ekkehard Ramm. "Displacement dependent pressure loads in nonlinear finite element analyses." In: *Computers & Structures* 18.6 (1984), pp. 1099–1114.
- [SS01] Alla Sheffer and Eric de Sturler. "Parameterization of faceted surfaces for meshing using angle-based flattening." In: *Engineering with Computers* 17.3 (2001), pp. 326–337.
- [STT95] V.P.W. Shim, V.B.C. Tan, and T.E. Tay. "Modelling deformation and damage characteristics of woven fabric under small projectile impact." In: *International Journal of Impact Engineering* 16.4 (Aug. 1995), pp. 585–605.
- [Top07] B. H. V. Topping. *Computer aided design of cable membrane structures*. In collab. with P. Iványi. Saxe-Coburg publications on computational engineering. Kippen, Stirlingshire, Scotland: Saxe-Coburg Publications, 2007. 233 pp.
- [Tre44] L. R. G. Treloar. "Stress-strain data for vulcanised rubber under various types of deformation." In: *Transactions of the Faraday Society* 40 (1944), pp. 59–70.
- [UEG13] P.-A. Ubach, C. Estruch, and J. Garcia-Espinosa. "On the interpolation of normal vectors for triangle meshes." In: *International Journal for Numerical Methods in Engineering* (Sept. 2013), n/a–n/a.
- [Van01] Garret N Vanderplaats. *Numerical optimization techniques for engineering design*. Colorado Springs, Colo.: Vanderplaats Research and Development, Inc., 2001.
- [Wak99] D. S. Wakefield. "Engineering analysis of tension structures: theory and practice." In: *Engineering structures* 21.8 (1999), pp. 680–690.
- [WB05] R. Wüchner and K.-U. Bletzinger. "Stress-adapted numerical form finding of pre-stressed surfaces by the updated reference strategy." In: *International Journal for Numerical Methods in Engineering* 64.2 (Sept. 14, 2005), pp. 143–166.
- [Web11] C. Weber. *Fritz Leonhardt - "Leichtbau - eine Forderung unserer Zeit. Anregungen für den Hoch- und Brückenbau". Zur Einführung baukonstruktiver Prinzipien im Leichtbau in den 1930er- und 1940er-Jahren*. Materialien zu Bauforschung und Baugeschichte. KIT Scientific Publ., 2011.
- [Wer83] H. Werkle. "Standesicherheit von Schalterfundamenten bei dynamischer Beanspruchung durch Kurzschlußkräfte." In: *Bautechnik* (1983).
- [Wil11] Monika Wilfling. *Experimentelle Formfindung von Minimalflächen*. München: Technische Universität München, 2011.
- [WKB07] Roland Wüchner, Alexander Kupzok, and Kai-Uwe Bletzinger. "A framework for stabilized partitioned analysis of thin membrane–wind interaction." In: *International Journal for Numerical Methods in Fluids* 54.6 (June 30, 2007), pp. 945–963.
- [WM95] Werkbund Bayern and Museum Villa Stuck. *Frei Otto, Bodo Rasch: finding form: towards an architecture of the minimal*. Stuttgart?: Axel Menges, 1995. 239 pp.

- [Woo50] M. Woodbury. *Inverting modified matrices*. Memorandum Report 42. Princeton: University of Princeton, 1950.
- [Wri08] P. Wriggers. *Nonlinear finite element methods*. Berlin: Springer, 2008. 559 pp.
- [WS90] P. Wriggers and J. C. Simo. “A general procedure for the direct computation of turning and bifurcation points.” In: *International Journal for Numerical Methods in Engineering* 30.1 (July 1990), pp. 155–176.
- [Wüc07] Roland Wüchner. “Mechanik und Numerik der Formfindung und Fluid-Struktur-Interaktion von Membrantragwerken.” PhD thesis. Aachen: Shaker, 2007.
- [WWB12] Armin Widhammer, Roland Wüchner, and Kai-Uwe Bletzinger. “Drape simulation for non-developable multi-layered CFRP structures focusing on optimized cutting patterns.” In: *Proceedings of the 6th European Congress on Computational Methods in Applied Sciences and Engineering 2012*. ECCOMAS 2012. Wien, 2012.
- [XN11] Weijie Xia and Ben Nadler. “Three-scale modeling and numerical simulations of fabric materials.” In: *International Journal of Engineering Science* 49.3 (Mar. 2011), pp. 229–239.
- [Zie00] O. C. Zienkiewicz. *The finite element method*. In collab. with Robert L. Taylor. 5th ed. Vol. Volume 1. Oxford ; Boston: Butterworth-Heinemann, 2000. 3 pp.
- [Zie01] René Ziegler. *Theorie und Numerik für den Entwurf von vorgespannten Membrantragwerken*. Karlsruhe: Inst. für Baustatik, 2001.
- [ZP06] T.I. Zohdi and D. Powell. “Multiscale construction and large-scale simulation of structural fabric undergoing ballistic impact.” In: *Computer Methods in Applied Mechanics and Engineering* 195.1 (2006), pp. 94–109.